~~SECRET~~

ORNL
MASTER COPY

AEC RESEARCH AND DEVELOPMENT REPORT

ORNL 1616
Special

LABORATORY RECORDS
1954

LID TANK SHIELDING TESTS FOR THE REFLECTOR-MODERATED REACTOR

F. H. Abernathy
A. P. Fraas
M. E. LaVerne
R. M. Spencer
F. N. Watson
F. R. Westfall

CLASSIFICATION CANCELLED
DATE JUL 13 1979

By authority of
AEC 9/21/1970
F. E. Evans
For A. T. Roy, Secretary
Laboratory Records Dept
ORNL

OAK RIDGE NATIONAL LABORATORY
OPERATED BY
CARBIDE AND CARBON CHEMICALS COMPANY
A DIVISION OF UNION CARBIDE AND CARBON CORPORATION
UCC
POST OFFICE BOX P
OAK RIDGE, TENNESSEE

~~RESTRICTED DATA~~

~~This document contains Restricted Data as defined in the Atomic Energy Act of 1946. Its transmittal or the disclosure of its contents in any manner to an unauthorized person is prohibited.~~

~~SECRET~~

SECRET

CENTRAL RESEARCH LIBRARY
DOCUMENT COLLECTION

AEC RESEARCH AND DEVELOPMENT REPORT

MARTIN MARIETTA ENERGY SYSTEMS LIBRARIES
3 4456 0349584 9

ORNL 1616
Special 44A

DECLASSIFIED
Classification Changed To: UCNI
By Authority Of: 9-24-70
By: [illegible] 3-10-71

LID TANK SHIELDING TESTS FOR THE REFLECTOR-MODERATED REACTOR

F. H. Abernathy
A. P. Fraas
M. E. LaVerne
R. M. Spencer
F. N. Watson
F. R. Westfall

CENTRAL RESEARCH LIBRARY
DOCUMENT COLLECTION
LIBRARY LOAN COPY
DO NOT TRANSFER TO ANOTHER PERSON
If you wish someone else to see this document, send in name with document and the library will arrange a loan.

OAK RIDGE NATIONAL LABORATORY
OPERATED BY
CARBIDE AND CARBON CHEMICALS COMPANY
A DIVISION OF UNION CARBIDE AND CARBON CORPORATION
UCC
POST OFFICE BOX P
OAK RIDGE, TENNESSEE

RESTRICTED DATA
This document contains Restricted Data as defined in the Atomic Energy Act of 1946. Its transmittal or the disclosure of its contents in any manner to an unauthorized person is prohibited.

SECRET

[redacted]

ORNL-1616

This document consists of 243 pages.
Copy 44 of 155 copies. Series A.

Contract No. W-7405-eng-26

LID TANK SHIELDING TESTS FOR THE REFLECTOR-MODERATED REACTOR

F. H. Abernathy
A. P. Fraas
M. E. LaVerne
R. M. Spencer*
F. N. Watson
F. R. Westfall*

* U. S. Air Force

DATE ISSUED

OCT 5 1954

OAK RIDGE NATIONAL LABORATORY
Operated by
CARBIDE AND CARBON CHEMICALS COMPANY
A Division of Union Carbide and Carbon Corporation
Post Office Box P
Oak Ridge, Tennessee

[redacted]

MARTIN MARIETTA ENERGY SYSTEMS LIBRARIES

3 4456 0349584 9

[redacted]

ORNL 1616
Special

INTERNAL DISTRIBUTION

1. F. H. Abernathy
2. H. Bethe (consultant)
3. E. P. Blizard
4. C. E. Center
5. R. A. Charpie
6. C. E. Clifford
7. G. T. Chapman
8. R. G. Cochran
9. Sylvan Cromer
10. J. B. Dee
11. L. B. Emlet (K-25)
12. W. K. Ergen
13. A. P. Fraas
14. H. E. Hungerford
15. W. H. Jordan
16. J. A. Lane
17. C. E. Larson
18. M. E. LaVerne
19. F. C. Maienschein
20. J. L. Meem
21. K. Z. Morgan
22. F. H. Murray
23. R. H. Ritchie
24. A. Simon
25. A. H. Snell
26. R. M. Spencer
27. H. E. Stern
28. C. L. Storrs
29. F. N. Watson
30. A. M. Weinberg
31. T. A. Welton
32. H. P. Yockey
33. Biology Library
34. Health Physics Library
35-40. ANP Library
41. Metallurgy Library
42. Reactor Experimental Engineering Library
43-48. Central Research Library
49. Laboratory Records, ORNL-RC
50-55. Laboratory Records Department

EXTERNAL DISTRIBUTION

56. Air Force Engineering Office, Oak Ridge
57. Air Force Plant Representative, Burbank
58. Air Force Plant Representative, Seattle
59. Air Force Plant Representative, Wood-Ridge
60. ANP Project Office, Fort Worth
61-63. Argonne National Laboratory (Kermit Anderson, J. W. Butler, and J. R. Dietrich)
64. Armed Forces Special Weapons Project (Sandia)
65. Armed Forces Special Weapons Project, Washington (E. C. LaVier)
66-75. Atomic Energy Commission, Washington (1 copy to Col. M. J. Nielsen, Col. T. A. Redfield, C. R. Horner, and A. F. Thompson)
76. Battelle Memorial Institute
77-78. Boeing Airplane Company (C. J. Leisy)
79. Brookhaven National Laboratory (M. Fox)
80. Bureau of Aeronautics (R. Zirkind)
81. Bureau of Ships (T. Rockwell)
82. Carbide and Carbon Chemicals Company (K-12 Plant)
83. Chief of Naval Research
84. Commonwealth Edison Company
85-86. Convair, Fort Worth (R. N. Little)
87. Convair, San Diego (C. H. Helms)

[redacted]

[redacted]

88-89. Curtiss-Wright Corporation, Wright Aeronautical Division (K. Campbell and H. Reese)
90. Department of the Navy - OP-362
91. Detroit Edison Company
92. duPont Company, Augusta
93. duPont Company, Wilmington
94. Foster Wheeler Corporation
95. General Dynamics Corp., Electric Boat Division
96-97. General Electric Company, ANPD (G. Thornton)
98. General Electric Company, Richland
99. Glenn L. Martin Company (T. F. Nagey)
100-101. Knolls Atomic Power Laboratory (H. E. Stone and L. H. Weinberg)
102. Lockheed Aircraft Company (F. A. Cleveland)
103. Lockland Area Office
104. Los Alamos Scientific Laboratory
105. Materials Laboratory (WADC) (Col. P. L. Hill)
106. Monsanto Chemical Company
107. National Advisory Committee for Aeronautics, Cleveland (A. Silverstein)
108. National Advisory Committee for Aeronautics, Washington
109. Naval Research Laboratory (J. R. Faust)
110. North American Aviation, Inc.
111-114. Nuclear Development Associates, Inc. (H. Goldstein)
115-119. Nuclear Powered Aircraft Branch, Weapon Systems Division (WADC) (Col. C. D. Gasser)
120. Oak Ridge Operations (H. M. Roth)
121. Patent Branch, Washington
122. Phillips Petroleum Company
123-126. Powerplant Laboratory (WADC) (A. Nelson and F. M. Westfall)
127-128. Pratt and Whitney Aircraft Division (Fox Project) (C. F. deGanahl)
129. Rand Corporation
130. San Francisco Operations Office
131. USAF Headquarters
132. U. S. Naval Radiological Defense Laboratory
133. University of California Radiation Laboratory, Berkeley
134. University of California Radiation Laboratory, Livermore
135. Walter Kidde Nuclear Laboratories, Inc.
136-137. Westinghouse Electric Corporation (J. J. Taylor)
138-155. Technical Information Service, Oak Ridge

[redacted]

[redacted]

TABLE OF CONTENTS

		Page
I.	ABSTRACT	1
II.	INTRODUCTION AND GENERAL OBJECTIVES	5
	Preliminary Studies of Shield Configurations for Circulating-Fuel Reactors	6
III.	INTERPRETATION OF LID TANK TESTS	15
	RMR Configurations	15
	Neutron Measurements	16
	Gamma-Ray Measurements	17
	Effect of variations in gamma shield	17
	Attempts to minimize effect of iron in reflector and to increase reflector thickness	22
	Effect of substituting oil in liquid neutron shield	23
	Effect of variations in pressure shell and moderator region	23
	Effect of substituting tungsten carbide in gamma shield	24
	Mockup modifications to improve RMR-shield simulation	25
	Effect of boron in shield	30
	Elimination of plain water gap between dry tank and borated water tank	31
	Effect of beryllium density	31
	Effect of plexibor inserted at various points in the shield	32
	Effect of heat exchanger thickness	33
	Effect of increasing beryllium reflector thickness	34
	Effect of substituting uranium in gamma shield	34
	Effect of varying boron concentration in water	35
	Effect of substituting lithium in heat exchanger region	36
	Lead Optimization Experiments	37
	Activation of the Secondary Coolant	43
	Sodium Activation Measurements in the Lid Tank	44
	Relative Activation Measurements of Sodium, Potassium, and Rubidium at the BSF	46
	Conclusions	61

[redacted]

[redacted]

	Page
IV. APPLICATION OF DATA TO DESIGNED-RMR SHIELD	63
Fast-Neutron Data Corrected to Designed RMR-Shield	63
Gamma-Ray Data Corrected to Designed RMR-Shield	69
Shields with 6 and 7.5 in. of lead	69
Shields with 4.5 in. of lead	72
Results	77
Equation for Calculation of Shield Weights	77
Sample Calculation of a Specific Shield Weight	79
V. PROBLEMS FOR FUTURE INVESTIGATION	82
Air and Structure Scattering	82
Heat Exchanger Region	82
Optimizations	83
Ducts and Voids	85
VI. LID TANK CONFIGURATIONS AND MEASUREMENTS	87
Lid Tank Facility	87
Techniques Pertinent to the RMR Tests	87
Description of Tanks Used in Mockups	89
Instrumentation	90
RMR Mockups (Configurations 1 through 77)	93
Radiation Measurements behind RMR Mockups	93

[redacted]

[redacted]

LIST OF FIGURES

Figure Number	Title	Page
II-1	Longitudinal Section through a Tandem Reactor--Heat Exchanger Assembly	7
II-2	Tandem Heat Exchanger Arrangement for a Circulating-Fuel Reactor	9
II-3	Annular Heat Exchanger Arrangement for a Circulating-Fuel Reactor	11
II-4	Spherical Heat Exchanger Arrangement for a Circulating-Fuel Reactor	12
III-1	Summary of Sodium Activation Data from Lid Tank Tests	45
III-2	Rubidium Decay Schemes	48
III-3	Observed Activity as a Function of Decay Time for Sodium Fluoride and Potassium Fluorids Samples	49
III-4	Corrected Activity as a Function of Decay Time for Sodium and Potassium Samples	50
III-5	Observed Activity as a Function of Decay Time for Rubidium Fluoride Samples	51
III-6	Corrected Activity as a Function of Decay Time for Rubidium Samples; 19.5-Day Activity Subtracted	52
III-7	Activity of Long-Lived Rb^{86} as a Function of Decay Time for Three Irradiation Times	54
III-8	Activity of Long-Lived Rb^{86} as a Function of Irradiation Time	55
III-9	Rubidium-to-Sodium Dose Ratio as a Function of Decay Time for Various Irradiation Times -- No Lead Shielding	56
III-10	Rubidium-to-Sodium Dose Ratio as a Function of Irradiation Time for Various Lead Thicknesses	57
III-11	Rubidium-to-Sodium Dose Ratio as a Function of Lead Thickness for Various Decay Times	58
III-12	Potassium-to-Sodium Dose Ratio as Functions of Decay Time, Irradiation Time, and Lead Thickness	59

[redacted]

[redacted]

Figure Number	Title	Page
IV-1	Fast-Neutron Attenuation Data Used to Obtain Representative Fast-Neutron Dose Curve for Designed RMR-Shield Assembly	64
IV-2	Lid Tank Fast-Neutron Dose Curves Corrected to Designed RMR-Shield Assembly	68
IV-3	Lid Tank Gamma-Ray Dose Curves Corrected to Designed RMR-Shield Assembly for 4.5, 6.0, and 7.5 in. of Lead	70
IV-4	Lid Tank Gamma-Ray Dose Curves Corrected to Designed RMR-Shield Assembly with Various Thicknesses of Lead	71
VI-1 through VI-28	Lid Tank Mockups of Reflector-Moderated Reactor and Shield	
VI-1	Configurations 1, 1a, 22	102
VI-2	Configurations 3, 4, 5	104
VI-3	Configurations 6, 7	106
VI-4	Configurations 8, 9	108
VI-5	Configurations 10, 11	110
VI-6	Configurations 12, 13, 14	112
VI-7	Configurations 15, 16, 17	114
VI-8	Configurations 18, 19	116
VI-9	Configurations 20a, b, c, d, e	118
VI-10	Configurations 21, 22, 23	120
VI-11	Configurations 24, 25, 26	122
VI-12	Configurations 27, 28, 29	124
VI-13	Configurations 30, 31, 32	126
VI-14	Configurations 33, 34, 35	128
VI-15	Configurations 36, 37, 38	130
VI-16	Configurations 39, 40, 41	132
VI-17	Configurations 42, 43, 44	134
VI-18	Configurations 45, 46, 47	136
VI-19	Configurations 48, 49, 50	138
VI-20	Configurations 51, 52, 53	140
VI-21	Configurations 54, 55, 56	142
VI-22	Configurations 57, 58, 59	144
VI-23	Configurations 60, 61, 62	146
VI-24	Configurations 63, 64, 65	148
VI-25	Configurations 66, 67, 68	150
VI-26	Configurations 69, 70, 71	152
VI-27	Configurations 72, 73, 74, 75	154
VI-28	Configurations 76, 77	156

[redacted]

[redacted]

Figure Number	Title	Page
VI-29 through VI-47	Gamma-Ray Dose Measurements behind Lid Tank Mockups of Reflector-Moderated Reactor and Shield	
VI-29	Configurations 1, 1a, 2, 3, 4, 5	158
VI-30	Configurations 6, 7, 9, 10, 8	159
VI-31	Configurations 11, 12, 13, 14	160
VI-32	Configurations 15, 16, 17, 18	161
VI-33	Configurations 19, 20a, b, c, d, e	162
VI-34	Configuration 21	163
VI-35	Configurations 22, 27, 28	164
VI-36	Configurations 22, 23, 24, 25, 26, 29, 30	165
VI-37	Configurations 31, 32	166
VI-38	Configurations 32, 35, 36, 37, 38, 33, 34	167
VI-39	Configurations 39, 40, 41, 42, 44, 43	168
VI-40	Configurations 45, 46, 47, 48, 49, 50	169
VI-41	Configurations 48, 51, 52, 53, 54	170
VI-42	Configurations 55R, 56, 57, 58, 59, 60, 61	171
VI-43	Configurations 62, 63, 64, 65	172
VI-44	Configurations 66, 67, 68, 69	173
VI-45	Configurations 70, 71, 72	174
VI-46	Configurations 55R, 73, 74, 75	175
VI-47	Configurations 64R, 76, 77	176
VI-48 through VI-61	Thermal-Neutron Flux Measurements behind Lid Tank Mockups of Reflector-Moderated Reactor and Shield	
VI-48	Configurations 1, 1a, 2, 3, 4, 5	177
VI-49	Configurations 6, 7, 9, 10	178
VI-50	Configurations 11, 12, 13, 14	179
VI-51	Configurations 15, 16	180
VI-52	Configurations 18, 19	181
VI-53	Configurations 22, 23, 24, 25, 26, 30	182
VI-54	Configurations 22, 27, 28	183
VI-55	Configurations 29, 31, 32	184
VI-56	Configurations 35, 36, 37, 38	185
VI-57	Configurations 39, 46, 47	186
VI-58	Configurations 51, 53, 54	187
VI-59	Configurations 55, 56	188
VI-60	Configurations 63, 70, 72	189
VI-61	Configurations 74, 75	190

[redacted]

[redacted]

Figure Number	Title	Page
VI-62 through VI-66	Fast-Neutron Dose Measurements behind Lid Tank Mockups of Reflector-Moderated Reactor and Shield	
VI-62	Configurations 1, 2, 3, 4	191
VI-63	Configuration 15	192
VI-64	Configuration 31	193
VI-65	Configuration 39	194
VI-66	Configuration 75	195

[redacted]

[redacted]

ACKNOWLEDGMENTS

The authors wish to acknowledge the helpful guidance and assistance received during this series of tests from E. P. Blizard, J. L. Meem, C. B. Mills, C. L. Storrs and J. B. Trice. Special thanks are also due for the effort and cooperation of those of the Lid Tank staff, J. D. Flynn, G. T. Chapman, J. M. Miller, J. L. Hull, W. J. Maynard, and J. N. Money. Finally, the authors wish to express their indebtedness to L. S. Abbott for her help in the collection of the reported material and in its preparation for publication.

[redacted]

I. ABSTRACT

Approximately 80 configurations simulating the preliminary basic shield design for the reflector-moderated reactor have been tested in the Lid Tank Shielding Facility. From these experiments it has been concluded that:

1. The beryllium reflector region should be about 12 in. thick to minimize the over-all reactor shield weight and still remain consistent with core reactivity requirements.
2. The thickness of the heat exchanger region has relatively little effect on neutron and gamma dose curves as a function of distance from the source plate.
3. The substitution of lead for water over the range covered (0 to 7.5 in.) in the region just outside of the heat exchanger has practically no effect on the neutron attenuation curve well out in the shield. The effect of lead in this region on the gamma dose is greatest for the first 4 in. and is appreciably smaller for thicknesses greater than about 7 in.
4. A 0.13 in. thick layer of B^{10} (density = 2.1) is as effective in depressing the thermal-neutron flux and consequent capture gammas as 1 in. of B_4C (density = 1.95).
5. Dividing the lead region into layers separated by borated hydrogenous material gives some reduction in the gamma dose for a given thickness of lead; however, the full-scale shield design is simplified structurally by placing all of the lead together just outside the pressure shell. While lumping the lead in this fashion increases the lead thickness required, keeping its radius to a minimum largely compensates for this so that very nearly minimum

over-all shield weights can be obtained in this manner for lead thicknesses up to 6.0 in.

6. Transformer oil is as effective as water on a volumetric basis for attenuating the neutron flux. Since its density is about 0.87, an appreciable saving in shield weight can be obtained through its use provided it can be borated to a few percent by weight by the addition of some compound such as borazole ($B_3N_3H_6$, B.P. = 53°C) or trimethylborate [$B(OCH_3)_3$, B.P. = 69°C]. Some of this weight saving is offset by the fact that the thickness of the lead layer must be increased because the attenuation of the gamma flux is not as great in the oil.

7. Beryllium is more effective than water on a thickness basis for neutron attenuation. (This can be seen from Fig. IV-2 by comparing the pure water curve and the curve representing the data with part of the water replaced by beryllium.)

8. It is important that a boron curtain be used between the heat exchanger and the pressure shell as well as between the reflector and the heat exchanger.

9. It does not appear worth while to use rubidium in place of sodium or NaK as a secondary coolant. Potassium is preferable to sodium with regard to activation, but it is inferior as a heat transfer medium.

As a consequence of these measurements, an effective preliminary shield was designed. Dose rate curves were obtained for the designed shield by correcting observed data from configurations which closely approximated it. These in turn can be used for shield weight calculations.

Air and structure scattering, the heat exchanger region, ducts and voids, and optimization of the shield size and weight pose problem areas that require further investigation.

II. INTRODUCTION AND GENERAL OBJECTIVES

A. P. Fraas

The circulating-fuel reactor presents some particularly difficult and complex shielding problems. The first design study that was attempted considered circulation of the fuel directly to the engine radiator.[1] It was immediately evident that the radiator installation was so large that shielding the fission product decay gammas emitted from the fuel circulated through it was out of the question. While the crew compartment could be protected with an unusually massive shield, the over-all shield weight was high even with an exceptionally large reactor-crew separation distance. Further, the radiation level in the vicinity of the airplane would no doubt make ground handling and maintenance work difficult. In addition, the radiation damage to all organic material in the airplane including lubricants, tires, gaskets, etc., would be so high as to require replacement of these materials after from 1 to 10 hr of full-power operation. A series of design studies was then directed toward the possibility of employing an intermediate heat transfer fluid to take heat from the fuel through a heat exchanger inside the reactor shield. With this arrangement activation of the intermediate fluid by neutrons leaking from the core and by delayed neutrons emitted from the fuel in the heat exchanger itself constituted a major problem. It was also found that for most layouts the volume of the intermediate heat exchanger resulted in a very large increase in the over-all shield weight.

---

1 R. W. Schroeder and B. Lubarsky, "A Design Study of a Nuclear-Powered Airplane in Which Circulating Fuel Is Piped Directly to the Engine Air Radiators," ORNL-1287 (March 31, 1953).

This report briefly summarizes the preliminary design work both to show the basis for the selection of the design proposed and to point out the questions that developed as the designs took form. The shielding tests run in the Lid Tank to resolve these questions are covered in detail. Altogether some eighty-three different configurations involving different thicknesses and compositions of the reflector, heat exchanger, pressure shell, gamma shielding and outer hydrogenous shielding regions were tested and the results analyzed. A series of tests on the activation of secondary fluids in the intermediate heat exchanger was carried out in conjunction with this work and is also reported. The final section of the report shows the application of the test data to typical designs and compares the results to the corresponding preliminary design studies.

While it is appreciated that the main body of the report -- the section covering the details of the configurations tested and the test results -- will prove confusing at first glance, it does not appear possible to present the results of so complex and extensive a set of work in such a fashion that it can be assimilated easily after a cursory examination.

Preliminary Studies of Shield Configurations for Circulating-Fuel Reactors

It is instructive to review the evolution of the shield configurations on which this report is centered. The work began in November 1951 with the analysis of a tandem reactor--intermediate heat exchanger design in which the reactor and intermediate heat exchanger were placed end-to-end as shown in Figs. II-1 and II-2. This design analysis disclosed that the salient problems in the design of any circulating fuel reactor--heat exchanger--shield system are: (1) activation of the fluid in the secondary coolant system, (2) secondary gamma production from neutron captures in the pressure shell and lead regions and in the neutron shield region, and (3) gamma heating of the pressure shell.

[redacted]
DWG Y-F7-171A

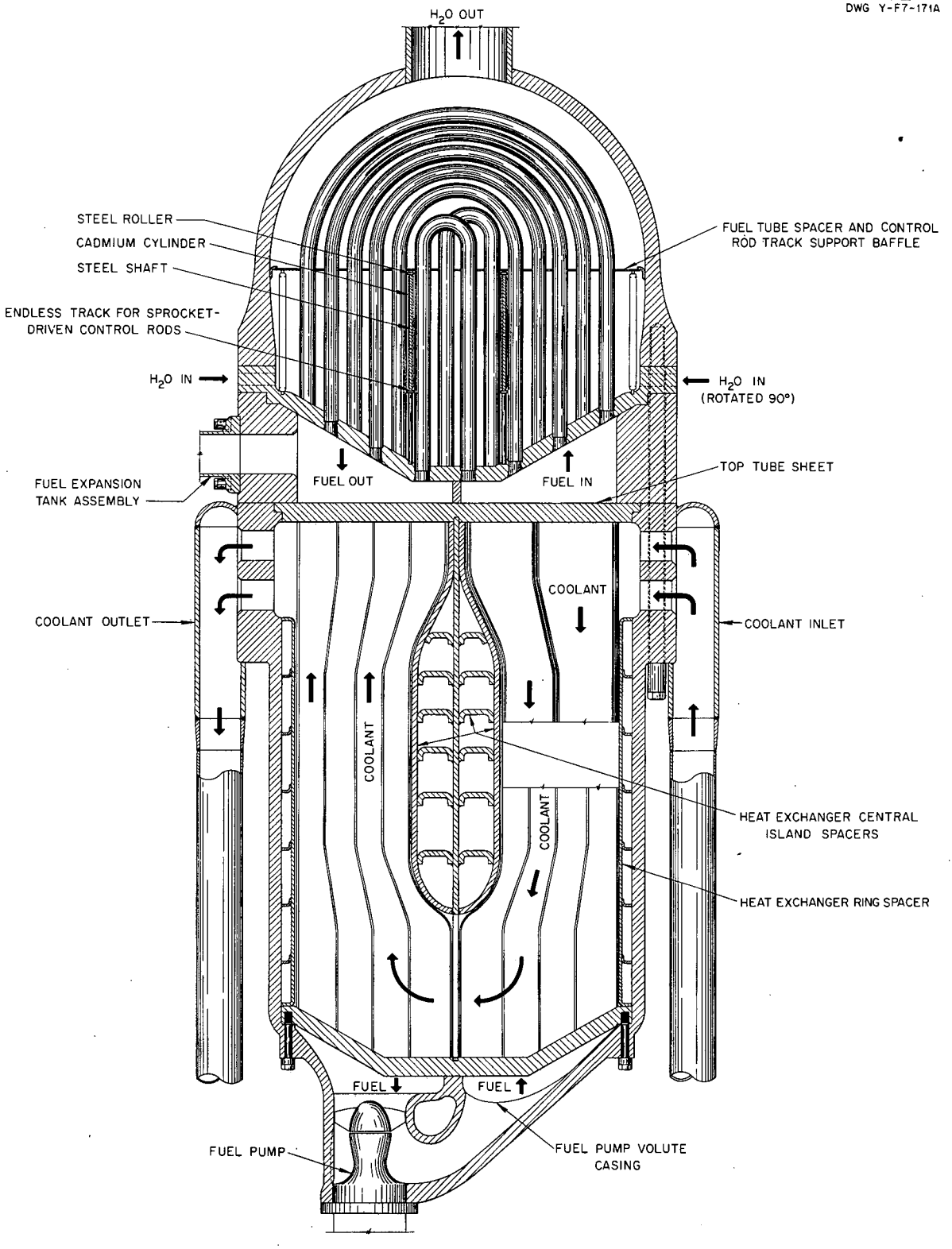

Fig. II-1. Longitudinal Section Through a Tandem Reactor-Heat Exchanger Assembly.

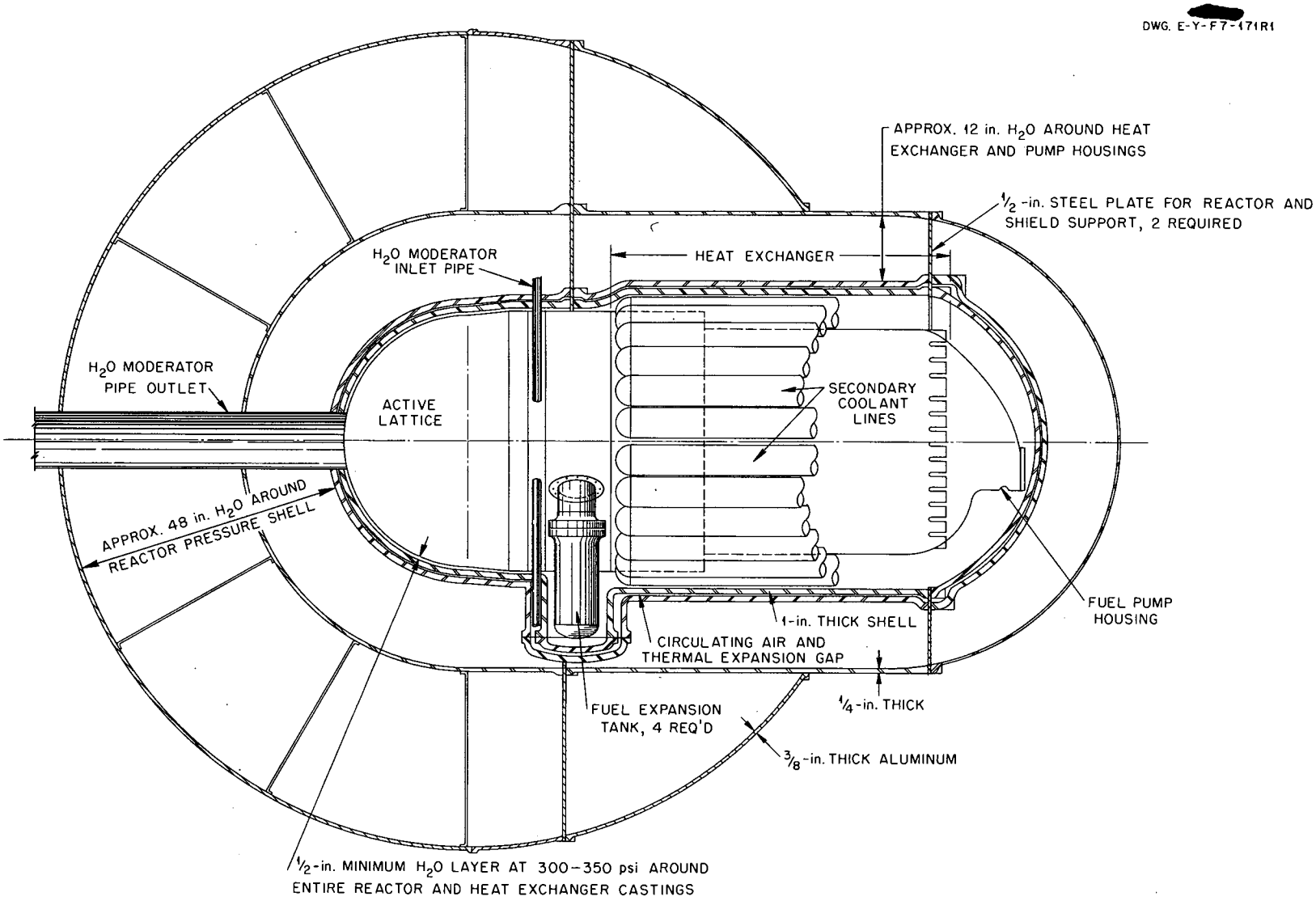

Fig. II-2. Tandem Heat Exchanger Arrangement for a Circulating-Fuel Reactor.

When the most careful design work failed to reduce the over-all weight of the tandem reactor--heat exchanger arrangement to an acceptable value, a completely different geometry was considered. It was found that by using the annular heat exchanger arrangement of Fig. II-3 a major savings in shield weight could be effected. The work carried out on this design indicated that still more weight might be saved by going to the spherical shell heat exchanger arrangement shown in Fig. II-4. The estimated shield weights and other pertinent data for each of these configurations are presented in Table II-1.[2,3]

If Figs. II-1, II-3, and II-4 are re-examined it will be evident that three different types of reactor cores were employed. While these were considered to be essentially interchangeable, they indicate some important steps in the evolution of a reactor design. In the first design the fluoride flowed through closely spaced tubes while water flowed between the tubes, presenting some formidable problems in preventing freezing of the fluoride at low-power outputs. More important from the shielding standpoint was the fact that with the thin reflector of Fig. II-1 the pressure shell appeared to be a much more serious source of gammas than the reactor core. Another important concept developed in the course of the design was that approximately 30 cm of moderating material followed by a boron curtain should be placed between the reactor core and the heat exchanger to reduce the neutron flux from the core to the heat exchanger to the level of that from the delayed neutrons emitted from the fuel in the heat exchanger.

The reactor core design employed in Fig. II-3 capitalized on the above concepts. Yet another feature was also interjected, i.e., the core matrix

2 A. P. Fraas, "ANP Quarterly Progress Report, March 10, 1952," ORNL-1227, p. 7.
3 A. P. Fraas, "ANP Quarterly Progress Report, June 10, 1952," ORNL-1294, p. 7.

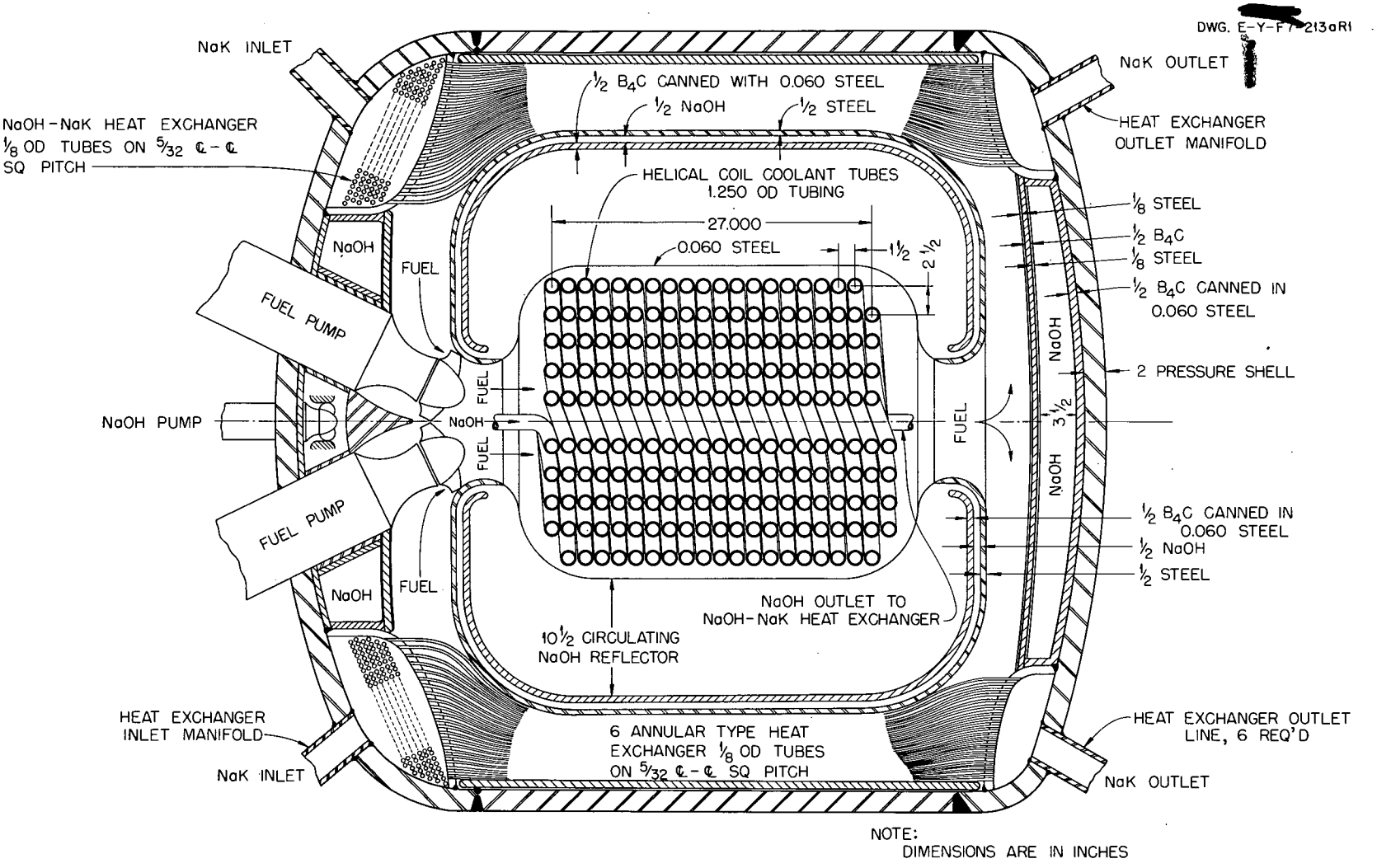

Fig. II-3. Annular Heat Exchanger Arrangement for a Circulating-Fuel Reactor.

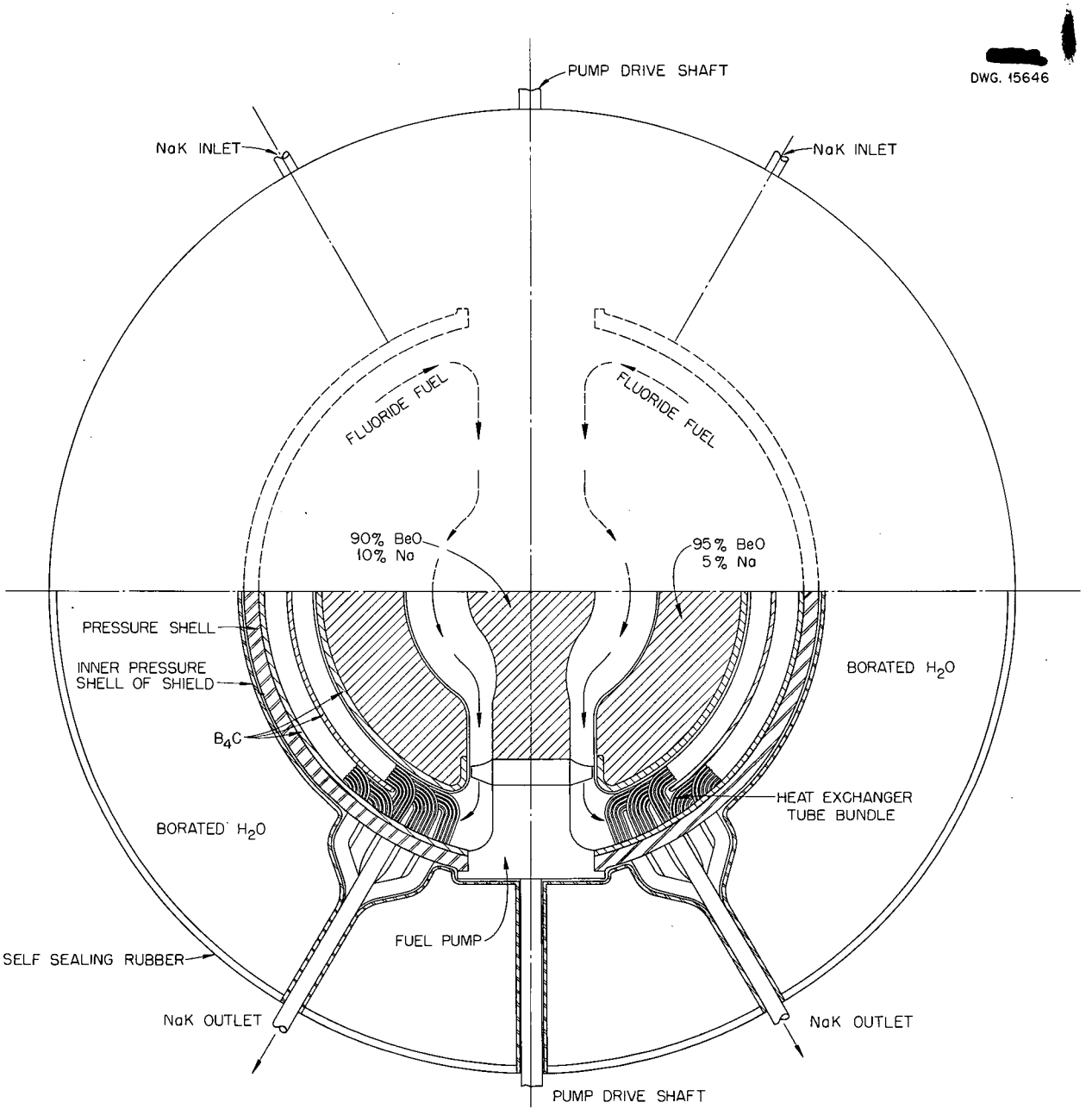

Fig. II-4. Spherical Heat Exchanger Arrangement for a Circulating-Fuel Reactor.

TABLE II-1

PARTIALLY DIVIDED SHIELDS FOR CIRCULATING-FUEL REACTORS WITH VARIOUS INTERMEDIATE HEAT EXCHANGERS

	Tandem Heat Exchanger				Annular Heat Exchanger			Spherical Heat Exchanger		
	1	2	3	4	1	2	3	1	2	3
Reactor shield diameter (in.)	150	150	121	121	148	118	118	148	118	118
Crew shield weight (lb)	5,000	11,000	36,000	14,000	5,000	36,000	14,000	5,000	36,000	14,000
Weight of reactor, intermediate heat exchanger, and reactor shield (lb)	151,000	130,000	75,000	75,000	123,000	62,000	62,000	115,000	54,000	54,000
Total weight of reactor, intermediate heat exchanger, and all shielding (including crew shield) (lb)	156,000	141,000	111,000	89,000	128,000	98,000	76,000	120,000	90,000	68,000
Reactor power (kw)	4000,000	400,000	400,000	400,000	400,000	400,000	400,000	400,000	400,000	400,000
Diameter of reactor core (in.)	32	32	32	32	32	32	32	32	32	32
Liquids in primary and secondary circuits	Fluoride-NaK	Fluoride-NaK	Fluoride-NaK	Fluoride-NaK	Fluoride-NaK	Fluoride-NaK	Fluoride-NaK	Fluoride-NaK	Fluoride-NaK	Fluoride-NaK
Temperature loss in intermediate heat exchanger (°F)	100	100	100	100	100	100	100	100	100	100
Pressure loss in intermediate heat exchanger (psi)	100	100	100	100	100	100	100	100	100	100
Crew shield size (ft)	$6\frac{1}{2} \times 7\frac{1}{2} \times 12\frac{1}{2}$	$6\frac{1}{2} \times 7\frac{1}{2} \times 12\frac{1}{2}$	$6\frac{1}{2} \times 7\frac{1}{2} \times 12\frac{1}{2}$	$5 \times 5 \times 12\frac{1}{2}$	$6\frac{1}{2} \times 7\frac{1}{2} \times 12\frac{1}{2}$	$6\frac{1}{2} \times 7\frac{1}{2} \times 12\frac{1}{2}$	$5 \times 5 \times 12\frac{1}{2}$	$6\frac{1}{2} \times 7\frac{1}{2} \times 12\frac{1}{2}$	$6\frac{1}{2} \times 7\frac{1}{2} \times 12\frac{1}{2}$	$5 \times 5 \times 12\frac{1}{2}$
Reactor-crew separation distance (ft)	50	50	50	120	50	50	120	50	50	50
Radiation inside crew compartment (r/hr)	1	1	1	1	1	1	1	1	1	1
Radiation 5 ft from center of reactor (r/hr)	300	2,400	380,000	380,000	300	380,000	380,000	300	380,000	380,000
Radiation 50 ft from center of reactor (r/hr)	7	36	5,600	5,600	7	5,600	5,600	7	5,500	5,600
Radiation 300 ft from center of reactor (r/hr)	1	6	156	156	1	156	156	1	156	156

geometry was changed to reduce the proportion of moderator. In principle, this should permit a smaller reactor core because the power density in the liquid fuel itself appears to control the reactor core diameter. A careful examination of this second design disclosed that the thick reflector could make a major contribution to the neutron economy if the poison concentration in it could be kept down.[4] At the same time it was evident that a more nearly spherical configuration would reduce the over-all weight substantially. As a result the simple reactor design of Fig. II-4 was evolved in March 1952. A detailed exposition of these three designs and the analysis on which they were based has been reported.[5]

The layout of Fig. II-4 appeared so promising that a series of multigroup calculations was carried out for a wide range of reactor core sizes and materials of construction. It soon developed that the exceptionally high atomic density of beryllium coupled with its comparatively high scattering cross section for neutron energies above 3 Mev make it a very nearly optimum material from the standpoint of both shielding and reactor physics considerations.[6]

As the result of the above described process of evolution a more or less definite arrangement of core, reflector, heat exchanger, pressure shell, and shield was decided upon which seemed feasible for the production of useful power and at the same time appeared to be very nearly optimum in shield weight economy. In order to obtain a more definite evaluation of shield weights and shield arrangements necessary to yield tolerable doses in the vicinity of the reactor, the Lid Tank tests as described in the following sections were performed.

4 C. B. Mills, "The Fireball, A Reflector-Moderated Circulating-Fuel Reactor," Y-F10-104 (June 20, 1952).
5 A. P. Fraas, "Three Reactor--Heat Exchanger--Shield Arrangements for Use with Fused Fluoride Circulating Fuel," Y-F15-10 (June 30, 1952).
6 C. B. Mills, "ANP Quarterly Progress Report, March 10, 1953," ORNL-1515, p. 49.

III. INTERPRETATION OF LID TANK TESTS

RMR Configurations

F. H. Abernathy and R. Spencer

Inasmuch as the RMR is unique in that no clear cut boundary exists between the reactor and shield, in the Lid Tank experiments it was necessary to simulate the reactor shield assembly from the core shell outward. Thus, the mockups consisted of materials that simulated the reflector, heat exchanger, pressure shell, heavy gamma shield, and final neutron shield in that order. In addition, thin layers of neutron-absorbing materials were inserted between the various components to ascertain the effectiveness of such curtains.

The composition and thickness of the reflector and the heat exchanger regions will of course be partially dictated by other than shielding considerations. For this reason these regions were mocked up with materials which approximated as closely as possible the contemplated finished product. The composition and thickness of the other regions could be varied to give a shield of minimum weight consistent with desired dose levels and sound engineering practice.

It must be pointed out that some of the mockups in the Lid Tank tests were less than satisfactory approximations of what was desired. In some instances materials needed either were not available or differed from the form in which they would ultimately be used. Because it was desirable to investigate the shielding properties of a large number of materials and configurations for the RMR and because there was of course a time limitation involved, the experiments on some of the materials were by no means complete. In this respect this series of tests should be considered preliminary. It is felt, however, that these tests do provide a reasonably sound basis for early RMR shield designs and also afford a basis for deciding on future experiments which should serve to refine and expand the conclusions reached here.

It should also be explained that at the time the Lid Tank tests were started there was not enough beryllium available in slab form to simulate the required reflector region. To compensate for this a tank 11.5 in. thick filled with beryllium pellets was used with a solid beryllium slab 3.6 in. thick. The density of the beryllium in the tank was only 1.23 g/cc as compared to 1.84 g/cc in the solid slab, making a density correction necessary in order to arrive at an equivalent reflector thickness. Later in the experiment beryllium blocks were obtained from the Critical Assembly Facility and it was then possible to simulate a solid beryllium reflector.

Neutron Measurements

An examination of the neutron data obtained behind the various configurations reveals that the fast-neutron dose (as measured directly or as correlated with the thermal-neutron flux well out in the water region) is rather insensitive to changes made in the heat exchanger, pressure shell, and heavy gamma shield regions. This is due to the fact that on a thickness basis the materials that were placed in these regions have about the same effectiveness as water in attenuating fast neutrons (e.g., as in the case of lead and the materials used in the heat exchanger region) or that the thicknesses used were so thin compared to the total neutron shield as to have only a small effect. An exception to this was the substitution of uranium for lead in the gamma shield region. A comparison of the thermal-neutron data behind configurations 63 and 72, which are similar except for the fact that No. 63 contained 6 in. of lead in the gamma shield region while No. 72 contained 3 in. of uranium, indicates that if uranium were to be used for the heavy gamma shield region a saving in the neutron shield weight could be effected. The data available is insufficient to determine an exact saving, as is discussed more fully under "Gamma-Ray Measurements" below.

Because of this insensitivity of the fast-neutron dose to the changes in the various sections of the shield, the bulk of the discussion on the Lid Tank results is centered on the gamma data.

Gamma-Ray Measurements

The first mockups tested for the RMR in the Lid Tank included (1) a reflector region consisting of 11.5 in. of beryllium pellets plus 3.6 in. solid beryllium (2) a 2.75-in. heat exchanger region made up of NaF-filled iron tanks, (3) neutron curtains consisting of 1 in. thick B_4C-filled tanks placed before and after the heat exchanger region, (4) a pressure shell composed of 1.75 in. of iron, (5) a gamma shield region of lead, and (6) the water in the Lid Tank. The lead thickness was varied to determine the effect on the gamma dose at the shield surface.

Effect of Variations in Gamma Shield. In an effort to exclude water from the reflector region in configuration 1* an aluminum wafer filled with pressurized air was inserted between the tank of beryllium pellets and the solid beryllium slab. The wafer was removed in configuration 1A and the gamma dose fell slightly below the data with the wafer; this difference can possibly be attributed to the neutron attenuation in the water that filled the space between the two beryllium regions, thus giving a slightly reduced level of secondary gammas. Since the thickness of the wafer was difficult to control because of variations in the air supply pressure and since it did not appear to make much difference in the measurements, it was removed. In subsequent configurations an effort was made to keep the water gap as small as possible.

Traverse measurements were made in the water behind configurations 1, 2, 3, and 4 for lead gamma shield thicknesses of 0.0, 2.5, 4.5, and 7.5 in., respectively. Because of sensitivity limitations, lead thicknesses beyond

* See section VI for sketches of configurations and corresponding data.

7.5 in. were not used. The difference in the slope of the gamma curve of configuration 2 as compared to those of configurations 3 and 4 is attributed to the air void in the latter configurations which places the source of the soft capture gammas from water closer to the detector. In configurations 3 and 4 the primary photons from the source plate and the secondary photons from the region inside the pressure shell have been greatly attenuated by the additional lead, while the capture gammas from the water remained undiminished or perhaps even increased.

An examination of configurations 4 and 5 and their associated gamma data indicates that the addition of approximately 20 cm of water to the second dry tank in configuration 5 decreased the gamma dose by a factor of 6. Since the relaxation length of gammas in water is known to be at least 20 to 25 cm, the addition of the water could account for no more than a factor of 3 in direct attenuation. While it would appear that the additional water could affect the gamma dose by direct attenuation only, further examination indicates that the water is responsible for two other phenomena that substantially decreased the doses of configuration 5. First and perhaps foremost is the decrease in the number of capture gammas from the wall of the dry tank nearest the receiver. Previously the only attenuation of the neutron flux from the outer surface of the lead to the tank wall was a very small geometric decrease; the addition of the water decreased the neutron flux at the tank wall and resulted in a decrease of capture gammas from the tank wall by at least a factor of 10. The importance of these capture gammas from the iron wall is clearly illustrated by the results of the tests behind configurations 39, 40, 41, and 42.

The other phenomenon that decreased the gamma dose when the water was added in configuration 5 was the replacement of the air gaps with water between the lead slabs. Unfortunately, when this particular test was run, there was a shortage of 1.5-in. lead slabs and 1-in. slabs were used. The framework supporting the slabs separated them by at least 0.5 in.; with the addition of water to the tank the water gaps between the slabs were possibly larger than 0.5 in. since the slabs were warped. It was felt that this probably resulted in the thermalization and capture in the water of many of the epithermal neutrons that would have otherwise been thermalized and captured in the lead. The energy of the photon resulting from thermal-neutron capture by hydrogen is about 2.2 Mev, which is far lower than the approximately 7-Mev gamma from neutron capture in lead, and hence is more easily attenuated by the material between the point of capture and the receiver. The water between the lead slabs further helped to reduce the gamma dose because of the fact that water, with a very much lower atomic weight than lead, more readily thermalizes neutrons, thereby increasing the probability of the neutron capture in either the lead region or the water itself. This process places more gamma shielding material between the secondary source of photons and the position of measurement than would be present if there were no water in the lead region.

Because of the lack of precision in measuring the water thickness between slabs and the engineering incentive to construct the heavy shielding material in one piece, the water in the region at this point of the experiment was an undesired evil. The best that could be done at the time was to use lead slabs as thick as the frames in which they were supported. Every effort possible was made to keep the slabs of lead close together, thereby reducing the water thickness and its associated uncertainty as much as possible.

In configurations 6, 7, and 8 the lead slabs were spread out in the water region. As has been pointed out previously, moving the lead away from the pressure shell increased its shielding effectiveness. However, an aircraft shield requires a minimum shield weight, and it is obvious that moving the lead layers of a spherical shield outward would increase their weight. The data from these tests and the lead optimization experiment indicate, although not conclusively, that for lead thicknesses up to 6 in. for RMR shields under consideration the increased shielding effectiveness of separating the lead layers was not great enough to compensate for the increased weight due to the increase in lead radius.

Configurations 9 through 14 were tested to determine the effect of borating the water in the neutron shield on the gamma dose. Boron competes with hydrogen for neutron capture, and neutron capture in B^{10} in the majority of cases results in the emission of an easily absorbed alpha particle and a 0.43-Mev gamma ray from the compound nucleus, rather than the 2.2-Mev capture gamma from water. The macroscopic thermal-neutron absorption cross section of natural boron in a 1% borated water solution is roughly 20 times the cross section for capture in the hydrogen atoms of the same solution. If all of the gamma dose measured well out in the shield came from hydrogen capture gammas, the addition of 1% by weight of boron to the water would decrease the measured gamma dose by a factor of 20. The data taken with configurations 5 and 10 show that the addition of 1% boron to the water decreased the gamma dose by a factor of 4.5, indicating that iron and lead secondary gammas and source gammas were also important.

The reasons for testing configurations 9 through 14 are self-evident except for configuration 11. The data obtained behind this mockup should be used with caution. Configuration 11 was the first test in which an attempt

was made to increase the boron concentration in the water above 1%. In order to increase the solubility of B_2O_3 in the solution, KOH was added. Because this reaction is exothermic in nature the initial temperature of the mixture was considerably above room temperature, though it rapidly decreased to that of the rest of the Lid Tank. This decrease in temperature was accompanied by the precipitation of what appeared to be B_2O_3 crystals on the tank walls, lead slabs, etc. Thus the attempt was a failure, for a chemical analysis of the water solution actually showed a decrease in the boron concentration. In order to prevent this precipitation in later tests in which boron was used in concentrations higher than 1%, all the water in the Lid Tank was held at an elevated temperature ($\sim 110^{\circ}F$).

After the first 14 configurations were run the entire set of tanks and slabs simulating the reactor and shield were removed from the Lid Tank, and traverses with all instruments were made in pure water to check their calibration. In the interim enough 1.5-in. lead slabs were obtained so that they could be used exclusively throughout the rest of the experiment, thus reducing the number of unnecessary air and water gaps in the gamma shield section.

Four of the most useful mockups for designing present RMR shields were configurations 15, 16, 17, and 18 which represent the logical buildup of a typical gamma shield from which the thickness of lead required at the reactor shield can be determined. In these tests four NaF-filled tanks simulated a heat exchanger thickness of 7 in. (The average density of this region was approximately 2.5 g/cc. This is lower than the 3.15-g/cc density contemplated in the present RMR designs, but a correction can be made by applying a simple density ratio.) These tests were not run at this time with the borated water extending to the shield surface since it was feared that the aluminum in the instrument

carriage and in the instrument itself, would be strongly attacked by the caustic borated water solution. Thus, it was necessary to take measurements in plain water behind the borated water tank.

The data for configurations 17 and 18 indicate a decrease in the effectiveness per unit thickness of lead as the total thickness of the lead region is increased. The last 3 in. of lead in configuration 17 have a water replacement relaxation length of 2.9 cm, while the additional 1.5 in. of lead added in the next configuration has a water replacement relaxation length of 4.1 cm. This clearly shows the increased importance of secondary gamma production as the lead region becomes thicker.

Attempts to Minimize Effect of Iron in Reflector and to Increase Reflector Thickness. In the first 18 RMR configurations there was more iron (in tank walls) in the simulated beryllium reflector region than is contemplated in the actual reactor. This iron constituted an excessive source of secondary gammas in the mockups, and in an effort to minimize its importance, a water layer was inserted in the reflector region (configurations 19 through 30). It was felt that the water layer would also serve to increase the reflector thickness since no additional beryllium was available at that time. Later in the experiment, however, beryllium blocks were obtained from the Critical Experiments Facility and tests were made with the desired beryllium reflector thickness. The correlation between these tests and those with the water layer was poor, and it is recommended that the absolute values of both the neutron and the gamma data taken behind mockups 19 through 30 be used with extreme caution unless a water layer in the beryllium reflector region of an actual reactor is anticipated.

While the meaning of the absolute values of the data of configurations 19 through 30 is in question, the measurements relative to other measurements

in the same group are very useful. Configuration 21 represents the first RMR test with "unfamiliar shielding materials," that is, materials other than lead, iron, and plain or borated water.

Effect of Substituting Oil in Liquid Neutron Shield. In configuration 21 a 15-in. tank of oil substituted for water in the liquid neutron shield decreased the fast-neutron dose and increased the gamma dose. This can be explained by the fact that a greater density of hydrogen atoms makes oil more effective than water in attenuating fast neutrons, although water is more effective for gamma rays because of its greater electron density.

Effect of Variations in Pressure Shell and Moderator Region. Data taken behind configurations 22 through 26, 29, and 30 show the effect on the gamma dose of varying the material used in the pressure shell. Iron, copper, nickel and inconel were used and since some of the slabs were too large to fit into the dry tank all the measurements were made with the pressure shell material placed in the water.

The results of these tests indicate that copper possesses the best properties of attenuation at this particular position in the shield. Nickel, iron and inconel followed in that order. The gamma doses measured well out in the water region behind the materials with no lead shielding showed that the dose with copper in the configurations was only 35% lower than that using inconel and that iron was only slightly better than inconel. The structural properties of inconel, however, override the small shielding disadvantage and it will probably be used in the pressure shell for the RMR. If a more precise comparison of these data becomes desirable it should be kept in mind that the iron and nickel thicknesses were made up of two slabs with an unknown amount of water between them, whereas the copper and inconel slabs were in one piece.

Configurations 31 and 32 were run to determine the effect on the external gamma dose of placing 1-1/2 in. of lead between the source and the beryllium. It is possible that at some future date the problems associated with containing lead at high temperatures will be solved and it would be desirable to use lead as a moderator coolant provided a weight saving could be realized. The data indicates that 1.5 in. of lead when placed next to the source reduced the external gamma dose by only 18% because of the high secondary production in this region of high neutron flux.

Effect of Substituting Tungsten Carbide in Gamma Shield. Since the gamma shield material of an aircraft reactor contributes a major fraction of the total installation weight, any means of reducing the weight of this particular region is worth serious investigation. The substitution of tungsten or tungsten carbide, both very dense materials, for lead has been considered and since some WC was available, a group of experiments was devised to determine its effect.

The WC was in granular form (average density = 8.05 g/cc) and filled a 2 in. thick tank. In configurations 33, 34, and 35 the WC tank was placed just outside the pressure shell. Because it was felt that there might be considerable capture of thermal neutrons in the iron tank walls, giving a gamma source that should not be charged against the WC, tests were made with a boral slab preceding and following the WC. There was no appreciable difference in the gamma dose with or without the boral and it appeared that the capture gamma source in the tank walls was small.

Lead was then added outside of the WC tank (configurations 36 and 37) to gain some insight into the gamma spectrum from neutron capture in WC. After a total of 3 in. of lead had been added, the order of the materials was reversed

(configuration 38). If the secondary gamma production rate times the self-absorption per gram were the same for WC and lead this reversal would make little difference in the dose. Earlier data clearly indicates that production of secondary gammas in the first few inches of lead outside the pressure shell has little effect on the total gamma dose. That is, there would be little difference in the external dose if the first of three slabs next to the pressure shell were tungsten instead of lead, provided the grams of material per square centimeter of the slabs were the same. Following this line of argument, it can be seen from the data for configurations 37 and 38 that placing the WC closer to the source than the lead gave a gamma dose roughly 40% lower than when the order of the slabs was reversed. Thus, the gamma shielding properties of lead appear to be clearly superior to WC in a region of important secondary gamma production.

The 6-in. slab of lead next to the pressure shell showed a relaxation length of 2.8 cm, whereas the WC tank plus 3 in. of lead showed 3.2 cm. It is just possible that by using metallic tungsten in place of WC the thermalization of neutrons and hence the production of capture gammas might be inhibited sufficiently to make the tungsten-lead combination as good as the lead alone. While the Lid Tank tests indicate that using tungsten in place of all of the lead would result in a heavier shield, a composite gamma shield employing tungsten for the inner layer and lead for the outer layer might be as light as an all-lead shield for the ideal case, and would have the advantage of being much stronger than the lead alone. Further experiments would be needed to prove this point.

Mockup Modifications to Improve RMR-Shield Simulation. After the first 38 configurations were tested, the removal of the entire mockup from the Lid Tank

and an extended shutdown were required to permit installation of a new shutter behind the Lid Tank source plate. During this period the previous tests were reviewed to determine what modifications in the reactor and shield simulation would more nearly approximate the RMR configuration.

As was mentioned previously, not enough solid beryllium was available to simulate the entire reflector region during the earlier tests and a tank (iron walls) of beryllium pebbles was substituted. Inasmuch as there was considerable uncertainty involved in correcting the data for the low-density pebbles, a change to a completely solid reflector was desired. Fortunately it was possible to borrow enough beryllium from the Critical Experiments Facility. Since the beryllium was in the form of small blocks, aluminum and stainless steel could be inserted between the rows of blocks to simulate the reflector coolant and coolant tubes, respectively. (Aluminum was substituted for sodium which will most likely be used as the reflector coolant in the RMR. The two materials have approximately the same thermal-neutron macroscopic cross section, although the hard, nearly monoenergetic capture gamma from aluminum is somewhat more difficult to shield against than the capture gammas from sodium.)

Design studies for the RMR[1] indicated that the percentage of the total reflector volume taken up by the coolant tube walls for a small high power density reactor might be as much as 0.4% on the average, with 0.78% in the first 6 in. For the same conditions the sodium percentages would be 2.4% and 4.7% respectively. While neither these percentages nor the distribution of these poisons could be matched exactly because the simulating material could be placed only between rows of the beryllium blocks in thicknesses of the sheet

1 "Aircraft Nuclear Propulsion Project Quarterly Progress Report for Period Ending March 10, 1953," p. 41, ORNL-1515 (Apr. 16, 1953).

material available, the amount and position of the material did closely approximate the poisons for a 200-megawatt reactor having an 18-in. core diameter.

Between the fuel region and the reflector of the 200-megawatt RMR designs there is 0.125 in. inconel, 0.100 in. sodium, and 0.025 in. inconel, which compose the core shell, a sodium passage, and the inconel can around the beryllium. These layers were simulated by the 3/16-in. iron wall of a new dry tank and the 1/4-in. aluminum wall of the beryllium tank. The other wall of the beryllium tank was thicker than desired, but the absorption rate per unit volume in the aluminum following the beryllium was calculated to be approximately 1% of the absorption rate in the inconel core shell, hence the error was considered inconsequential. A table of the tank dimensions is presented on page 89.

It was felt that the elimination of water gaps between the lead slabs was necessary; consequently it was decided to construct a large tank that would hold all the dry components of the mockups. This arrangement had a disadvantage in that it was relatively inflexible; i.e., if it was desired to use a material which would not fit into the new tank exactly, either an air gap would be present or it would be necessary to place some of the material in the water region outside the tank. It was decided that the advantages of the new arrangement were more than worth the lack of versatility.

Advantage was also taken of an opportunity to test the effect of substituting B^{10} for the B_4C previously employed as a neutron curtain on one or both sides of the heat exchanger region. If B^{10} could be substituted for a similar number of thermal-neutron relaxation lengths, a considerable saving in the over-all reactor shield installation weight could be achieved by reducing the radius and hence the weight of the pressure shell and lead region. There was little doubt that this substitution could be made; however, since

the material was available it was thought best to conduct a test. The introduction of B^{10} into the configuration was not easily arranged. First the material was in powder form and could not be allowed to contaminate the surrounding area. Secondly, the thickness of the material desired for the test, approximately 0.7 g/cm^2, was much thinner than the required supporting structure. Since the B^{10} had to be returned in the same form as it had been received, it could not be hot pressed. It was finally decided best to prepare it in the form of a water "slip" that could be puddled into a 3/16 in. deep recess dished out of a piece of aluminum 3/4 in. thick. After drying, the boron was covered with a thin sheet of stainless steel pulled down over the boron much like a drum head tightened over a drum. A description of this container and a list of the thicknesses is contained in another section of this report.

With the modifications described above it was expected that the gamma dose behind configuration 39 would be about a factor of 6 higher than the dose measured behind configuration 17. A factor of 3 was expected because configuration 39 did not have borated water behind the lead region, and a factor or 2 was expected from the elimination of the water gaps in the lead region. It was found, however, that the dose behind configuration 39 was a factor of 25 higher than that behind configuration 17. Since only a factor of 6 could be definitely accounted for, an intensive search was undertaken to uncover the remaining factor of 4. The first investigation was centered around the iron tank wall following the lead region.

As was described previously, the iron tank wall separated the dry lead region from the liquid neutron shield, and it was felt that there might be a significant amount of neutron capture in the iron. In configurations 40, 41,

and 42 boral was placed before, after, and on both sides of the wall, and the respective gamma doses indicated that there was an appreciable amount of capture in the iron, both from neutrons emerging from the lead and from neutrons that were thermalized in the water and reflected back into the iron. Although use of the boral resulted in a considerable reduction in the dose, the experimental arrangement with a boral slab following the iron was never completely satifactory. Even under the best conditions there was enough water pressure to bow the tank wall inward, leaving a water gap between the iron and the boral. In later configurations the water region itself was borated and the captures in the iron were sufficiently suppressed by neutrons thermalized in the water. The boral slab on the other side of the iron partition removed the thermal neutrons from the outward bound current at the surface of the lead. Thus, the effect on the external gamma dose of the iron in the partition of the dry tank that followed the lead region was small when boron was present on both sides of the partition. In actual RMR designs there will probably be no iron outside of the lead region because the addition of a small amount of calcium or tellurium to the lead should increase its strength to the point that it will be self-supporting.

Since the dish of B^{10} was only 34 in. in diameter it was thought possible that the streaming of thermal neutrons around the B^{10} could affect the gamma dose. In configuration 43 the B^{10} tank was spliced out on each side with 1/4 in. thick boral slabs, but the difference in the gamma dose with and without the boral was so small as to be negligible.

In configuration 44 a 3/4-in. water gap was inserted between the second and third lead slabs to test the effect of the water gaps in the lead region. Since there was no change in the dose, configuration 45 was installed to

determine the effect of boron in the lead. It can be seen that the gamma dose behind configuration 45 is a factor of 2.3 lower than that behind configuration 39; however, all but about a factor of 1.5 of the reduction can be attributed to the tybor between the last lead slab and the dry tank wall. This would seem to indicate that there was no great amount of neutron capture in the 6 in. thick lead region. These results for configurations 44 and 45 coupled with the results of later tests indicate that the effect of the water gaps between the lead slabs in all mockups prior to configuration 39 was small and that the production of secondary gammas in the lead, even when it was in a solid slab next to the pressure shell, was not excessive.

Effect of Boron in Shield. The B^{10} placed in front of the heat exchanger region was loaned to the Laboratory for only a short time and it became necessary to remove it from the configuration. In configuration 46 it was replaced with a 1-in. B_4C slab and there was a slight reduction in the gamma dose. Most of this difference can be attributed to the removal of the stainless steel which formed the drumhead over the B^{10} dish. This stainless steel -- or more correctly inconel -- will be necessary in the actual reactor designs, however.

In configuration 47 the addition of a 15-in. tank of 1% borated water behind the lead region reduced the gamma dose at a distance of 160 cm by a factor of 3.0. Although this mockup was similar to configuration 17, its gamma dose was higher by a factor of 2.2. An effort was then made to eliminate the gap of unborated water between the two iron tank walls. In an effort to remove this region an air wafer was inserted between the tanks in configuration 48, but the dose remained unchanged. It was then decided to weld a 60-cm extension on the dry tank to hold the borated water, thus completely eliminating the water gap. This modification was introduced in configuration 55.

Elimination of Plain Water Gap between Dry Tank and Borated Water Tank. In addition to eliminating the water layer between the iron tank walls, the extension of the mockup tank had several other advantages. The approximately 23 in. of borated water was more realistic than 15 in. as a typical thickness which might be used in the RMR. In addition, it provided enough space for a few measurements to be taken inside the borated water tank. It must be remembered that the fast-neutron flux in the Lid Tank Facility is too small to be measured accurately behind a full-scale shield, hence the thermal-neutron flux in equilibrium with the fast flux is taken as the measure of the fast flux after a suitable correlation is made between them. This correlation in borated water is dependent upon the not very well-known boron concentration, hence it was advisable to obtain some thermal-neutron data in pure water behind the full shield.

While the above modification was being made, configurations 49 through 53 were run with some variations in lead, boral, tybor, and water thicknesses in the lead gamma shield region. The data from configurations 51 and 52 revealed that there is some advantage in placing a strong neutron absorber such as B_4C or B^{10} between the heat exchanger and the pressure shell to reduce secondary gamma production in the pressure shell.

Effect of Beryllium Density. A comparison of the data taken behind configuration 55 (this was the first time the two-section mockup tank was used) with the data of configuration 17 showed that their gamma doses were approximately the same.

In order to make a precise comparison it is necessary to know how to correct for the low-density beryllium present in configuration 17. Inasmuch as the origin of the gammas measured in the water behind the shield mockup is

not known, this correction cannot accurately be made. If the dominant source of gamma rays is on the far side (as viewed from the detector) of the low-density region, then to the simple thickness correction must be added another correction to take account of the difference in distance between source and detector. A total correction for configuration 17 would then amount to about a 16% increase. However, if the secondary gammas originate in regions outside of the reflector, only a small geometric correction is needed.

It is probable that a combination of these factors was present, with the former assuming the greater importance for thin lead regions and the latter assuming greater importance as the lead thickness is increased. Certainly with 7.5 in. of lead in the configuration the majority of the measured gamma dose is coming either from the lead region or from the water immediately outside the lead region as evidenced by the marked increase in the water replacement relaxation length for the fifth lead slab.

A case in which the reflector region may be an important contributor to the secondary gamma-ray intensity as measured outside the shield, even with as much as 6 in. of lead, is shown in configuration 55 for which this production was probably increased owing to the addition of stainless steel to the reflector region to simulate structure.

Tests are underway at the time of writing to determine whether the beryllium reflector will have to be canned in inconel (as assumed in the subject tests) or whether it may be operated without cladding in sodium at 1200°F.

Effect of Plexibor Inserted at Various Points in the Shield. In configurations 56 through 59 slabs of plexibor of density 1.6 were placed at different points in the configuration to determine their effectiveness in reducing the gamma dose. Configuration 56 was run with 3/16 in. of plexibor in place of the 1-in. slab

of B_4C behind the heat exchanger. The gamma dose was increased by a factor of only 1.2. This would seem to indicate that the amount of boron in the plexibor is very nearly adequate for thermal flux depression in this region.

The use of plexibor between the lead slabs is of more doubtful utility. Configuration 58, which had plexibor on both sides of all four of the lead slabs, shows a decrease in the gamma dose by a factor of 1.1 over the dose of configuration 57, which had plexibor on both sides of the fourth lead slab only. When all the plexibor in the lead region was removed as in configuration 59, there was an extrapolated increase in the dose over configuration 58 by a factor of 1.35. However, a computation of the shield weight for a 6-in. lead region for contemplated RMR designs shows that insertion of the plexibor has very little effect on the over-all lead region weight.

It is evident from the configurations together with the lead optimization experiments that for RMR shields requiring up to 6 in. of lead the lead region can be constructed in an integral piece and placed next to the pressure shell with only a trivial weight penalty involved. However, an examination of the gamma data behind configurations 59 and 60 reveals that the water replacement relaxation length for an additional 1.5 in. of lead is 5.7 cm. This indicates a marked decrease in the effectiveness of this lead slab. An optimization experiment is clearly required to determine how much weight could be saved by inserting a borated hydrogenous region between the first 6 in. of lead and any additional lead required. It is possible that the weight involved would be sufficient to offset the engineering incentive to construct the entire lead region in an integral piece.

Effect of Heat Exchanger Thickness. By comparing configuration 59 with 62 and configuration 58 with 63 and 64, it is possible to estimate the effect of

the heat exchanger thickness on the gamma dose well out in the shield. After adjusting the data of configurations 62, 63, and 64 to account for the air gaps left by removing part of the heat exchanger, it is found that the water well behind the 60-cm borated water tank has roughly the same effectiveness on a thickness basis in reducing the gamma dose as the material in the heat exchanger region. This can be attributed to the fact that the gammas are induced by neutrons passing through the heat exchanger region.

Effect of Increasing Beryllium Reflector Thickness. In configuration 66 the reflector thickness was increased to 15 in. by adding a layer of solid beryllium blocks behind the beryllium tank. There was no major reduction in the gamma dose over previous configurations (see for instance configuration 63). From the standpoint of shielding the RMR it would certainly not be advisable to use a reflector thickness of 15 in. because of the heavy weight penalty incurred by increasing the radius of the lead and pressure shell regions.

Effect of Substituting Uranium in Gamma Shield. Configurations 70, 71, and 72 were run to determine the desirability of replacing lead with uranium. Inasmuch as the density and the mass absorption coefficient for gammas is greater in uranium than in lead, uranium should be a better gamma shield than lead provided the production of gammas from neutron capture and inelastic scattering is not excessive. In configuration 70 there were 3/16-in. plexibor slabs on both sides of a 3-in. uranium slab to inhibit neutron capture in the uranium. The gamma traverse obtained behind this configuration was considerably higher than expected. Inasmuch as the uranium slab was only 3 ft wide the possibility of streaming existed. In configuration 72 a lead collar was placed around the slab and the gamma measurements were significantly lower than those for configuration 70. A comparison of the gamma traverses of configurations 68

and 72 indicates that the slope of the curve in the water behind the 4.5 in. of lead is steeper than that with uranium, although at 170 cm the doses are practically the same. By using a water replacement length for gamma rays of 2.65 cm for the lead thickness between 4.5 and 6 in. obtained from configurations 66 and 68, it was found that 3 in. of uranium would give the same gamma dose at a distance of 150 cm from the source as 4.7 in. of lead.

It is rather difficult to apply these data to an RMR shield inasmuch as the experimental setup was not as clean as desired and because of the fact that there was no direct comparison between the effectiveness of lead and uranium for total shield thicknesses under consideration. It is obvious that more experiments are needed in which lead and uranium are compared directly for varying thicknesses of both materials and for total shield thicknesses that are under consideration for RMR shield designs.

Effect of Varying Boron Concentration in Water. Measurements behind configurations 73, 74, and 75 indicate that a 1% borated water solution decreases the gamma dose over that for plain water by a factor of 2.4, whereas a solution borated to 0.5% decreases the dose by a factor of 2.25 over the plain water. It is evident from these and previous comparisons of borated and plain water that the factor by which the gamma dose is reduced is dependent on the lead thickness in the configuration. These results become clear if the percentage of the total gamma dose that results from capture gammas from the water is taken into consideration. It is evident that this percentage is larger for the thicker lead regions, which will yield a larger factor of comparison between borated and plain water than if the comparison were made using a thinner lead region.

Effect of Substituting Lithium in Heat Exchanger Region. Configuration 77 was the last configuration tested. It was run to determine the desirability, from the standpoint of shielding, of using natural lithium in place of sodium as the secondary coolant. In view of the better heat transfer characteristics and the shorter half-life of the neutron activated emitter, lithium might well prove to be better than sodium as the secondary coolant provided materials can be found that will contain it at the temperatures envisioned. The configuration tested had two lithium-filled tanks in place of two of the four NaF tanks used previously. The data for this configuration can be compared directly with the data of the repeat run for configuration 64. There was no observable difference in the gamma traverses obtained. From the data at hand lithium appears to offer no shielding advantage over sodium other than the inevitably lower activation.

Lead Optimization Experiments

F. N. Watson

In experimentally examining the proposed shield for the RMR at the Lid Tank, optimization was attempted for several configurations. Since at that time and to the date of writing no method better than a trial and error method of optimizing a shield has been found, a perfect optimization was not arrived at owing to time limitations. Enough data were taken, however, to indicate that with 6 in. of lead shield no spectacular weight saving will result from lead-water spacing. A precise optimization will be attempted when the over-all reactor design is more complete.

The theory for weight optimization of a two-component spherically symmetric reactor shield has been developed by Blizard[1] and generalized by Goldstein and Blizard.[2] The condition for weight optimization is that the product of R^2 and $\ell(R)$ be constant for all R covered by the two-component region, where R is the radial distance from the core center and $\ell(R)$ is the "effective attenuation length" or "replacement length" defined by the relation

$$\ell(R) = \frac{t}{\ln \frac{\Gamma_1(R)}{\Gamma_2}}$$

where

Γ_2 = gamma-ray dose (more exactly it should be the total dose) for a configuration which is presumed to be optimized,

1 "ANP Quarterly for Period Ending Aug. 31, 1950," ORNL 858, p. 17; see also E. P. Blizard, "Introduction to Shield Design - II," CF-51-10-70, Part II Revised (Mar. 7, 1952); E. P. Blizard, "Shield Optimization," ORNL-1471, p. 10 (Feb. 18, 1953).

2 H. Goldstein and E. P. Blizard, "A Criterion for the Experimental Optimization of Two-component Unit Shields," Reactor Sci. Tech. 1, No. 2, TID-72, p. 88 (1951).

$\Gamma_1(R)$ = gamma-ray dose for the same configuration with a lead layer removed at position R,

t = thickness of the slab removed.

In the data given below R is the distance from the source to the center of the slab plus an assumed radius of the core (22.86 cm) minus a correction for the low density of the beryllium pellets (9.45 cm) minus any air in the dry tank preceding the lead-borated water tank.

In configuration 8 the effect of each of the four lead slabs (spaced 4 cm apart) was determined by comparison of gamma-ray measurements behind the total shield with measurements behind the shield with one slab removed. The data and the resulting $R^2\ell$ values are given in Table III-1; for convenience a sketch of the lead-water section of the mockup is given with the table. The total configuration is shown in Fig. VI-4.

In another group of measurements an attempt was made to determine the optimum position of each slab added to the mockup. In this case the water contained 2.8% boron by weight, and the water temperature was held at 42°C to maintain the boron content. The data for these measurements and the calculated $R^2\ell$ values are given in Table III-2; again sketches of the lead-water sections are included. The elements preceding this section are the same as shown in configuration 16, Fig. VI-7.

It is seen from Table III-2 that the minimum $R^2\ell$ for each slab occurred at G = 0. This was not the expected result, and therefore this method was not so good a first step toward optimization as had been hoped. It is of course true that the high boron content tends to decrease the value of G at which a minimum $R^2\ell$ will occur. It should be noted that $\ell_{G=10.16}$, $\ell_{G=4}$ and $\ell_{G=0}$ are very nearly constant for any of slabs 1, 2 and 3. This indicates that nearly maximum

Table III-1

$R^2\ell$ Values for Four Lead Slabs in Plain Water

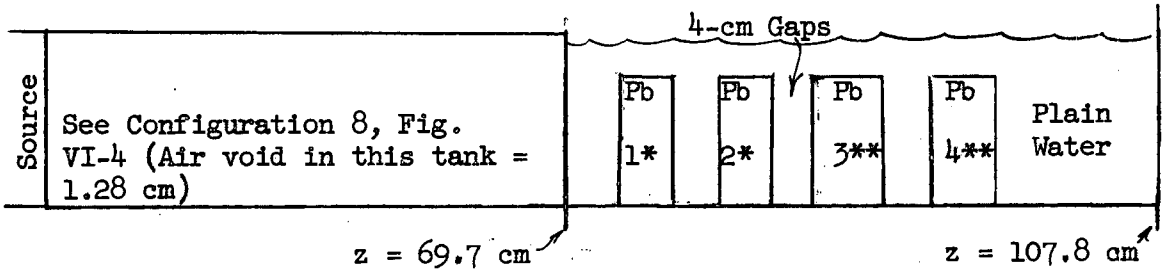

Removed Slab No.	Gamma Dose (mr/hr) at z = 151.3 cm		Calculated Values of $R^2\ell$ for Removed Slab		
	Actual Measurement	Average Measurement	R (cm)	ℓ [a]	$R^2\ell$
None	1.86×10^{-2} 1.83×10^{-2}	1.85×10^{-2}			
1	2.72×10^{-2} 2.55×10^{-2} 2.87×10^{-2} 2.88×10^{-2}	2.76×10^{-2}	87.42	6.37	4.94×10^{4}
2	2.76×10^{-2} 2.52×10^{-2} 2.46×10^{-2}	2.58×10^{-2}	93.96	6.98	6.16×10^{4}
3	4.05×10^{-2} 4.03×10^{-2}	4.04×10^{-2}	101.14	4.88	4.99×10^{4}
4	5.59×10^{-2} 5.10×10^{-2} 5.97×10^{-2}	5.55×10^{-2}	108.95	3.47	4.12×10^{4}

* 1-in. Pb slabs.

** 1-1/2-in. Pb slabs.

a In another configuration (No. 9) borated water (1% boron by weight) was substituted for plain water; otherwise the configurations were the same. The gamma dose behind configuration 9 was lower by a factor of 2.58 which accounts for the ℓ's listed above being large.

Table III-2

$R^2\ell$ Values for Four Lead Slabs in Borated Water

Lead--2.8% Borated Water Section of Mockup (1-1/2-in. Pb Slabs)	Gap Thickness, G(cm)	Gamma Dose (mr/hr) at z = 140 cm	Calculated Values of $R^2\ell$ for Last Slab in Configuration		
			R (cm)	ℓ	$R^2\ell$
No lead in tank z=68.7 cm 106.8 cm		1.39×10^{1}			
←G→ Pb 1	10.16	2.66×10^{0}	94.50	2.31	2.063×10^{4}
	4	2.65×10^{0}	88.34	2.30	1.995×10^{4}
	0	2.69×10^{0}	84.34	2.32	1.650×10^{4}
Pb 1 ←G→ Pb 2	10.16	5.18×10^{-1}	98.31	2.31	2.233×10^{4}
	4	5.19×10^{-1}	92.15	2.316	1.967×10^{4}
	0	5.22×10^{-1} [a]	88.15	2.325	1.807×10^{4}
Pb 1 Pb 2 ←G→ Pb 3	10.16	1.20×10^{-1}	102.12	2.59	2.700×10^{4}
	4	1.16×10^{-1}	95.96	2.53	2.330×10^{4}
	0	1.17×10^{-1}	91.96	2.55	2.157×10^{4}
Repeat run	10.16	1.60×10^{-1} [b]	102.12	2.76	2.878×10^{4}
	4	1.67×10^{-1} [b]	95.96	2.85	2.624×10^{4}
	0	1.75×10^{-1} [b]	91.96	2.95	2.495×10^{4}
No. 3 slab removed		6.37×10^{-1} [a]			
Pb 1 Pb 2 Pb 3 ←G→ Pb 4	15.24	3.45×10^{-2}	111.01	2.35	2.896×10^{4}
	10.16	3.40×10^{-2}	105.93	2.32	2.603×10^{4}
	4	4.14×10^{-2}	99.77	2.64	2.628×10^{4}
	0	4.62×10^{-2}	95.77	2.86	2.623×10^{4}
Pb 1 Pb 2 ←G→ Pb 3 ←G→ Pb 4	4 each	3.71×10^{-2}	103.77	2.53	2.724×10^{4}

[a] These measurements should agree.
[b] These repeat measurements should agree with original measurements above.

effectiveness is being obtained from the lead at any of these positions, G = 0 being the most desirable position. The variation between ℓ_{1stPb}, ℓ_{2ndPb} and ℓ_{3rdPb} may be attributed to the fact that the remaining components of the gamma spectrum during the process of attenuation have longer and longer relaxation lengths. The variation of ℓ_{4thPb} with G indicates that an optimum positioning of this slab is required. A calculation of the $R^2\ell$'s for this slab shows that a minimum value occurs at $G \cong 0$.[3] The indication is that for a fifth slab the minimum $R^2\ell$ would not occur at G = 0.

The summary of $R^2\ell$'s indicates that the theoretical condition for optimum placement of lead, viz. $R^2\ell$ = constant, has not been achieved. As mentioned previously, time considerations prevented any further investigation of the possibilities of weight saving through optimization. However, if the structural problems involved in arranging water and lead in spaced spherical shells is considered, such a spacing is not desirable unless a significant weight saving is to be obtained.

A few $R^2\ell$'s were calculated for configurations containing 7-1/2 in. of lead and are given with the gamma dose measurements in Table III-3. As in the cases above a single configuration of the many possible configurations was considered, and not enough data were taken to indicate an optimum lead-water spacing.

---

3 The low value of $\ell_{G=10.16}$ appears to be the result of faulty data.

Table III-3

$R^2\ell$ Values for Five Lead Slabs in Borated Water

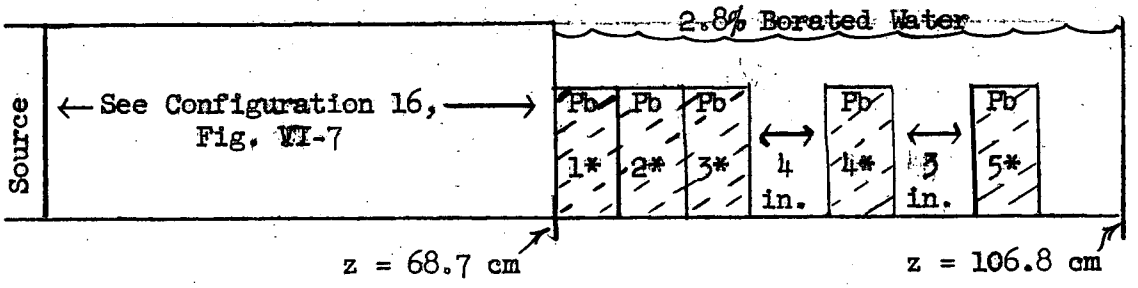

Removed Slab No.	Gamma Dose (mr/hr) at z = 140 cm	Calculated Values of $R^2\ell$ for Removed Slab		
		R(cm)	ℓ	$R^2\ell$
None	1.125×10^{-2}			
1	3.30×10^{-2}	84.34	3.54	2.52×10^{4}
2	3.12×10^{-2}	88.15	3.73	2.90×10^{4}
3	3.22×10^{-2}	91.96	3.63	3.07×10^{4}
4	3.44×10^{-2}	105.93	3.41	3.83×10^{4}
5	3.40×10^{-2}	117.36	3.45	4.74×10^{4}

* 1-1/2-in. Pb slabs.

Activation of the Secondary Coolant

M. E. LaVerne

The contribution to the total gamma dose of the secondary coolant passing through the intermediate heat exchanger becomes a limiting factor in the over-all shield design if the shielding at the reactor is increased to approach a unit shield. The activity of the secondary coolant in the heat exchanger of a circulating fuel reactor depends on many factors. The composition and thickness of the reflector and the boron-bearing curtain determine the rate of leakage of neutrons from the core to the heat exchanger region. The number of delayed neutrons released within the heat exchanger depends upon the fuel fraction in that region, while the percentage of these neutrons escaping from the heat exchanger will depend on its thickness; i.e., the thinner the heat exchanger the greater the escape probability. A boron curtain between the heat exchanger and the pressure shell will reduce the albedo of neutrons from the pressure shell and gamma shielding regions. Finally, the neutron absorption cross section in the intermediate energy range varies with the various secondary coolant materials.

In the RMR Lid Tank experiments the sodium activation within the NaF-filled heat exchanger tanks was measured for various thicknesses of the NaF region and for various materials around the region. In order to explore the possibility of reducing the secondary coolant activation by using potassium or rubidium in place of sodium, another series of tests was made in which NaF, KF, and RbF were irradiated at the Bulk Shielding Facility and their activations were compared. Both series of tests are described below.

Sodium Activation Measurements in the Lid Tank

Experimental Procedure. The heat exchanger in the RMR configurations was simulated by using thin slab-shaped steel tanks that were 3.5 cm thick and filled with NaF. The steel tank walls represented the matrix of tubing that would be present in a full-scale heat exchanger. Even though the heat exchanger tanks were loaded with NaF in as dry a condition as possible and were closed off, it was feared that the moisture content might change during the course of the test and have an effect on the amount of neutron moderation in the simulated heat exchanger. Therefore the central position of each heat exchanger tank was filled with cans of sodium rather than with NaF powder.

For activation measurements of the sodium, one NaF capsule encased in 0.250-in.-OD aluminum tubing attached to the lower end of a 0.250-in.-dia aluminum rod was lowered into each NaF tank. The activity of each capsule was plotted directly (decays/min/g) in Fig. III-1 with no attempt to correct to a common geometry. The disposition of the materials in the immediate vicinity of the simulated heat exchanger in the various tests is also indicated in Fig. III-1.

Analysis of Data. Tests 1 and 2 show the dual effect of increasing the heat exchanger thickness: (1) the total activity increases simply because more material is present, and (2) because of the reduced neutron escape probability in the thicker heat exchanger the activation does not fall off so rapidly with distance from the source, thereby raising the average level.

The effect of increasing the B_4C thickness on the source side of the heat exchanger is shown by a comparison of test 3 with test 2. The general level of activation is reduced by a factor of roughly 2, with little effect on the slope of the curve.

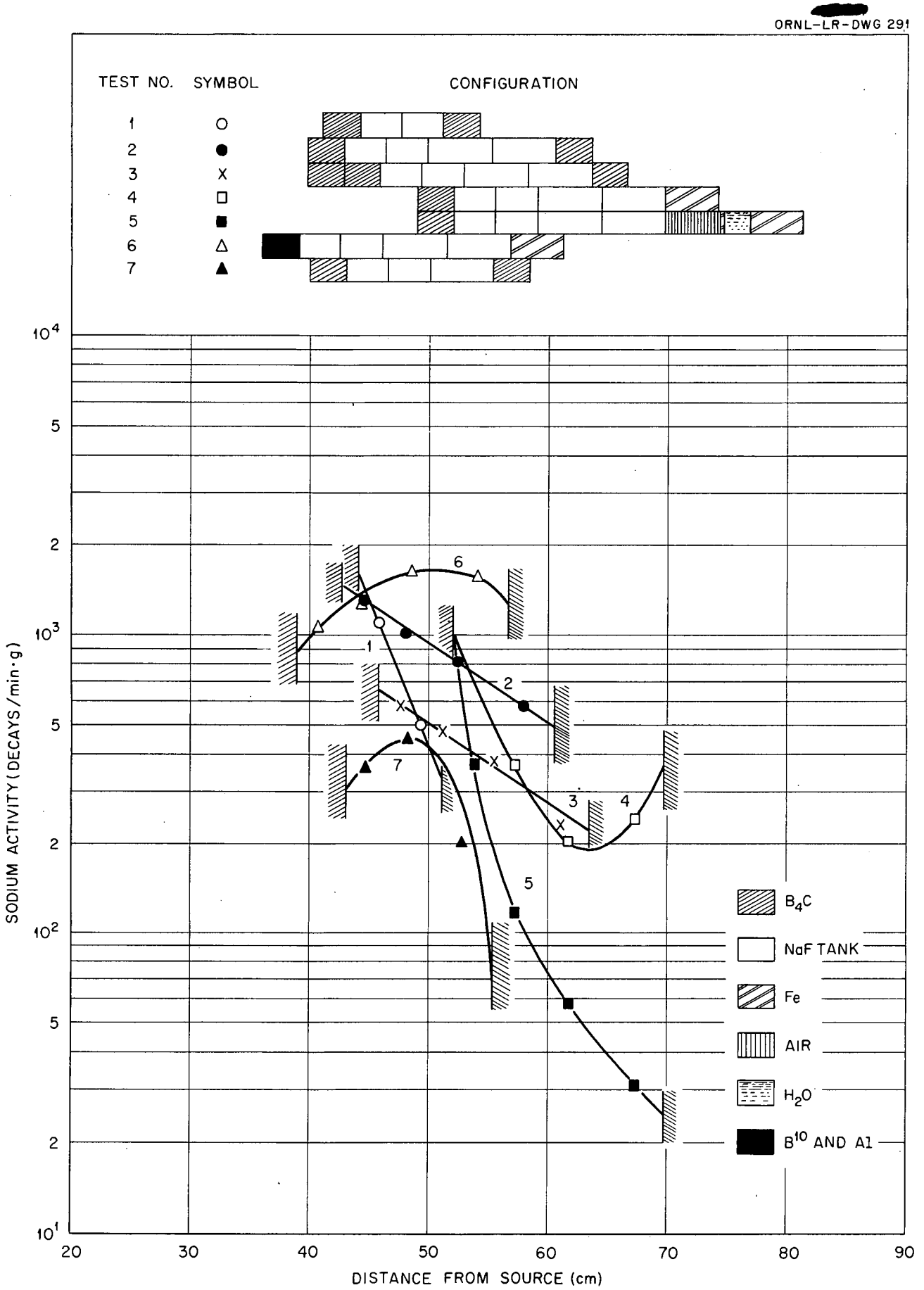

Fig. III-1. Summary of Sodium Activation Data from Lid Tank Tests.

Removal of the B_4C on the pressure shell side produces the effect shown in test 4. The sharp rise at the right is, presumably, the result of scattering of neutrons back into the heat exchanger mockup from the heavy iron slabs immediately outside. In test 5 this presumption has been tested by interposing a 2-cm water layer between the iron slabs and the heat exchanger. The marked reduction in activation is traceable to slowing down in the water layer resulting in absorption in the iron rather than reflection.

Tests 6 and 7 are unexplained as yet. There are only two obvious differences between these two tests and those preceding them. First, solid beryllium was used throughout the reflector instead of principally pellet beryllium with a small amount of solid beryllium. Second, the reflector and heat exchanger regions were placed in the same dry tank whereas previously the beryllium pellet tank and the tank containing the remaining beryllium and the heat exchanger were separately immersed in the water of the Lid Tank.

Relative Activation Measurements of Sodium, Potassium, and Rubidium at the BSF

Experimental Procedure. Samples of anhydrous fluorides of sodium, potassium, and rubidium were held in individual aluminum capsules. In an effort to approximate the spectrum seen by the secondary coolant in the full-scale heat exchanger, the capsules were surrounded by a 1 in. thick natural boron powder layer (density = 1 g/cm^3) encased in an aluminum can. This layer simulated the boron curtains adjacent to the heat exchanger in the full-scale design. The entire assembly was then placed on top of the reflector of the Bulk Shielding Reactor and irradiated for 9 to 12 hr in a thermal flux of approximately 10^{12} neutrons/cm^2/sec (at 50 and 100-kw reactor power). After irradiation the samples were transferred to unirradiated containers. The RbF was placed as quickly as possible in a high-pressure ion chamber and counted for 30 to 40 min, after which the NaF and KF samples were counted.

A Brown Recorder was used to obtain a continuous record of activity on a strip chart. Elapsed times from withdrawal of the samples to the beginning of the count ranged from 1-1/2 to 2-1/2 min, the length of time necessary to reach the nearest ion chamber. Further brief counts were made over a period of about two weeks to check the long-lived activities. All samples were then weighedd in order to convert activities to a per gram basis.

Three sets of samples were irradiated and counted as described above.

Analysis of Data. The largest obstacle to analysis of the data was the absence of clear-cut decay schemes for rubidium. Enough information[1-4] was found, however, to enable reasonable conjectures to be made with respect to rubidium, and the decay schemes shown in Fig. III-2 were finally settled on. Decay schemes used for sodium and potassium are given in Ref. (1), pages 19 and 36, respectively.

The observed activity (uncorrected data) of the NaF and KF samples are presented in Fig. III-3 in terms of ion chamber millivolts as a function of decay time. These curves have been drawn with the accepted slopes for sodium and potassium. In Fig. III-4 the data for these elements has been corrected for reactor power (to 100-kw), sample weight, and irradiation time. The corrections for power and weight were assumed to be simple proportionalities. The irradiation time was considered infinite.

The observed activity of the RbF sample is shown in Fig. III-5. The corrected Rb activity (minus the 19.5-day activity) is given in Fig. III-6 as

1 Nuclear Data, NBS Circular 499, p. 86 (Sept. 1, 1950).
2 A. Flammersfeld, "Rb^{86}, A New Isomer of 1.06-Minute Half-Life," Z. Naturforsch. 6a, p. 559 (1951).
3 M. E. Bunker, L. M. Langer, and R. J. D. Moffat, "The Disintegration of Rb^{88}," Phys. Rev. 81, p. 30 (1951).
4 K. Geiger, "Complex β-Decay of Rb^{88}," Ann. Physik 9, p. 293 (1951).

[redacted]

ORNL-LR-DWG 292

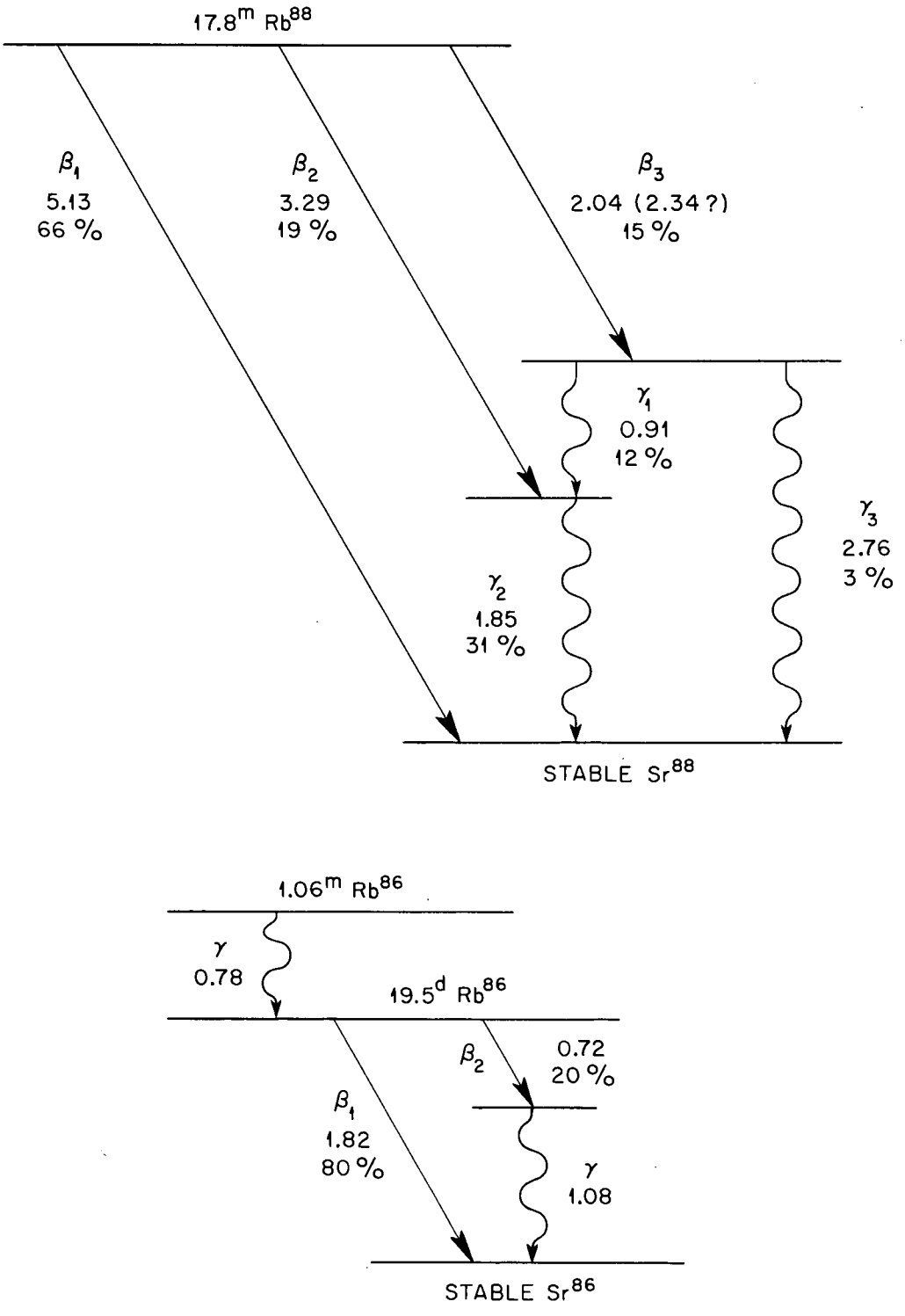

Fig. III-2. Rubidium Decay Schemes.

[redacted]

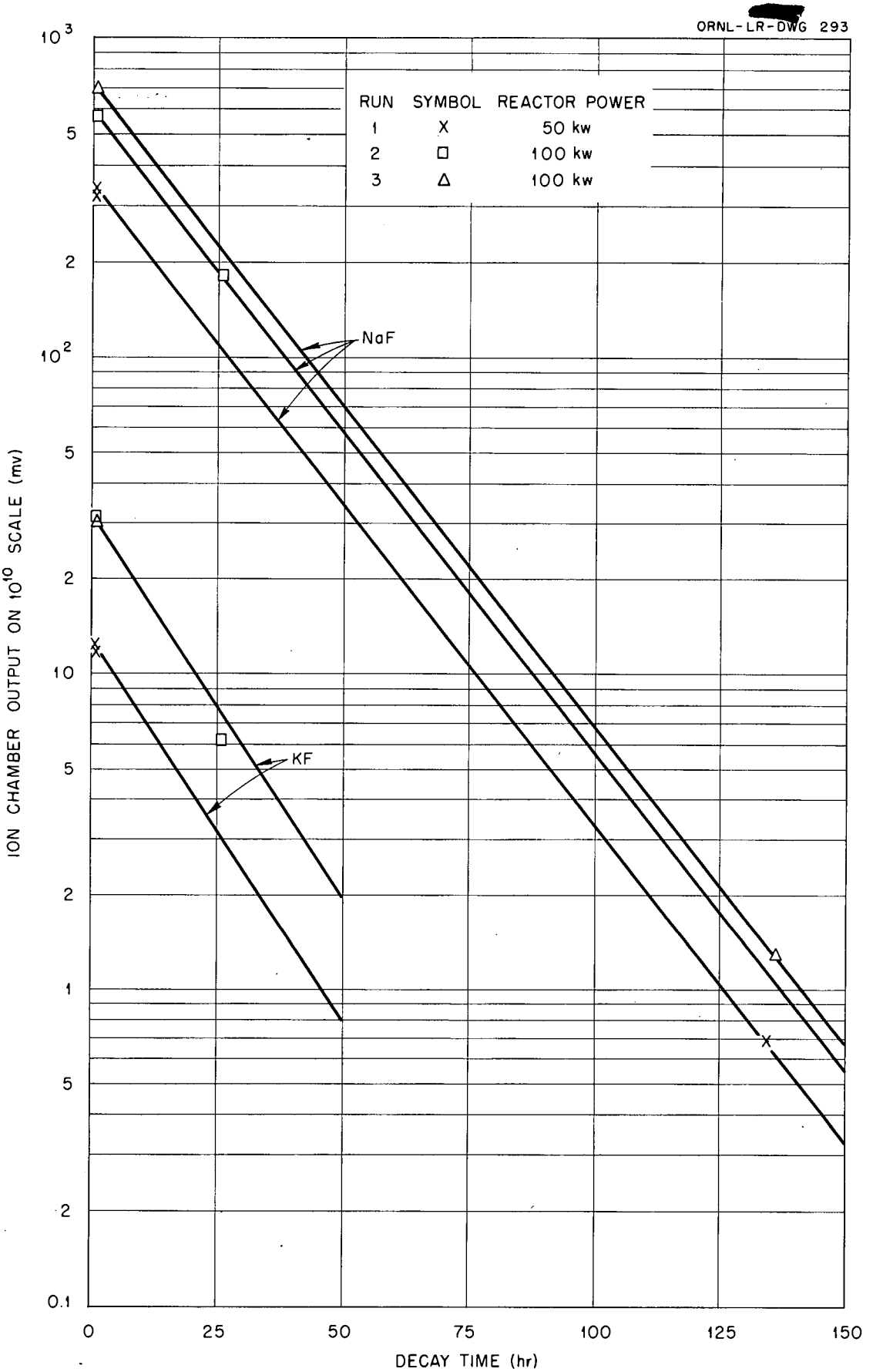

Fig. III-3. Observed Activity as a Function of Decay Time for Sodium Fluoride and Potassium Fluoride Samples.

[redacted]

ORNL-LR-DWG 294

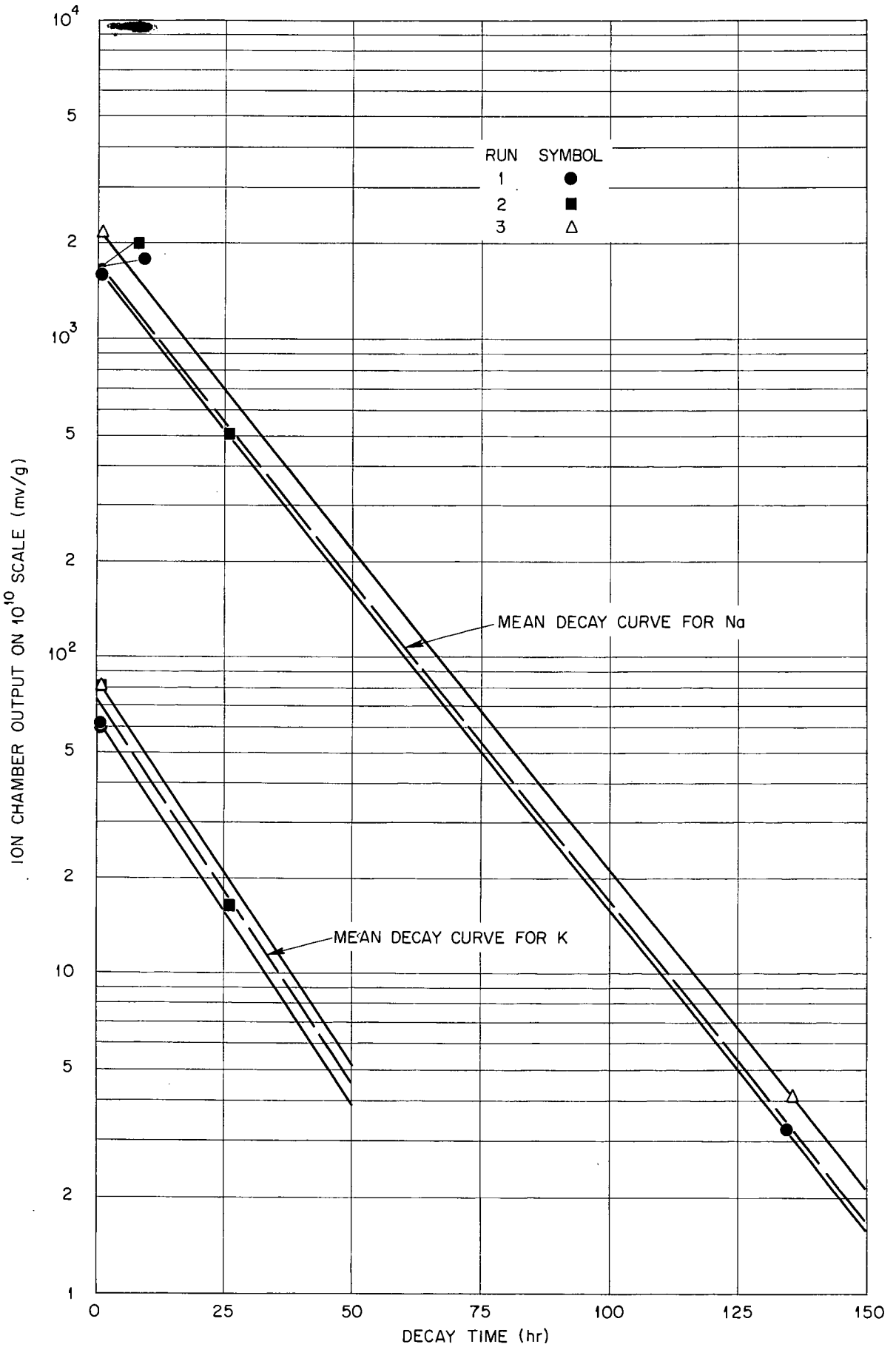

Fig. III-4. Corrected Activity as a Function of Decay Time For Sodium and Potassium Samples. (Note: Activity Corrected to Saturation)

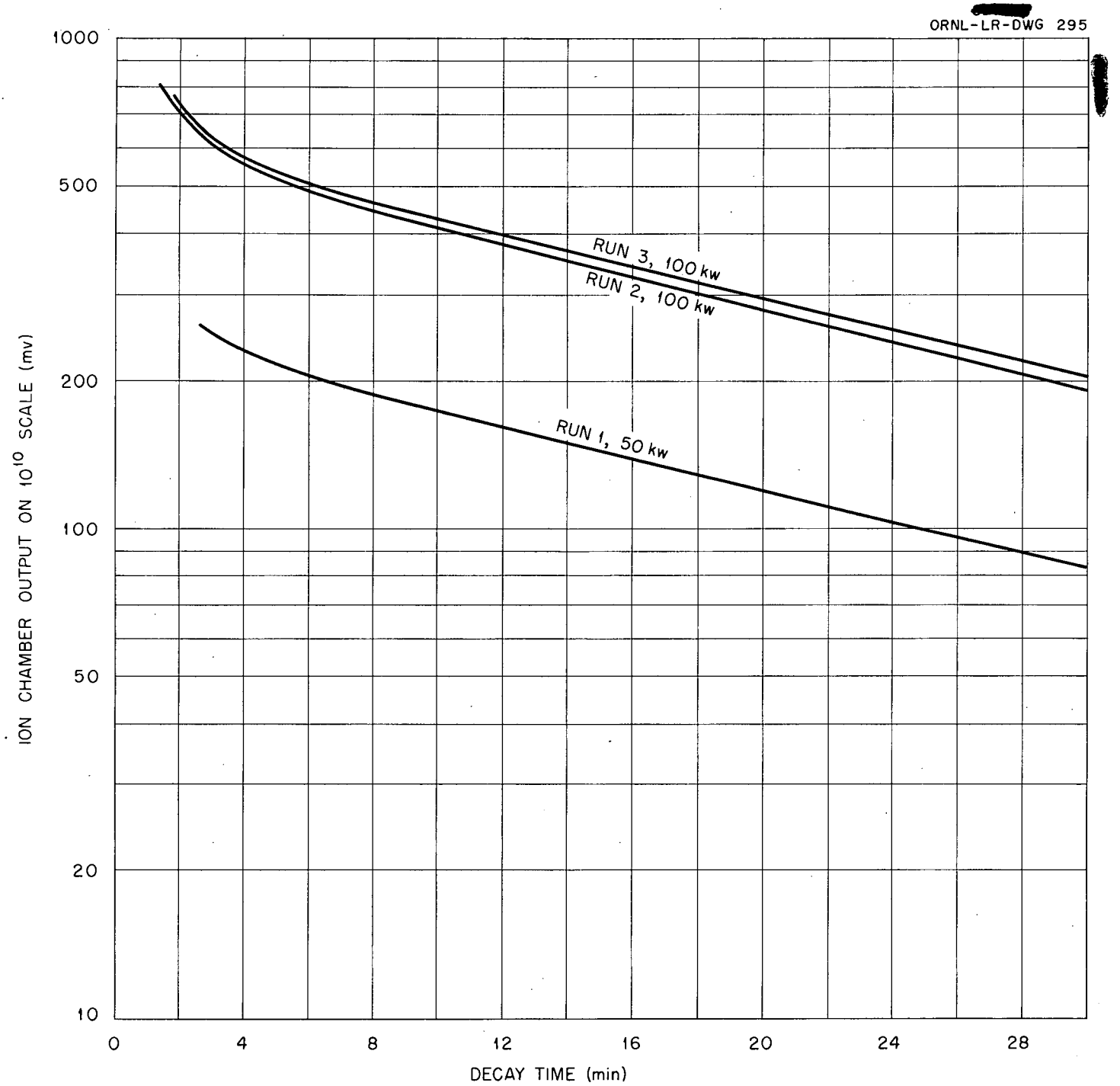

Fig. III-5. Observed Activity as a Function of Decay Time for Rubidium Fluoride Samples.

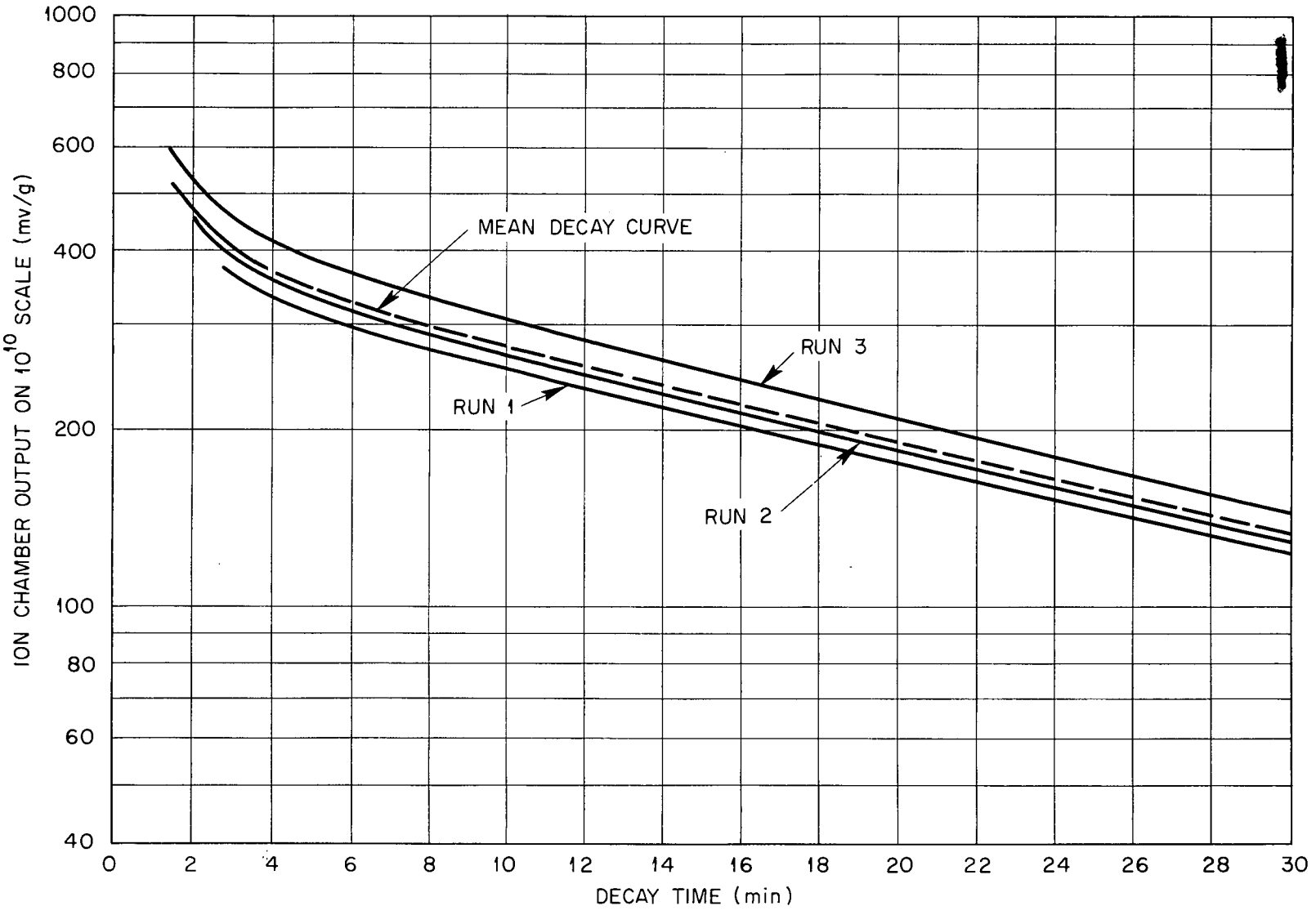

Fig. III-6. Corrected Activity as a Function of Decay Time for Rubidium Samples; 19.5-day Activity Subtracted.

a function of decay time. The data are corrected for reactor power and sample weight. No correction was needed for irradiation time, both short-lived activities being essentially saturated in much less than the shortest irradiation time.

The activity for the long-lived Rb^{86} isomer is given in Fig. III-7 for three irradiation times. These curves have been drawn with a slope corresponding to a 19.5-day half-life.

For irradiation times that are small compared to isotope half-life, the exponential buildup of activity is ordinarily well approximated by a linear term. However, in the irradiation of the RbF this did not prove to be so; an increase in irradiation time of 33% resulted in an activity increase of only 15%. The indication then is that a considerable portion of the long-lived Rb^{86} is being formed from the quickly saturated 1.06-min isomer. This circumstance together with the absence of a known 0.87-Mev excited state of Sr^{86} led to the selection of the Rb^{86} decay scheme in Fig. III-2.

The activity of the long-lived Rb^{86} for zero decay time is cross-plotted in Fig. III-8 as a function of irradiation time. The data are well fitted in the vicinity of 12 hr by the straight line shown. The coefficients of the exponential terms were determined by linearizing in the neighborhood of 12 hr and comparing the terms with those of the straight line. The fit is undoubtedly better than the data really justify.

For each of the three salts tested the corrected data were combined to give a single mean curve. These mean curves were then analyzed for their component activities. Finally, analytic expressions were determined for the gamma dose from each activity in terms of irradiation and decay times and shielding. These expressions were then used to compute the families of curves in Figs. III-9 through III-12.

[redacted]

ORNL-LR-DWG. 297

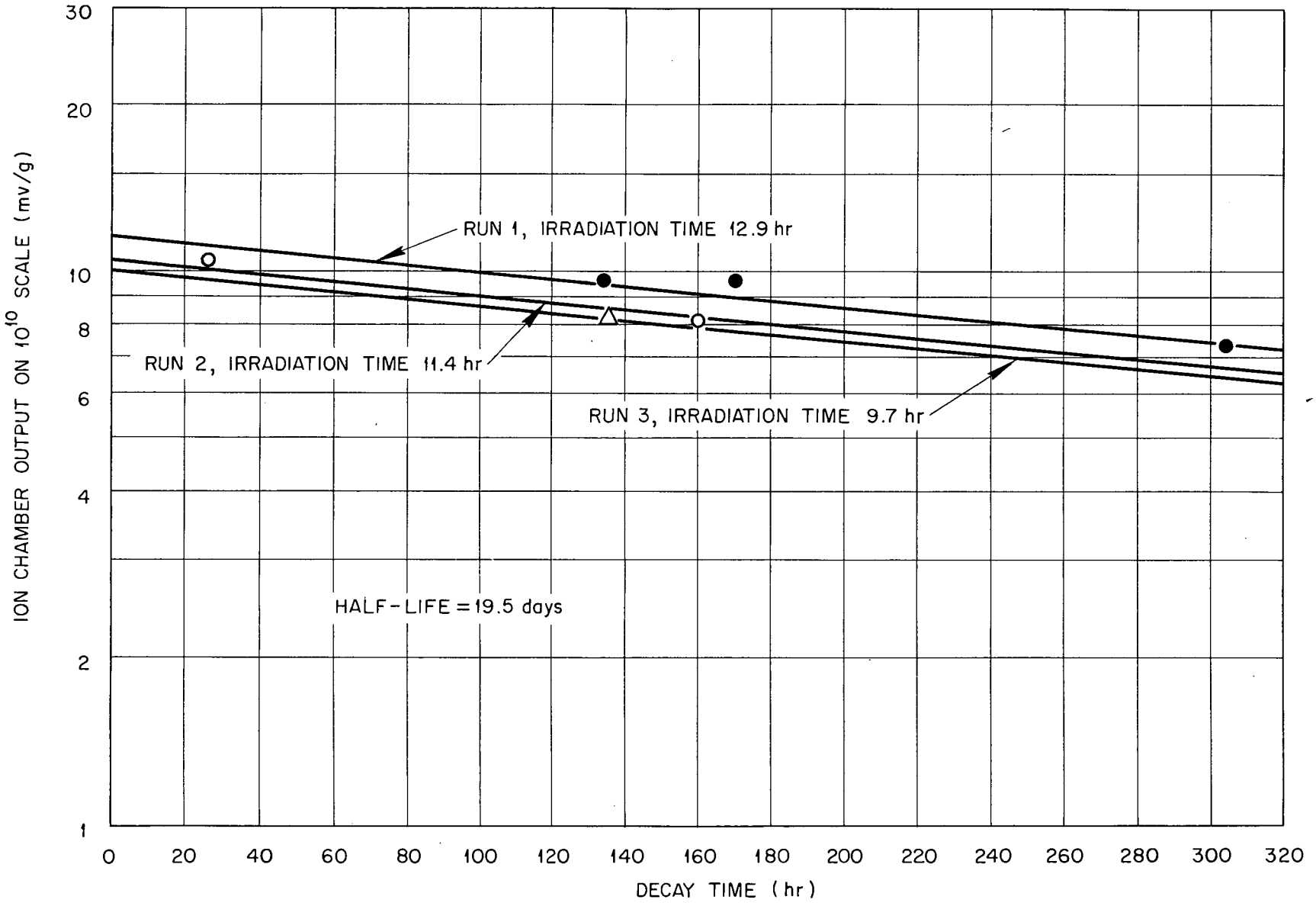

Fig. III-7. Activity of Long-Lived Rb^{86} as a Function of Decay Time for Three Irradiation Times.

[redacted]

ORNL-LR-DWG 298

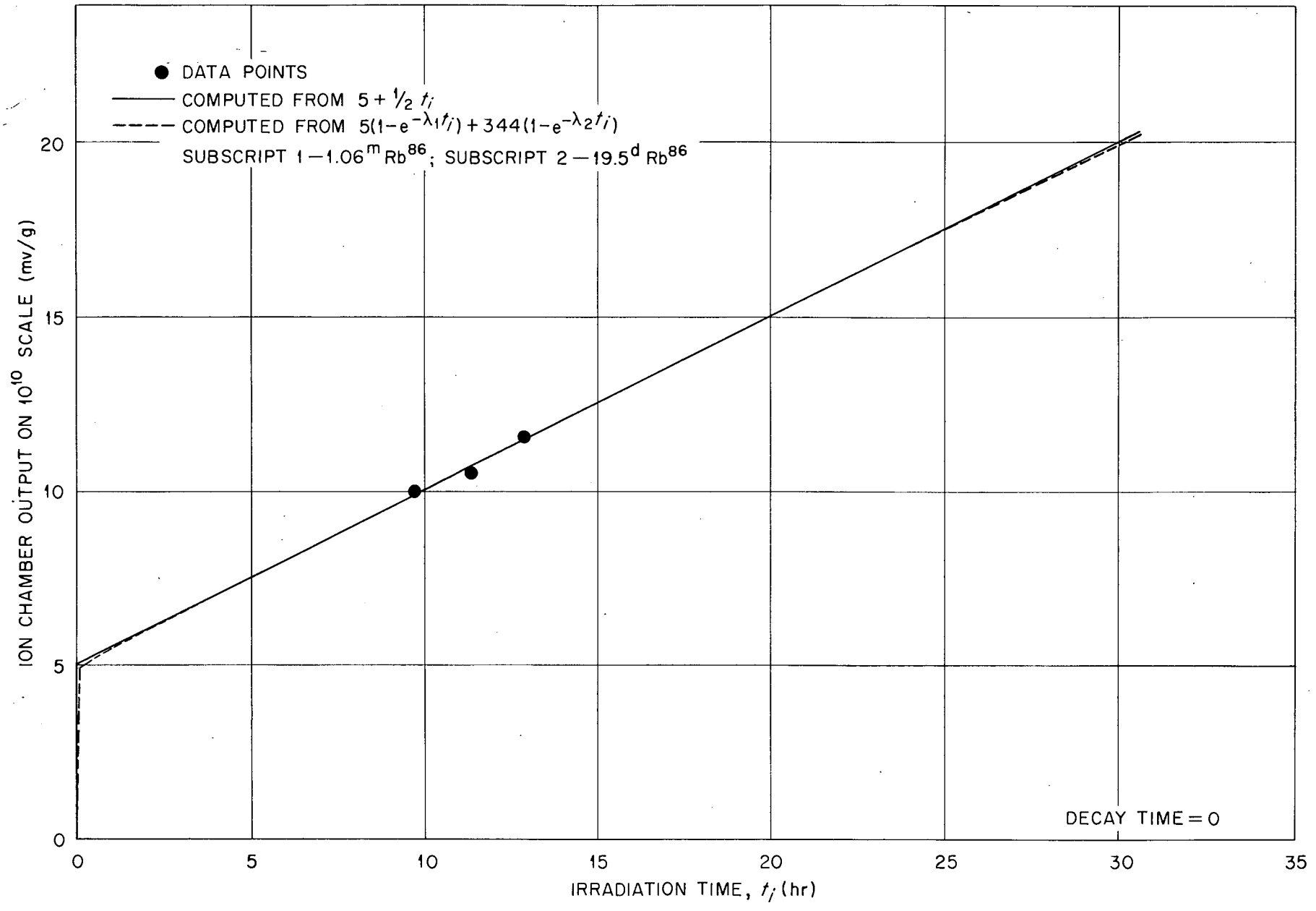

Fig. III-8. Activity of Long-Lived Rb^{86} as a Function of Irradiation Time.

[redacted]

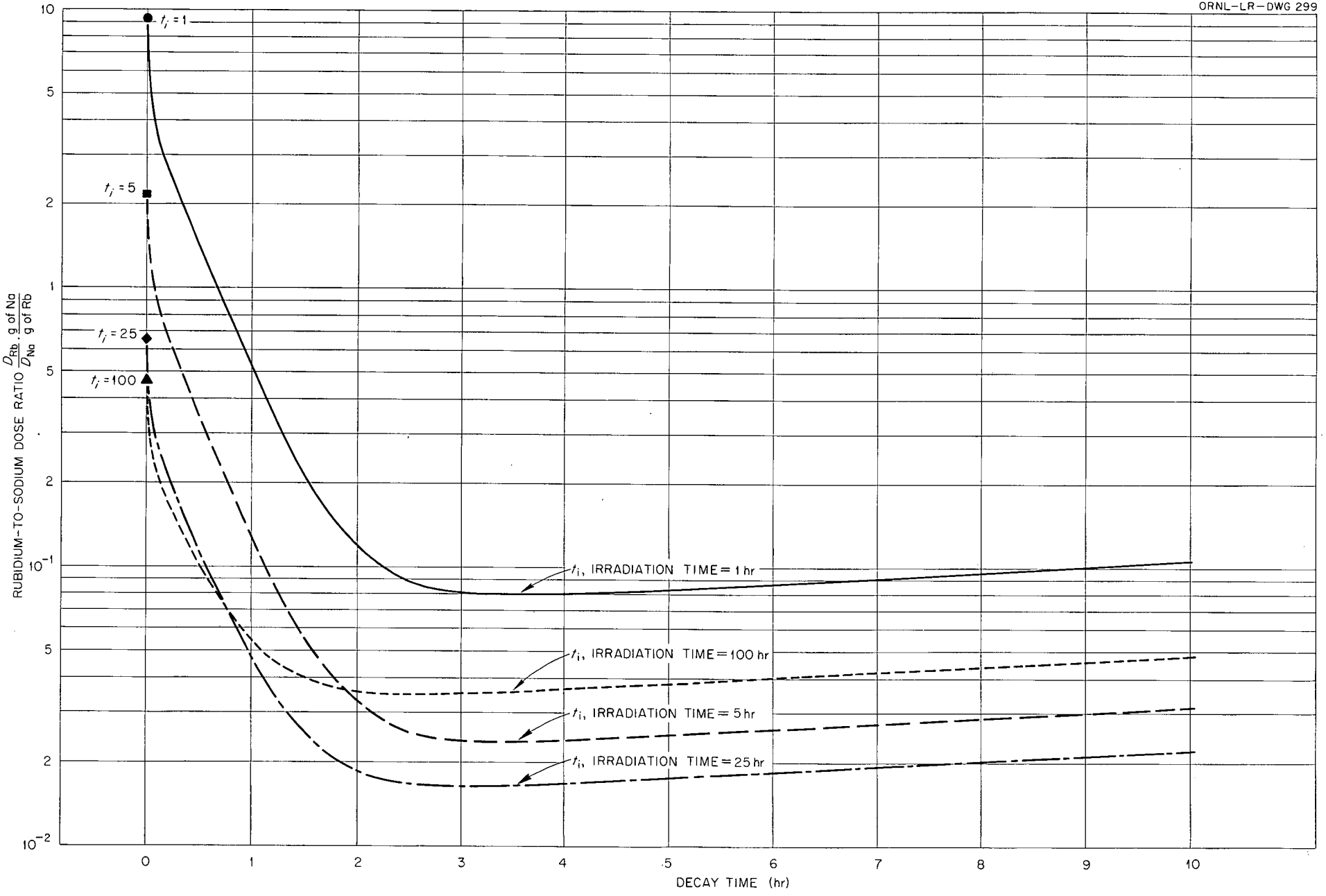

Fig. III-9. Rubidium-to-Sodium Dose Ratio as a Function of Decay Time for Various Irradiation Times—No Lead Shielding.

[redacted]

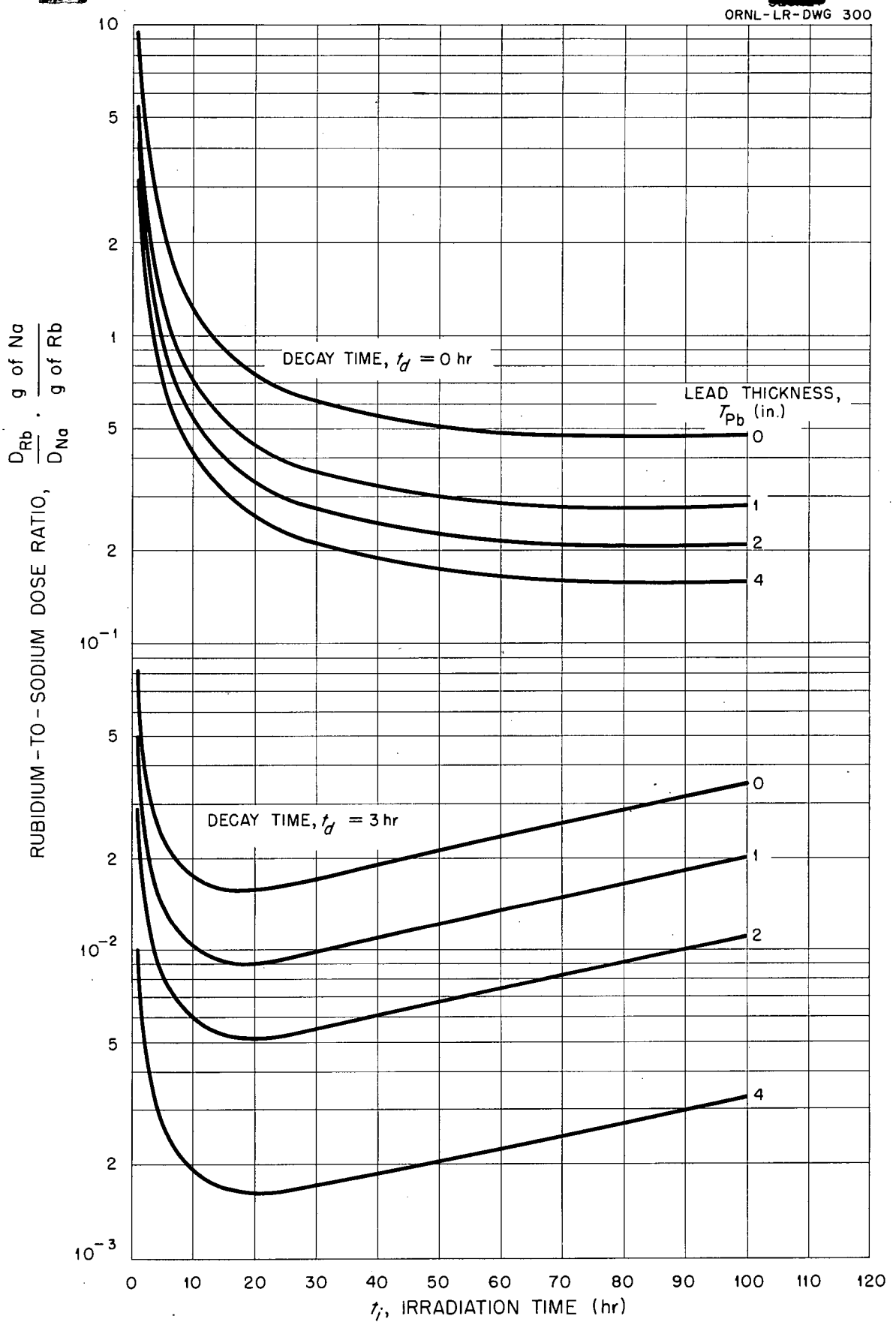

Fig. III-10. Rubidium-to-Sodium Dose Ratio as a Function of Irradiation Time for Various Lead Thicknesses.

[redacted] [redacted]

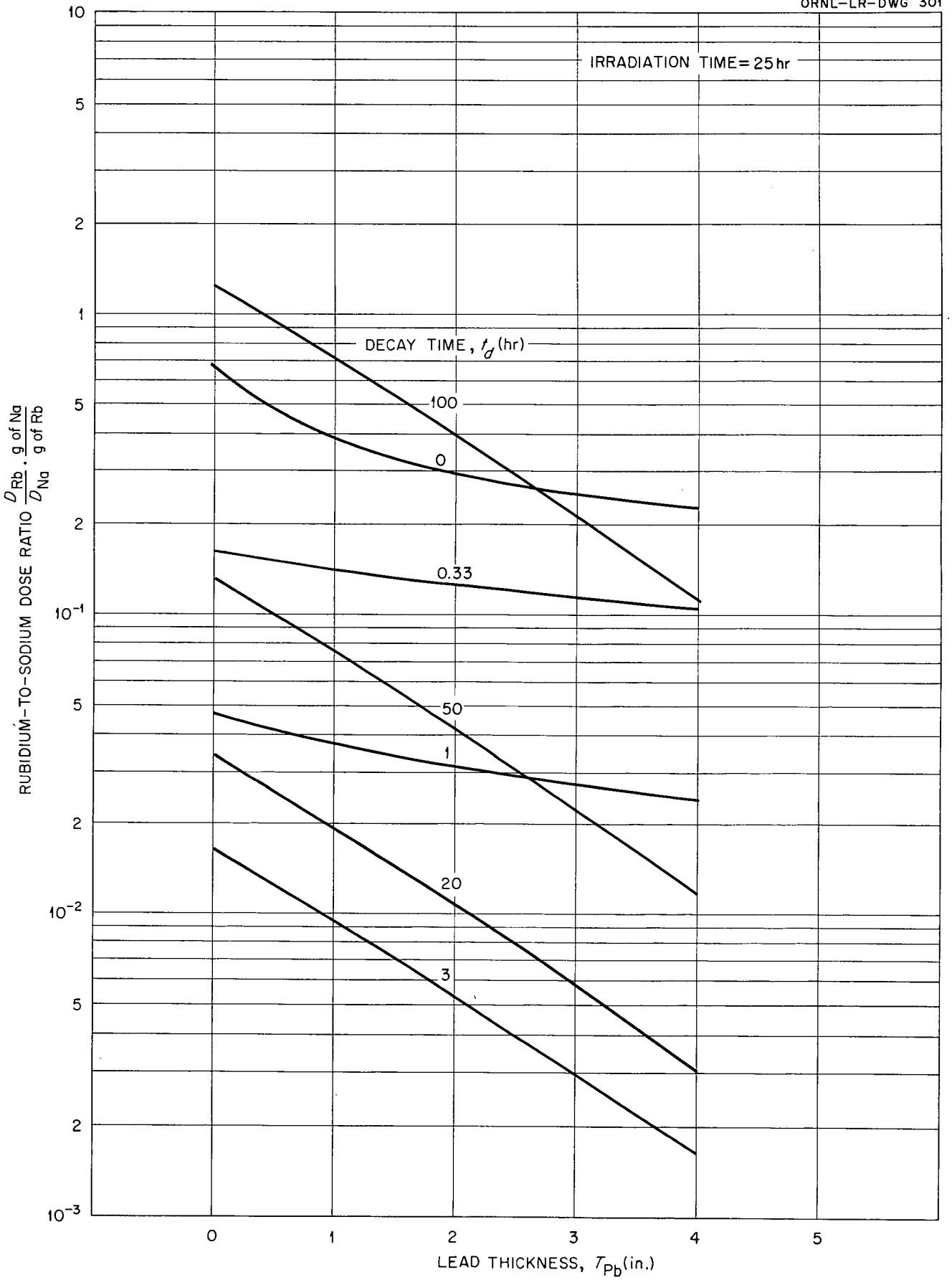

Fig. III-11. Rubidium-To-Sodium Dose Ratio as a Function of Lead Thickness for Various Decay Times.

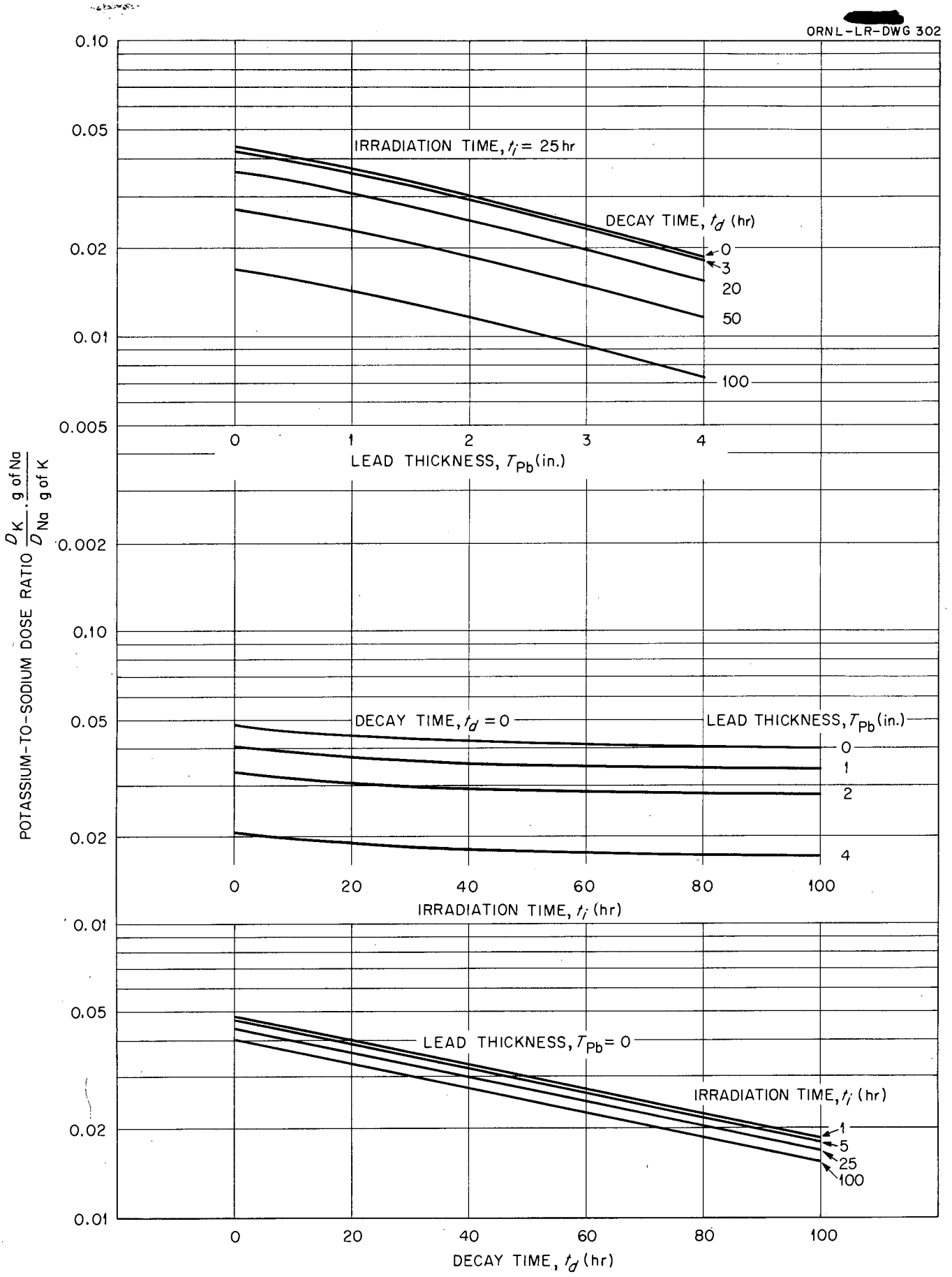

Fig. III-12. Potassium-to-Sodium Dose Ratio as Functions of Decay Time, Irradiation Time, and Lead Thickness.

Discussion of Results. Figure III-9 presents the gamma dose ratio for rubidium relative to sodium as a function of decay time for several irradiation times. For moderate irradiation times (less than about 13 hr) and short decay times (less than 1 hr) the rubidium dose is from 1 to 10 times that from sodium. For moderate decay times (3 to 10 hr) the dose from rubidium is only 2 to 10% of the dose from sodium. For long decay times (of the order of 60 to 90 hr, depending on irradiation time) the dose ratio again becomes and now remains greater than 1, increasing with time. These results are all with no shielding.

The rubidium-to-sodium dose ratio is presented in Fig. III-10 as a function of irradiation time for several thicknesses of lead shielding and two decay times. Note that for zero decay time (corresponding to in-flight conditions) the dose ratio falls precipitately for about 20 hr, then decreases more gently to a minimum at about 80 hr irradiation, increasing slowly thereafter. For a 3-hr decay time, the minimum is reached much sooner (about 20 hr irradiation) and the initial rate of increase is much greater. However, the dose ratios in the second case are lower than in the first by as much as a factor of 100.

Hardening of the complex rubidium gamma spectrum is apparent from the upper family in Fig. III-10. The first inch of lead is roughly as effective as the next 3 in., while the second inch is about as effective as the next 2 in. This effect, of course, is absent from the lower set of curves where the decay time has been sufficient that the short-lived activities are virtually non-existent. Here each inch of lead is about as effective as the next.

Figure III-11 shows the effect of lead shield thickness on the rubidium-to-sodium dose ratio for various decay times with a 25-hr irradiation time. The spectral changes referred to above are even more apparent here. Note that after a

3-hr decay time the changes are nearly complete as evidenced by the small change in curve shape from then on. The slight concavity downward in the curves for decay times of 3 hr or more results from the sodium emission of two gammas of appreciably different energies in cascade.

The complete results for potassium are shown in Fig. III-12. This conciseness results from the uncomplicated gamma output of potassium and extends to this statement of the results: For irradiation and decay times up to 100 hr and lead thicknesses up to 4 in. the dose from potassium is roughly 1 to 5% that from sodium.

The dose ratio as a function of decay time is a simple exponential with a 73.9-hr half-life. The effect of irradiation time on dose ratio is exceedingly small, amounting to a decrease of only one-sixth in dose ratio in the range of zero to infinite irradiation time. The dose ratio as a function of lead thickness shows a slight concavity downward as a result of the sodium cascade gammas. These curves are nearly exponential with a half-thickness of about 3.3 in.

Conclusions

Irrespective of the secondary coolant, its activation will be minimized if a boron curtain is placed between the heat exchanger and the pressure shell as well as between the reflector and the heat exchanger.

Rubidium does not appear to be a worth-while prospect in the search for a secondary coolant less subject to activation than sodium or a sodium-potassium alloy. First, its advantages under some operating conditions of interest are balanced, if not overbalanced, by its decided disadvantages under other operating conditions, also of interest. Second, the meager physical property data on rubidium indicate that it is poor (compared to sodium) as a heat transfer

medium. Finally, there is the matter of economics; rubidium would be much more expensive than sodium.

In general, the results indicate that potassium is far superior to sodium, the relative gamma dose from potassium being from 1 to 5% that from sodium for almost any combination of conditions. Furthermore, expense is not a determining factor, since the cost of potassium is comparable to that of sodium. However, as a heat transfer medium potassium is inferior to sodium (although better than rubidium) so that the use of potassium as a secondary coolant may well depend more on its effects on the heat exchanger and fluid system design than on nuclear considerations.

IV. APPLICATION OF DATA TO DESIGNED RMR-SHIELD

F. R. Westfall

The data obtained in this series of tests not only will serve as a guide to possible future experiments but can be immediately applied in a calculation of a shield weight for a specific situation. As mentioned previously, an effective preliminary shield has been designed for the RMR on the basis of these Lid Tank experiments. Unfortunately, experimental difficulties prevented the testing of an exact mockup of this "designed RMR-shield," but configuration 62 closely approximates it as is shown in Table IV-1. In this section both gamma and fast-neutron measurements are corrected to the designed RMR-shield and then applied to a sample calculation of the shield weight.

Fast-Neutron Data Corrected to Designed RMR-Shield

The attenuation of fast neutrons behind several RMR-shield configurations is shown in Fig. IV-1. A corrected fast-neutron curve is given in Fig. IV-2 and can be used for preliminary shield calculations regardless of the experimental configuration chosen. It essentially represents a corrected mean and and is presented to facilitate calculations. The manner in which this curve evolved is briefly described.

Of the configurations tested, those including full-density beryllium are of prime interest since they require less correction and adjustment; therefore, configurations 39 and 75 were selected and their fast-neutron data are plotted in Fig. IV-1. This data is not available for $z \gtrsim 110$ cm because of fast-neutron dosimeter sensitivity limitations. However, on the basis of Lid Tank experience with neutron data in water, the fast-neutron dose can be estimated from the thermal flux.[1] In order to determine a trend for the extrapolation of the

1 Notes from lectures by E. P. Blizard.

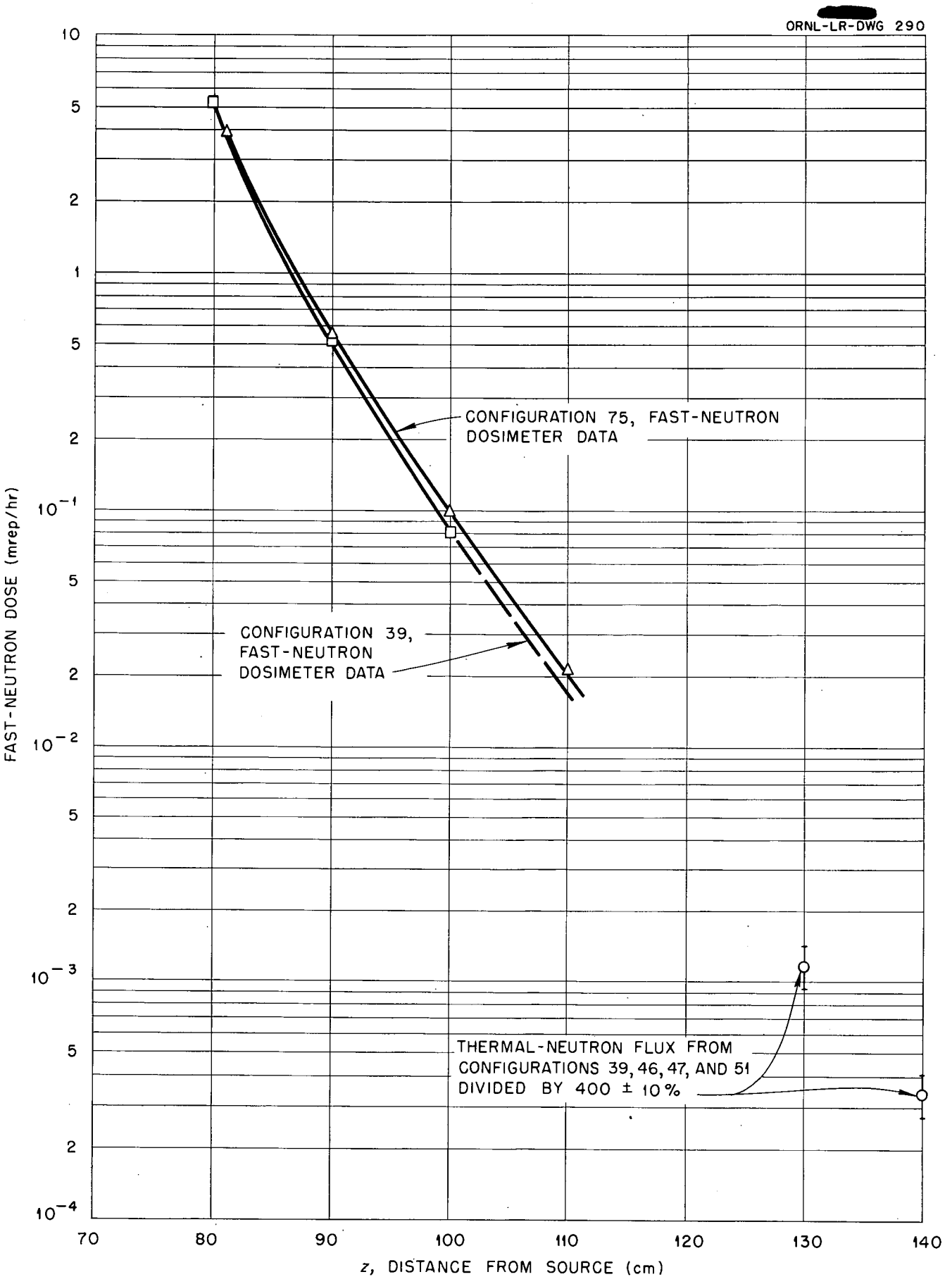

Fig. IV-1. Fast-Neutron Attenuation Data Used to Obtain Representative Fast-Neutron Dose Curve for Designed RMR-Shield Assembly.

Table IV-1

Comparison of Designed RMR-Shield Assembly with Configuration 62

Designed RMR-Shield		Configuration 62	
Component[a]	Thickness (in.)	Component[a]	Thickness (in.)
		H_2O	1.06
Inconel	0.125	Fe	0.19
Be (Na cooled)	12.0	Be Tank 2[b]	12.20
Inconel	0.0625		
B^{10}	0.13	B_4C Tank[b]	1.19
Heat Exchanger Region	X[c]	NaF Tank 1[b]	1.38
		NaF Tank 2[b]	1.38
		NaF Tank 4[b]	2.12
Inconel	0.125		
B^{10}	0.13	B_4C Tank	1.19
Inconel	1.50	Fe	1.75
Insulation	0.5		
Pb	Y[d]	Pb	6.00
		Plexibor	0.19
		Air	1.42
		Fe	0.19
H_2O (1% B)	Z[d]	H_2O (1% B)	24.22
		Fe	0.19
Rubber	2.00		
Total	16.6975+X+Y+Z		54.60

[a] Components listed in sequence from surface of source.
[b] See description of tanks in section VI, p. 89.
[c] The heat exchanger region varies in thickness according to the power of the reactor under design. The curves in Figs. IV-1 through IV-4 are based on an assumed value of 5 in.
[d] The gamma and neutron shield layers are dependent upon the design conditions.

of the fast-neutron curve, the thermal-neutron data for configurations 39, 46, 47 and 51 were chosen since these data were well suited for the purpose. It is of interest to note that the thermal-neutron flux measured between z = 130 cm and z = 140 cm varied less than ± 10% from the average for all these mockups.

The curve which was taken as representative of the fast-neutron attenuation is, then, a mean between configurations 39 and 75 out to 110 cm. It was extended to 140 cm by the points obtained from thermal-neutron data. Some correction to the curve was necessary in order to resolve the more apparent differences between the mockups and the RMR-designed shield. Those considered follow:

(1) Difference in Heat Exchanger Densities

	Density (g/cc)	Thickness (cm)
Designed	3.15	x
Configurations 39, 46, 47, and 51	2.42	17.8

Adjustment to z = 17.8 - 17.8 (2.42/3.15)

= 4.1-cm shift toward source

Adjusted z (cm)	Geometry Factor*
76	1.10
86	1.10
96	1.09
106	1.08
116	1.07
126	1.06
136	1.06

(2) Correction for Air Gaps. The air gaps for configurations 39, 46, 47, and 51 varied approximately from 0.3 to 2.1 cm. For this reason a shift of the median curve 1 cm to the left seemed appropriate.

* This is an inverse distance squared correction to take account of the extra distance from source to detector.

The result of these corrections is the fast-neutron attenuation curve representative of the designed RMR-shield that appears in Fig. IV-2. It is of interest to note where neutron data of various configurations fall with respect to the mean curve. This is shown in Table IV-2 which gives the dose after corrections have been made for the air gaps and the low-density beryllium.

Table IV-2

Fast-Neutron Dose for Several Configurations Corrected for Air Gaps and Low-Density Beryllium

	Measured			Corrected	
Configuration	z, Distance from Source (cm)	Thermal-Neutron Flux (nv_{th})	Flux Divided by 400	z, Distance from Source (cm)	Fast Neutron Dose* (mrep/hr)
15, 16	140	2.8×10^{-1}	7.0×10^{-4}	130	8.04×10^{-4}
19	140	3.32×10^{-1}	8.32×10^{-4}	129	9.55×10^{-4}
22, 27, 28	140	3.46×10^{-1}	8.65×10^{-4}	130	9.95×10^{-4}
53	140	1.49×10^{-1}	3.73×10^{-4}	140	3.73×10^{-4}

* Product of Flux/400 and geometry factors.

By comparing the data of Table IV-2 with that in Fig. IV-2, it is seen that the fast-neutron attenuation varied little with the changes made in the configurations throughout the experiment. Thus, the use of the representative curve appears valid and is worth while since it will simplify calculation procedures of preliminary shield weights considerably.

[redacted]

ORNL-LR-DWG 122

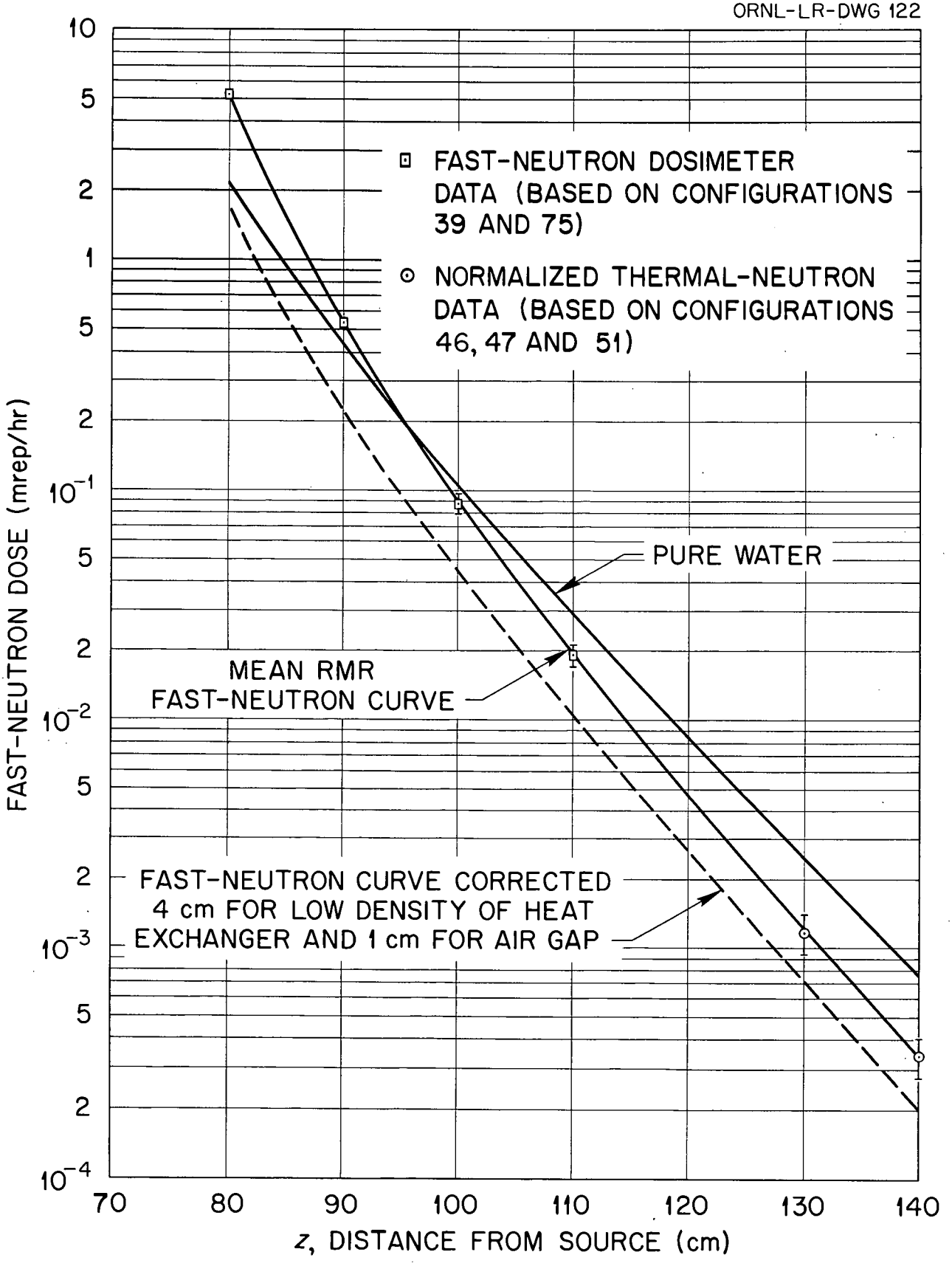

Fig. IV-2. Lid Tank Fast-Neutron Dose Curves Corrected to Designed RMR-Shield Assembly.

Gamma-Ray Data Corrected to Designed RMR-Shield

The gamma dose curves used in the sample calculation below are presented in Figs. IV-3 and IV-4. Figure IV-3 gives the gamma attenuation that should be expected with a designed RMR-shield incorporating 4.5, 6, and 7.5 in. of lead, respectively. Figure IV-4 restates Fig. IV-3 in a form that facilitates preliminary shield calculations. These curves were obtained from experimental data corrected as explained below.

Shields with 6 and 7.5 in. of Lead

For the cases of 6 and 7.5 in. of lead, the data of configurations 61 and 62 required little correction. The comparison of configuration 62 with the designed RMR-shield appears in Table IV-1. The only differences between configurations 61 and 62 were that the air gap in configuration 61 was 3.2 cm instead of 3.6 cm and, of course, configuration 61 had 7.5 in. of lead. The corrections to the gamma curves for configurations 61 and 62 are outlined briefly:

(1) Difference in Heat Exchanger Densities

	Density (g/cc)	Thickness (cm)
Designed	3.15	12.7
Configurations 61 and 62	2.53	12.4

Factor = 0.711 (where $\lambda \cong 25/\text{density}$ when the value is not available)

(2) Difference in Boron Curtains

	Density (g/cc)	Thickness (cm)
Designed (B^{10})	2.54	0.66
Configurations 61 and 62 (B_4C)	1.9	6.04

Factor = 1.48

[redacted]

ORNL-LR-DWG 120

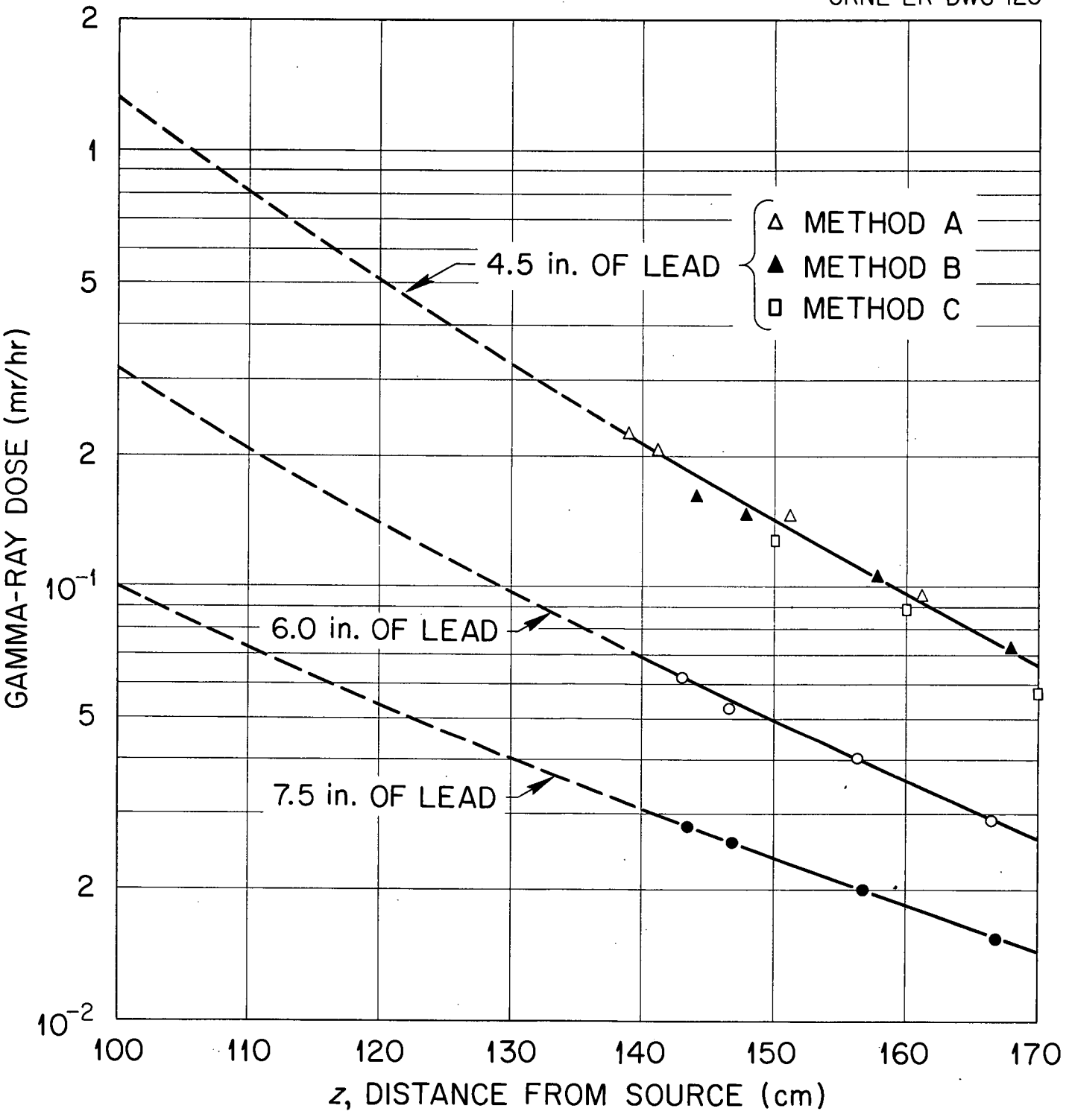

Fig. IV-3. Lid Tank Gamma-Ray Dose Curves Corrected to Designed RMR-Shield Assembly for 4.5, 6.0, and 7.5 in. of Lead.

[redacted]

ORNL-LR-DWG 121

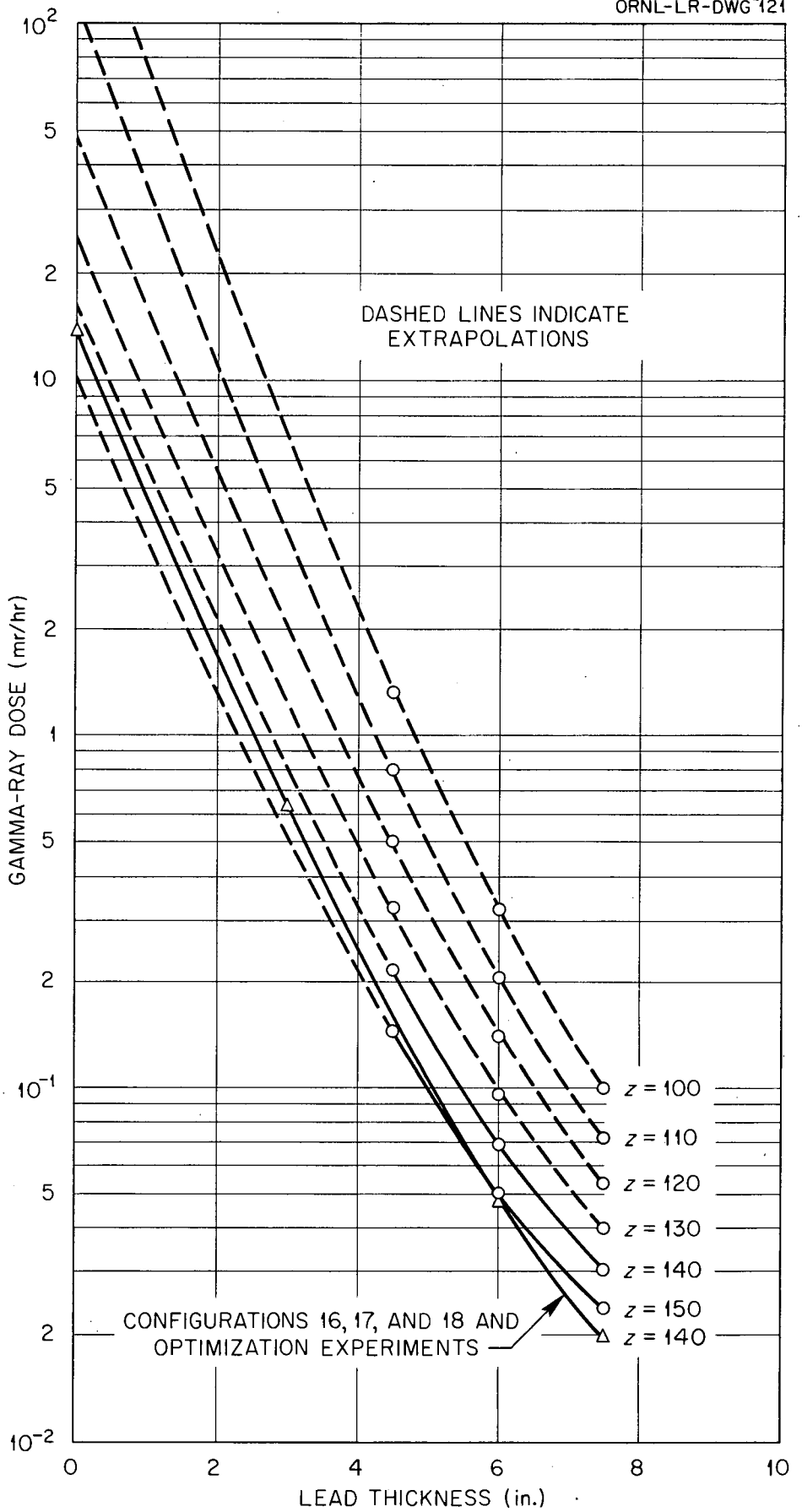

Fig. IV-4. Lid Tank Gamma-Ray Dose Curves Corrected to Designed RMR-Shield Assembly with Various Thicknesses of Lead.

(3) Difference in Pressure Shell Thicknesses

	Material	Thickness (cm)
Designed	Fe	3.81
Configurations 61 and 62	Fe	4.44

Factor = 1.19

(4) Corrections for Air Gaps

Configuration 61	z shifted toward source 3.2 cm
Configuration 62	z shifted toward source 3.6 cm

Factor ≅ 1.05

(5) Total Correction Factor for Configuration 61 or 62

$$(0.711)(1.48)(1.19)(1.05) = 1.32$$

The results of these corrections are given in Tables IV-3 and IV-4.

Shields with 4.5 in. of Lead

The curve that expresses the gamma dose for the designed shield with 4.5 in. of lead required corrections of greater uncertainty than those used for 6.0 and 7.5 in. of lead. Therefore, three different approaches were taken. The fact that the results from each of these methods agree closely provides some assurance that the curve presented in Fig. IV-3 is realistic.

Method A. Consideration of configuration 65 shows that it had the same differences from the designed RMR-shield as configuration 62 with the exceptions of a larger air gap (8.9 cm as compared to 3.6 cm), less lead (4.5 in. as compared to 6.0 in.) and the deletion of heat exchanger tank 2. (Study of configurations 63 and 64 showed that any corrections other than the air gap correction to account for the absence of heat exchanger tank 2 was for all intents and purposes unnecessary.) It further differed from the designed shield in that the three lead slabs, each 1.5 in. thick, were separated by 3/16-in. plexibor layers. A summary of the corrections for configuration 65 follows:

Table IV-3

Gamma Dose for Configuration 61 Corrected to Designed RMR-Shield -- 7.5 in. of Lead

Measured		Corrected to Designed RMR-Shield	
z, Distance from Source (cm)	Gamma Dose (mr/hr)	z, Distance from Source (cm)	Gamma Dose[a] (mr/hr)
146.6	2.10×10^{-2}	143.4	2.77×10^{-2}
150	1.95×10^{-2}	146.8	2.57×10^{-2}
160	1.52×10^{-2}	156.8	2.00×10^{-2}
170	1.17×10^{-2}	166.8	1.54×10^{-2}

[a] Product of configuration 61 gamma dose and correction factor 1.32.

Table IV-4

Gamma Dose for Configuration 62 Corrected to Designed RMR-Shield -- 6 in. of Lead

Measured		Corrected to Designed RMR-Shield	
z, Distance from Source (cm)	Gamma Dose (mr/hr)	z, Distance from Source (cm)	Gamma Dose[a] (mr/hr)
146.5	4.73×10^{-2}	142.9	6.24×10^{-2}
150	4.00×10^{-2}	146.4	5.28×10^{-2}
160	3.07×10^{-2}	156.4	4.04×10^{-2}
170	2.20×10^{-2}	166.4	2.90×10^{-2}

[a] Product of configuration 62 gamma dose and correction factor 1.32.

(1) Corrections for Heat Exchanger Densities, Boron Curtains, and Pressure Shell Thicknesses

Same as listed in items (1), (2), and (3) for configurations 61 and 62

Factor = 1.25

(2) Correction for Air Gaps

z shifted toward source 8.9 cm

Factor = 1.13

(3) Correction for Plexibor Layers

Factor between configurations 76 and 64	1.3
Factor between configurations 62 and 63	1.2

Mean value factor = 1.25

(4) Total Correction Factor for Configuration 65

$(1.25)(1.13)(1.25) = 1.76$

The points of the curve based on data corrected by this approach appear in Table IV-5.

Table IV-5

Gamma Dose for Configuration 65 Corrected to Designed RMR-Shield by Method A -- 4.5 in. of Lead

Measured		Corrected to Designed RMR-Shield	
z, Distance from Source (cm)	Gamma Dose (mr/hr)	z, Distance from Source (cm)	Gamma Dose[a] (mr/hr)
147.7	1.27×10^{-1}	138.8	2.23×10^{-1}
150	1.17×10^{-1}	141.1	2.06×10^{-1}
160	8.17×10^{-2}	151.1	1.44×10^{-1}
170	5.41×10^{-2}	161.1	9.53×10^{-2}

[a] Product of configuration 65 gamma dose and correction factor 1.76.

Method B. Configuration 73 was also used as a basis to obtain a gamma dose curve for the designed shield with a 4.5-in. lead layer. (In this case heat exchanger tank 3 had been added to the mockup, but once again its effect was considered negligible as is shown by comparing configurations 60 and 61.) The following corrections were necessary:

(1) Corrections for Heat Exchanger Densities, Boron Curtains, and Pressure Shell Thicknesses

Same as listed in items (1), (2), and (3) for configurations 61 and 62

Factor = 1.25

(2) Correction for Air Gap

z adjusted toward source 2.3 cm

Geometry factor = 1.03

(3) Correction for Plexibor Layers

Factor = 1.10

(4) Total Correction Factor for Configuration 73

$$(1.25)(1.03)(1.10) = 1.42$$

The results of these corrections are given in Table IV-6.

Method C. A third method involved finding a ratio between curves for two configurations which differed only in gamma shield thickness and then applying this to the 6-in. lead curve already obtained for the designed shield.

Two configurations that met this requirement were configurations 55R (6 in. of lead) and 73 (4.5 in. of lead) which were run consecutively. Since the outside 1.5-in. layer of lead was in borated water in configuration 55R, it was necessary to estimate a correction factor for the effect of this borated water. A comparison of configurations 55R and 59 indicated that the factor was approximately 1.35.

Table IV-6

Gamma Dose for Configuration 73 Corrected to Designed RMR-Shield by Method B -- 4.5 in. of Lead

Measured		Corrected to Designed RMR-Shield	
z, Distance from Source (cm)	Gamma Dose (mr/hr)	z, Distance from Source (cm)	Gamma Dose[a] (mr/hr)
146.3	1.13×10^{-1}	144	1.60×10^{-1}
150	1.03×10^{-1}	147.7	1.46×10^{-1}
160	7.36×10^{-1}	157.7	1.05×10^{-1}
170	5.08×10^{-2}	167.7	7.23×10^{-2}

[a] Product of configuration 65 gamma dose and correction factor 1.42.

Table IV-7

Gamma Dose for Designed RMR-Shield Obtained by Method C -- 4.5 in. of Lead

z, Distance from Source (cm)	Configuration 55R Gamma Dose (mr/hr)		Configuration 73 Measured Gamma Dose (mr/hr)	Ratio: C-73 Dose / C-55R Dose	Gamma Dose for Designed RMR-Shield (mr/hr)	
	Measured	Corrected[a]			With 6-in. Lead[b]	With 4.5 in. Lead[c]
150	2.96×10^{-2}	3.99×10^{-2}	1.03×10^{-1}	2.58	4.93×10^{-2}	1.27×10^{-1}
160	2.20×10^{-2}	2.97×10^{-2}	7.36×10^{-2}	2.48	3.57×10^{-2}	8.85×10^{-2}
170	1.75×10^{-2}	2.36×10^{-2}	5.08×10^{-2}	2.15	2.62×10^{-2}	5.64×10^{-2}

[a] Product of configuration 55R gamma dose and correction factor of 1.35 for borated water effect.
[b] Read from Fig. IV-3.
[c] Product of value for 6 in. of lead and ratio of C-73 Dose/C-55R Dose.

A ratio of this corrected data for configuration 55R and the measured data for configuration 73 applied to the curve for 6 in. of lead (Fig. IV-3) gave the gamma dose for the designed RMR-shield with 4.5 in. of lead as shown in Table IV-7.

Results

As mentioned previously, the curves in Fig. IV-4 are restatements of those in Fig. IV-3 and they are drawn to facilitate the calculation of specific shield weights. A curve based on observed data for configurations 16, 17, and 18 and the optimization experiments is included for purposes of comparison. This tends to substantiate the rather large extrapolations for the designed RMR-shield curves. The steeper slope can be explained by the fact that the lead gamma shields of these configurations are immersed in borated water.

Equation for Calculation of Shield Weights

The data shown in Figs. IV-2 and IV-4 were used to determine a specific shield weight by applying it to the following equation:[2]

$$D_{LT} = D_{RMR}\left(\frac{x}{R_S}\right)^2 \left(\frac{S_{LT}}{S_{RMR}}\right)\left(\frac{R_S}{R_C}\right)\left(\frac{1}{h}\right)$$

where

D_{LT} = Lid Tank dose,

D_{RMR} = dose desired at distance x from shielded reflector-moderated reactor,

x = distance from reactor center to crew position,

S_{LT} = Lid Tank surface source strength

= 9.04×10^{-4} watts/cm^2 (a constant, since the data were always normalized to a power of 6 watts; the self-absorption factor is 0.6, and the source area is 3970 cm^2),

2 "Report of the 1953 Summer Shielding Session," ORNL-1575 (June 11, 1954).

S_{RMR} = equivalent RMR surface source strength (given in Table IV-8 for a range of core diameters and a power of 1 watt),

R_S = shield outer radius,

R_C = core radius,

h = Hurwitz correction

$= 0.5 + 2(\lambda/a)^2 \left[(z/\lambda) + 1\right]$,

λ = relaxation length for use with Hurwitz correction

= 7.5 cm for both neutrons and gamma rays,

a = radius of Lid Tank source = 35.6 cm,

$z = R_S - R_C$.

Table IV-8

Equivalent RMR Surface Source Strengths for Various Core Diameters and a Power of 1 Watt[a]

Core Diameter (in.)	S_{RMR} (watts/cm^2)
14.3	2.29×10^{-6}
18	1.32×10^{-6}
22.7	7.8×10^{-5}
28.5	4.6×10^{-5}
36	2.66×10^{-5}
45.3	1.52×10^{-5}

[a] "Report of the 1953 Summer Shielding Session," ORNL-1575 (June 11, 1954).

A trial and error method of solution must be applied to the equation in conjunction with the fast-neutron and gamma-ray dose curves already presented. Fortunately, convergence is rapid. The shield outer radius, R_S, is the factor whose value is assumed in order to start this process.

Sample Calculation of a Specific Shield Weight

A sample calculation of the designed RMR-shield weight can now be made using the above equation and the following assumptions:

Beryllium reflector thickness	12 in.
Reactor power	50 megawatts
x	50 ft
D_{RMR}	10 rem/hr
Gammas	3/4 of total dose
Neutrons	1/4 of total dose
R_C	9 in. (23 cm)
S_{RMR} (see Table IV-8)	$1.32 \times 10^{-6} \frac{\text{watts/cm}^2}{\text{watt}} \times (5 \times 10^7 \text{ watts})$

For the first trial assume

$$z = 110 \text{ cm}$$

Therefore

$$R_S = R_C + z = 133 \text{ cm}$$

$$h = 1.89$$

and

$$D_{LT} = 10\left(\frac{1520}{133}\right)^2\left(\frac{9.04 \times 10^{-4}}{(13.2 \times 10^{-5})(5 \times 10^7)}\right)\left(\frac{133}{23}\right)\left(\frac{1}{1.89}\right)$$

$$= 5.5 \times 10^{-4} \text{ rem/hr}$$

$$(\text{Gamma dose})_{LT} = 0.75\ D_{LT} = 4.13 \times 10^{-1} \text{ mr/hr}$$

$$(\text{Neutron dose})_{LT} = 0.25\ D_{LT} = 1.37 \times 10^{-2} \text{ mrep/hr}$$

$$\text{RBE} = 10$$

The Lid Tank neutron dose at z = 110 according to Fig. IV-2 is 1×10^{-2}. Since $1.37 \times 10^{-2} > 1 \times 10^{-2}$, another trial is necessary. If z = 105 is assumed, then

$$(\text{Gamma dose})_{LT} = 0.75(5.87 \times 10^{-4})\text{rem/hr} = 4.40 \times 10^{-1}\ \text{mr/hr}$$

$$(\text{Neutron dose})_{LT} = 0.25(5.87 \times 10^{-4})\text{rem/hr} = 1.47 \times 10^{-2}\ \text{mrep/hr}$$

The dose for z = 105 from Fig. IV-2 is 2×10^{-2} mrep/hr. In this case the measured dose is greater than the calculated dose, $2 \times 10^{-2} > 1.47 \times 10^{-2}$, and the approximate value of z is determined by interpolation to be 107 cm. Thus, R_S = 130 cm gives the desired neutron attenuation. From Fig. IV-4 the gamma shield necessary is read directly as 5.3 in. of lead.

The weight of the neutron and gamma shields can be computed once their distance from the center of the reactor is determined. The necessary dimensions are presented in Table IV-1. For a 50-megawatt reactor of 18-in. core diameter, a 1.6-in. heat exchanger seems reasonable.[2] Thus, the inner radius of the lead layer is ~25.3 in. and its weight is approximately 21,600 lb. The inner radius of the neutron shield is 30.6 in. and its outer radius is 51.3 in., so the neutron shield weighs 15,900 lb. Thus, the total basic shield weight is 37,500 lb.

Approximate weights of the reactor--heat exchanger--pressure vessel components may be determined by a volume-density calculation. Tables conveniently presenting such data appear in Refs. (2) and (3). If this weight is added to the shield, the designed reactor and its shield assembly is found to weigh 44,500 lb.

The shield above is essentially a basic shield. There are problems such as the emission of fission product decay gammas in the intermediate heat exchanger and the leakage of radiation through passages in the shield that

3 A. P. Fraas and C. B. Mills, "A Reflector-Moderated Circulating Fuel Reactor for an Aircraft Power Plant," CF-53-3-210 (Mar. 27, 1953).

require further addition to the shield weight. Such refinements are not treated in the foregoing calculation because these experiments do not contribute to their resolution. However, these areas are treated in Ref. (2).

In conclusion, then, the data from these experiments have been reduced to the neutron and gamma attenuation curves shown in Figs. IV-1 through IV-4. It is felt that shields based on these data represent the closest approximation to the envisioned shield for the designed RMR-shield assembly that has been determined to date.

V. PROBLEMS FOR FUTURE INVESTIGATION

F. R. Westfall and R. M. Spencer

There are problem areas throughout the RMR-shield that have not been investigated to satisfaction. The resolution of these problems might be described as refinements to the basic shield design, although the nature or magnitude of the part they play is not definitely known. The elimination of such areas of uncertainty will contribute to the goal of a complete, accurate, and optimized shield. An effort is made here to present those areas of principal concern as recognized at this time.

Air and Structure Scattering

Air and structure scattering play important roles in determining the division between the shield at the reactor and crew compartment and the total shield weight. A better grasp of the over-all effect of the scattering phenomena should be possible as soon as measurements are available from the TSF. The pertinence of these data to the RMR design is highly dependent upon achieving a close approximation to the RMR of the angular distribution and spectrum of the radiation escaping from the mocked-up shield assembly. Whether this can be done by enclosing the TSF reactor with beryllium is as yet not known with any certainty.

Heat Exchanger Region

In the heat exchanger region several events take place that are of interest from the shielding point of view. Delayed neutrons and fission product decay gammas are released from the fuel which is cycled through the region. Since the energy of delayed neutrons is of the order of 0.5 Mev they are not expected to be important contributors to the neutron dose; however, their effect

on gamma dose may be of some significance. This can be attributed to coolant activation and to some extent to secondary gamma production. Fission product decay gammas inject an uncertainty in the gamma dose because of the scarcity of information on the spectra of short half-life fission products. At present, efforts are being made at ORNL to obtain data on the spectra and intensities of these gamma rays. The importance to shielding of the events already pointed out is affected by three principal factors: (1) the thickness of the beryllium reflector, boron curtain, and the heat exchanger; (2) the cycling time of the fuel, and (3) the choice of secondary coolant. An experiment is being considered that will simulate the passage of fuel through the heat exchanger region in which the effects of these factors will be measured.

Optimizations

The application of the RMR to the propulsion of aircraft increases the importance of efforts to optimize the shield assembly with respect to size and weight. Both of these factors play vital roles in the determination of airplane performance. Since the reactor--heat exchanger--pressure shell assembly is an integral part of the shield, any alteration of these components will affect the optimization of the outer shield region. So the heavy gamma shield and hydrogenous layer for the final design cannot be accurately optimized until the component thicknesses and materials of the inner region are completely specified. However, preliminary attempts are necessary to expose the significant parameters of the inner region from a shielding point of view. If areas that contribute significantly to the dose are revealed and a selection of thickness and/or composition of such areas is possible, the choice should be influenced by shielding considerations. Some examples are cited here.

The effect of the inconel core shell and reflector coolant liners may be significant, particularly for a thin gamma shield. If such is the case, there would be an incentive, in addition to that of reactivity requirements, to make the core shell as thin as is structurally possible and to eliminate the lining of the coolant passages. Also, if sodium is used as the reflector coolant, it will constitute a source of hard gammas. Thus, it is desirable to investigate various possible coolants to determine which have the least effect on gamma dose.

The thickness of the beryllium region is primarily dictated by the neutron moderation and reflection required. For these purposes, it must be at least 10 in. thick and perhaps will have to be as thick as 16 in. Multigroup calculations and critical experiments are proceeding, however, which will enable a closer determination. Since this thickness affects the shield weight, the radius of the outer heavy regions being dependent upon it, a more thorough study than has been undertaken to date could better define the optimum reflector thickness within existing limits from a shielding standpoint.

The heat exchanger region obviously is of concern to any effort toward reducing the size and weight of the reactor-shield assembly. Hence, it is important to attempt to simulate it in any future optimization experiment as pointed out in the preceding section.

Insulation will separate the pressure shell from the gamma shield region. This layer has not been included in these experiments, but it will have a small effect on optimization because of its thickness. The delayed neutron flux escaping from the heat exchanger region is not likely to be significantly reduced by the boron curtain following the heat exchanger because the energy is too high. Since these neutrons may give rise to secondary gammas in the gamma

and hydrogenous shield region, a further effort to reduce their number is warranted. This might be done by incorporating boron in the insulation to make this layer advantageous to the shield.

A complete optimization of the shield involves a determination of the optimum arrangement of the heavy gamma shield within the assembly. The preliminary experiments that have been described indicate that for lead thicknesses up to 6 in., the layer can be constructed in an integral piece and placed next to the pressure shell. This conclusion needs to be checked with the optimization parameters described previously taken into consideration. An extension for thicknesses beyond 6 in. is also in order.

In addition, the possibility exists that some advantage can be gained by the substitution of other materials for part or all of the lead in the heavy gamma shield. These advantages could take the form of a weight reduction, a decrease in the over-all shield diameter, an increase in structural strength without an excessive weight penalty, or a combination of these. Some investigation of these possibilities was attempted in the preliminary tests, but the results were inconclusive, and further work is necessary.

Ducts and Voids

The final design must allow for the presence of ducts and voids within the shield assembly. These can be placed in three categories: (1) the fuel passage through the beryllium at the top and bottom of the reactor, (2) the pump housing within the shield at the top of the reactor, and (3) the secondary coolant ducts that pass through the shield. Since these irregularities have not been simulated in any experiment to date, the streaming of radiation and the enhanced possibility for secondary gamma production in these vicinities are unknown. Because these regions are concentrated at the top and bottom of

the reactor, there is not such a stringent requirement on the magnitude of the allowed dose. However, it is necessary to determine the amount and kind of radiation escaping through these regions in order to shield them.

Comments

As experiments are undertaken to resolve the problem areas already pointed out, continual efforts to minimize inconsistencies in the simulated configurations introduced by experimental setups are important. The presence of air voids, water gaps, and other materials foreign to the contemplated design introduce uncertainties in the application of the data that should be avoided wherever possible.

VI. LID TANK CONFIGURATIONS AND MEASUREMENTS

F. N. Watson

In the preceding sections of this report the interpretation and application of the data from the tests on the RMR shield assembly have been discussed. In this section all the configurations and corresponding gamma and neutron measurements are presented together with a brief description of the Lid Tank Facility and the special techniques, materials, and instruments used.

Lid Tank Facility

The Lid Tank Facility consists of a large water tank adjacent to an opening in the concrete shield of the Oak Ridge Graphite Reactor (X-10 Pile). A shield mockup is inserted in the tank and the transmitted radiation is measured behind it. Sections of the shield which should be kept dry are usually held in one or more of the standard 15-in. tanks which are open at the top and are 64 in. wide by 60 in. high. The 1/8 in. thick steel walls of these tanks are held under drum head tension but are subject to deformation when inside pressure is not equal to outside pressure. Obviously when one of these tanks is placed in a mockup there are water gaps between the tank walls and adjacent materials; these gaps generally cannot be measured directly and their thicknesses are calculated on the basis of measurable quantities.

The lead slabs used in the tests were either 1 or 1-1/2 in. thick as noted. All the slabs were mounted in 1 1-1/2 in. thick iron frames which caused a 1/4-in. gap between a 1-in. slab and any non-liquid adjacent material.

Techniques Pertinent to the RMR Tests

As the RMR tests progressed some changes in the basic experimental arrangement of the shield mockups were made. These changes are listed below:

Configuration 1. In configuration 1 an air-filled aluminum wafer was inserted between the beryllium pellet tank and the 15-in. dry tank. Since its thickness was unstable and immeasurable it was not used in the mockups which followed.

Configurations 1 through 38. The beryllium used in the first 38 mockups was in two forms: (1) beryllium pellets held in a waterproof iron container and (2) a slab of solid beryllium held (with other materials) in a dry iron tank.

Configurations 39 through 77. The beryllium used in these mockups was of solid form held in an aluminum tank with the exception of configuration 54 which was a repeat of configuration 17.

Configurations 39 through 53. A special 30-in. dry tank which held all the dry components of the mockups was used in these configurations.

Configuration 43. The B^{10} tank used in this experiment had an effective diameter of 34-1/2 in. As it was felt that neutrons perhaps were passing around this tank, 1/4-in. boral slabs 2 ft wide were inserted to the left and right of the B^{10} tank for this configuration.

Configurations 55 through 77. A 24-in. extension was welded to the 30-in. tank mentioned above. It was filled with borated water, and the plain water gap between the dry tank and the borated water tank was eliminated.

Configurations 70 through 72. The 3-in. thick natural uranium used in configurations 70 and 71 was 3 by 3 ft. Since there was some streaming around the uranium slab, a 4-in. thick lead brick yoke was built around it to reduce the streaming in configuration 72.

Description of Tanks Used in Mockups

Throughout the tests tanks containing various materials simulated sections of the RMR and shield. These tanks with their thicknesses and densities are listed as follows:

Tank	Material and Density	Thickness (cm)
Be Pellet Tank 1	Fe wall	0.3
	Be Pellets (ρ = 1.233 g/cc)	28.5
	Fe Wall	0.3
		29.1
B_4C Tanks	Al Wall	0.16
	B_4C* (ρ = 1.9 g/cc)	2.70
	Al Wall	0.16
		3.02
NaF Tanks 1 and 2	Fe Wall	0.48
	NaF (ρ = 0.96 g/cc)	2.54
	Fe Wall	0.48
		3.50
NaF Tanks 3 and 4	Fe Wall	0.48
	NaF (ρ = 0.96 g/cc)	4.44
	Fe Wall	0.48
		5.40
WC Tank	Fe Wall	0.635
	WC (ρ = 8.05 g/cc)	5.08
	Fe Wall	0.635
		6.35
Be Tank 2	Al Wall	0.64
	Be (ρ = 1.84 g/cc)	7.30
	Al	0.16
	Stainless Steel	0.03
	Be (ρ = 1.84 g/cc)	7.30
	Al	0.16
	Stainless Steel	0.02
	Be (ρ = 1.84 g/cc)	14.61
	Blotter Paper	0.15
	Al Wall	0.64
		31.01
B^{10} Tank	Stainless Steel	0.05
	B^{10} Powder	1.53
	Aluminum	1.52
		3.1

* 45.9% boron, 36.9% carbon, plus silicon oxide and organic compounds.

Tank	Material and Density	Thickness (cm)
Li Tank 1	Fe Wall	0.64
	Lithium (ρ = 0.534 g/cc)	2.54
	Fe Wall	0.64
		3.82
Li Tank 2	Fe Wall	0.48
	Lithium (ρ = 0.534 g/cc)	3.65
	Fe Wall	0.48
		4.61
Air Wafer	Al Wall	0.16
	Air	Variable
	Al Wall	0.16
		Variable

Instrumentation

All radiation measurements were taken in plain water behind each configuration except for those measurements made inside the borated water section of the shield. Since, as is usually the case in shield testing, wide ranges of intensities were encountered, a number of instruments were used as follows:

Gamma-Ray Dose Measurements

(1) CO_2-filled ion chamber, 10^{10} ohms to ground, with electrometer circuit;

(2) 1/2-in. anthracene crystal with photomultiplier tube and electrometer circuit;[1]

(3) 1-1/4-in. anthracene crystal with photomultiplier tube and electrometer cricuit;[1]

(4) 1-1/4-in. anthracene crystal with photomultiplier tube, preamplifier, A-1 amplifier, pulse sorter, and binary scaler.[1]

1 F. K. McGowan and C. E. Clifford, "Application of a Scintillation Detector to Gamma-ray Dosimetry," CF-51-10-212 (Oct. 16, 1951).

Thermal-Neutron Flux Measurements

(1) 3-in. U^{235} fission plate with preamplifier, A-1 amplifier, pulse height selector, and scaler;

(2) 12-1/2-in. BF_3 "single barrel" counter with preamplifier, A-1 amplifier, pulse height selector, and scaler;

(3) 12-1/2-in. BF_3 "double barrel" counter with preamplifier, A-1 amplifier, pulse height selector, and scaler.

Fast-Neutron Dose Measurements

(1) Hurst-type fast-neutron dosimeter with preamplifier, A-1 amplifier, pulse sorter, and binary scaler.[2]

The gamma data for this experiment ranged from 10^3 to 10^{-3} mr/hr and neutron data ranged from 10^8 to 10^{-2} neutrons/(cm^2·sec) and the errors encountered varied somewhat with the intensity of the radiation to be measured. The probable sources of error and approximate contributions of each major type of error are listed as follows:

Counting Errors	±8% (for normal data)
	±12% (for low-intensity data*)

(1) Varying backgrounds;

(2) With large amounts of lead shielding the background outside the Lid Tank is at a higher level than gamma dose inside the tank;

(3) Extraneous pulses may be thrown into counting circuits from other electrical apparatus;

(4) Counter position may be incorrectly recorded;

(5) Operator's techniques vary slightly;

(6) Temperature fluctuations in Lid Tank water and in instrument room air may alter response of instrument.

2 G. S. Hurst, "Fast Neutron Count-Rate Dosimetry," ORNL-589 (Feb. 17, 1950).
* Gamma data less than 5×10^{-2} mr/hr.

Calibration Errors ±2% (for normal data)

±12% (for low-intensity data*)

(1) Varying backgrounds;

(2) Wall scattering effects on indoor calibrations;

(3) Variations in source spectra.

The repeatability of the data may be observed and is quite valuable in shield comparisons. In considering curves only and not individual points, gamma dose values appear to be repeatable with variations of less than ±15% for gamma doses less than 10^{-1} mr/hr and with variations less than ±10% for gamma doses greater than 10^{-1} mr/hr. Neutron curves are repeatable to ±10%.

As an example, configuration 54 was a repetition of configuration 17 except that the borated water in 54 contained 1% boron by weight whereas borated water in 17 contained 2.8% boron. In configuration 54 the gamma doses were 5% lower than in configuration 17 and should have been less than 1% higher. A period of 10 weeks elapsed between these measurements and different operators ran the instruments. The same calibration techniques and the same shielding materials were used.

In another case configuration 64 was repeated after a period of two weeks. In configuration 64R the gamma dose was 10% higher.

Some error is introduced in the measurement of the thicknesses of the various components of the shield mockups. This error is the greater of ±2 mm or ±2% but not exceeding ±2 cm and is attributed to:

(1) Warpage of slabs;

(2) Bulging of tank walls;

---

* Gamma data less than 5×10^{-2} mr/hr.

(3) Inability to measure air and water gaps as a result of items (1) and (2) which tends to make a cumulative error in gap measurements.

RMR Mockups (Configurations 1 through 77)

A summary of the Lid Tank mockups of the RMR and shield is given in Table VI-1. The configurations are given in more detail in Figs. VI-1 through VI-28 in which schematic diagrams of all the mockups are shown. Tabulated thicknesses of all the shield components are presented on pages opposite the sketches.

The reporting of certain shield component thicknesses to the nearest hundredth of a centimeter and others to the nearest tenth of a centimeter is an apparent inconsistency. This was permitted in view of the fact that even the smallest thicknesses of such components as steel, water, and boron may be extremely important while the specification of the thicknesses of other materials to this accuracy is unnecessary.

Radiation Measurements behind RMR Mockups

Since the gamma dose behind the RMR mockups was of primary concern in these tests, gamma-ray measurements were made behind each configuration. These measurements are presented in Figs. VI-29 through VI-47 and Tables VI-2 through VI-20. Reference should be made to sections III and IV of this report for interpretation of the data.

As was mentioned in section III, the neutron dose was relatively insensitive to most changes in the shield. Because of this, neutron measurements were not made behind each mockup. In regions where the fast-neutron dosimeter could not be used, thermal-neutron flux measurements were made. The thermal-neutron data are given in Figs. VI-48 through VI-61 and Tables VI-21 through

VI-34. Fast-neutron measurements are presented in Figs. VI-62 through VI-66 and Tables VI-35 through VI-37.

It should be noted that for configuration 15 (Fig. VI-63 and Table VI-36) the fast-neutron data is presented in such a manner as to enable one to approximate fast-neutron dose from thermal-neutron flux where the relaxation length of the thermal-neutron flux curve is greater than 8 cm.

TABLE VI-1 SUMMARY OF LID TANK MOCKUPS OF REFLECTOR-MODERATED REACTOR AND SHIELD

CONFIGURATION NUMBER	REFLECTOR	NEUTRON CURTAIN	HEAT EXCHANGER	NEUTRON CURTAIN	PRESSURE SHELL	GAMMA SHIELD[a]	LIQUID NEUTRON SHIELD[b]	OTHER INFORMATION
1	Be pellet tank,[c] 9.2 cm of solid Be	B_4C tank[d]	NaF tanks[e] 1, 2	B_4C tank	1 3/4 in. of Fe	None	Plain H_2O	Air wafer[f] inserted between Be reflector elements
1a	"	"	"	"	"	"	"	No air wafer used
2	"	"	"	"	"	2 1/2 in. of Pb (D)	"	
3	"	"	"	"	"	4 1/2 in. of Pb (D)	"	Last 2 in. of Pb in 15-in. dry tank, leaving large (~11 in.) air void after Pb
4	"	"	"	"	"	7 1/2 in. of Pb (D)	"	Large air void after Pb
5	"	"	"	"	"	2 1/2 in. of Pb (D), 5 in. of Pb (W)	"	Air void replaced with H_2O
6	"	"	"	"	"	"	"	Outer 3 in. of Pb moved out, leaving 12-cm H_2O gap
7	"	"	"	"	"	2 1/2 in. of Pb (D), 2 in. of Pb (W)	"	Same as configuration 3 except air void replaced with H_2O
8	"	"	"	"	"	2 1/2 in. of Pb (D), 5 in. of Pb (W)	"	4-cm H_2O gap preceded each of last four Pb slabs
9	"	"	"	"	"	"	10 in. of borated H_2O (1% B)	Borated H_2O replaced plain H_2O in 15-in. tank; 4-cm borated H_2O gap preceded each of last four Pb slabs
10	"	"	"	"	"	"	"	Last four Pb slabs moved toward source
11	"	"	"	"	"	"	10 in. of borated H_2O (0.9% B)	Last four Pb slabs moved toward source
12	"	"	"	"	"	"	10 in. of borated H_2O (2.8% B)	4-in. borated H_2O gap preceded last 3 in. of Pb
13	"	"	"	"	"	"	"	Last 3 in. of Pb moved toward source
14	"	"	"	"	"	2 1/2 in. of Pb (D), 2 in. of Pb (W)	13 in. of borated H_2O (2.8% B)	
15	"	"	NaF tanks 1, 2, 3, 4	"	"	None	Plain H_2O	
16	"	"	"	"	"	3 in. of Pb (W)	12 in. of borated H_2O (2.8% B)	
17	"	"	"	"	"	6 in. of Pb (W)	9 in. of borated H_2O (2.8% B)	
18	"	"	"	"	"	7 1/2 in. of Pb (W)	7 1/2 in. of borated H_2O (2.8% B)	
19	Be pellet tank, 1/4 in. of boral, 3 1/4 in. of H_2O, 1/4 in. of boral, 9.2 cm of solid Be	"	"	None	"	"	7 1/2 in. of borated H_2O (2.3% B)	
20a	"	"	"	"	"	3 in. of Pb (W)	12 in. of borated H_2O (2.3% B)	

TABLE VI-1 (continued)

CONFIGURATION NUMBER	REFLECTOR	NEUTRON CURTAIN	HEAT EXCHANGER	NEUTRON CURTAIN	PRESSURE SHELL	GAMMA SHIELD	LIQUID NEUTRON SHIELD	OTHER INFORMATION
20*b*	Be pellet tank, 1/4 in. of boral, 3 1/4 in. of H_2O, 1/4 in. of boral, 9.2 cm of solid Be	B_4C tank	NaF tanks 1, 2, 3, 4	None	1 3/4 in. of Fe	4 1/2 in. of Pb (W)	10 1/2 in. of borated H_2O (2.3% B)	
20*c*	"	"	"	"	"	6 in. of Pb (W)	9 in. of borated H_2O (2.3% B)	
20*d*	"	"	"	"	"	7 1/2 in. of Pb (W)	7 1/2 in. of borated H_2O (2.3% B)	
20*e*	"	"	"	"	"	7 1/2 in. of Pb (W), 1/8 in. of boral (W)	7 3/8 in. of borated H_2O (2.3% B)	
21	"	"	"	"	"	6 in. of Pb (W)	9 in. of borated H_2O (2.3% B), 15 in. of oil	Oil (ρ = 0.88 g/cm^3) placed in 15-in. tank behind borated H_2O tank
22	"	"	"	"	"	None	Plain H_2O	
23	"	"	"	"	"	"	"	Fe pressure shell in plain H_2O just outside dry tank, leaving 5-cm air void in tank
24	"	"	"	"	2 in. of Ni	"	"	Ni pressure shell in plain H_2O just outside dry tank
25	"	"	"	"	2 in. of Cu	"	"	Cu pressure shell in plain H_2O just outside dry tank
26	"	"	"	"	2 in. of Cu, 2 in. of Ni	"	"	Cu and Ni pressure shell in plain H_2O just outside dry tank
27	Be pellet tank, 3 in. of H_2O, 9.2 cm of solid Be	"	"	"	1 3/4 in. of Fe	"	"	
28	Be pellet tank, 1/4 in. of boral, 9/10 in. of H_2O, 1/4 in. of boral, 9.2 cm of solid Be	"	"	"	"	"	"	
29	Be pellet tank, 1/4 in. of boral, 3 1/4 in. of H_2O, 1/4 in. of boral, 9.2 cm of solid Be	"	"	"	None	"	"	
30	"	"	"	"	2 in. of Inconel	"	"	Inconel pressure shell in plain H_2O just outside dry tank
31	1 1/2 in. of Pb, Be pellet tank, 9.2 cm of solid Be	"	"	"	1 3/4 in. of Fe	"	"	
32	Be pellet tank, 9.2 cm of solid Be	"	"	"	"	"	"	
33	"	"	"	"	"	1/4 in. of boral (W), WC tank[g] (W)	"	
34	"	"	"	"	"	WC tank (W), 1/4 in. of boral (W)	"	
35	"	"	"	"	"	WC tank (W)	"	
36	"	"	"	"	"	WC tank (W), 1 1/2 in. of Pb (W)	"	
37	"	"	"	"	"	WC tank (W), 3 in. of Pb (W)	"	

TABLE VI-1 (continued)

CONFIGURATION NUMBER	REFLECTOR	NEUTRON CURTAIN	HEAT EXCHANGER	NEUTRON CURTAIN	PRESSURE SHELL	GAMMA SHIELD	LIQUID NEUTRON SHIELD	OTHER INFORMATION
38	Be pellet tank, 9.2 cm of solid Be	B_4C tank	NaF tanks 1, 2, 3, 4	None	1 3/4 in. of Fe	3 in. of Pb (W), WC tank (W)	Plain H_2O	
39	Be tank[h]	B^{10} tank[i]	"	"	"	6 in. of Pb (D)	"	Began using new tank which held all dry components of shield
40	"	"	"	"	"	"	"	1/4 in. of boral in plainwater just outside large dry tank
41	"	"	"	"	"	"	"	1/4 in. of boral just inside and 1/4 in. of boral just outside large tank
42	"	"	"	"	"	"	"	1/4 in. of boral just inside large tank
43	"	"	"	"	"	"	"	B^{10} tank spliced out 2 ft on each side with 1/4 in.-thick boral slabs
44	"	"	"	"	"	3 in. of Pb (D), 3/4 in. of H_2O,[j] 3 in. of Pb (D)	"	Boral splicing removed
45	"	"	"	"	"	1 1/2 in. of Pb (D), 1/4 in. of boral (D), 3 in. of Pb (D), 1/4 in. of boral (D), 1 1/2 in. of Pb (D), 1/4 in. of Tybor[k]	"	
46	"	B_4C tank	"	"	"	"	"	
47	"	"	"	"	"	"	15 in. of borated H_2O (1% B)	
48	"	"	"	"	"	"	"	Air wafer inserted between borated H_2O tank and preceding tank
49	"	"	"	"	"	1 1/2 in. of Pb (D), 1/4 in. of boral (D), 3 in. of Pb (D), 1/4 in. of boral (D), 1 1/2 in. of Pb (D), 1/4 in. of Tybor (D), 1 1/2 in. of Pb (W)	13 1/2 in. of borated H_2O (1% B)	
50	"	"	"	"	"	1 1/2 in. of Pb (D), 1/4 in. of boral (D), 3 in. of Pb (D), 1/4 in. of boral (D)	15 in. of borated H_2O (1% B)	
51	"	"	"	B_4C tank	"	6 in. of Pb (D)	"	
52	"	"	"	None	"	3 in. of Pb (D), 3/4 in. of borated H_2O,[j] 3 in. of Pb (D)	"	
53	1 1/4 in. of Al, Be tank	"	"	"	"	6 in. of Pb (D)	"	
54	Same as configuration 17 except borated H_2O was 1% B instead of 2.8% B							
55	Be tank	"	"	B_4C tank	"	3 in. of Pb (D), 3/16 in. of plexibor[l] (D), 1 1/2 in. of Pb (D), 3/16 in. of plexibor (D), 1 1/2 in. of Pb (W)	22 1/2 in. of borated H_2O (1% B)	Section welded on tank containing dry components to hold liquid neutron shield and thus eliminate undesired water layers between tanks

TABLE VI-1 (continued)

CONFIGURATION NUMBER	REFLECTOR	NEUTRON CURTAIN	HEAT EXCHANGER	NEUTRON CURTAIN	PRESSURE SHELL	GAMMA SHIELD	LIQUID NEUTRON SHIELD	OTHER INFORMATION
56	Be tank	B_4C tank	NaF tanks 1, 2, 3, 4	3/16 in. of plexibor	1 3/4 in. of Fe	3 in. of Pb (D), 3/16 in. of plexibor (D), 1 1/2 in. of Pb (D), 3/16 in. of plexibor (D), 1 1/2 in. of Pb (W)	22 1/2 in. of borated H_2O (1% B)	
57	"	"	"	"	"	4 1/2 in. of Pb (D), 3/16 in. of plexibor (D), 1 1/2 in. of Pb (D), 3/16 in. of plexibor (D)	24 in. of borated H_2O (1% B)	
58	"	"	"	"	"	Four 1 1/2-in. Pb slabs (D), each preceded by 3/16 in. of plexibor; 3/16 in. of plexibor behind fourth slab	"	
59	"	"	"	B_4C tank	"	6 in. of Pb (D), 3/16 in. of plexibor (D)	"	
60	"	"	"	"	"	6 in. of Pb (D), 3/16 in. of plexibor (D), 1 1/2 in. of Pb (W)	22 1/2 in. of borated H_2O (1% B)	
61	"	"	NaF tanks 1, 2, 4	"	"	"	"	
62	"	"	"	"	"	6 in. of Pb (D), 3/16 in. of plexibor (D)	24 in. of borated H_2O (1% B)	
63	"	"	"	"	"	Four 1 1/2-in. Pb slabs (D), each preceded by 3/16 in. of plexibor; 3/16 in. of plexibor behind fourth slab	"	
64	"	"	NaF tanks 1, 4	"	"	Four 1 1/2-in. Pb slabs (D), each preceded by 3/16 in. of plexibor; 3/16 in. of plexibor behind fourth slab	"	
65	"	"	"	"	"	Three 1 1/2-in. Pb slabs (D), each preceded by 3/16 in. of plexibor; 3/16 in. of plexibor behind third slab	"	
66	Be tank, 9.2 cm of solid Be	"	"	"	"	Three 1 1/2-in. Pb slabs (D), 3/16 in. of plexibor behind each slab; 1 1/2 in. of Pb (W)	22 1/2 in. of borated H_2O (1% B)	
67	"	"	"	"	"	Three 1 1/2-in. Pb slabs (D), 3/16 in. of plexibor behind each slab; 3 in. of Pb (W)	21 in. of borated H_2O (1% B)	
68	"	"	"	"	"	Three 1 1/2-in. Pb slabs (D), 3/16 in. of plexibor behind each slab	24 in. of borated H_2O (1% B)	
69	"	"	NaF tanks 1, 2, 3, 4	"	"	1 1/2 in. of Pb (D), 3/16 in. of plexibor (D), 4 1/2 in. of Pb (W)	19 1/2 in. of borated H_2O (1% B)	
70	"	"	NaF tanks 1, 2, 4	"	"	3/16 in. of plexibor (D), 3 in. of U (D), 3/16 in. of plexibor (D)	24 in. of borated H_2O (1% B)	

TABLE VI-1 (continued)

CONFIGURATION NUMBER	REFLECTOR	NEUTRON CURTAIN	HEAT EXCHANGER	NEUTRON CURTAIN	PRESSURE SHELL	GAMMA SHIELD	LIQUID NEUTRON SHIELD	OTHER INFORMATION
71	Be tank, 9.2 cm of solid Be	B_4C tank	NaF tanks 1, 2, 4	B_4C tank	1 3/4 in. of Fe	3/16 in. of plexibor (D), 3 in. of U (D), 3/16 in. of plexibor (D), 1 1/2 in. of Pb (W)	22 1/2 in. of borated H_2O (1% B)	
72	"	"	"	"	"	3/16 in. of plexibor (D), 3 in. of U (D) plus Pb brick yoke,[m] 3/16 in. of plexibor (D)	24 in. of borated H_2O (1% B)	
73	Be tank	"	NaF tanks 1, 2, 3, 4	"	"	3 in. of Pb (D), 3/16 in. of plexibor (D), 1 1/2 in. of Pb (D), 3/16 in. of plexibor (D)	"	
74	"	"	"	"	"	"	24 in. of borated H_2O (0.5% B)	
75	"	"	"	"	"	"	24 in. of plain H_2O	
76	"	"	NaF tanks 1, 4	"	"	6 in. of Pb (D), 3/16 in. of plexibor (D)	24 in. of borated H_2O (1% B)	3-cm air void in gamma shield
77	"	"	Li tanks[n] 1, 2	"	"	Four 1 1/2-in. Pb slabs (D), each preceded by 3/16 in. of plexibor; 3/16 in. of plexibor behind fourth slab	"	This data should be compared with that taken behind configuration 64R rather than 64.

[a] Lead thicknesses in the gamma shield were made up of 1- and 1 1/2-in. slabs. Where possible, these slabs were grouped with the dry components of the shield, but in many cases it was necessary to place some of the slabs in the liquid neutron shield container. (D) indicates dry slabs; (W) indicates wet slabs, both for the plain and for the borated water.

[b] The borated water used in configurations 1 to 54 was contained in a separate tank. In configurations 55 to 77, the solution was contained in the wet section of a single large tank.

[c] Beryllium pellets (ρ = 1.233 g/cm^3) encased in iron; dimensions were 0.3 cm of Fe, 28.5 cm of Be, 0.3 cm of Fe, totaling 29.1 cm.

[d] Boron carbide (ρ = 1.9 g/cm^3) encased in aluminum; dimensions were 0.16 cm of Al, 2.70 cm of B_4C, 0.16 cm of Al, totaling 3.02 cm.

[e] Sodium fluoride (ρ = 0.96 g/cm^3) encased in iron; dimensions for tanks 1 and 2 were 0.48 cm of Fe, 2.54 cm of NaF, 0.48 cm of Fe, totaling 3.50 cm; dimensions for tanks 3 and 4 were 0.48 cm of Fe, 4.44 cm of NaF, 0.48 cm of Fe, totaling 5.40 cm.

[f] Air in wafer with 0.16-cm aluminum walls.

[g] Tungsten carbide pebbles (ρ = 8.05 g/cm^3) encased in iron; dimensions were 0.635 cm of Fe, 5.08 cm of WC, 0.635 cm of Fe, totaling 6.35 cm.

[h] Solid beryllium (ρ = 1.84 g/cm^3) blocks in aluminum tank. Additional aluminum and stainless steel within tank simulated reflector coolant tubes. Dimensions for the tank were 0.64 cm of Al, 7.30 cm of Be, 0.16 cm of Al, 0.03 cm of stainless steel, 7.30 cm of Be, 0.16 cm of Al, 0.02 cm of stainless steel, 14.61 cm of Be, 0.15 cm of blotter paper, 0.64 cm of Al, totaling 31.03 cm.

[i] Boron isotope 10; dimensions were 0.05 cm of stainless steel, 1.53 of B^{10} powder, 1.52 cm of Al, totaling 3.1 cm.

[j] The 3/4 in. of water was contained in a thin-walled aluminum tank.

[k] Tygon impregnated with boron.

[l] Plexiglas impregnated with boron.

[m] Uranium slab was 3 in. thick by 3 ft by 3 ft. Since the radiation cone from the source at the uranium slab position had a greater diameter than 3 ft, a 4-in.-thick yoke of lead bricks was built around the top and sides of the slab to reduce streaming.

[n] Lithium (ρ = 0.534 g/cm^3) encased in iron; dimensions for tank 1 were 0.64 cm of Fe, 2.54 cm of Li, 0.64 cm of Fe, totaling 3.82 cm; dimensions for tank 2 were 0.48 cm of Fe, 3.65 cm of Li, 0.48 cm of Fe, totaling 4.61 cm.

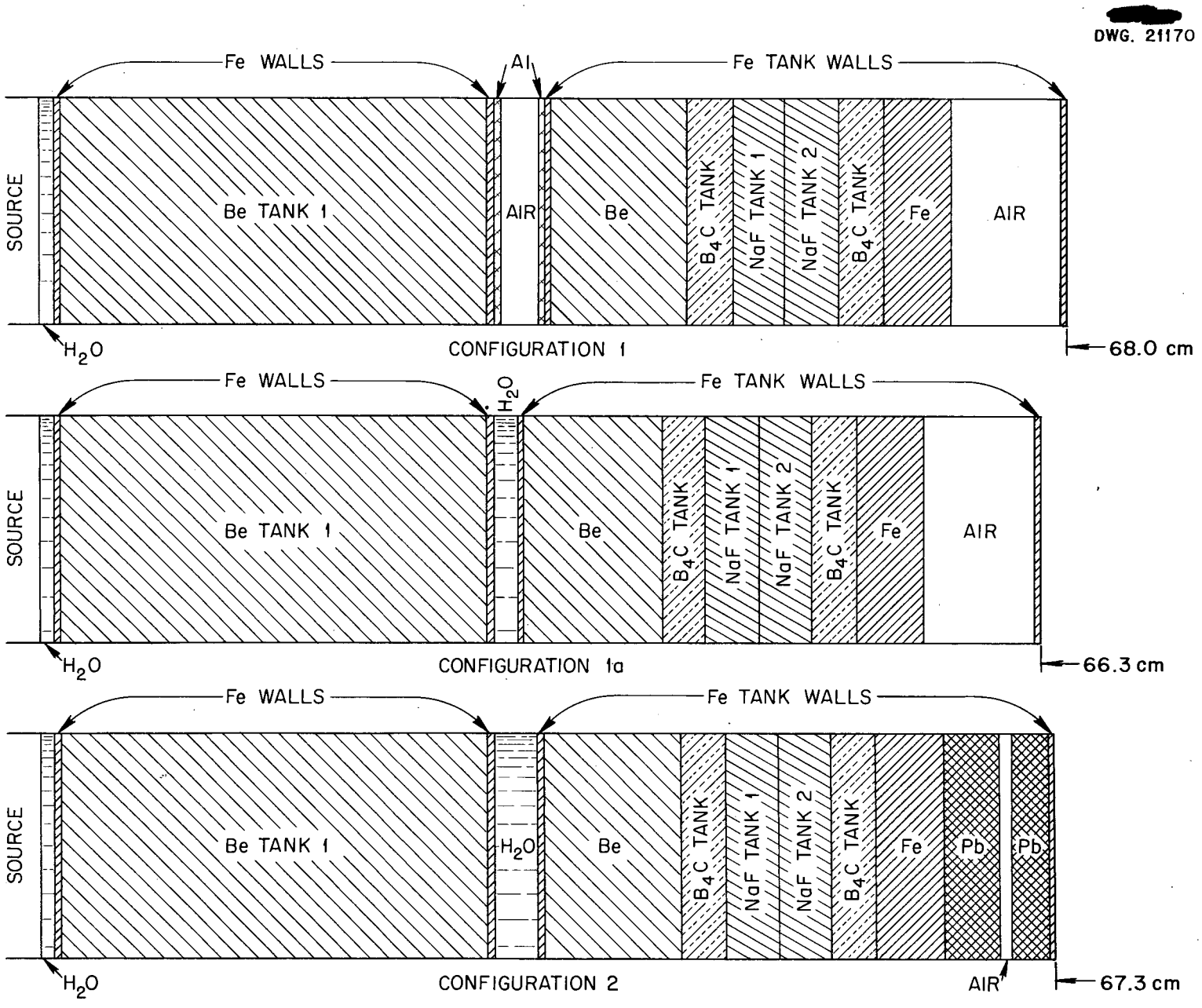

Fig. VI-1. Lid Tank Mockups of Reflector-Moderated Reactor and Shield

Configurations 1, 1a, and 2

Component	Thickness of Component (cm)		
	Configuration 1	Configuration 1a	Configuration 2
H_2O	0.9	0.9	0.9
Be Tank 1	29.1	29.1	29.1
Al	0.16	-	-
Air	3.0	-	-
Al	0.16	-	-
H_2O		1.6	3.0
Fe	0.32	0.32	0.32
Be (ρ = 1.84 g/cc)	9.2	9.2	9.2
B_4C Tank	3.0	3.0	3.0
NaF Tank 1	3.5	3.5	3.5
NaF Tank 2	3.5	3.5	3.5
B_4C Tank	3.0	3.0	3.0
Fe	4.45	4.45	4.45
Pb	-	-	3.81
Air	7.4	7.4	0.64
Pb	-	-	2.54
Fe	0.32	0.32	0.32
Total	68.0	66.3	67.3

[redacted]
DWG. 21171

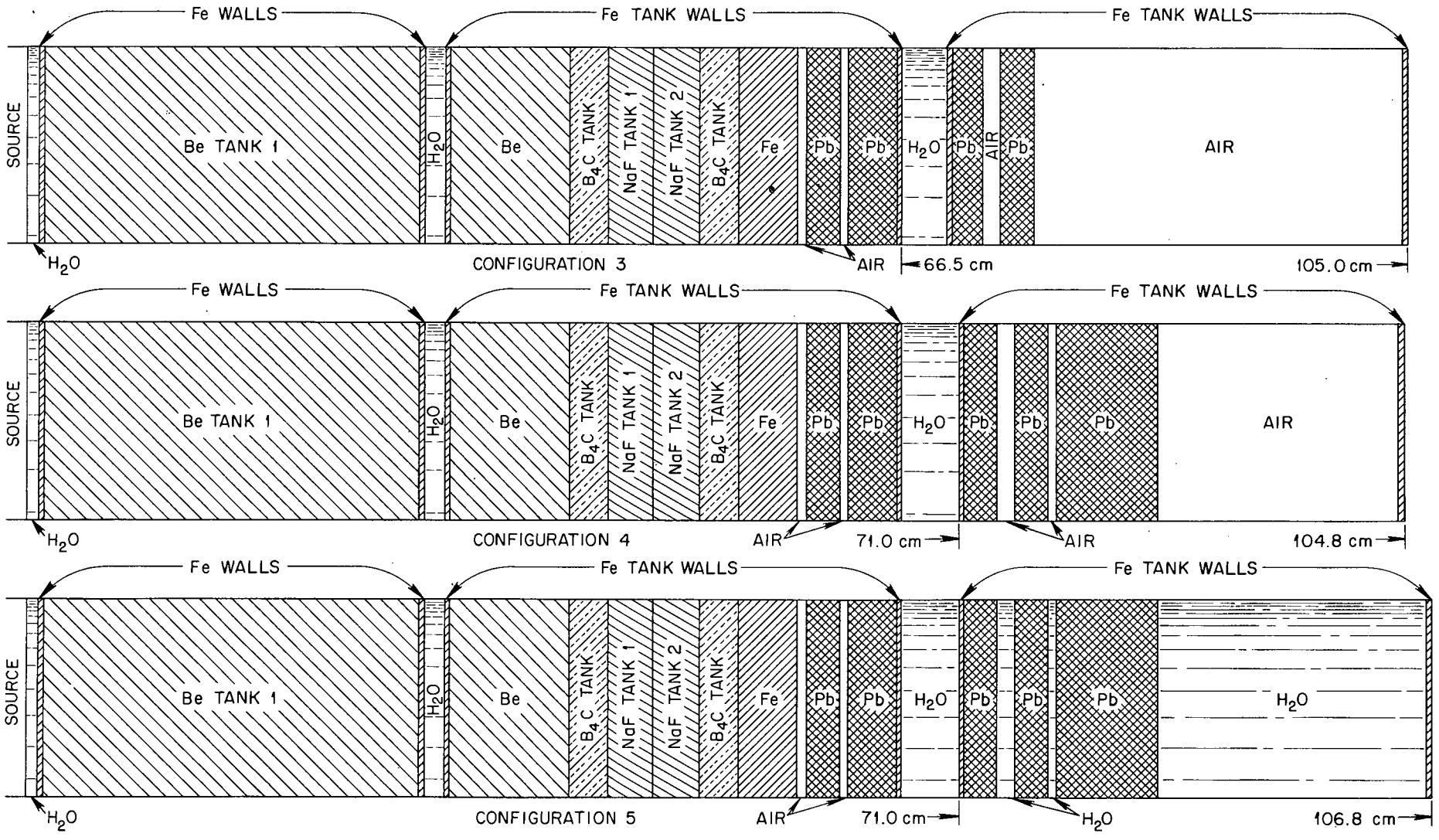

Fig. VI-2. Lid Tank Mockups of Reflector-Moderated Reactor and Shield.

Configurations 3, 4, and 5

Component	Thickness of Component (cm)		
	Configuration 3	Configuration 4	Configuration 5
H_2O	0.9	0.9	0.9
Be Tank 1	29.1	29.1	29.1
H_2O	1.6	1.6	1.6
Fe	0.32	0.32	0.32
Be (ρ = 1.84 g/cc)	9.2	9.2	9.2
B_4C Tank	3.0	3.0	3.0
NaF Tank 1	3.5	3.5	3.5
NaF Tank 2	3.5	3.5	3.5
B_4C Tank	3.0	3.0	3.0
Fe	4.45	4.45	4.45
Air	0.64	0.64	0.64
Pb	2.54	2.54	2.54
Air	0.64	0.64	0.64
Pb	3.81	3.81	3.81
Fe	0.32	0.32	0.32
H_2O	3.4	4.5	2.2
Fe	0.32	0.32	0.32
Pb	2.54	2.54	-
H_2O	-	-	0.64
Air	1.27	1.27	-
Pb	2.54	2.54	2.54
H_2O	-	-	1.27
Air	28.1	0.64	-
Pb	-	-	2.54
H_2O	-	-	0.64
Pb	-	7.62	7.62
Air	-	18.5	-
H_2O	-	-	22.2
Fe	0.32	0.32	0.32
Total	105.0	104.8	106.8

DWG. 21172

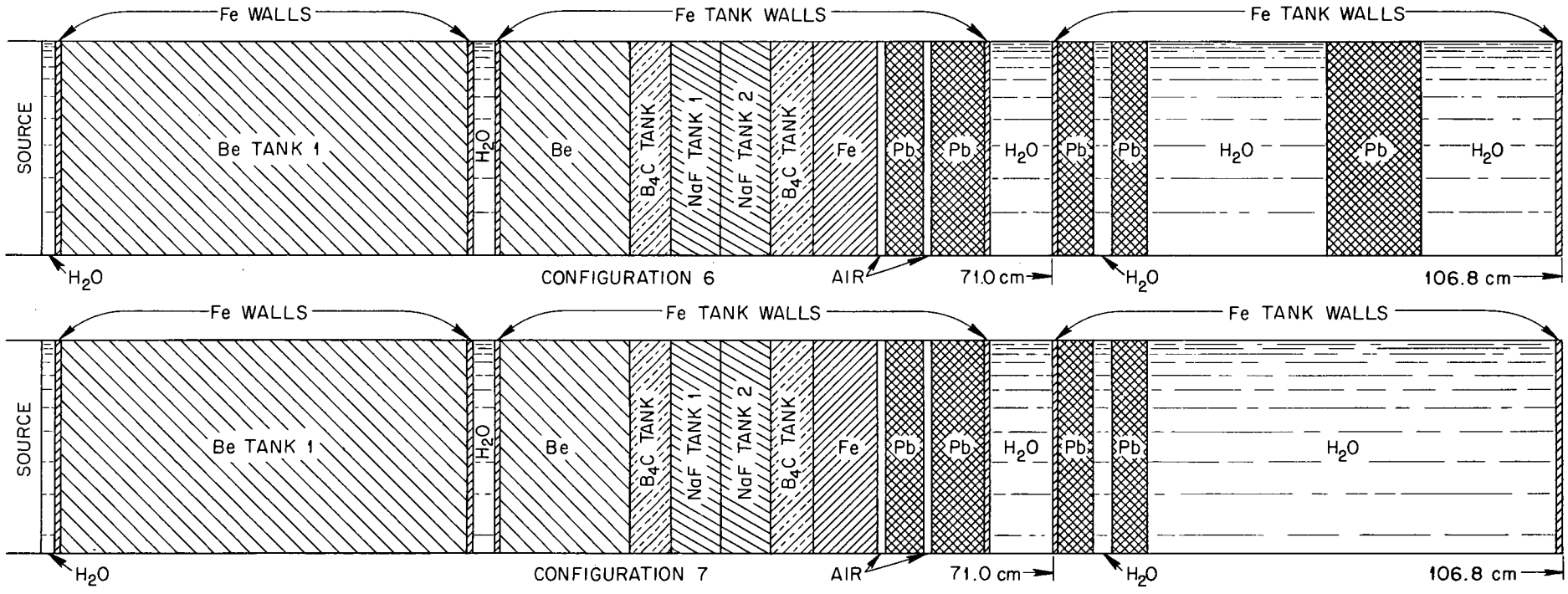

Fig. VI-3. Lid Tank Mockups of Reflector – Moderated Reactor and Shield.

Configurations 6 and 7

Component	Thickness of Component (cm)	
	Configuration 6	Configuration 7
H_2O	0.9	0.9
Be Tank 1	29.1	29.1
H_2O	1.6	1.6
Fe	0.32	0.32
Be (ρ = 1.84 g/cc)	9.2	9.2
B_4C Tank	3.0	3.0
NaF Tank 1	3.5	3.5
NaF Tank 2	3.5	3.5
B_4C Tank	3.0	3.0
Fe	4.45	4.45
Air	0.64	0.64
Pb	2.54	2.54
Air	0.64	0.64
Pb	3.81	3.81
Fe	0.32	0.32
H_2O	2.2	2.2
Fe	0.32	0.32
H_2O	0.64	0.64
Pb	2.54	2.54
H_2O	1.27	1.27
Pb	2.54	2.54
H_2O	12.64	30.5
Pb	7.62	-
H_2O	10.2	-
Fe	0.32	0.32
Total	106.8	106.8

[redacted]
DWG. 21173

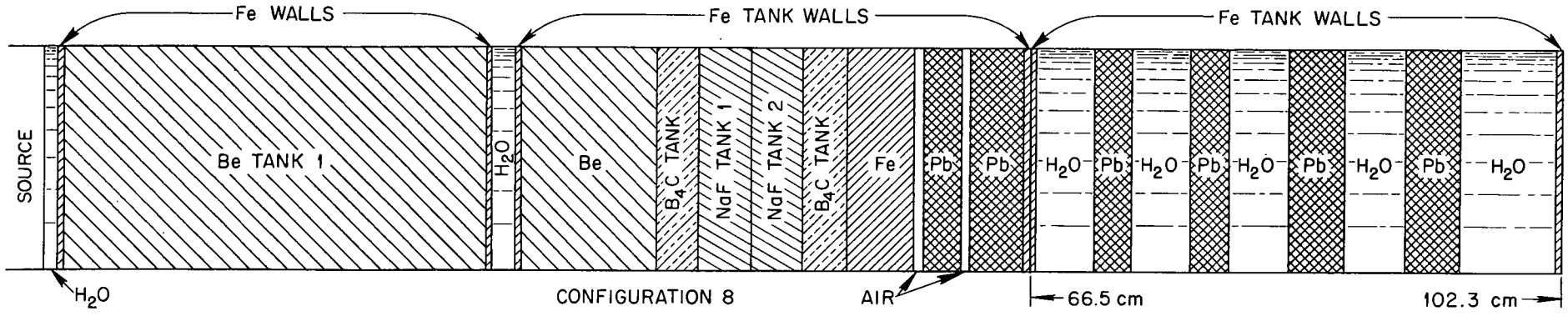

CONFIGURATION 9 SAME AS CONFIGURATION 8 EXCEPT H_2O IN Fe TANK WAS BORATED TO 1.0 % B BY WEIGHT.

Fig. VI-4. Lid Tank Mockups of Reflector - Moderated Reactor and Shield.

Configurations 8 and 9

Component	Thickness of Component (cm)	
	Configuration 8	Configuration 9
H_2O	0.9	0.9
Be Tank 1	29.1	29.1
H_2O	1.6	1.6
Fe	0.32	0.32
Be (ρ = 1.84 g/cc)	9.2	9.2
B_4C Tank	3.0	3.0
NaF Tank 1	3.5	3.5
NaF Tank 2	3.5	3.5
B_4C Tank	3.0	3.0
Fe	4.45	4.45
Air	0.64	0.64
Pb	2.54	2.54
Air	0.64	0.64
Pb	3.81	3.81
Fe[a]	0.64	0.64
H_2O	4.0	-
1% Borated H_2O	-	4.0
Pb	2.54	2.54
H_2O	4.0	-
1% Borated H_2O	-	4.0
Pb	2.54	2.54
H_2O	4.0	-
1% Borated H_2O	-	4.0
Pb	3.81	3.81
H_2O	4.0	-
1% Borated H_2O	-	4.0
Pb	3.81	3.81
H_2O	6.44	-
1% Borated H_2O	-	6.44
Fe	0.32	0.32
Total	102.3	102.3

(a) Two adjacent 0.32-cm tank walls.

[redacted]
DWG. 21174

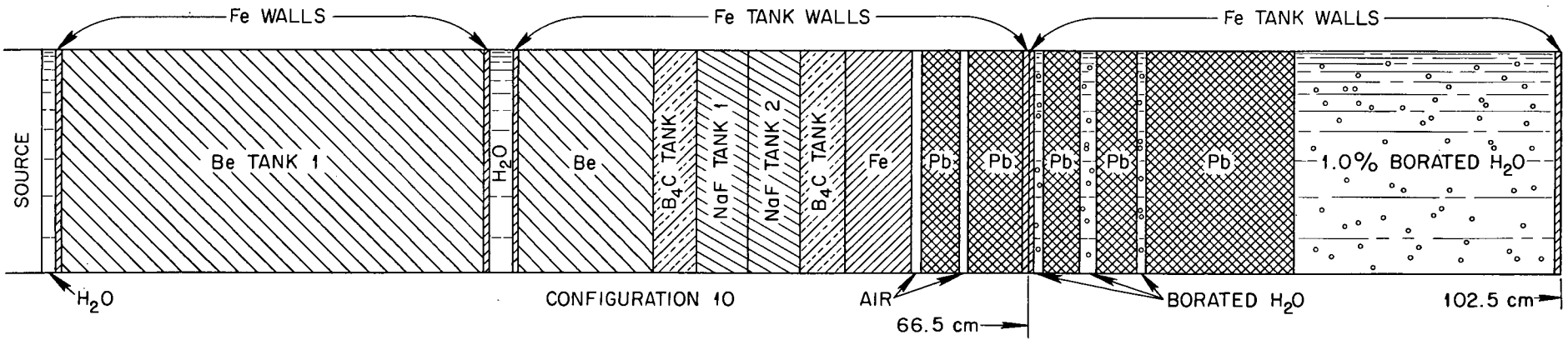

CONFIGURATION 11 SAME AS CONFIGURATION 10 EXCEPT H_2O WAS BORATED TO 0.9% B BY WEIGHT.

Fig. VI-5. Lid Tank Mockups of Reflector – Moderated Reactor and Shield.

Configurations 10 and 11

Component	Component Thickness (cm)	
	Configuration 10	Configuration 11
H_2O	0.9	0.9
Be Tank 1	29.1	29.1
H_2O	1.6	1.6
Fe	0.32	0.32
Be (ρ = 1.84 g/cc)	9.2	9.2
B_4C Tank	3.0	3.0
NaF Tank 1	3.5	3.5
NaF Tank 2	3.5	3.5
B_4C Tank	3.0	3.0
Fe	4.45	4.45
Air	0.64	0.64
Pb	2.54	2.54
Air	0.64	0.64
Pb	3.81	3.81
Fe[a]	0.64	0.64
1% Borated H_2O	0.64	-
0.9% Borated H_2O[b]	-	0.64
Pb	2.54	2.54
1% Borated H_2O	1.27	-
0.9% Borated H_2O[b]	-	1.27
Pb	2.54	2.54
1% Borated H_2O	0.64	-
0.9% Borated H_2O[b]	-	0.64
Pb	7.62	7.62
1% Borated H_2O	19.9	-
0.9% Borated H_2O[b]	-	19.9
Fe	0.32	0.32
Total	102.3	102.3

(a) Two adjacent 0.32-cm tank walls.

(b) In configuration 11 enough B_2O_3 was added to give a 2.8% borated H_2O solution; however, changes in temperature caused crystallization of the B_2O_3 on the Pb slabs and the resulting solution was 0.9% B by weight. The application of steam heat eliminated crystallization in the succeeding configurations.

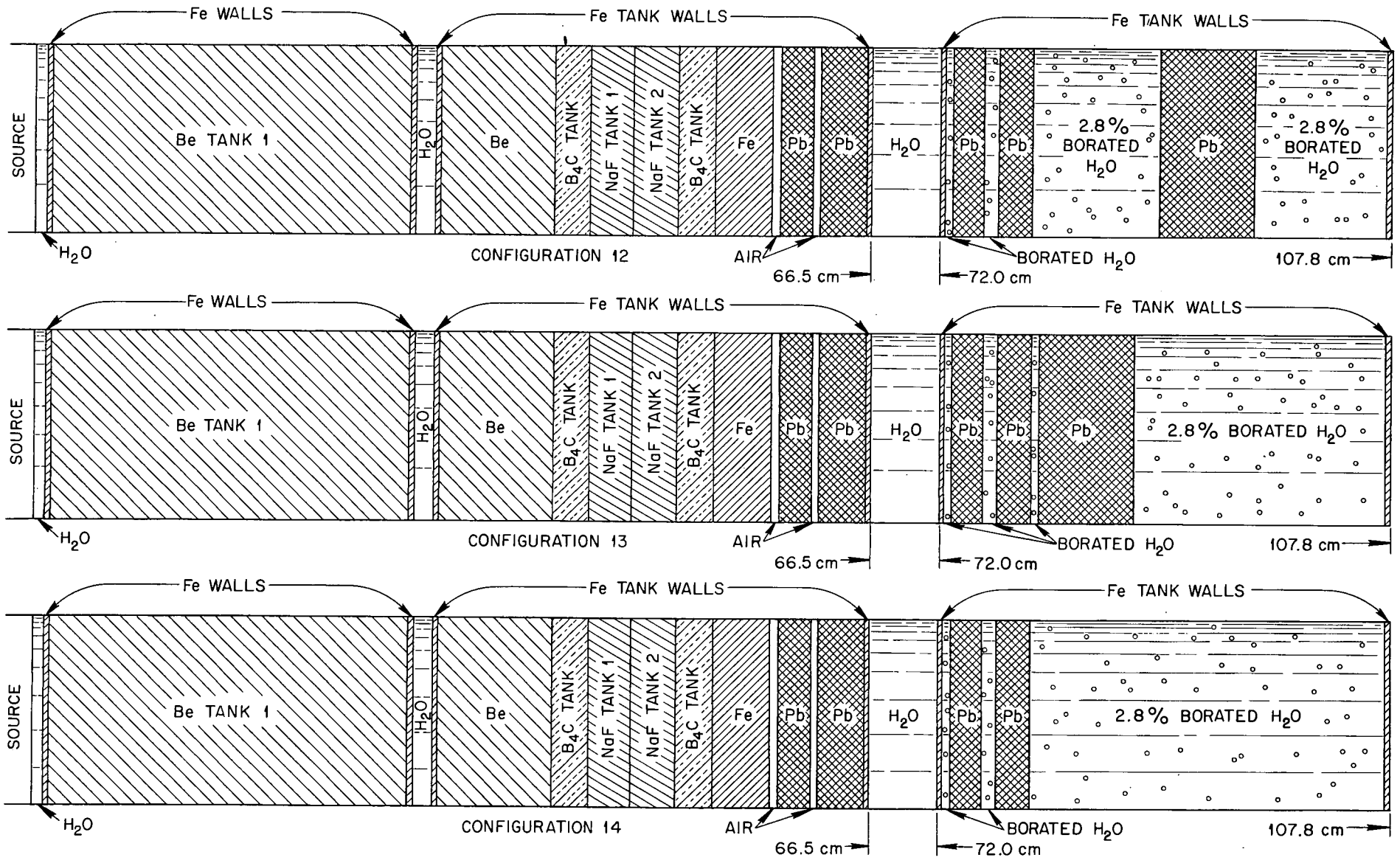

Fig. VI-6. Lid Tank Mockups of Reflector – Moderated Reactor and Shield.

Configurations 12, 13, and 14

Component	Component Thickness (cm)		
	Configuration 12	Configuration 13	Configuration 14
H_2O	0.9	0.9	0.9
Be Tank 1	29.1	29.1	29.1
H_2O	1.6	1.6	1.6
Fe	0.32	0.32	0.32
Be (ρ = 1.84 g/cc)	9.2	9.2	9.2
B_4C Tank	3.0	3.0	3.0
NaF Tank 1	3.5	3.5	3.5
NaF Tank 2	3.5	3.5	3.5
B_4C Tank	3.0	3.0	3.0
Fe	4.45	4.45	4.45
Air	0.64	0.64	0.64
Pb	2.54	2.54	2.54
Air	0.64	0.64	0.64
Pb	3.81	3.81	3.81
Fe	0.32	0.32	0.32
H_2O	3.1	3.1	3.1
Fe	0.32	0.32	0.32
2.8% Borated H_2O	0.64	0.64	-
2.9% Borated H_2O	-	-	0.64
Pb	2.54	2.54	2.54
2.8% Borated H_2O	1.27	1.27	-
2.9% Borated H_2O	-	-	1.27
Pb	2.54	2.54	2.54
2.8% Borated H_2O	10.2	0.64	-
2.9% Borated H_2O	-	-	30.56
Pb	7.62	7.62	-
2.8% Borated H_2O	12.7	22.3	-
Fe	0.32	0.32	0.32
Total	107.8	107.8	107.8

[redacted]

DWG. 21176

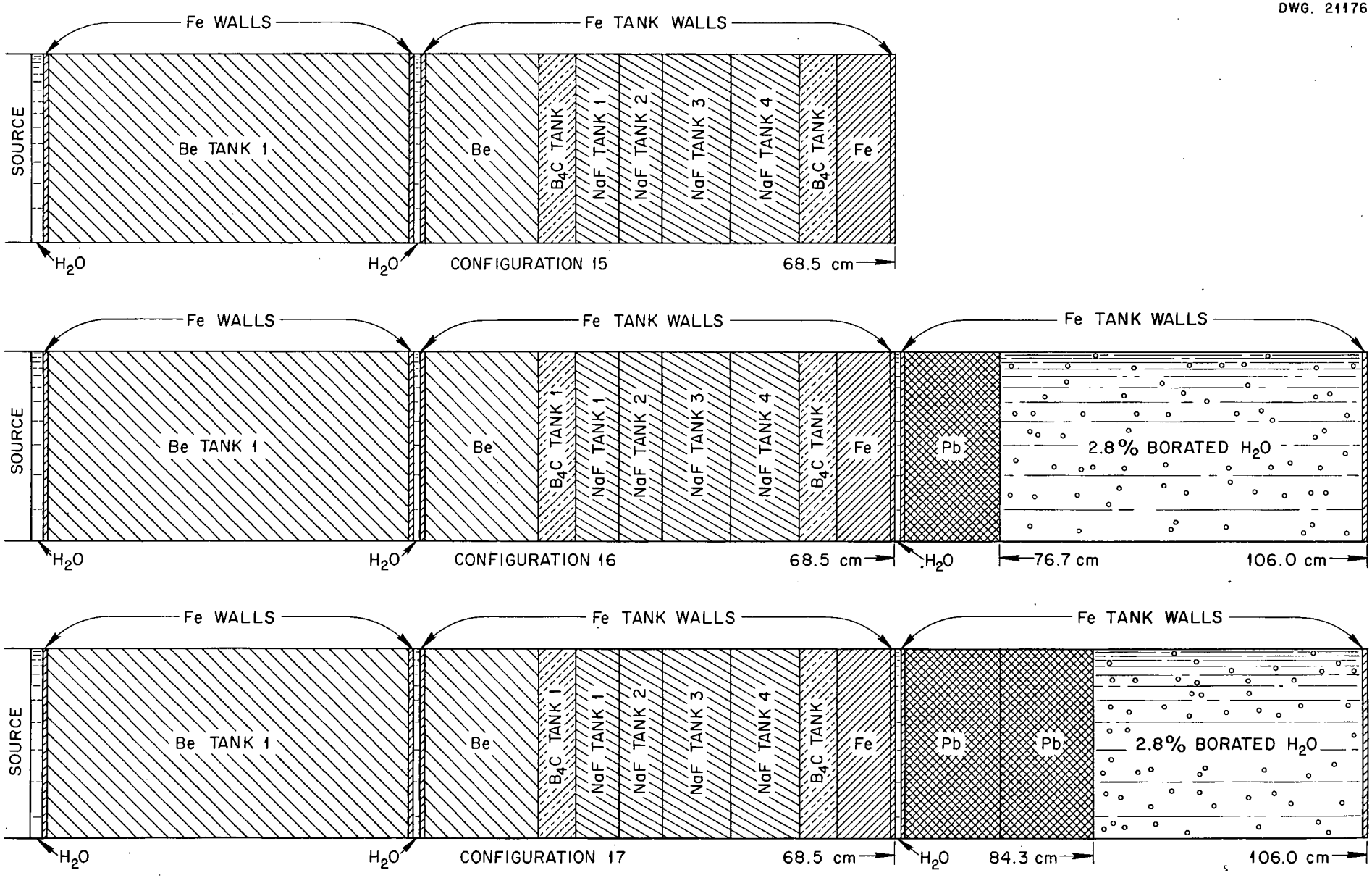

Fig. VI-7. Lid Tank Mockups of Reflector — Moderated Reactor and Shield.

Configurations 15, 16, and 17

Component	Component Thickness (cm)		
	Configuration 15	Configuration 16	Configuration 17
H_2O	0.9	0.9	0.9
Be Tank 1	29.1	29.1	29.1
H_2O	0.4	0.4	0.4
Fe	0.32	0.32	0.32
Be (ρ = 1.84 g/cc)	9.2	9.2	9.2
B_4C Tank	3.02	3.02	3.02
NaF Tank 1	3.5	3.5	3.5
NaF Tank 2	3.5	3.5	3.5
NaF Tank 3	5.4	5.4	5.4
NaF Tank 4	5.4	5.4	5.4
B_4C Tank	3.02	3.02	3.02
Fe	4.45	4.45	4.45
Fe	0.32	0.32	0.32
H_2O	-	0.2	0.2
Fe	-	0.32	0.32
Pb	-	7.62	15.24
2.8% Borated H_2O	-	28.98	22.16
Fe	-	0.32	0.32
Total	68.5	106.0	106.8

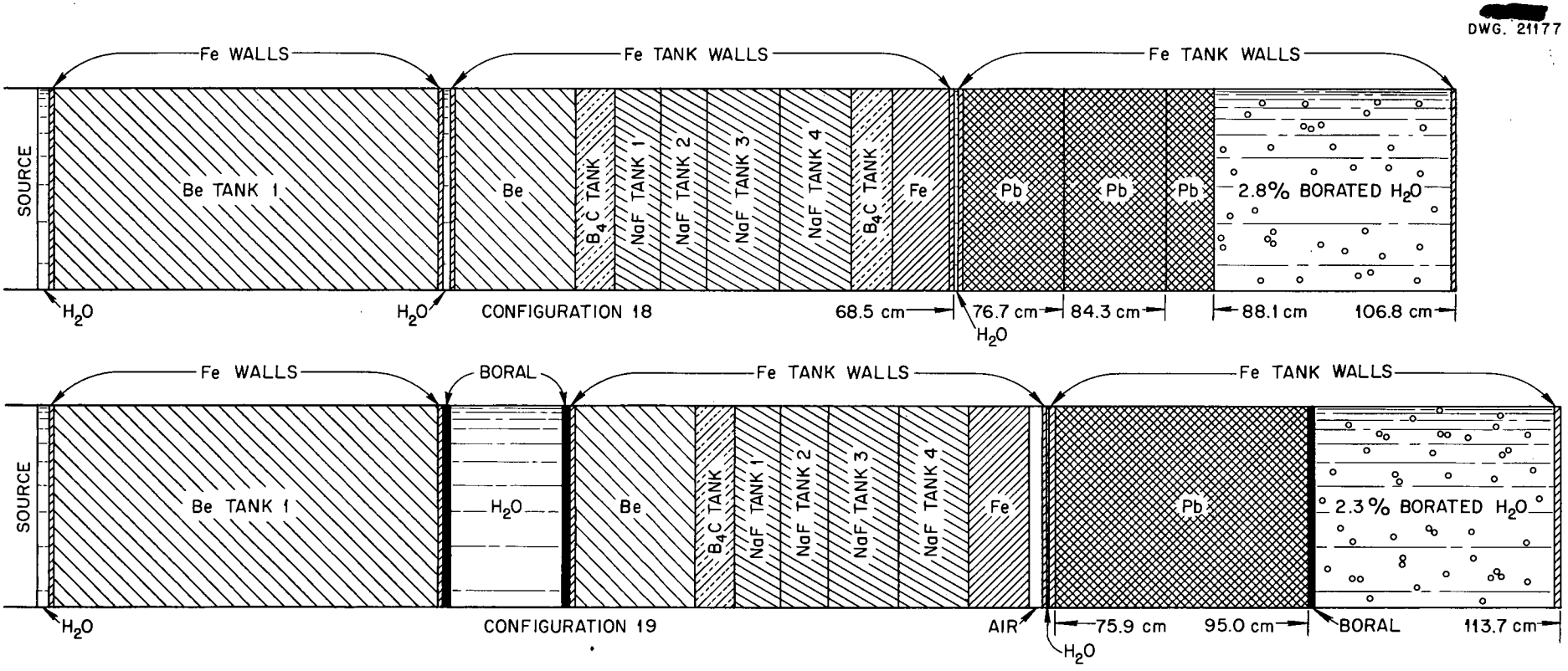

Fig. VI-8. Lid Tank Mockups of Reflector—Moderated Reactor and Shield.

Configurations 18 and 19

Component	Component Thickness (cm)	
	Configuration 18	Configuration 19
H_2O	0.9	0.9
Be Tank 1	29.1	29.1
Boral	-	0.64
H_2O	0.4	8.26
Boral	-	0.64
Fe	0.32	0.32
Be (ρ = 1.84 g/cc)	9.21	9.21
B_4C Tank	3.02	3.02
NaF Tank 1	3.5	3.5
NaF Tank 2	3.5	3.5
NaF Tank 3	5.4	5.4
NaF Tank 4	5.4	5.4
B_4C Tank	3.02	-
Fe	4.45	4.45
Air	-	0.9
Fe	0.32	0.32
H_2O	0.2	0.1
Fe	0.32	0.32
Pb	19.05	19.05
2.8% Borated H_2O	18.35	-
2.3% Borated H_2O	-	18.21
Fe	0.32	0.32
Total	106.8	113.7

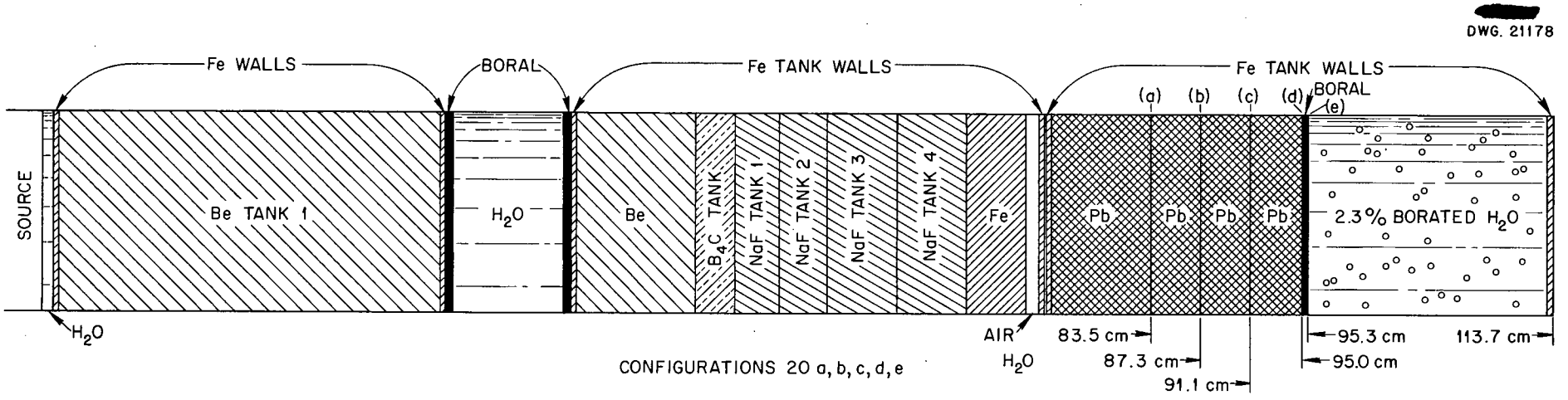

Fig. VI-9. Lid Tank Mockups of Reflector – Moderated Reactor and Shield.

Configurations 20 a, b, c, d, and e

Component	Component Thickness (cm)				
	Configuration 20				
	(a)	(b)	(c)	(d)	(e)
H_2O	0.9	0.9	0.9	0.9	0.9
Be Tank 1	29.1	29.1	29.1	29.1	29.1
Boral	0.64	0.64	0.64	0.64	0.64
H_2O	8.26	8.26	8.26	8.26	8.26
Boral	0.64	0.64	0.64	0.64	0.64
Fe	0.32	0.32	0.32	0.32	0.32
Be (ρ = 1.84 g/cc)	9.21	9.21	9.21	9.21	9.21
B_4C Tank	3.02	3.02	3.02	3.02	3.02
NaF Tank 1	3.5	3.5	3.5	3.5	3.5
NaF Tank 2	3.5	3.5	3.5	3.5	3.5
NaF Tank 3	5.4	5.4	5.4	5.4	5.4
NaF Tank 4	5.4	5.4	5.4	5.4	5.4
Fe	4.45	4.45	4.45	4.45	4.45
Air	0.9	0.9	0.9	0.9	0.9
Fe	0.32	0.32	0.32	0.32	0.32
H_2O	0.1	0.1	0.1	0.1	0.1
Fe	0.32	0.32	0.32	0.32	0.32
Pb	7.62	11.43	15.24	19.05	19.05
Boral	-	-	-	-	0.32
23% Borated H_2O	29.74	25.93	22.12	18.31	17.99
Fe	0.32	0.32	0.32	0.32	0.32
Total	113.7	113.7	113.7	113.7	113.7

[redacted]

DWG. 21179

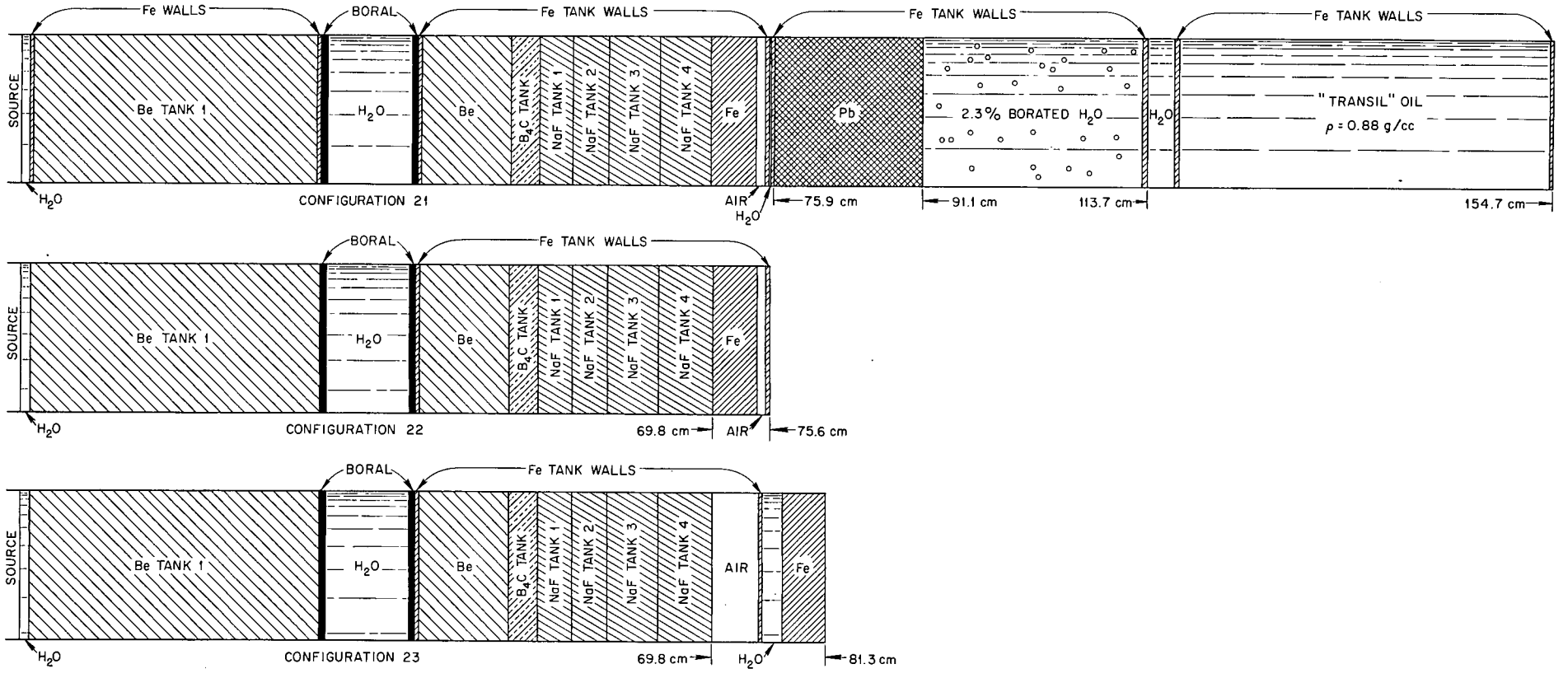

Fig. VI-10. Lid Tank Mockups of Reflector — Moderated Reactor and Shield.

Configurations 21, 22, and 23

Component	Component Thickness (cm)		
	Configuration 21	Configuration 22	Configuration 23
H_2O	0.9	0.9	0.9
Be Tank 1	29.1	29.1	29.1
Boral	0.64	0.64	0.64
H_2O	8.26	8.26	8.26
Boral	0.64	0.64	0.64
Fe	0.32	0.32	0.32
Be (ρ = 1.84 g/cc)	9.21	9.21	9.21
B_4C Tank	3.02	3.02	3.02
NaF Tank 1	3.5	3.5	3.5
NaF Tank 2	3.5	3.5	3.5
NaF Tank 3	5.4	5.4	5.4
NaF Tank 4	5.4	5.4	5.4
Fe	4.45	4.45	-
Air	0.9	1.0	4.63
Fe	0.32	0.32	0.32
H_2O	0.1	-	2.05
Fe	0.32	-	4.45
Pb	15.24	-	-
2.3% Borated H_2O	22.12	-	-
Fe	0.32	-	-
H_2O	2.9	-	-
Fe	0.32	-	-
Transil Oil (ρ = 0.88 g/cc)	37.5	-	-
Fe	0.32	-	-
Total	154.7	75.6	81.3

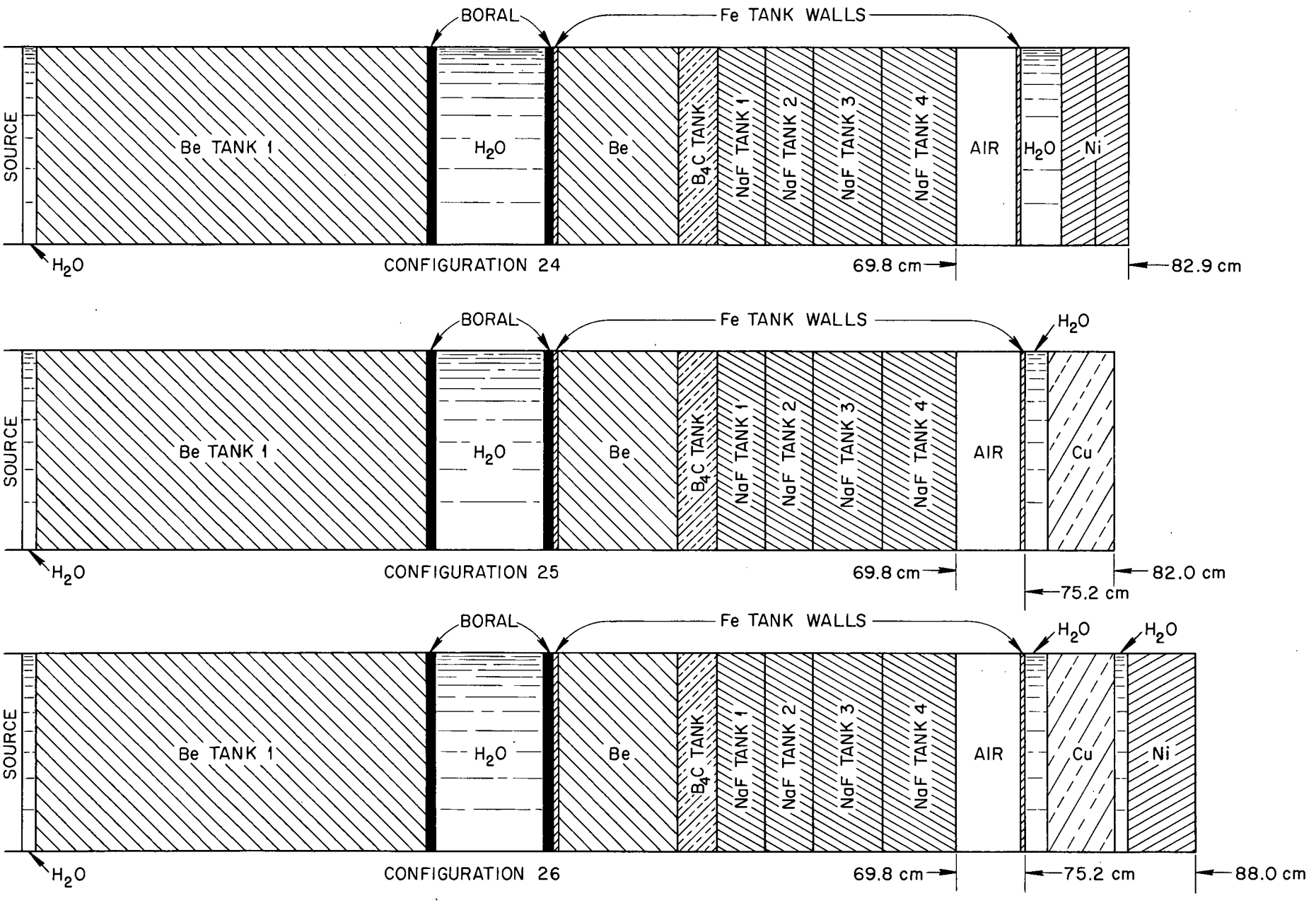

Fig. VI-11. Lid Tank Mockups of Reflector—Moderated Reactor and Shield.

Configurations 24, 25, and 26

Component	Component Thickness (cm)		
	Configuration 24	Configuration 25	Configuration 26
H_2O	0.9	0.9	0.9
Be Tank 1	29.1	29.1	29.1
Boral	0.64	0.64	0.64
H_2O	8.26	8.26	8.26
Boral	0.64	0.64	0.64
Fe	0.32	0.32	0.32
Be (ρ = 1.84 g/cc)	9.21	9.21	9.21
B_4C Tank	3.02	3.02	3.02
NaF Tank 1	3.5	3.5	3.5
NaF Tank 2	3.5	3.5	3.5
NaF Tank 3	5.4	5.4	5.4
NaF Tank 4	5.4	5.4	5.4
Air	4.63	5.03	5.03
Fe	0.32	0.32	0.32
H_2O	3.07	1.7	1.7
Ni	5.08	-	-
Cu	-	5.08	5.08
H_2O	-	-	0.94
Ni	-	-	5.08
Total	83.0	82.0	88.0

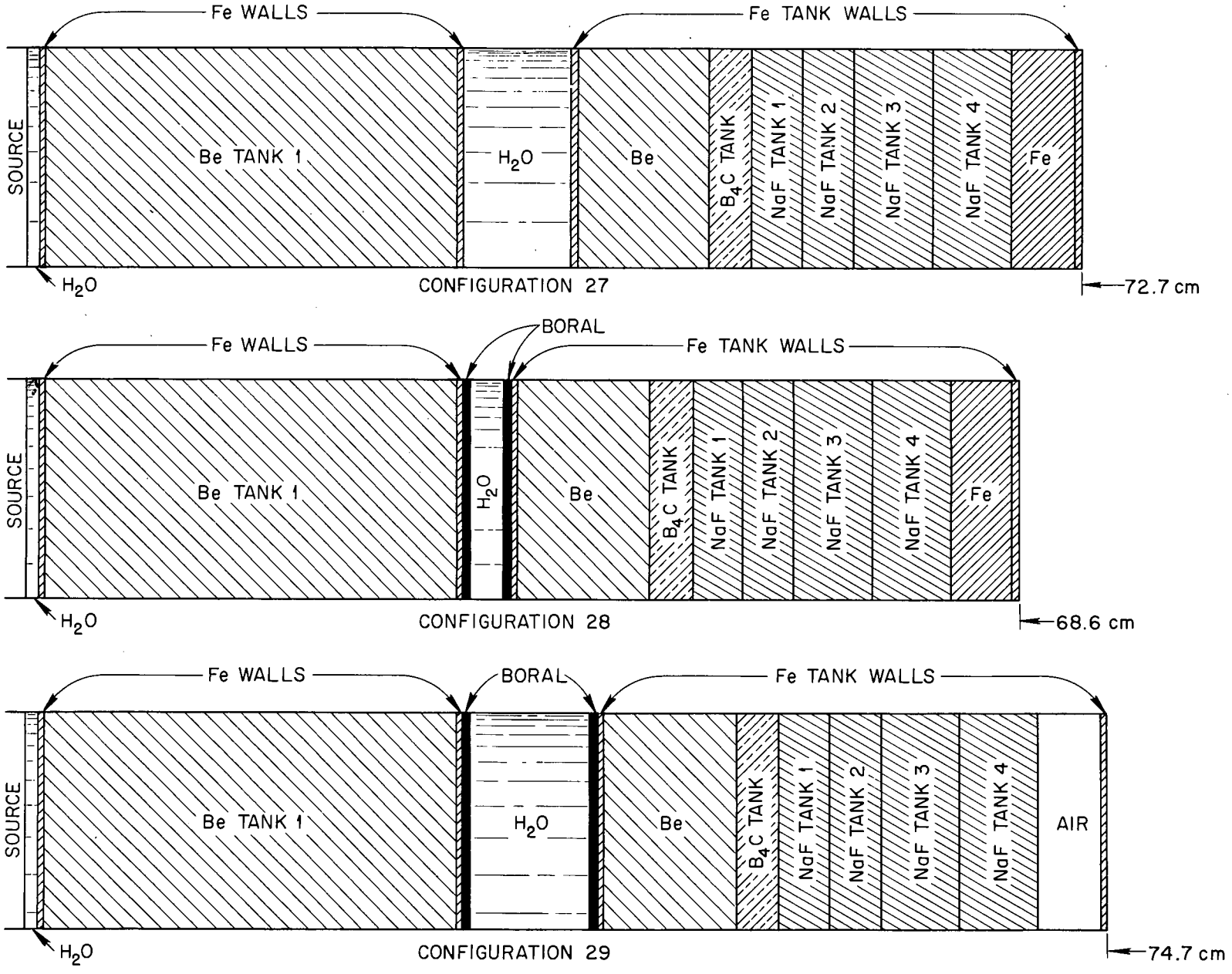

Fig. VI-12. Lid Tank Mockups of Reflector—Moderated Reactor and Shield.

Configurations 27, 28, and 29

Component	Component Thickness (cm)		
	Configuration 27	Configuration 28	Configuration 29
H_2O	0.9	0.9	0.9
Be Tank 1	29.1	29.1	29.1
Boral	-	0.64	0.64
H_2O	7.62	2.24	8.26
Boral	-	0.64	0.64
Fe	0.32	0.32	0.32
Be (ρ = 1.84 g/cc)	9.21	9.21	9.21
B_4C Tank	3.02	3.02	3.02
NaF Tank 1	3.5	3.5	3.5
NaF Tank 2	3.5	3.5	3.5
NaF Tank 3	5.4	5.4	5.4
NaF Tank 4	5.4	5.4	5.4
Fe	4.45	4.45	-
Air	-	-	4.5
Fe	0.32	0.32	0.32
Total	72.7	68.6	74.7

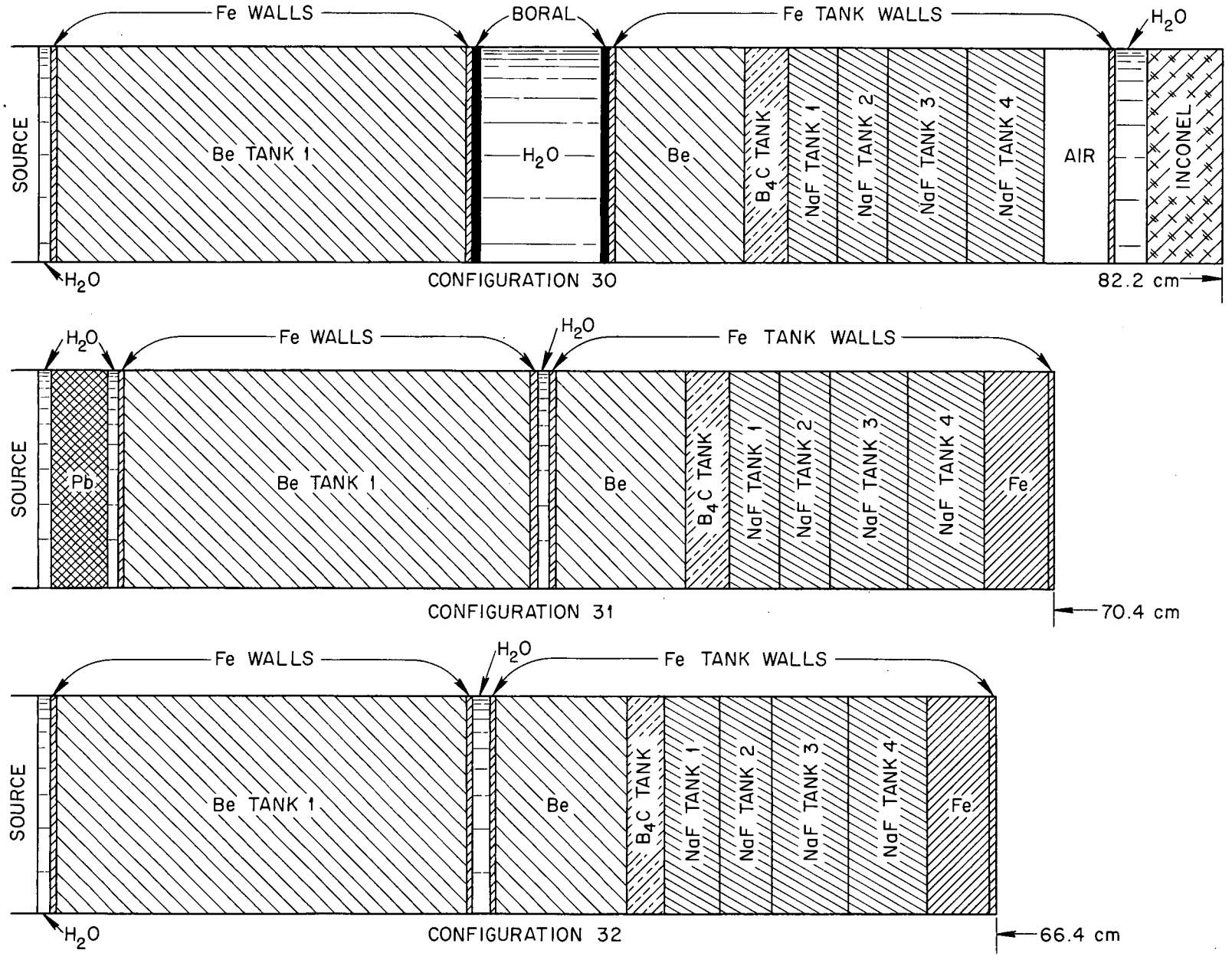

Fig. VI-13. Lid Tank Mockups of Reflector—Moderated Reactor and Shield.

Configurations 30, 31, and 32

Component	Thickness of Component (cm)		
	Configuration 30	Configuration 31	Configuration 32
H_2O	0.9	0.9	0.9
Pb	-	3.81	-
H_2O	-	0.75	-
Be Tank 1	29.1	29.1	29.1
Boral	0.64	-	-
H_2O	8.26	0.76	1.3
Boral	0.64	-	-
Fe	0.32	0.32	0.32
Be (ρ = 1.84 g/cc)	9.21	9.21	9.21
B_4C Tank	3.02	3.02	3.02
NaF Tank 1	3.5	3.5	3.5
NaF Tank 2	3.5	3.5	3.5
NaF Tank 3	5.4	5.4	5.4
NaF Tank 4	5.4	5.4	5.4
Air	4.5	-	-
Fe	-	4.45	4.45
Fe	0.32	0.32	0.32
H_2O	2.45	-	-
Inconel	5.08	-	-
Total	82.2	70.4	66.4

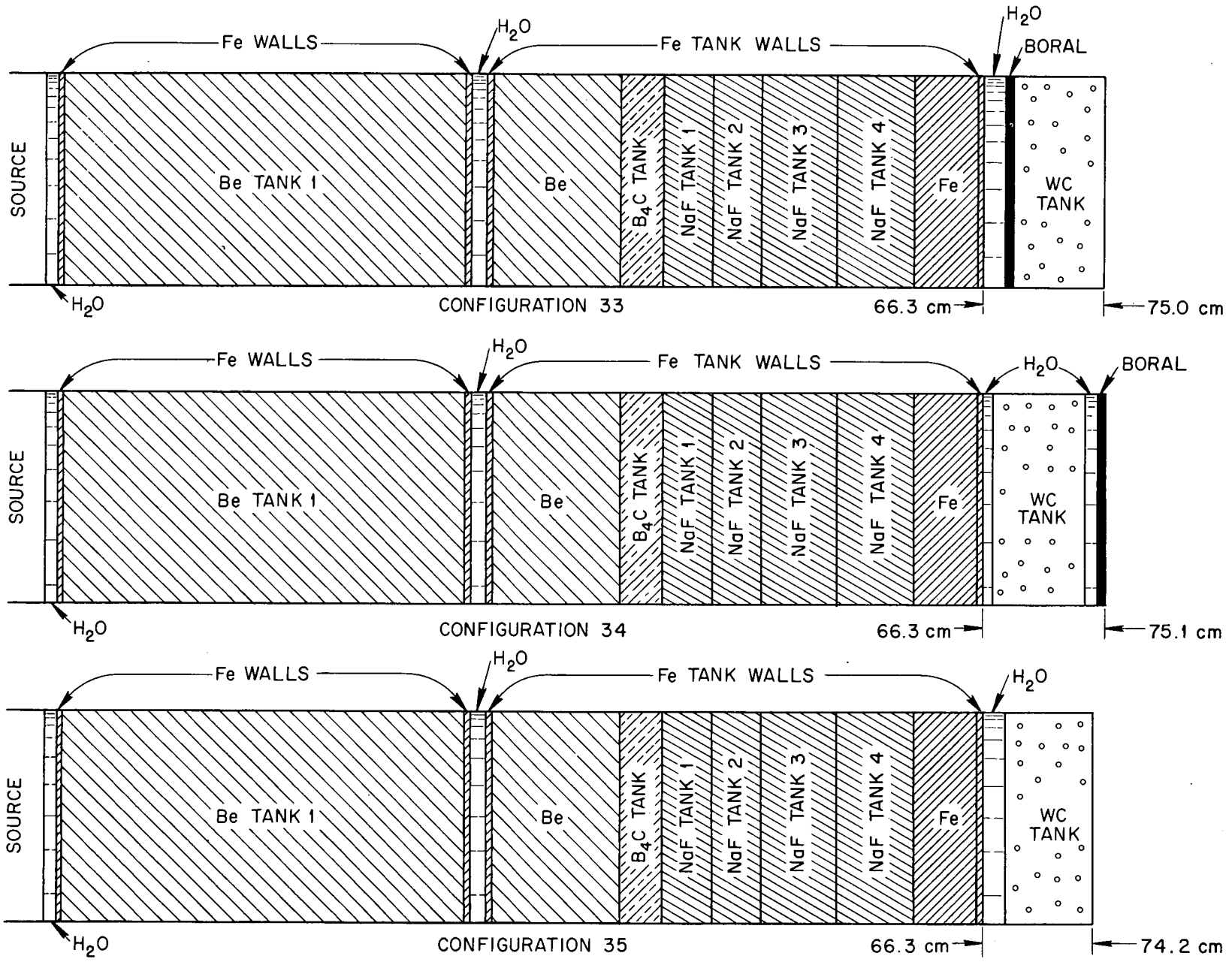

Fig. VI-14. Lid Tank Mockups of Reflector – Moderated Reactor and Shield.

Configurations 33, 34, and 35

Component	Component Thickness (cm)		
	Configuration 33	Configuration 34	Configuration 35
H_2O	0.9	0.9	0.9
Be Tank 1	29.1	29.1	29.1
H_2O	1.2	1.2	1.2
Fe	0.32	0.32	0.32
Be (ρ = 1.84 g/cc)	9.21	9.21	9.21
B_4C Tank	3.02	3.02	3.02
NaF Tank 1	3.5	3.5	3.5
NaF Tank 2	3.5	3.5	3.5
NaF Tank 3	5.4	5.4	5.4
NaF Tank 4	5.4	5.4	5.4
Fe	4.45	4.45	4.45
Fe	0.32	0.32	0.32
H_2O	1.7	0.9	1.5
Boral	0.64	-	-
WC Tank	6.35	6.35	6.35
H_2O	-	0.9	-
Boral	-	0.64	-
Total	75.0	75.1	74.2

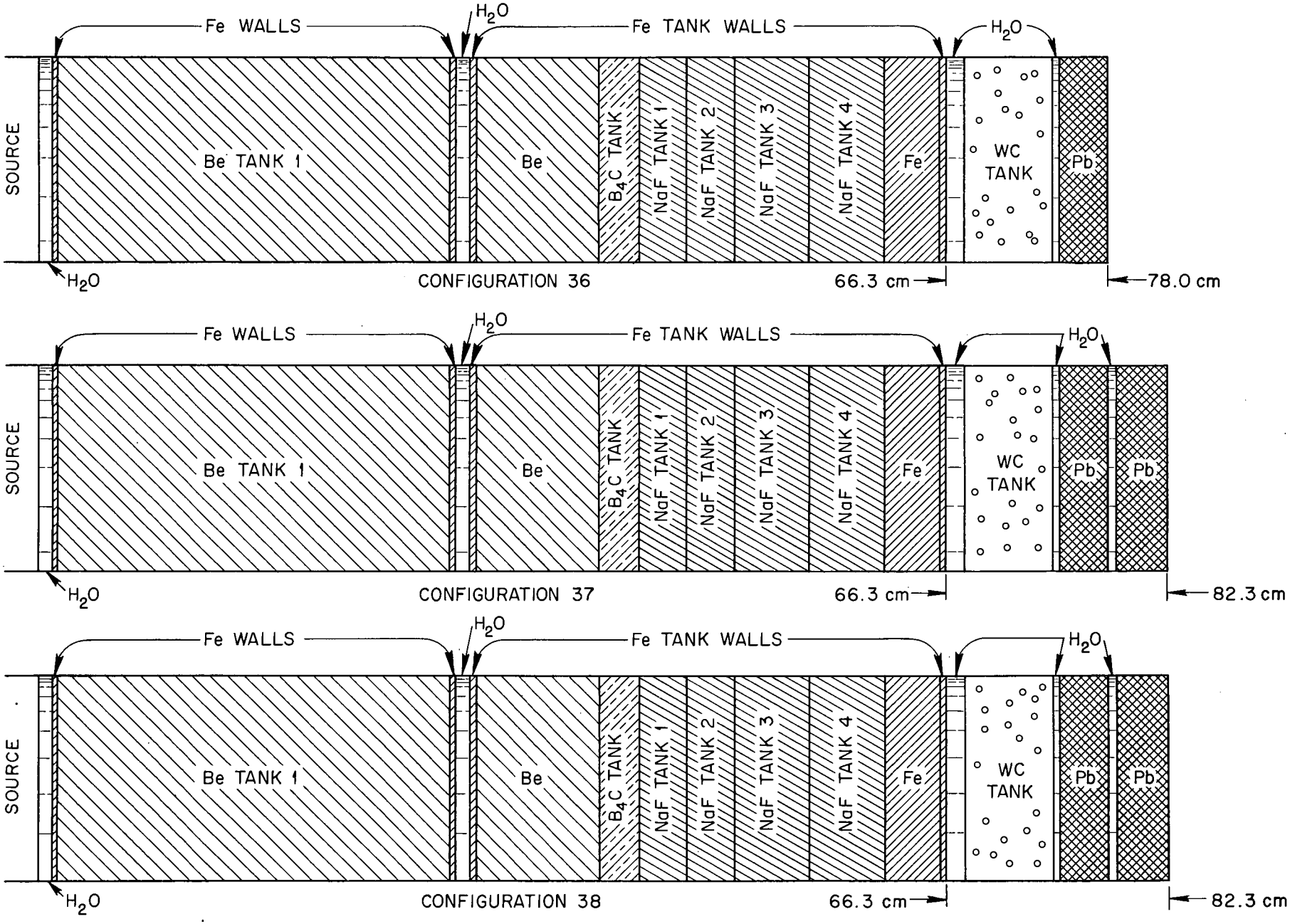

Fig. VI-15. Lid Tank Mockups of Reflector — Moderated Reactor and Shield.

Configurations 36, 37, and 38

Component	Component Thickness (cm)		
	Configuration 36	Configuration 37	Configuration 38
H_2O	0.9	0.9	0.9
Be Tank 1	29.1	29.1	29.1
H_2O	1.2	1.2	1.2
Fe	0.32	0.32	0.32
Be (ρ = 1.84 g/cc)	9.21	9.21	9.21
B_4C Tank	3.02	3.02	3.02
NaF Tank 1	3.5	3.5	3.5
NaF Tank 2	3.5	3.5	3.5
NaF Tank 3	5.4	5.4	5.4
NaF Tank 4	5.4	5.4	5.4
Fe	4.45	4.45	4.45
Fe	0.32	0.32	0.32
H_2O	1.2	1.2	0.8
Pb	-	-	3.81
H_2O	-	-	0.4
Pb	-	-	3.81
H_2O	-	-	0.4
WC Tank	6.35	6.35	6.35
H_2O	0.4	0.4	-
Pb	3.81	3.81	-
H_2O	-	0.45	-
Pb	-	3.81	-
Total	78.0	82.3	81.9

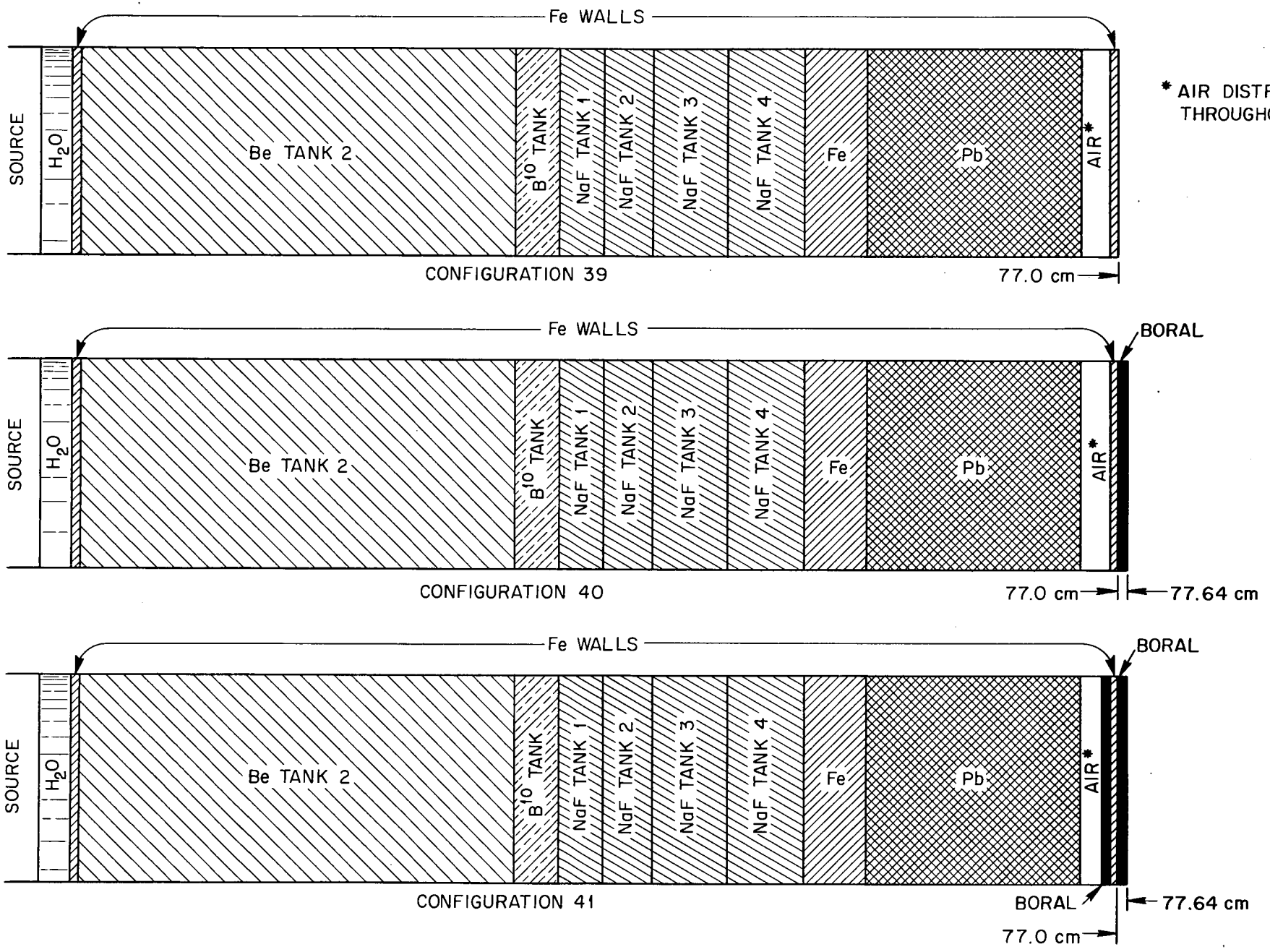

Fig. VI-16. Lid Tank Mockups of Reflector — Moderated Reactor and Shield.

Configurations 39, 40, and 41

Component	Component Thickness (cm)		
	Configuration 39	Configuration 40	Configuration 41
H_2O	2.3	2.3	2.3
Fe	0.48	0.48	0.48
Be Tank 2	31.01	31.01	31.01
B^{10} Tank	3.1	3.1	3.1
NaF Tank 1	3.5	3.5	3.5
NaF Tank 2	3.5	3.5	3.5
NaF Tank 3	5.4	5.4	5.4
NaF Tank 4	5.4	5.4	5.4
Fe	4.45	4.45	4.45
Pb	15.24	15.24	15.24
Boral	-	-	0.64
Air[a]	2.14	2.14	1.50
Fe	0.48	0.48	0.48
Boral	-	0.64	0.64
Total	77.0	77.64	77.64

(a) Air distributed throughout shield.

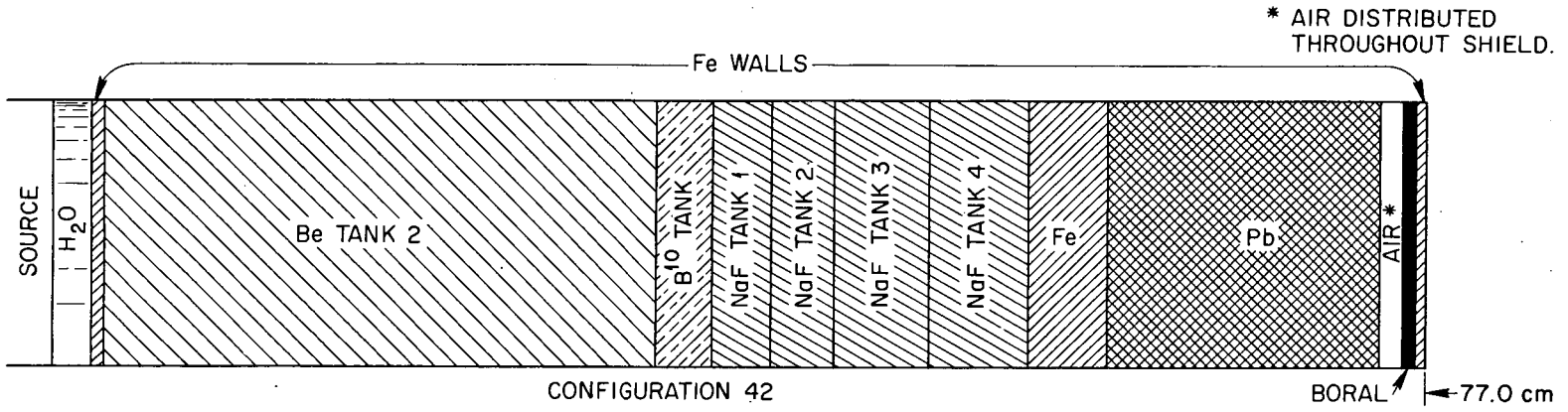

CONFIGURATION 42

CONFIGURATION 43 SAME AS CONFIGURATION 39 EXCEPT 34½-in. DIAMETER B^{10} TANK WAS SPLICED OUT 2 ft ON EACH SIDE WITH TWO ¼-in. THICK BORAL SHEETS (48 in. HIGH).

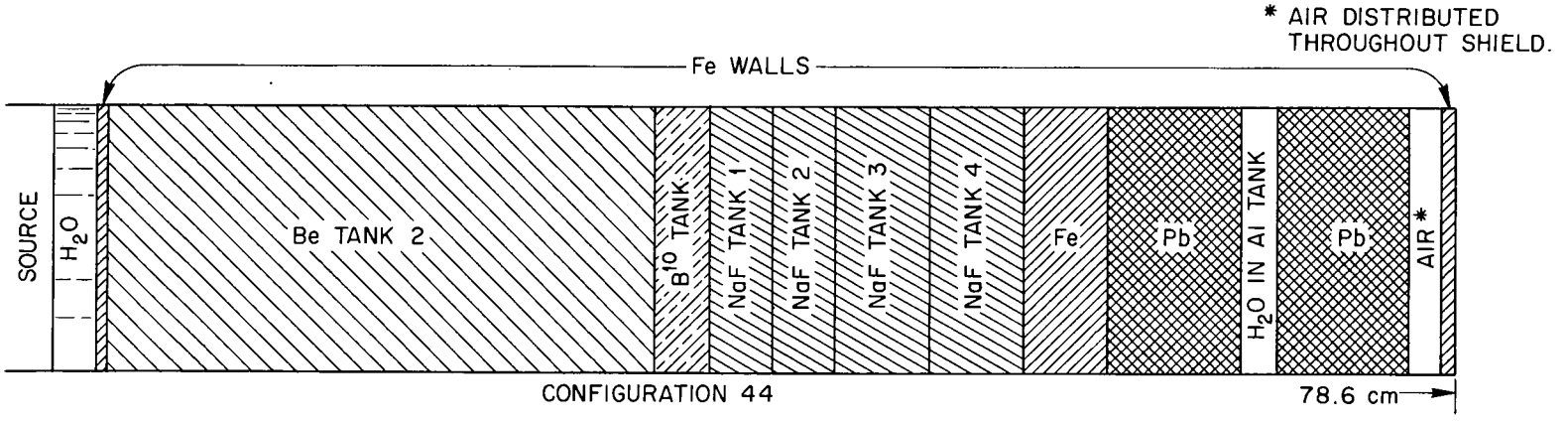

CONFIGURATION 44

Fig. VI-17. Lid Tank Mockups of Reflector – Moderated Reactor and Shield.

Configuration 42, 43, and 44

Component	Thickness of Component (cm)		
	Configuration 42	Configuration 43	Configuration 44
H_2O	2.3	2.3	2.3
Fe	0.48	0.48	0.48
Be Tank 2	31.01	31.01	31.01
B^{10} Tank	3.1	-	3.1
B^{10} Tank (Spliced out)[a]	-	3.1	-
NaF Tank 1	3.5	3.5	3.5
NaF Tank 2	3.5	3.5	3.5
NaF Tank 3	5.4	5.4	5.4
NaF Tank 4	5.4	5.4	5.4
Fe	4.45	4.45	4.45
Pb	15.24	15.24	7.62
H_2O	-	-	1.91
Pb	-	-	7.62
Boral	0.64	-	-
Air[b]	1.50	2.19	1.83
Fe	0.48	0.48	0.48
Total	77.0	77.5	78.6

(a) B^{10} tank spliced out 2 ft on each side with two 1/4 in. thick boral sheets (48 in. high).
(b) Air distributed throughout shield.

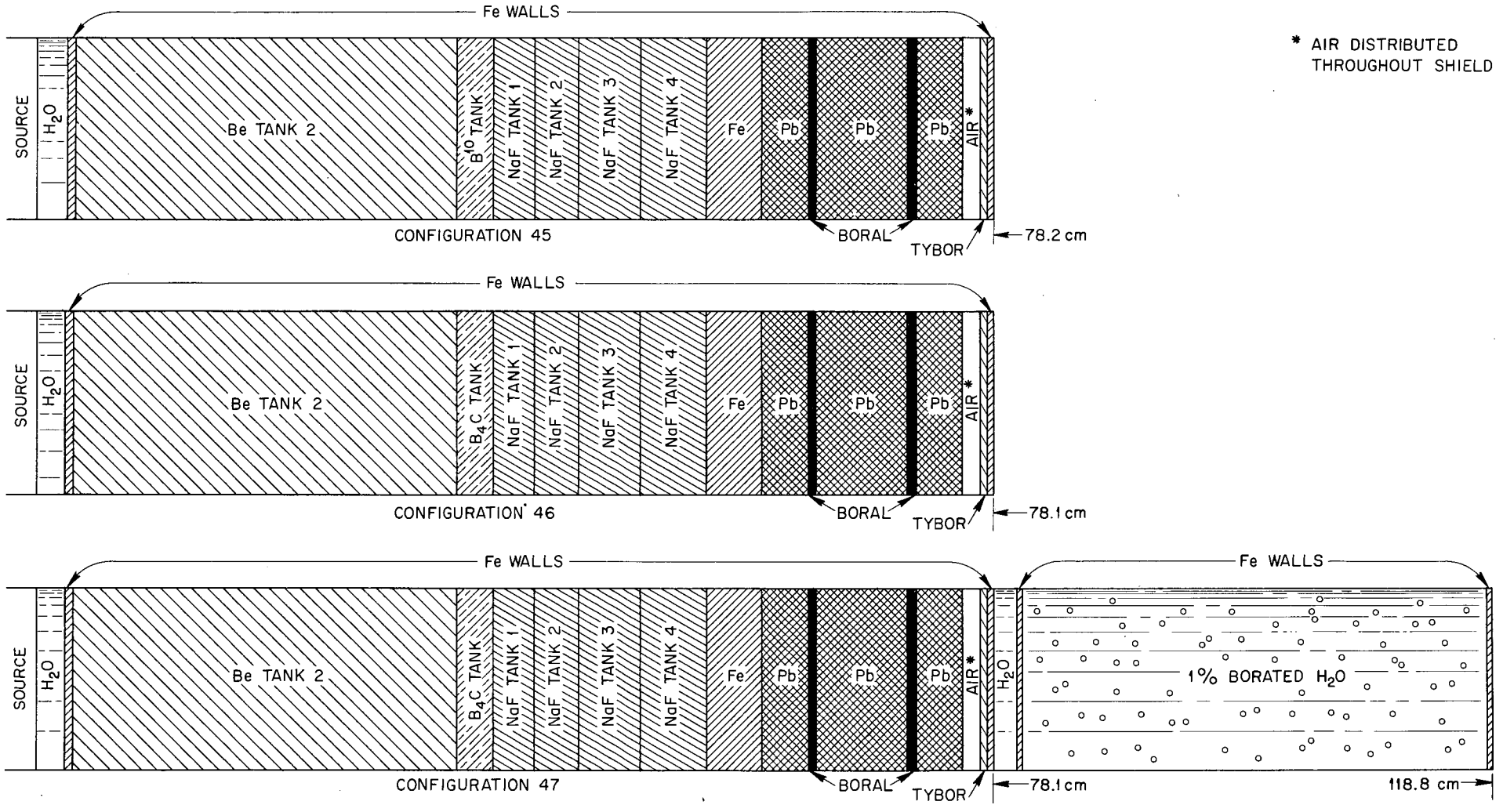

Fig. VI-18. Lid Tank Mockups of Reflector – Moderated Reactor and Shield.

Configurations 45, 46, and 47

Component	Thickness of Component (cm)		
	Configuration 45	Configuration 46	Configuration 47
H_2O	2.3	2.3	2.3
Fe	0.48	0.48	0.48
Be Tank 2	31.01	31.01	31.01
B^{10} Tank	3.1	-	-
B_4C Tank	-	3.02	3.02
NaF Tank 1	3.5	3.5	3.5
NaF Tank 2	3.5	3.5	3.5
NaF Tank 3	5.4	5.4	5.4
NaF Tank 4	5.4	5.4	5.4
Fe	4.45	4.45	4.45
Pb	3.81	3.81	3.81
Boral	0.64	0.64	0.64
Pb	7.62	7.62	7.62
Boral	0.64	0.64	0.64
Pb	3.81	3.81	3.81
Tybor	0.64	0.64	0.64
Air[a]	1.42	1.4	1.4
Fe	0.48	0.48	0.48
H_2O	-	-	1.96
Fe	-	-	0.32
1% Borated H_2O	-	-	38.1
Fe	-	-	0.32
Total	78.2	78.1	118.8

(a) Air distributed throughout dry section of shield.

DWG. 21188

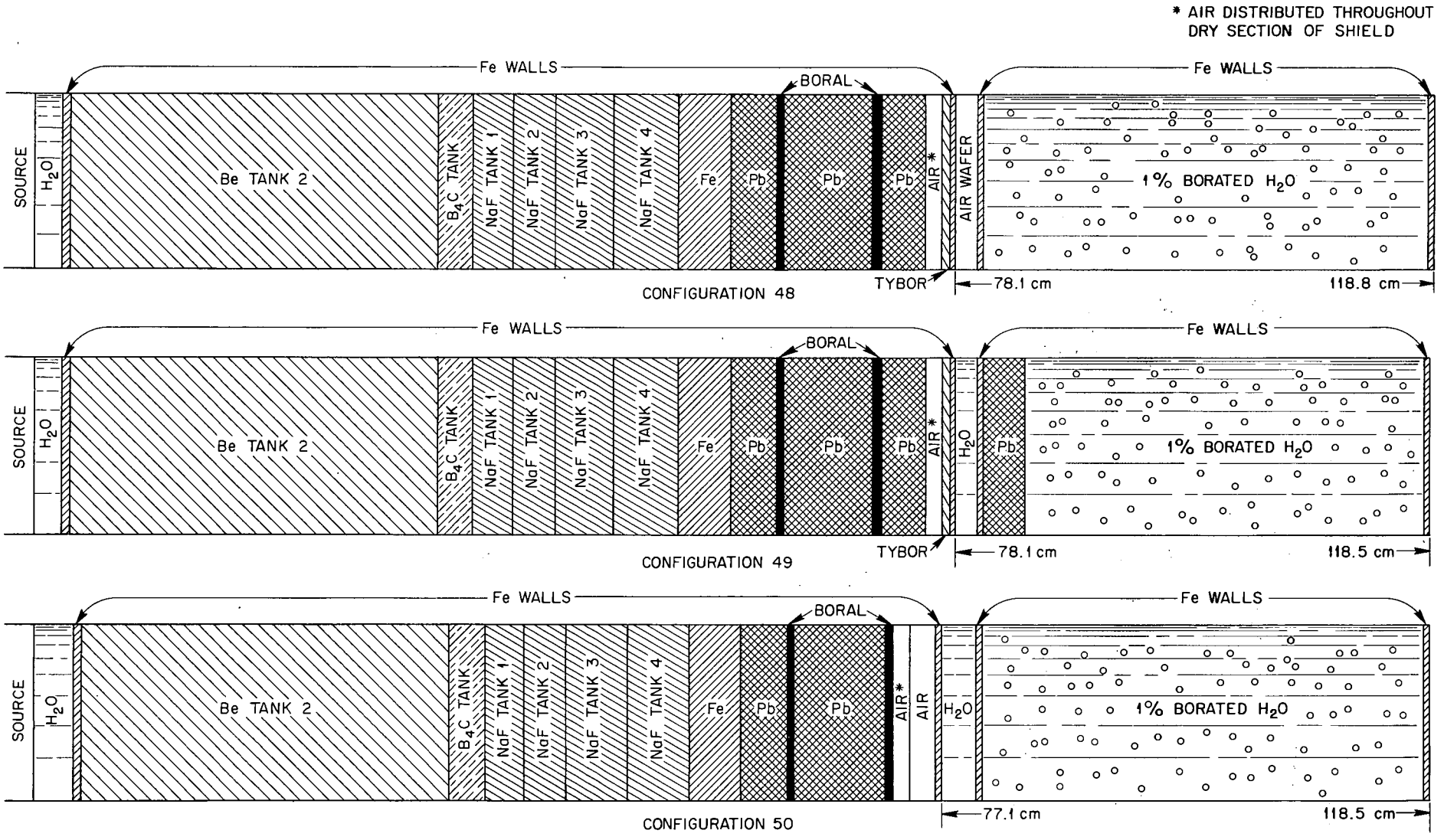

Fig. VI-19. Lid Tank Mockups of Reflector – Moderated Reactor and Shield.

Configurations 48, 49, and 50

Component	Thickness of Component (cm)		
	Configuration 48	Configuration 49	Configuration 50
H_2O	2.3	2.3	3.4
Fe	0.48	0.48	0.48
Be Tank 2	31.01	31.01	31.01
B_4C Tank	3.02	3.02	3.02
NaF Tank 1	3.5	3.5	3.5
NaF Tank 2	3.5	3.5	3.5
NaF Tank 3	5.4	5.4	5.4
NaF Tank 4	5.4	5.4	5.4
Fe	4.45	4.45	4.45
Pb	3.81	3.81	3.81
Boral	0.64	0.64	0.64
Pb	7.62	7.62	7.62
Boral	0.64	0.64	0.64
Pb	3.81	3.81	-
Tybor	0.64	0.64	-
Air[a]	1.4	1.4	1.52
Air	-	-	2.22
Fe	0.48	0.48	0.48
Al	0.16	-	-
Air	1.64	-	-
Al	0.16	-	-
H_2O	-	1.96	2.97
Fe	0.32	0.32	0.32
Pb	-	3.81	-
1% Borated H_2O	38.1	33.99	37.8
Fe	0.32	0.32	0.32
Total	118.8	118.5	118.5

[a] Air distributed throughout dry section of shield.

DWG. 21189

* AIR DISTRIBUTED THROUGHOUT DRY SECTION OF SHIELD

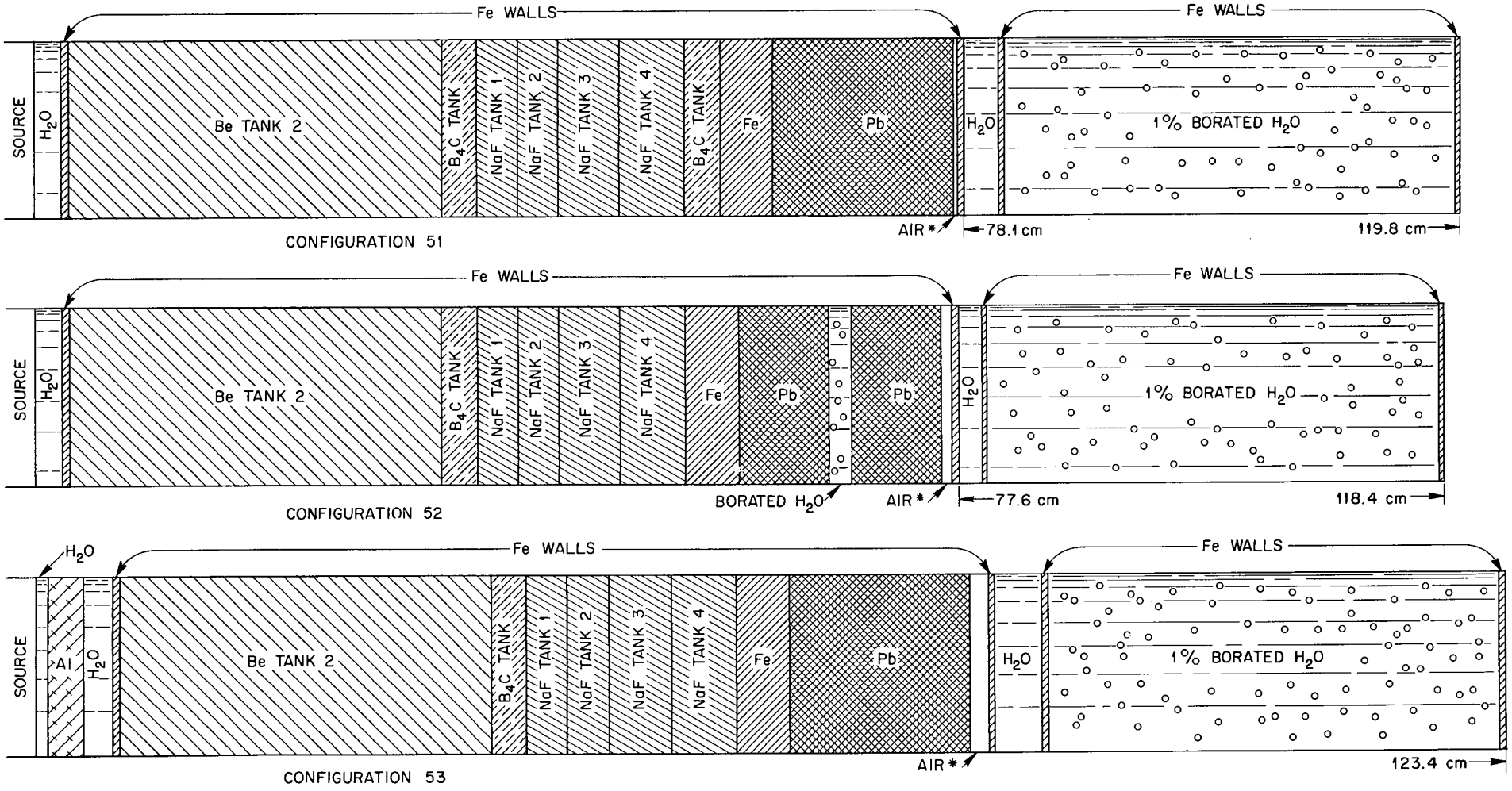

Fig. VI-20. Lid Tank Mockups of Reflector — Moderated Reactor and Shield.

Configurations 51, 52, and 53

Component	Thickness of Component (cm)		
	Configuration 51	Configuration 52	Configuration 53
H_2O	2.3	2.3	0.9
Al	-	-	3.18
H_2O	-	-	2.3
Fe	0.48	0.48	0.48
Be Tank 2	31.01	31.01	31.01
B_4C Tank	3.02	3.02	3.02
NaF Tank 1	3.5	3.5	3.5
NaF Tank 2	3.5	3.5	3.5
NaF Tank 3	5.4	5.4	5.4
NaF Tank 4	5.4	5.4	5.4
B_4C Tank	3.02	-	-
Fe	4.45	4.45	4.45
Pb	15.24	7.62	15.24
1% Borated H_2O	-	1.91	-
Pb	-	7.62	-
Air[a]	0.30	0.92	1.4
Fe	0.48	0.48	0.48
H_2O	2.96	2.05	4.4
Fe	0.32	0.32	0.32
1% Borated H_2O	38.1	38.1	38.1
Fe	0.32	0.32	0.32
Total	119.8	118.4	123.4

[a] Air distributed throughout dry section of shield.

CONFIGURATION 54 SAME AS CONFIGURATION 17 EXCEPT H_2O IN Fe TANK WAS BORATED TO 1.0% BY WEIGHT.

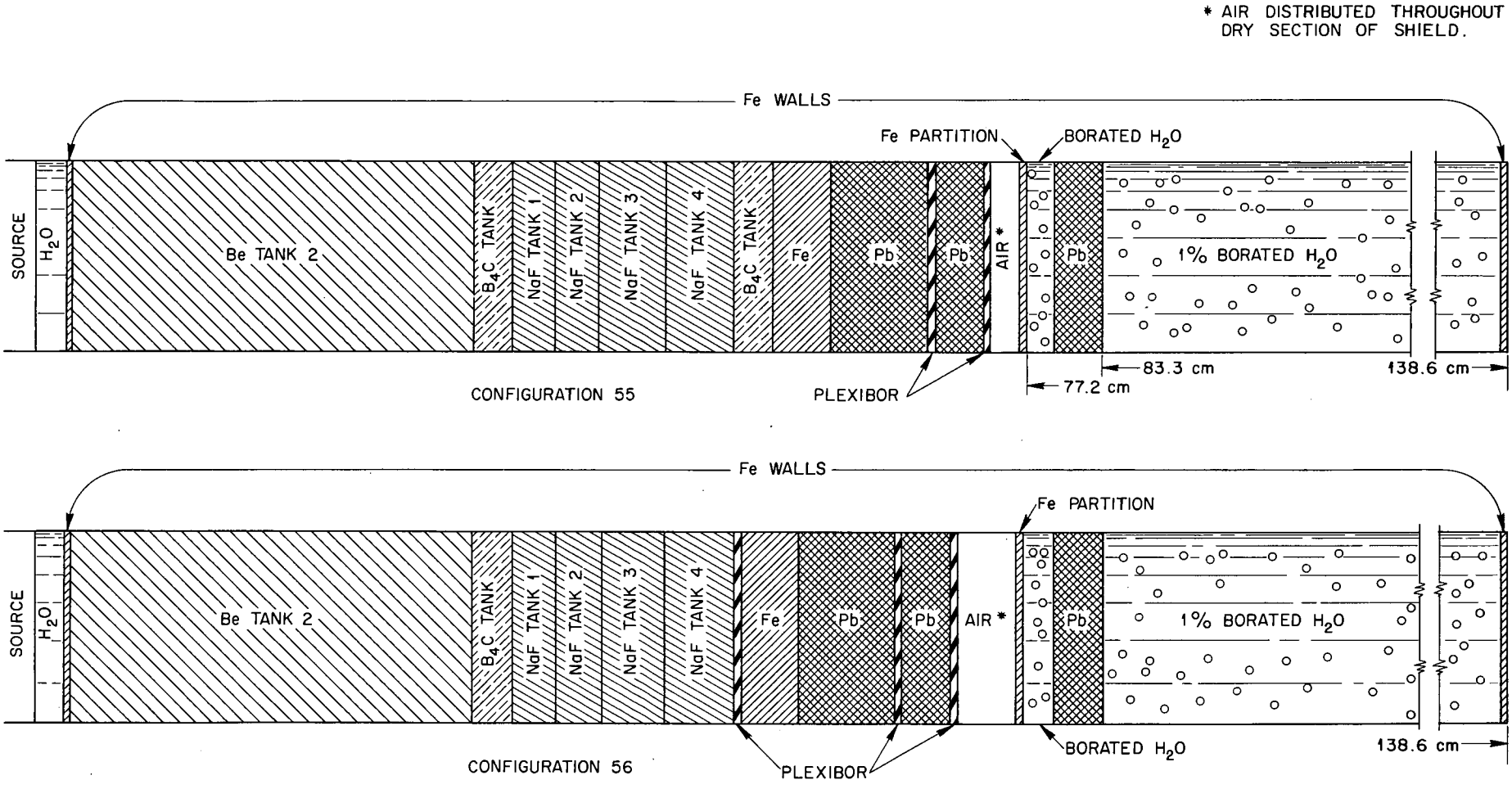

Fig. VI-21. Lid Tank Mockups of Reflector — Moderated Reactor and Shield.

Configurations 54, 55, and 56

Component	Thickness of Component (cm)		
	Configuration 54	Configuration 55	Configuration 56
H_2O	0.9	2.3	2.3
Fe	-	0.48	0.48
Be Tank 1	29.1	-	-
Be Tank 2	-	31.01	31.01
H_2O	0.4	-	-
Fe	0.32	-	-
Be (ρ = 1.84 g/cc)	9.21	-	-
B_4C Tank	3.02	3.02	3.02
NaF Tank 1	3.5	3.5	3.5
NaF Tank 2	3.5	3.5	3.5
NaF Tank 3	5.4	5.4	5.4
NaF Tank 4	5.4	5.4	5.4
B_4C Tank	3.02	3.02	-
Plexibor	-	-	0.48
Fe	4.45	4.45	4.45
Fe	0.32	-	-
H_2O	1.36	-	-
Fe	0.32	-	-
Pb	-	7.62	7.62
Plexibor	-	0.48	0.48
Pb	-	3.81	3.81
Plexibor	-	0.48	0.48
Air[a]	-	2.25	4.79
Fe	-	0.48	0.48
1% Borated H_2O	-	2.29	2.29
Pb	15.24	3.81	3.81
1% Borated H_2O	22.22	54.82	54.82
Fe	0.32	0.48	0.48
Total	108.0	138.6	138.6

(a) Air distributed throughout dry section of shield.

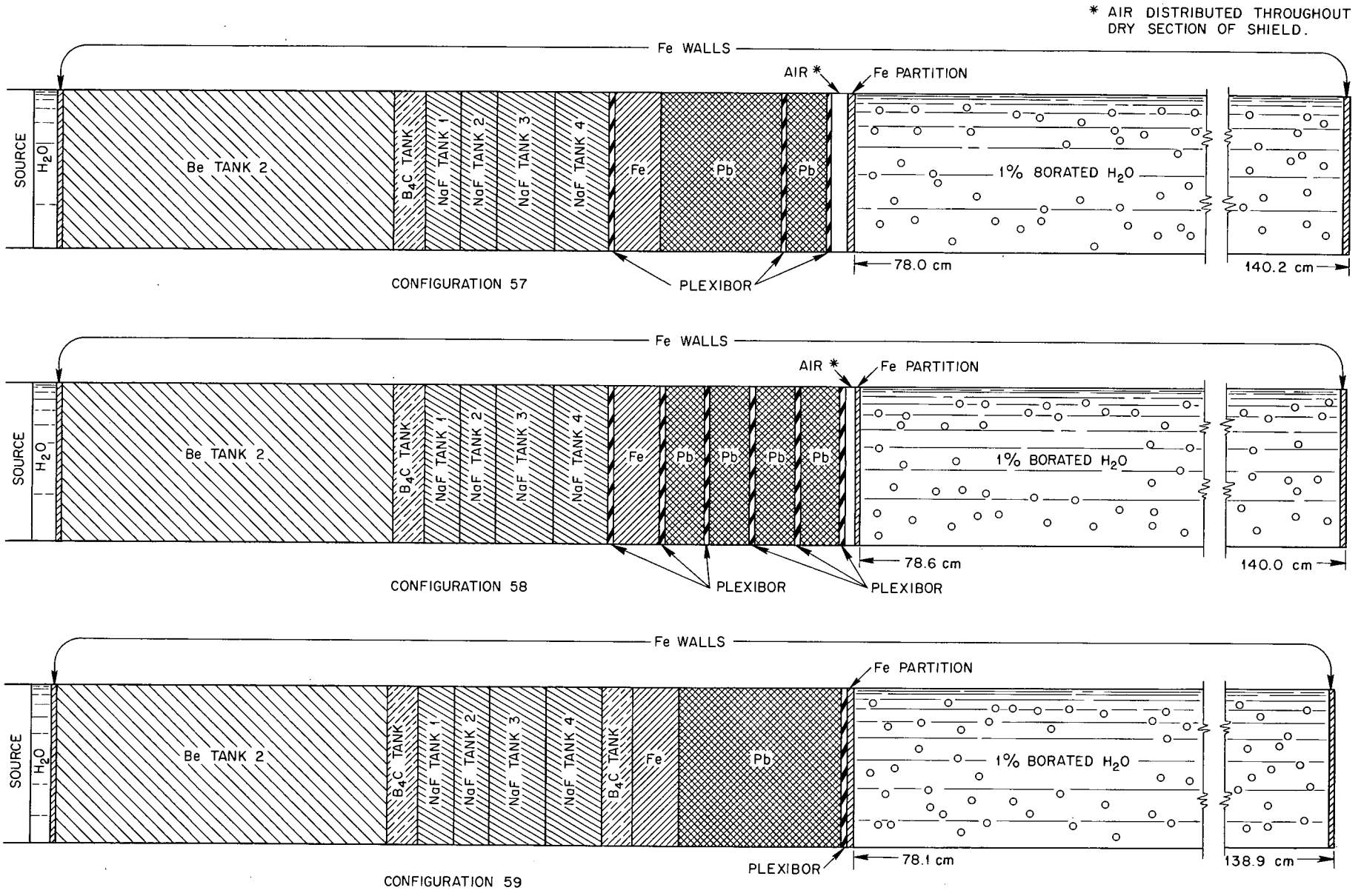

Fig. VI-22. Lid Tank Mockups of Reflector – Moderated Reactor and Shield.

Configurations 57, 58, and 59

Component	Thickness of Component (cm)		
	Configuration 57	Configuration 58	Configuration 57
H_2O	2.3	2.3	1.82
Fe	0.48	0.48	0.48
Be Tank 2	31.01	31.01	31.01
B_4C Tank	3.02	3.02	3.02
NaF Tank 1	3.5	3.5	3.5
NaF Tank 2	3.5	3.5	3.5
NaF Tank 3	5.4	5.4	5.4
NaF Tank 4	5.4	5.4	5.4
Plexibor	0.48	0.48	-
B_4C Tank	-	-	3.02
Fe	4.45	4.45	4.45
Plexibor	-	0.48	-
Pb	11.43	3.81	15.24
Plexibor	0.48	0.48	0.48
Pb	3.81	3.81	-
Plexibor	0.48	0.48	-
Pb	-	3.81	-
Plexibor	-	0.48	-
Pb	-	3.81	-
Plexibor	-	0.48	-
Air[a]	1.78	0.94	0.3
Fe	0.48	0.48	0.48
1% Borated H_2O	61.72	60.92	60.32
Fe	0.48	0.48	0.48
Total	140.2	140.0	138.9

(a) Air distributed throughout dry section of shield.

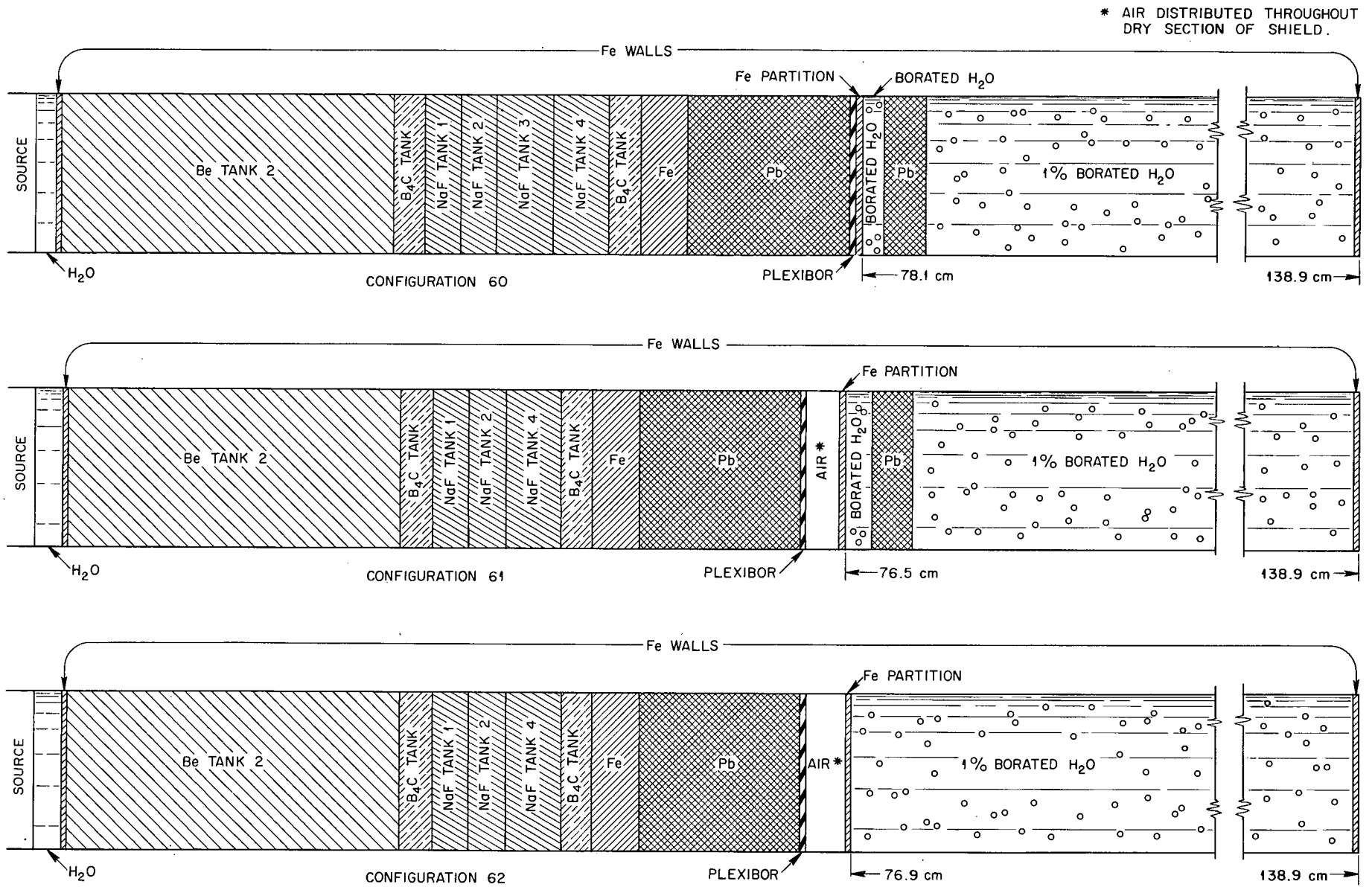

Fig. VI-23. Lid Tank Mockups of Reflector – Moderated Reactor and Shield.

Configurations 60, 61, and 62

Component	Thickness of Component (cm)		
	Configuration 60	Configuration 61	Configuration 62
H_2O	1.82	2.7	2.7
Fe	0.48	0.48	0.48
Be Tank 2	31.01	31.01	31.01
B_4C Tank	3.02	3.02	3.02
NaF Tank 1	3.5	3.5	3.5
NaF Tank 2	3.5	3.5	3.5
NaF Tank 3	5.4	-	-
NaF Tank 4	5.4	5.4	5.4
B_4C Tank	3.02	3.02	3.02
Fe	4.45	4.45	4.45
Pb	15.24	15.24	15.24
Plexibor	0.48	0.48	0.48
Air[a]	0.3	3.22	3.62
Fe	0.48	0.48	0.48
1% Borated H_2O	2.0	2.6	-
Pb	3.81	3.81	-
1% Borated H_2O	54.51	55.51	61.52
Fe	0.48	0.48	0.48
Total	138.9	138.9	138.9

(a) Air distributed throughout dry section of shield.

DWG. 21193

* AIR DISTRIBUTED THROUGHOUT DRY SECTION OF SHIELD.

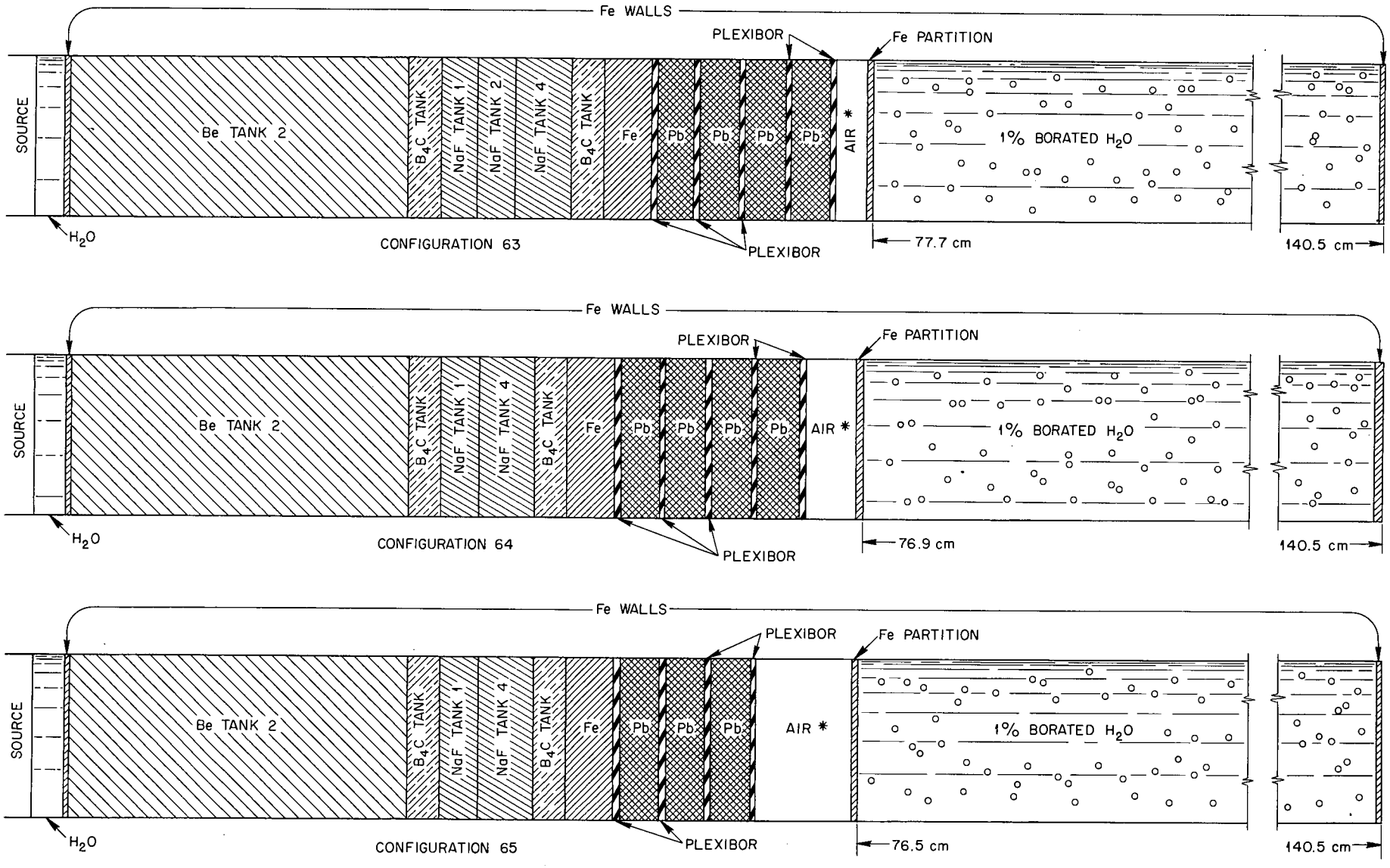

Fig. VI-24. Lid Tank Mockups of Reflector – Moderated Reactor and Shield.

Configurations 63, 64, and 65

Component	Thickness of Component (cm)		
	Configuration 63	Configuration 64	Configuration 65
H_2O	2.3	2.9	2.9
Fe	0.48	0.48	0.48
Be Tank 2	31.01	31.01	31.01
B_4C Tank	3.02	3.02	3.02
NaF Tank 1	3.5	3.5	3.5
NaF Tank 2	3.5	-	-
NaF Tank 4	5.4	5.4	5.4
B_4C Tank	3.02	3.02	3.02
Fe	4.45	4.45	4.45
Plexibor	0.48	0.48	0.48
Pb	3.81	3.81	3.81
Plexibor	0.48	0.48	0.48
Pb	3.81	3.81	3.81
Plexibor	0.48	0.48	0.48
Pb	3.81	3.81	3.81
Plexibor	0.48	0.48	0.48
Pb	3.81	3.81	-
Plexibor	0.48	0.48	-
Air[a]	2.9	4.8	8.89
Fe	0.48	0.48	0.48
1% Borated H_2O	62.32	63.12	63.52
Fe	0.48	0.48	0.48
Total	140.5	140.5	140.5

(a) Air distributed throughout dry section of shield.

* AIR DISTRIBUTED THROUGHOUT DRY SECTION OF SHIELD.

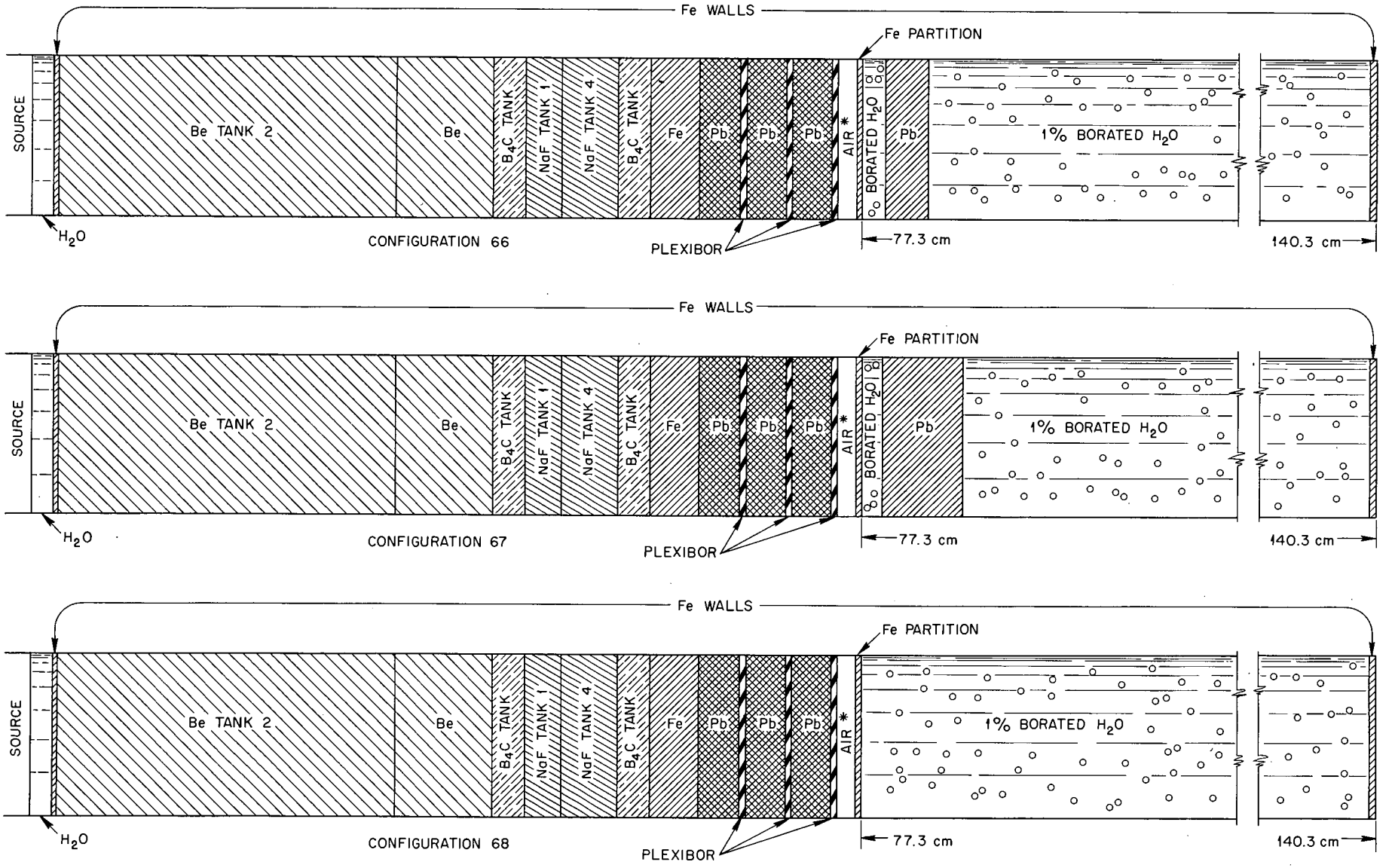

Fig. VI-25. Lid Tank Mockups of Reflector – Moderated Reactor and Shield.

Configurations 66, 67, and 68

Component	Thickness of Component (cm)		
	Configuration 66	Configuration 67	Configuration 68
H_2O	2.1	2.1	2.3
Fe	0.48	0.48	0.48
Be Tank 2	31.01	31.01	31.01
Be (ρ = 1.84 g/cc)	9.21	9.21	9.21
B_4C Tank	3.02	3.02	3.02
NaF Tank 1	3.5	3.5	3.5
NaF Tank 4	5.4	5.4	5.4
B_4C Tank	3.02	3.02	3.02
Fe	4.45	4.45	4.45
Pb	3.81	3.81	3.81
Plexibor	0.48	0.48	0.48
Pb	3.81	3.81	3.81
Plexibor	0.48	0.48	0.48
Pb	3.81	3.81	3.81
Plexibor	0.48	0.48	0.48
Air[a]	1.76	1.76	1.56
Fe	0.48	0.48	0.48
1% Borated H_2O	2.39	1.88	-
Pb	3.81	7.62	-
1% Borated H_2O	56.32	53.02	62.52
Fe	0.48	0.48	0.48
Total	140.3	140.3	140.3

[a] Air distributed throughout dry section of shield.

DWG. 21195

* AIR DISTRIBUTED THROUGHOUT DRY SECTION OF SHIELD.

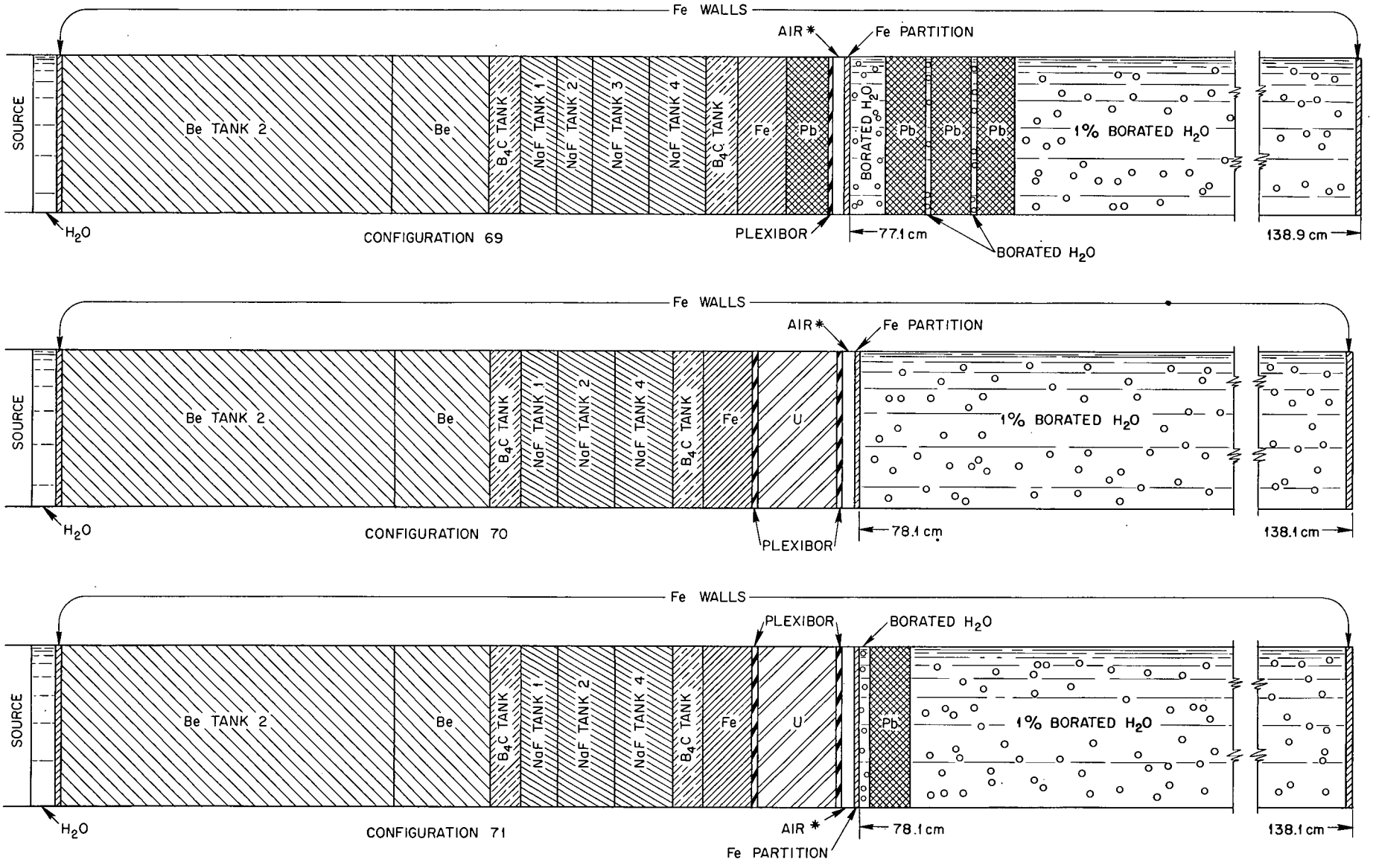

Fig. VI-26. Lid Tank Mockups of Reflector – Moderated Reactor and Shield.

Configurations 69, 70, and 71

Component	Thickness of Component (cm)		
	Configuration 69	Configuration 70	Configuration 71
H_2O	2.1	2.3	2.3
Fe	0.48	0.48	0.48
Be Tank 2	31.01	31.01	31.01
Be (ρ = 1.84 g/cc)	9.21	9.21	9.21
B_4C Tank	3.02	3.02	3.02
NaF Tank 1	3.5	3.5	3.5
NaF Tank 2	3.5	-	-
NaF Tank 3	5.4	5.4	5.4
NaF Tank 4	5.4	5.4	5.4
B_4C Tank	3.02	3.02	3.02
Fe	4.45	4.45	4.45
Pb	3.81	-	-
Plexibor	0.48	0.48	0.48
U	-	7.62	7.62
Plexibor	-	0.48	0.48
Air[a]	1.24	1.25	1.25
Fe	0.48	0.48	0.48
1% Borated H_2O	3.37	-	0.99
Pb	3.81	-	3.81
1% Borated H_2O	0.4	-	-
Pb	3.81	-	-
1% Borated H_2O	0.4	-	-
Pb	3.81	-	-
1% Borated H_2O	45.72	59.52	54.72
Fe	0.48	0.48	0.48
Total	138.9	138.1	138.1

(a) Air distributed throughout dry section of shield.

CONFIGURATION 72 SAME AS CONFIGURATION 70 EXCEPT A YOKE OF 4-in. THICK LEAD BRICKS WAS BUILT AROUND SIDES AND TOP OF 3-ft X 3-ft X 3-in. URANIUM SLAB IN AN EFFORT TO REDUCE STREAMING AROUND THE SLAB.

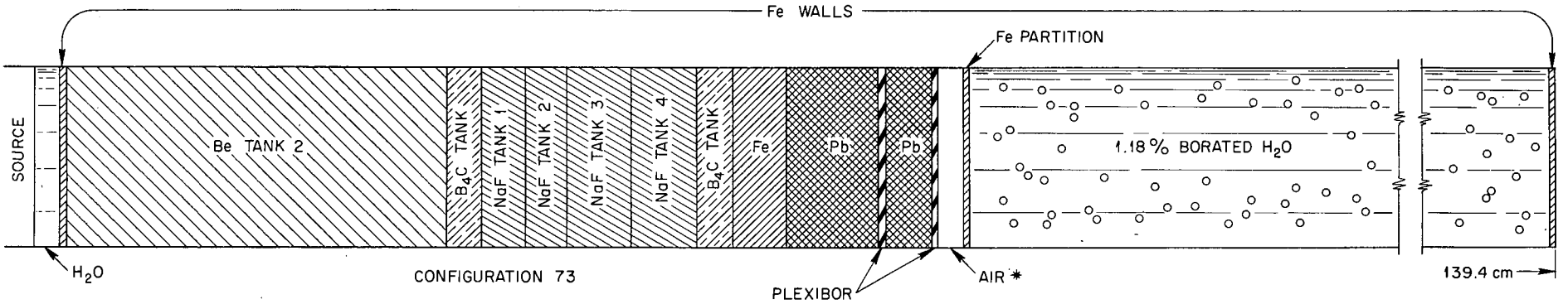

* AIR DISTRIBUTED THROUGHOUT DRY SECTION OF SHIELD.

CONFIGURATION 74 SAME AS CONFIGURATION 73 EXCEPT H_2O IN WET SECTION OF TANK WAS BORATED TO 0.5 % BORON BY WEIGHT.

CONFIGURATION 75 SAME AS CONFIGURATION 73 EXCEPT H_2O IN WET SECTION OF TANK CONTAINED NO BORON.

Fig. VI-27. Lid Tank Mockups of Reflector – Moderated Reactor and Shield.

Configurations 72, 73, 74, and 75

Component	Thickness of Component (cm)			
	Configuration 72	Configuration 73	Configuration 74	Configuration 75
H_2O	2.5	2.2	2.2	2.2
Fe	0.48	0.48	0.48	0.48
Be Tank 2	31.01	31.01	31.01	31.01
Be (ρ = 1.84 g/cc)	9.21	-	-	-
B_4C Tank	3.02	3.02	3.02	3.02
NaF Tank 1	3.5	3.5	3.5	3.5
NaF Tank 2	-	3.5	3.5	3.5
NaF Tank 3	5.4	5.4	5.4	5.4
NaF Tank 4	5.4	5.4	5.4	5.4
B_4C Tank	3.02	3.02	3.02	3.02
Fe	4.45	4.45	4.45	4.45
Pb	-	7.62	7.62	7.62
Plexibor	0.48	0.48	0.48	0.48
U	7.62	-	-	-
Pb	-	3.81	3.81	3.81
Plexibor	0.48	0.48	0.48	0.48
Air[a]	1.45	2.25	2.25	2.25
Fe	0.48	0.48	0.48	0.48
1% Borated H_2O	61.52	61.82	-	-
0.5% Borated H_2O	-	-	61.82	-
H_2O	-	-	-	61.82
Fe	0.48	0.48	0.48	0.48
Total	140.5	139.4	139.4	139.4

(a) Air distributed throughout dry section of shield.

DWG. 21197

* AIR DISTRIBUTED THROUGHOUT DRY SECTION OF SHIELD.

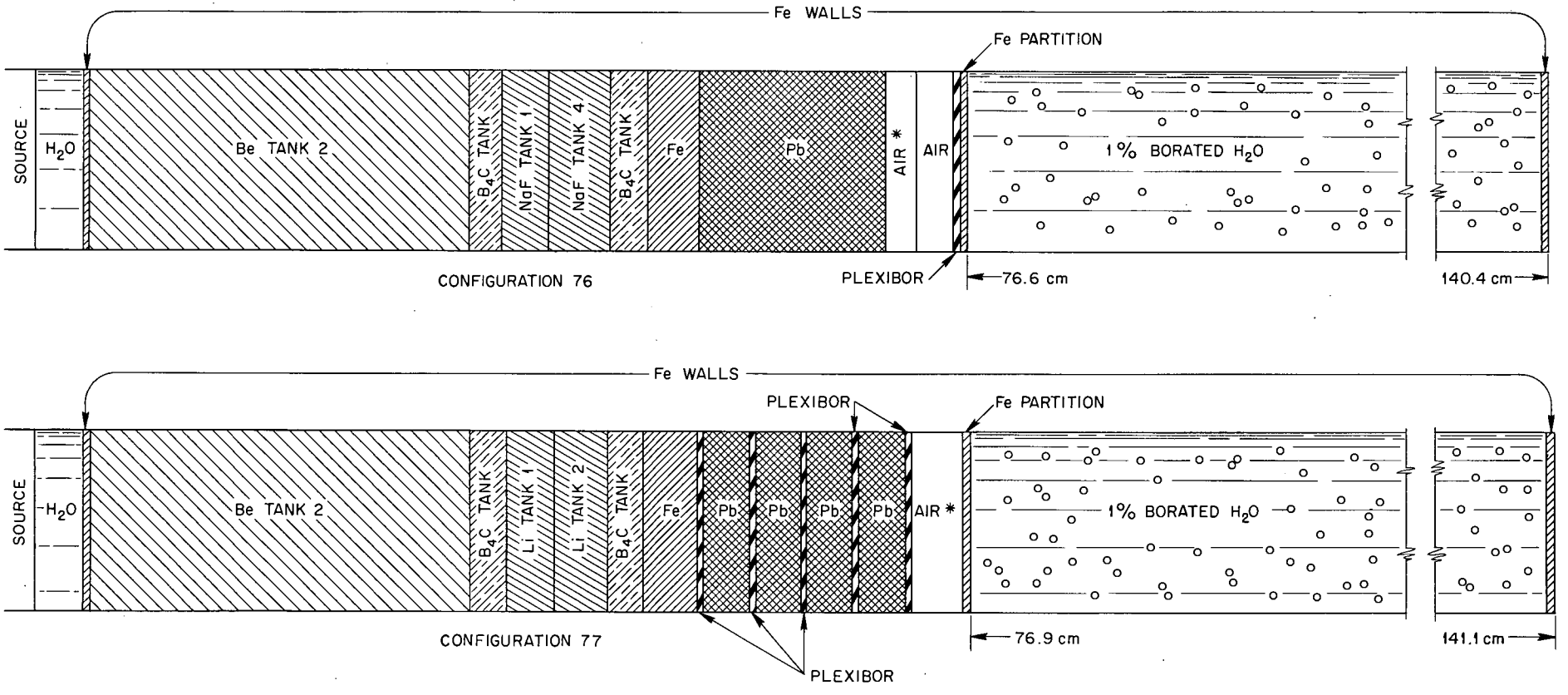

Fig. VI-28 Lid Tank Mockups of Reflector – Moderated Reactor and Shield.

Configurations 76 and 77

Component	Component Thickness (cm)	
	Configuration 76	Configuration 77
H_2O	3.9	4.1
Fe	0.48	0.48
Be Tank 2	31.01	31.01
B_4C Tank	3.02	3.02
NaF Tank 1	3.5	-
NaF Tank 4	5.4	-
Li Tank 1	-	3.82
Li Tank 2	-	4.61
B_4C Tank	3.02	3.02
Fe	4.45	4.45
Plexibor	-	0.48
Pb	15.24	3.81
Plexibor	-	0.48
Pb	-	3.81
Plexibor	-	0.48
Pb	-	3.81
Plexibor	-	0.48
Pb	-	3.81
Plexibor	-	0.48
Air[a]	2.42	4.27
Air	3.2	-
Plexibor	0.48	-
Fe	0.48	0.48
1% Borated H_2O	63.32	63.72
Fe	0.48	0.48
Total	140.4	141.1

[a]Air distributed throughout dry section of shield.

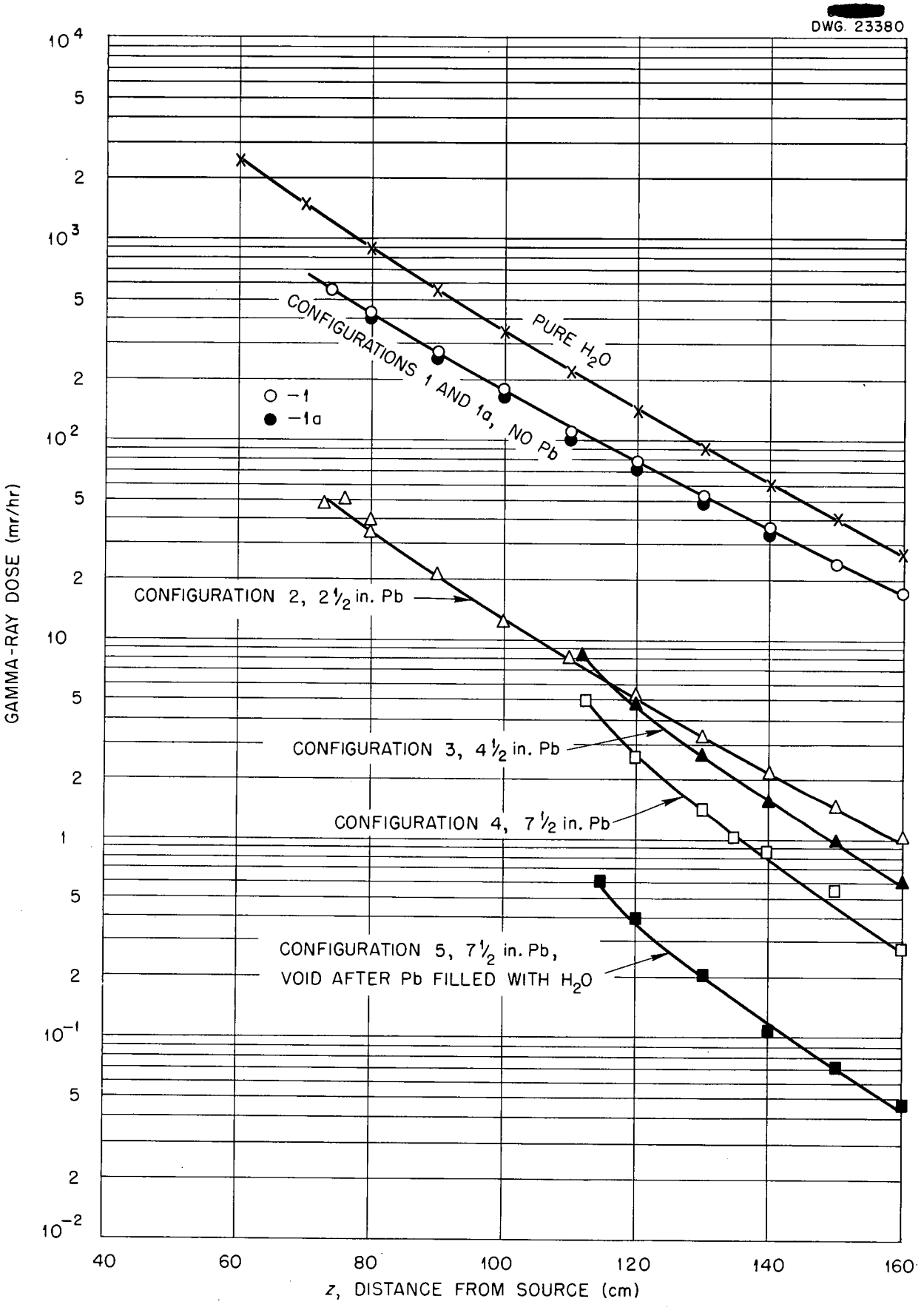

Fig. VI-29. Gamma-Ray Dose Measurements behind Lid Tank Mockups of Reflector-Moderated Reactor and Shield.

[redacted] [redacted]

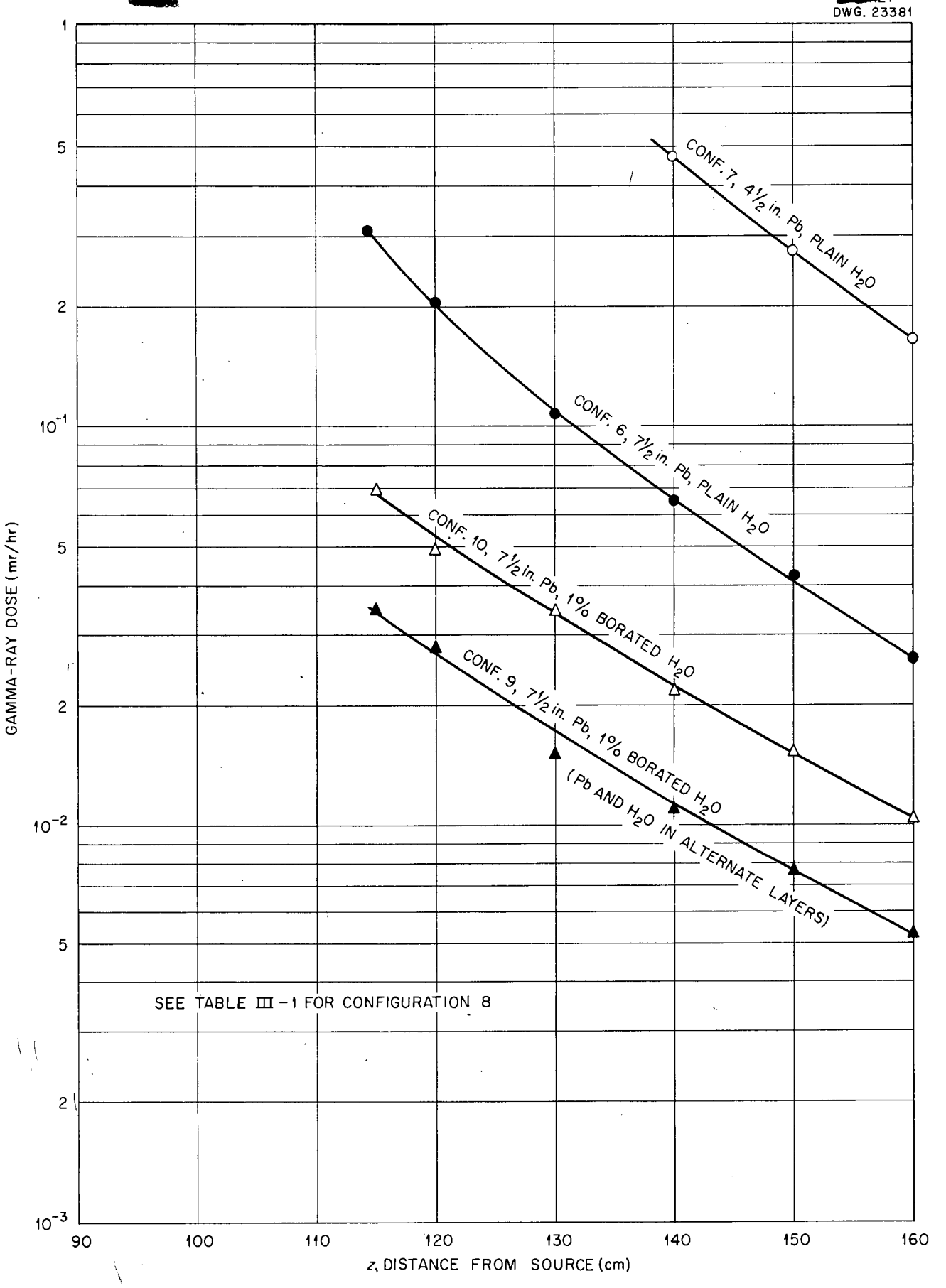

Fig. VI-30. Gamma-Ray Dose Measurements behind Lid Tank Mockups of Reflector-Moderated Reactor and Shield.

[redacted] [redacted]

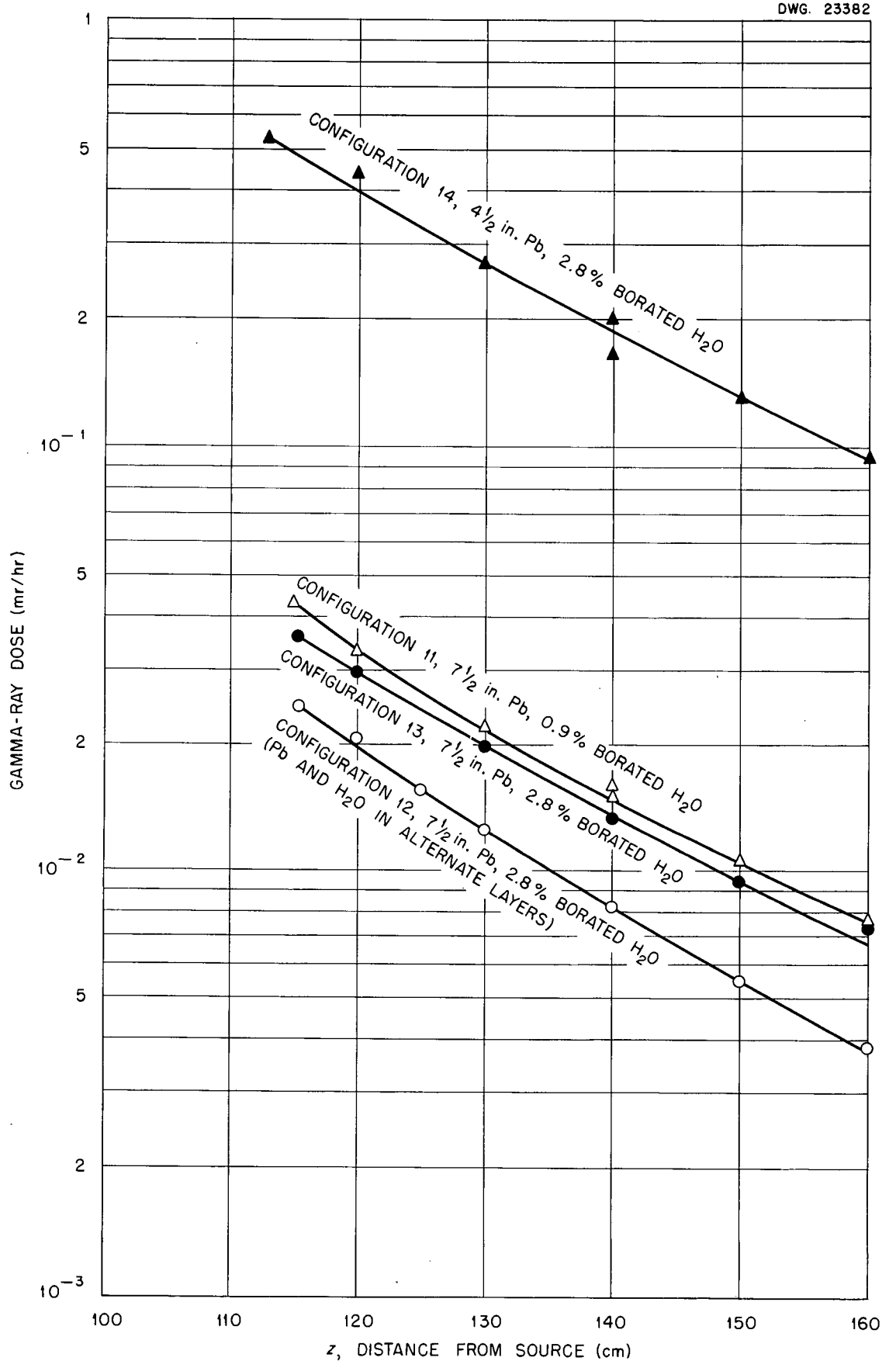

Fig. VI-31. Gamma-Ray Dose Measurements behind Lid Tank Mockups of Reflector-Moderated Reactor and Shield.

[redacted] [redacted]

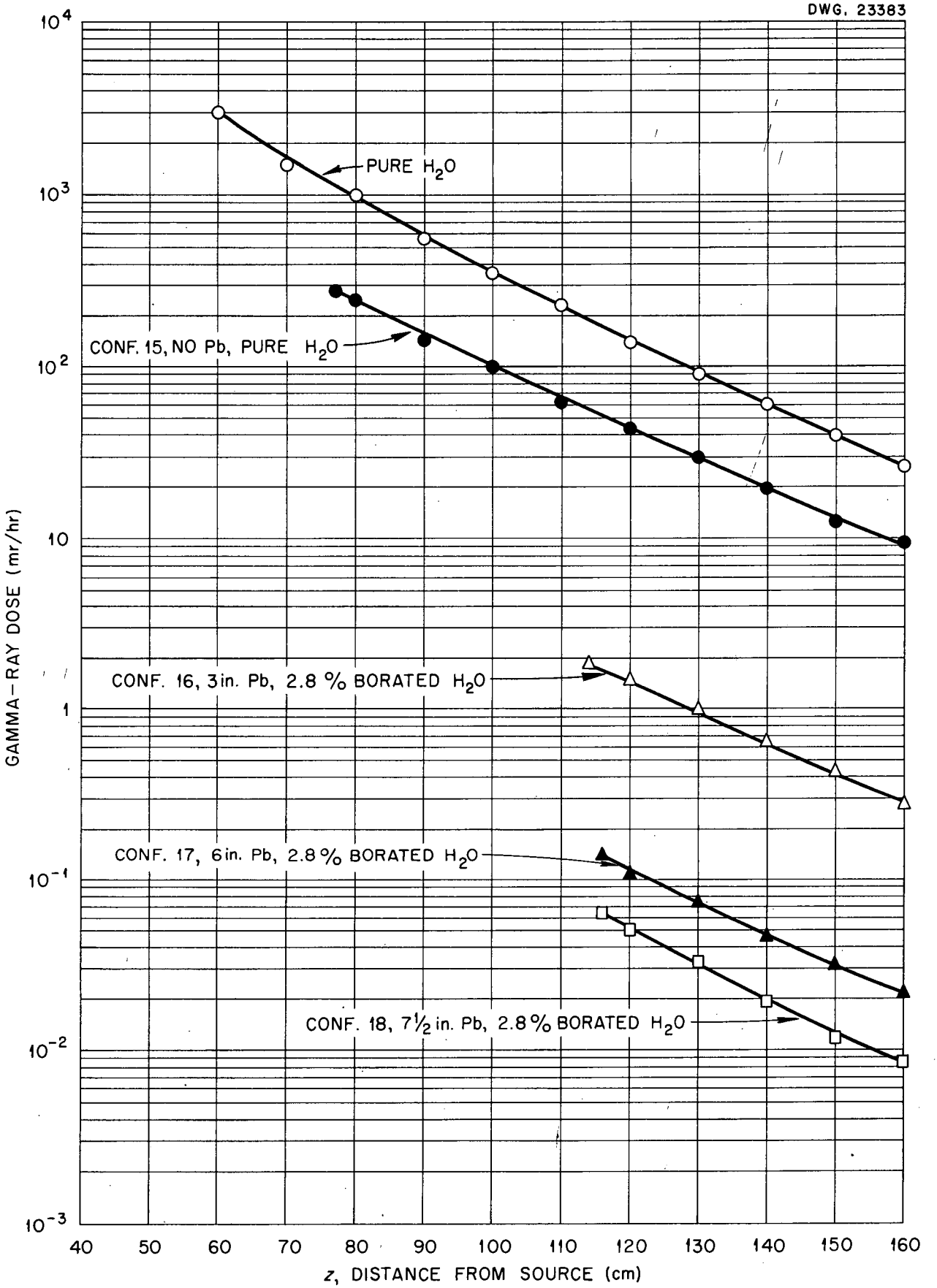

Fig. VI-32. Gamma-Ray Dose Measurements behind Lid Tank Mockups of Reflector-Moderated Reactor and Shield.

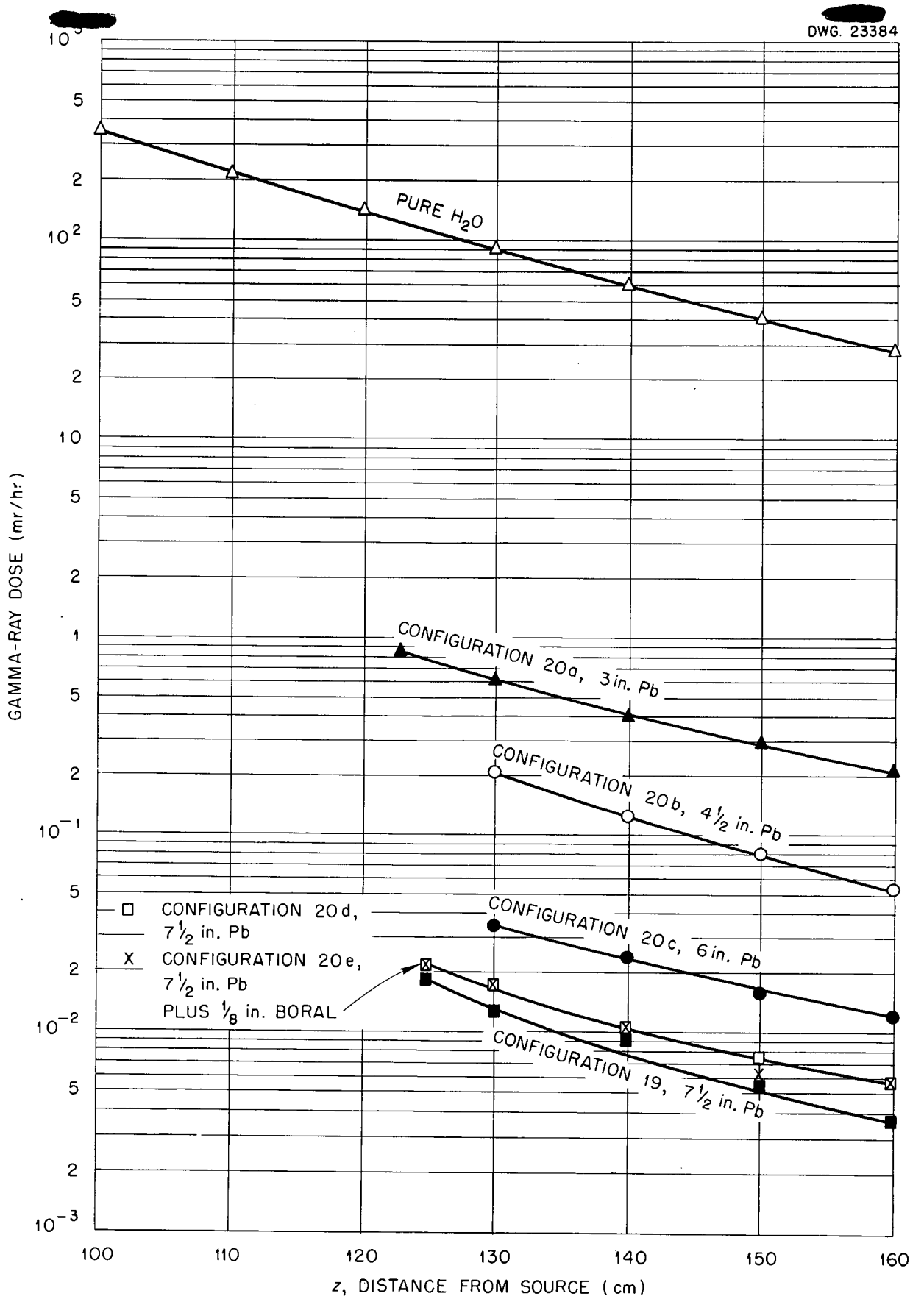

Fig. VI-33. Gamma-Ray Dose Measurements behind Lid Tank Mockups of Reflector-Moderated Reactor and Shield.

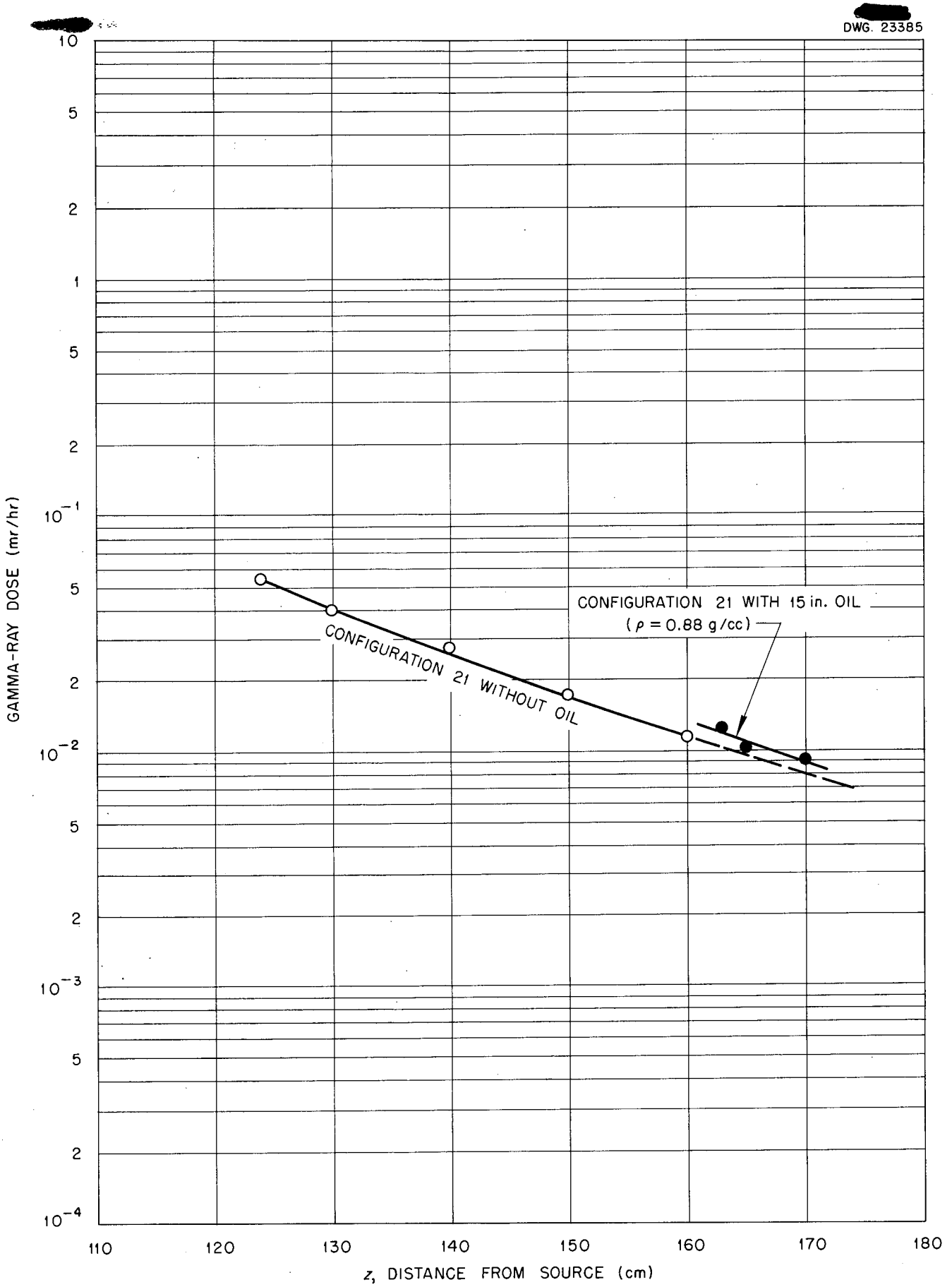

Fig. VI-34. Gamma-Ray Dose Measurements behind Lid Tank Mockups of Reflector-Moderated Reactor and Shield.

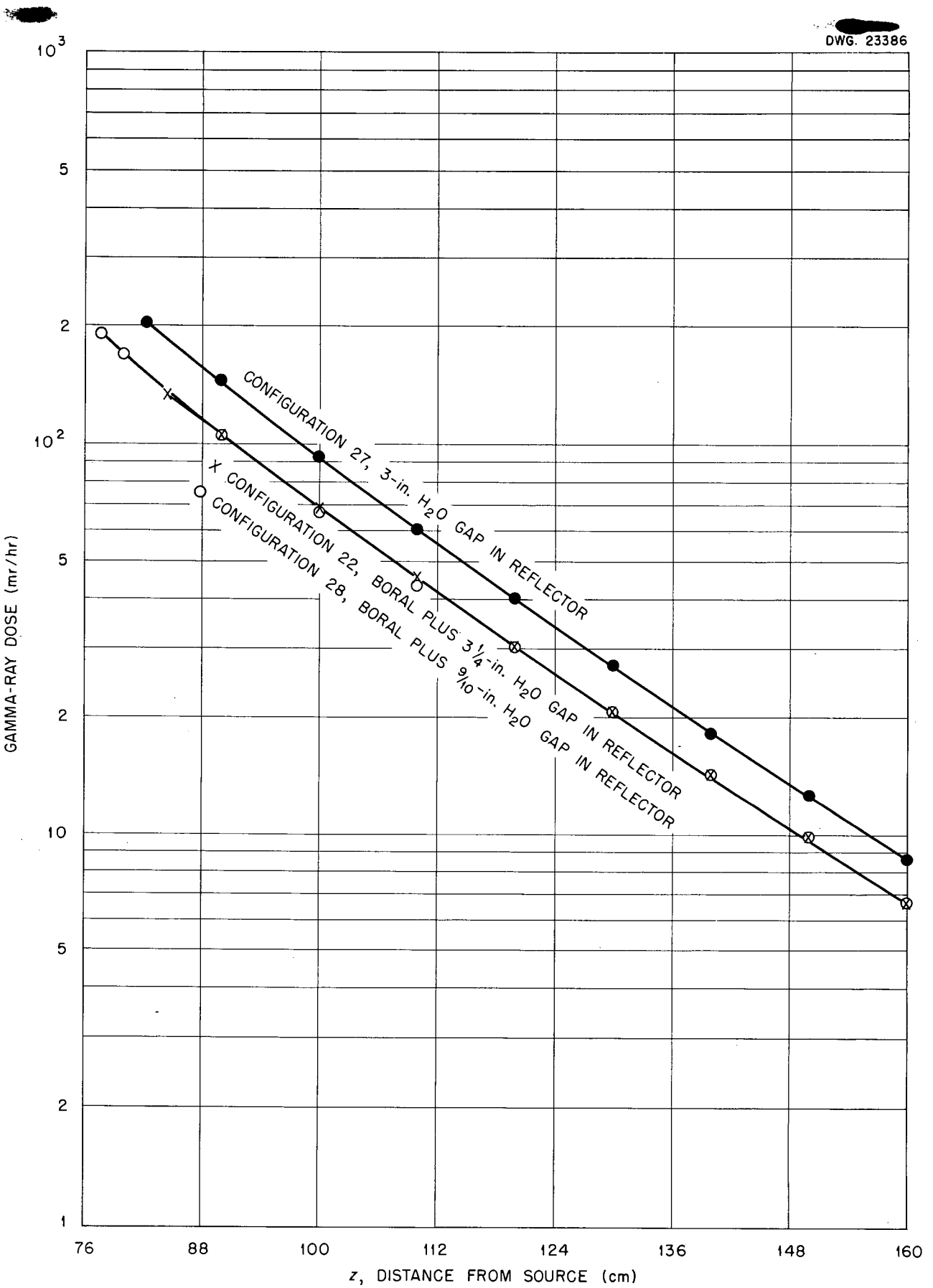

Fig. VI-35. Gamma-Ray Dose Measurements behind Lid Tank Mockups of Reflector-Moderated Reactor and Shield.

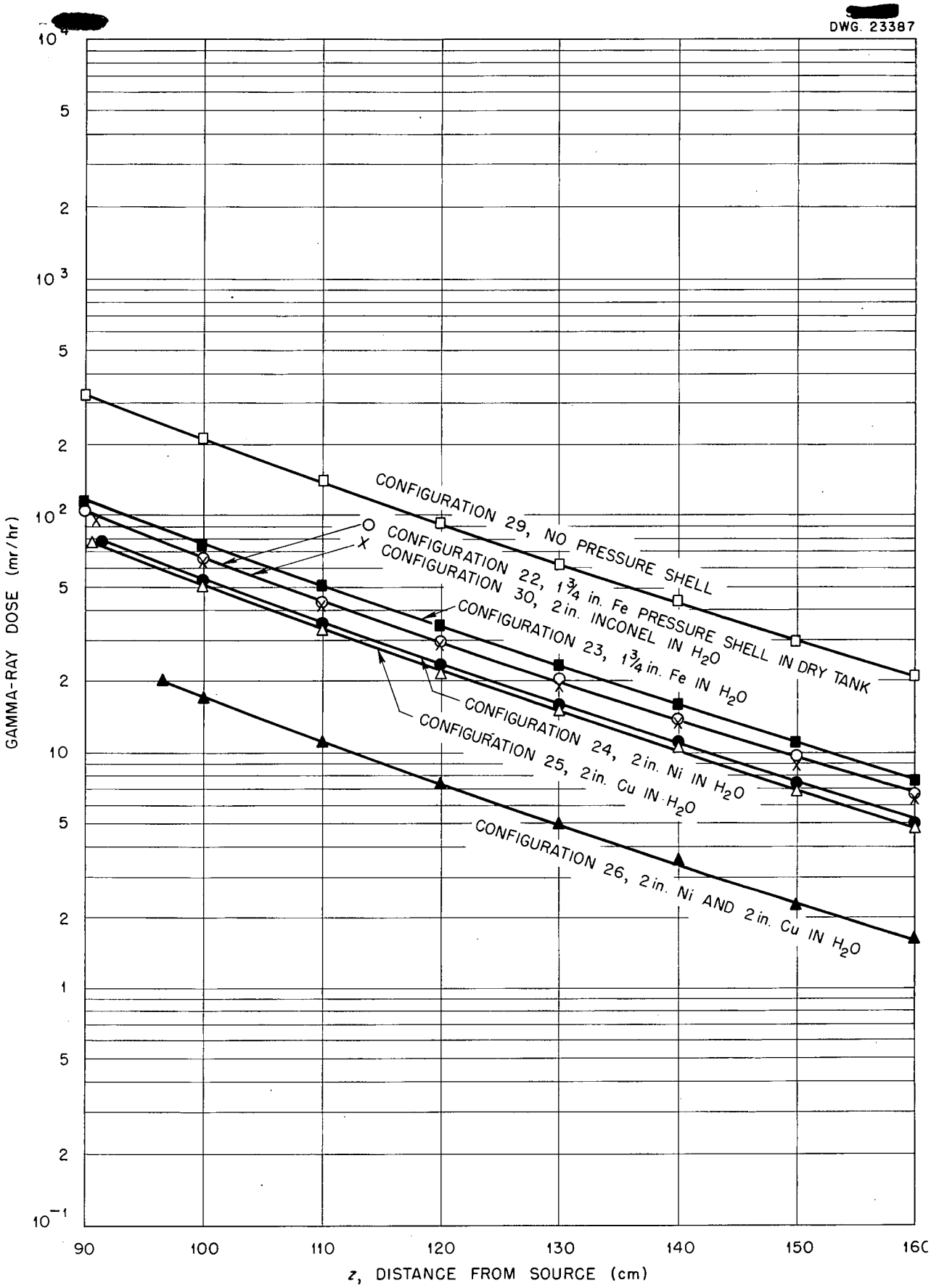

Fig. VI-36. Gamma-Ray Dose Measurements behind Lid Tank Mockups of Reflector-Moderated Reactor and Shield.

[redacted]

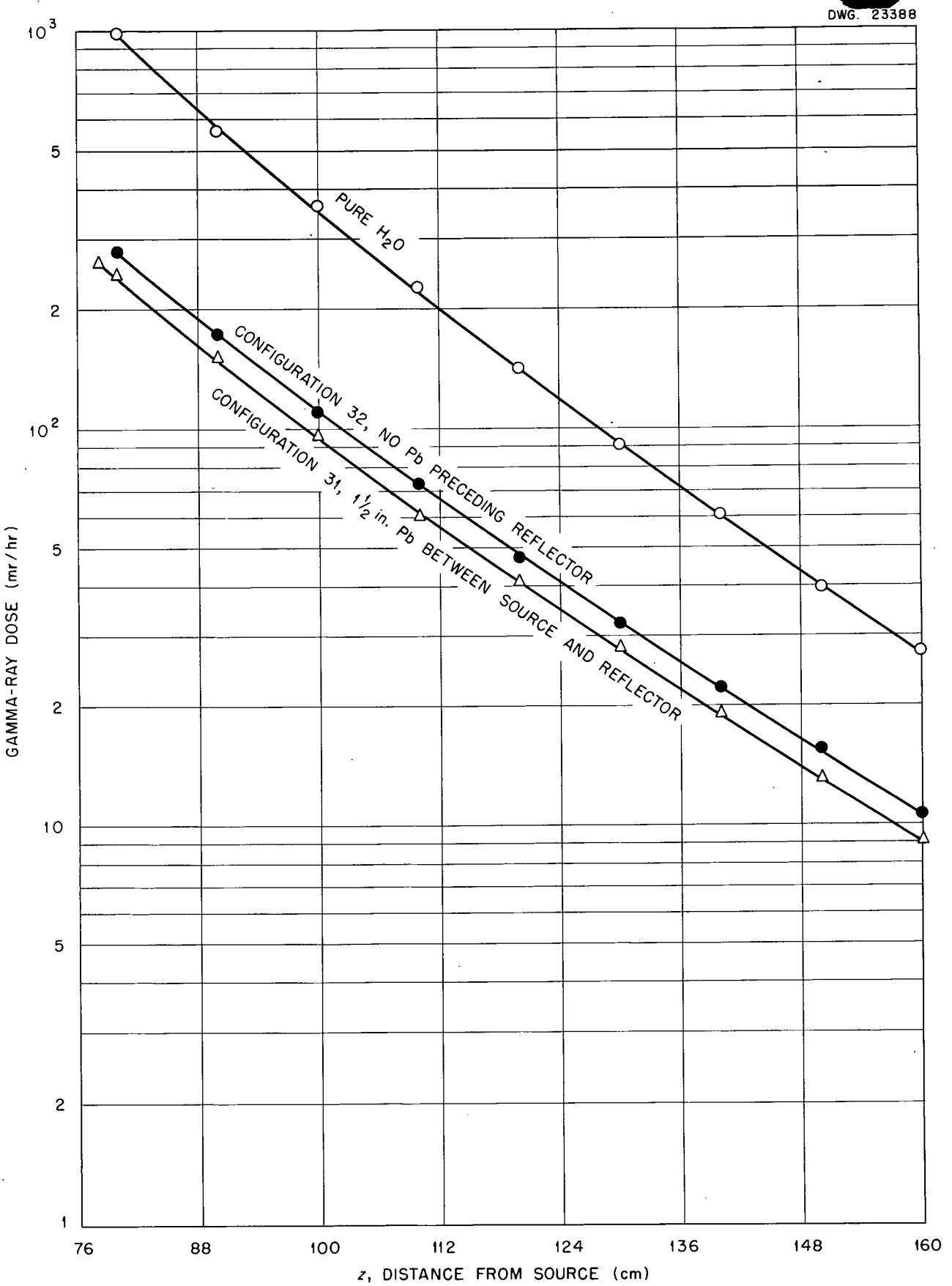

Fig. VI-37. Gamma-Ray Dose Measurements behind Lid Tank Mockups of Reflector-Moderated Reactor and Shield.

[redacted] [redacted]

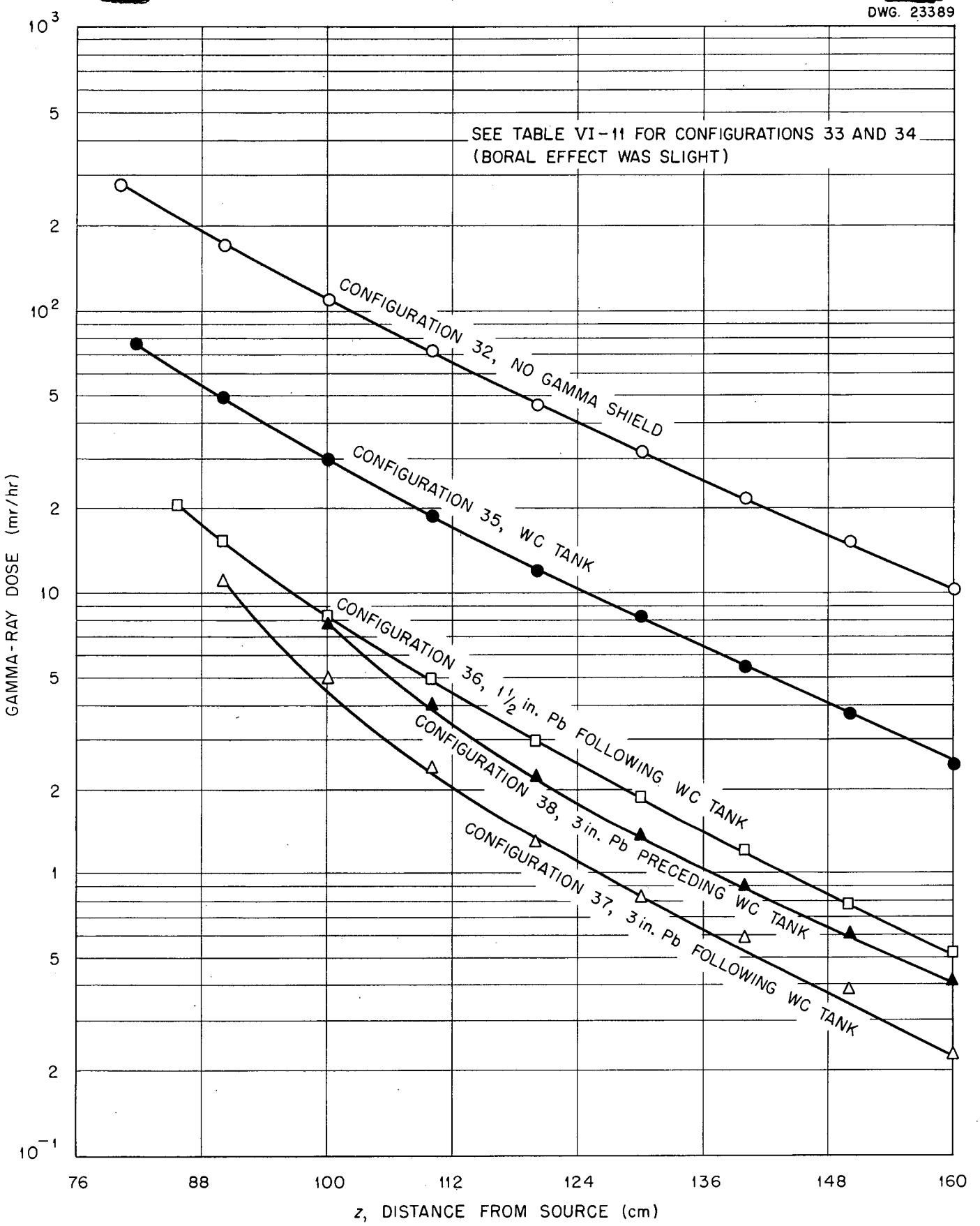

Fig. VI-38. Gamma-Ray Dose Measurements behind Lid Tank Mockups of Reflector-Moderated Reactor and Shield.

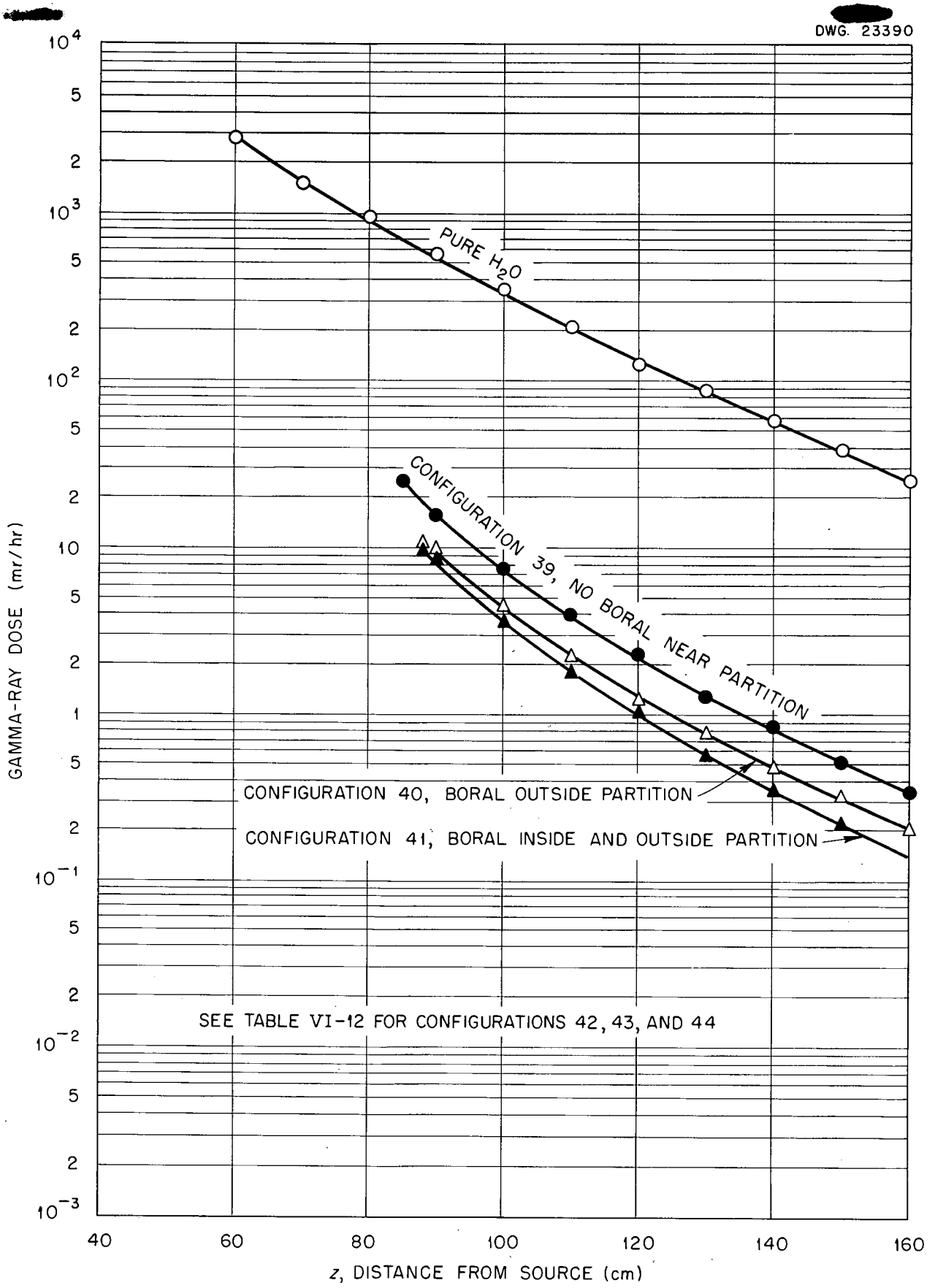

Fig. VI-39. Gamma Ray Dose Measurements behind Lid Tank Mockups of Reflector-Moderated Reactor and Shield.

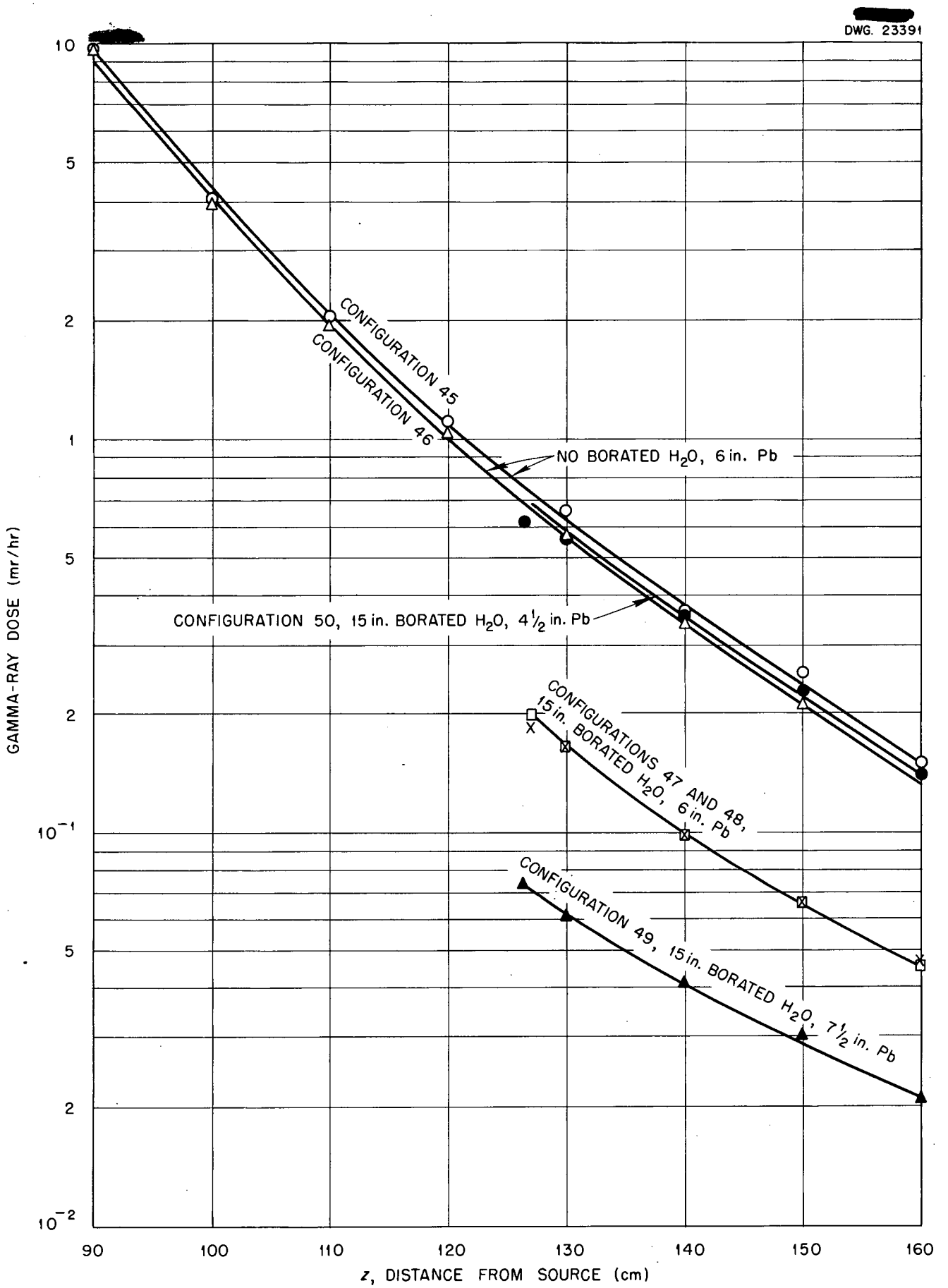

Fig. VI-40. Gamma-Ray Dose Measurements behind Lid Tank Mockups of Reflector-Moderated Reactor and Shield.

[redacted]

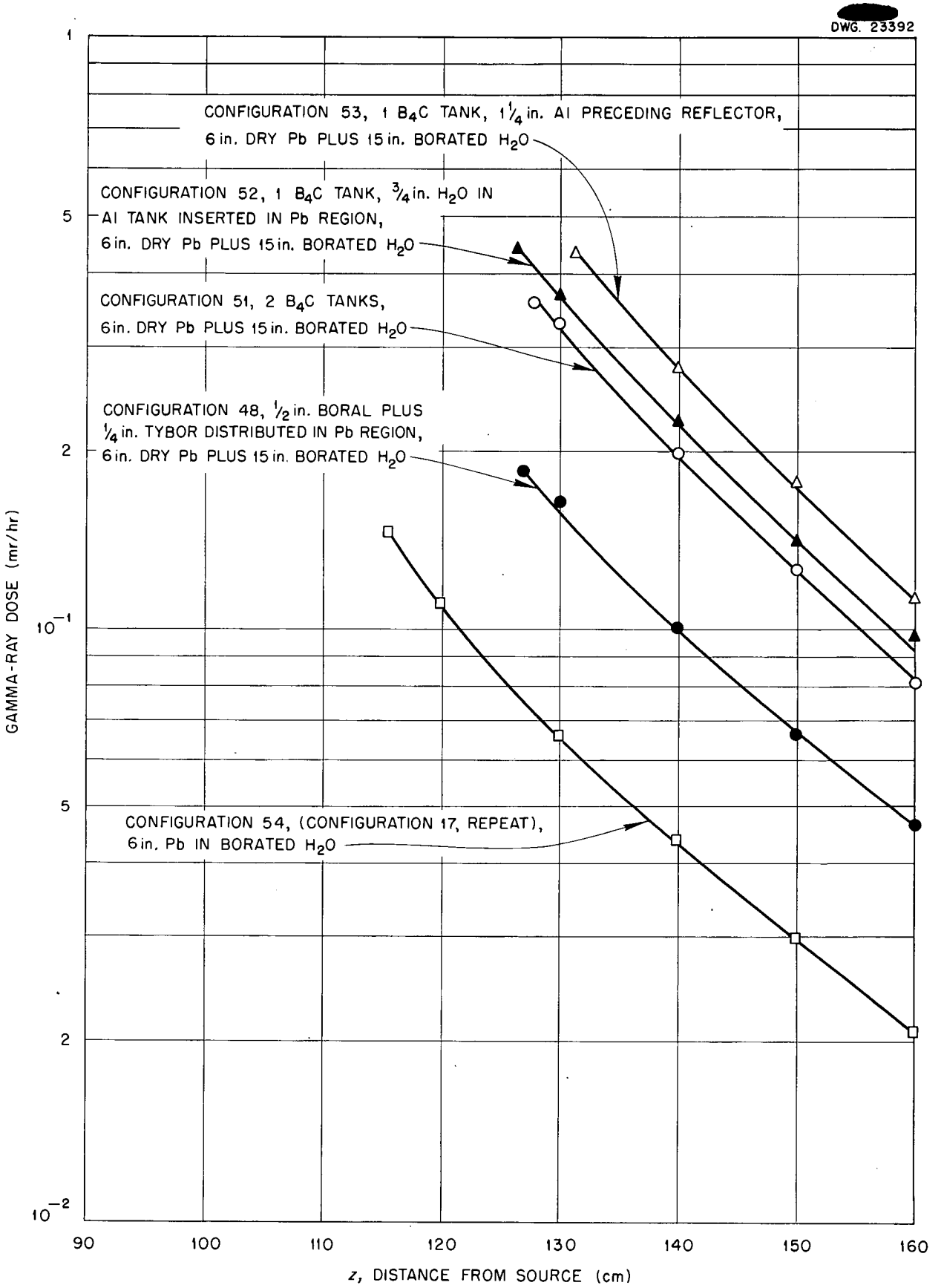

Fig. VI-41. Gamma-Ray Dose Measurements behind Lid Tank Mockups of Reflector-Moderated Reactor and Shield.

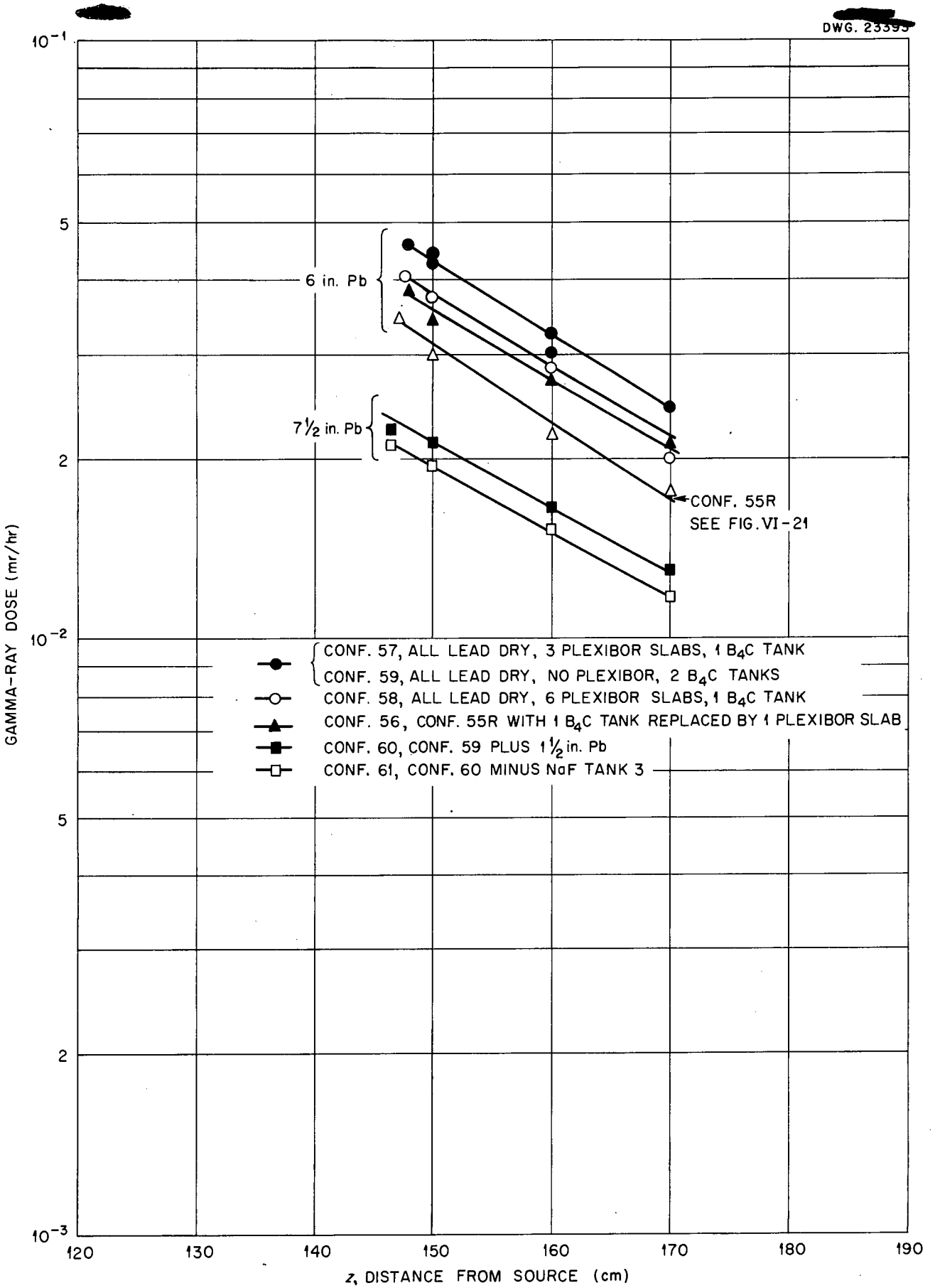

Fig. VI-42. Gamma-Ray Dose Measurements behind Lid Tank Mockups of Reflector-Moderated Reactor and Shield.

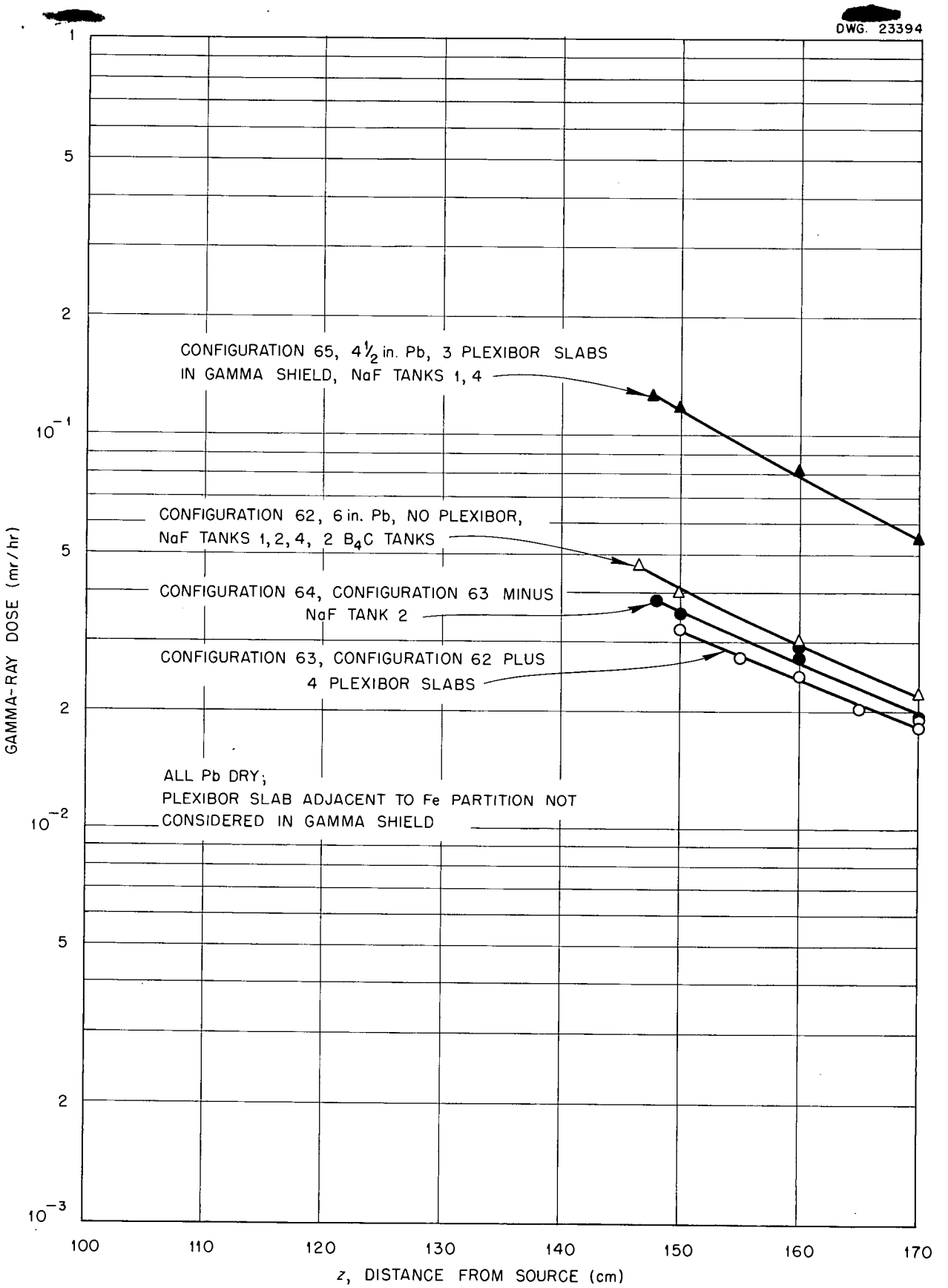

Fig. VI-43. Gamma-Ray Dose Measurements behind Lid Tank Mockups of Reflector-Moderated Reactor and Shield.

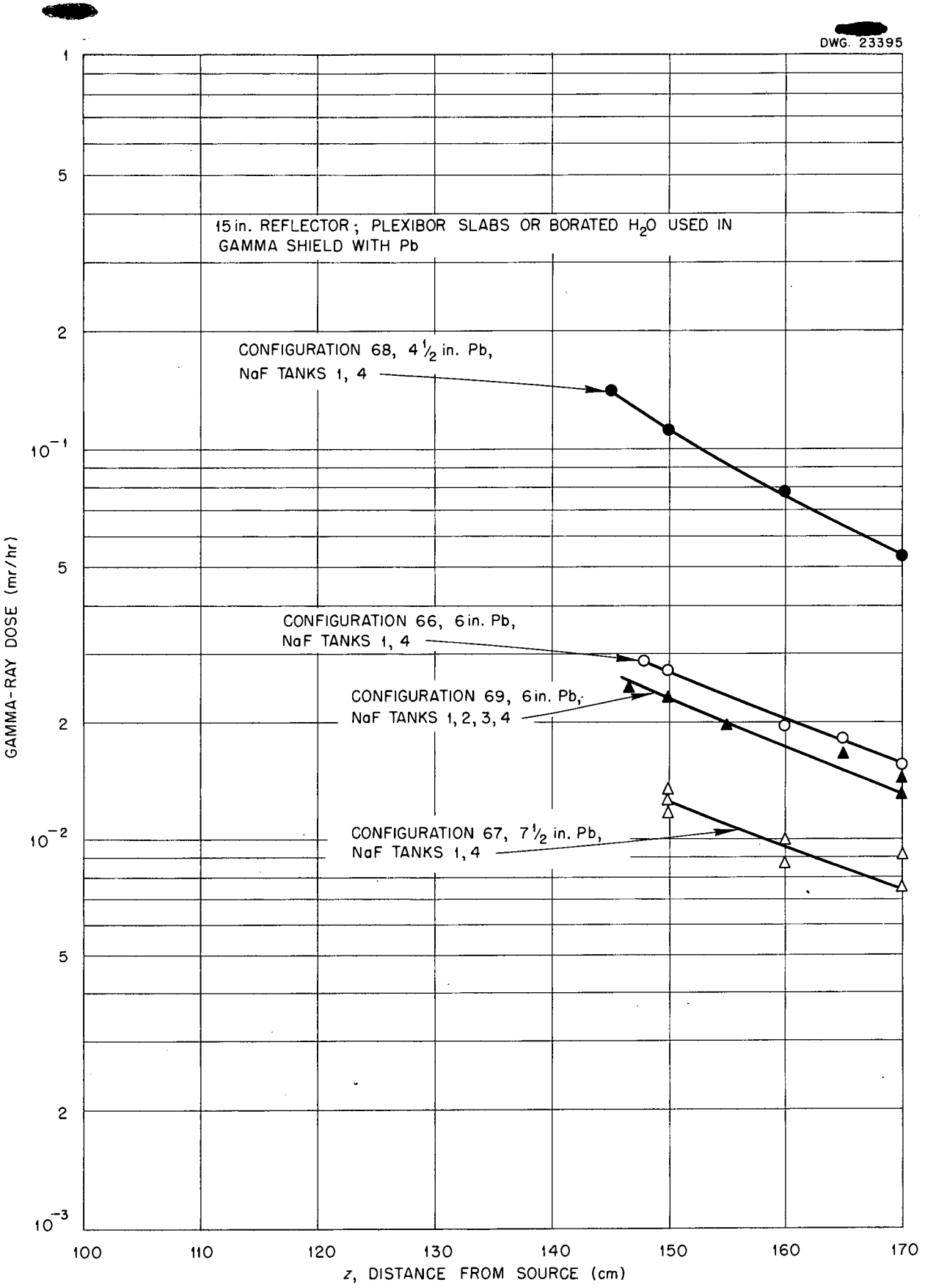

Fig. VI-44. Gamma-Ray Dose Measurements behind Lid Tank Mockups of Reflector-Moderated Reactor and Shield.

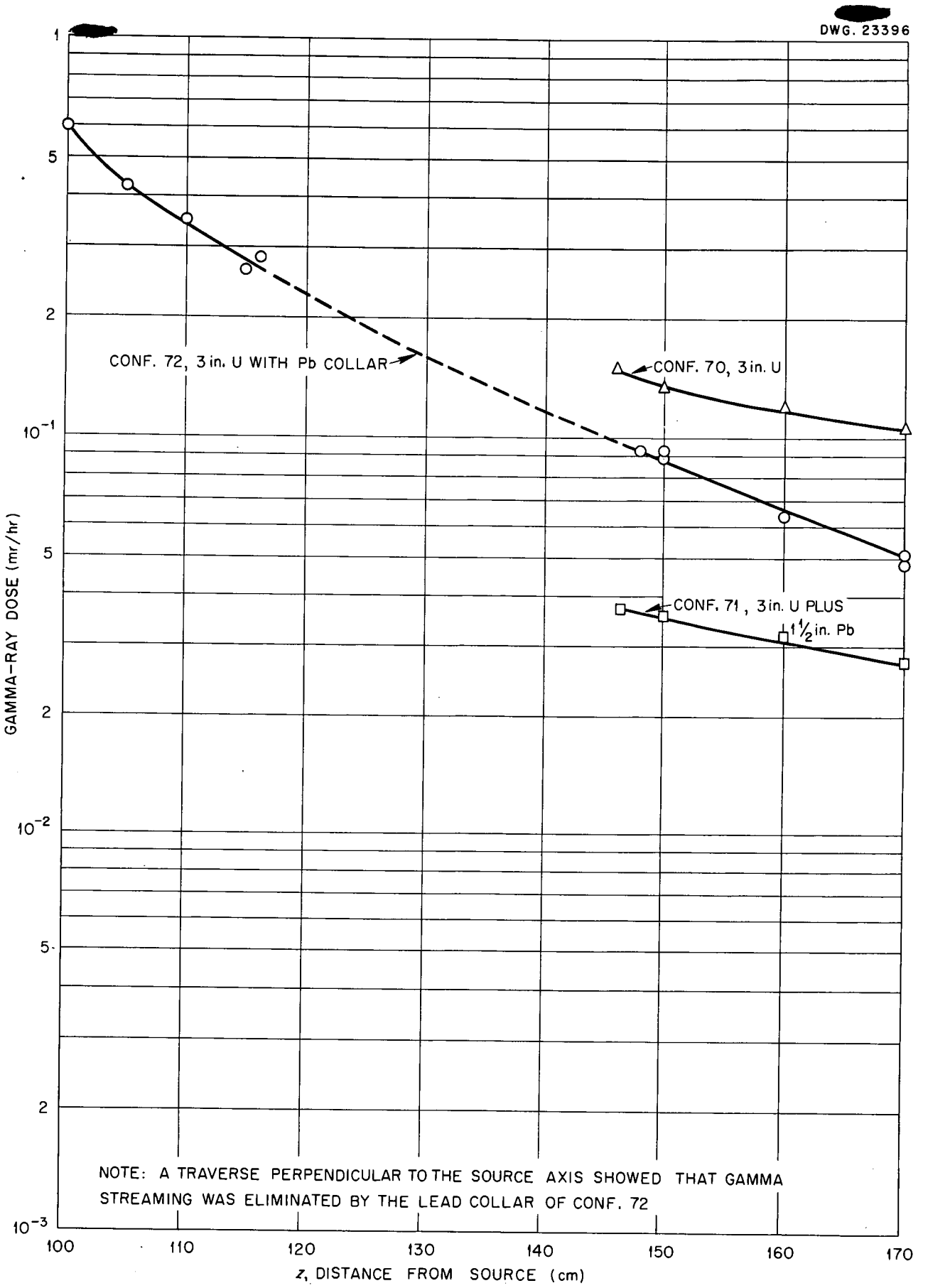

Fig. VI-45. Gamma-Rav Dose Measurements behind Lid Tank Mockups of Reflector-Moderated Reactor and Shield.

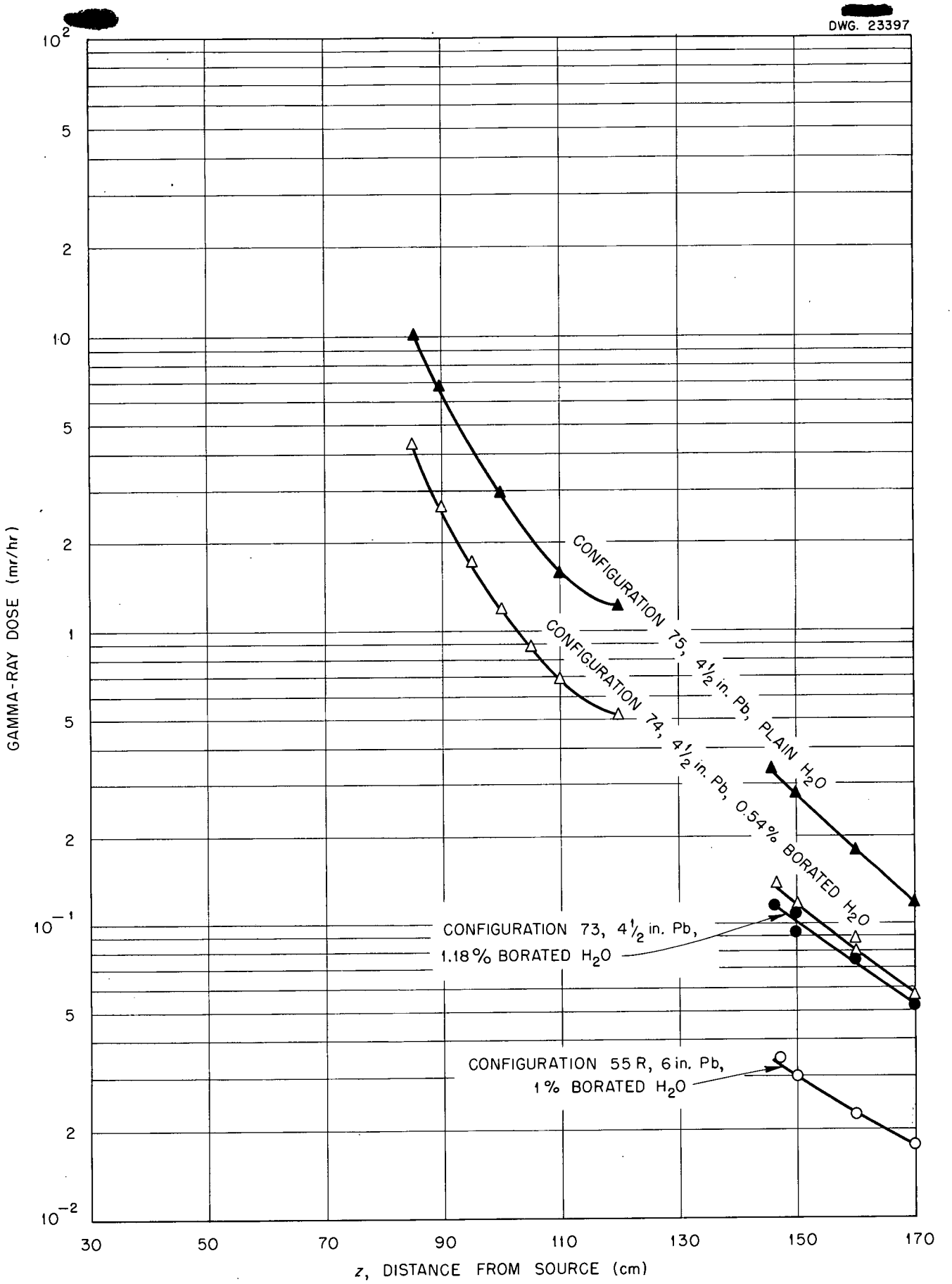

Fig. VI-46. Gamma-Ray Dose Measurements behind Lid Tank Mockups of Reflector-Moderated Reactor and Shield.

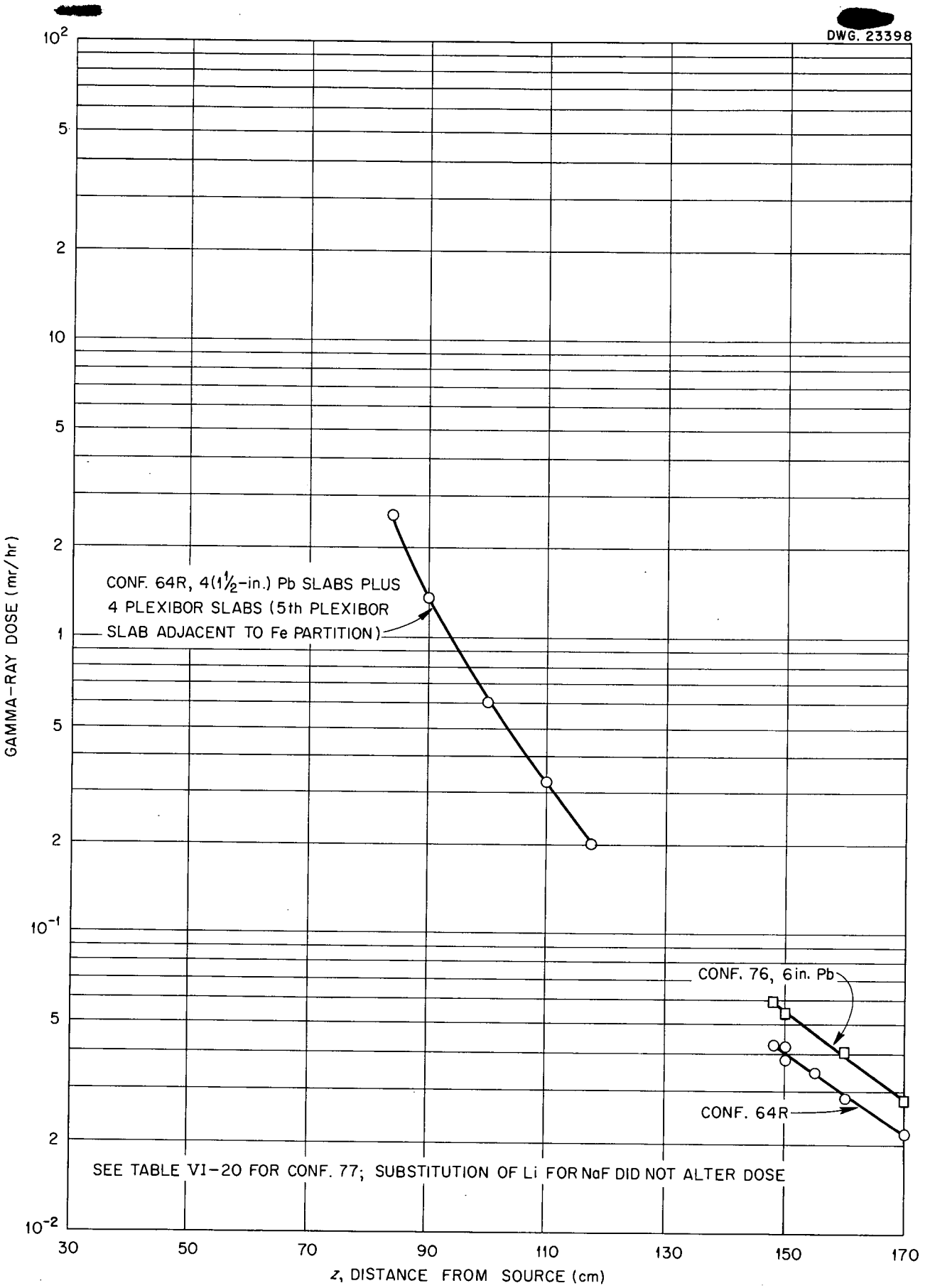

Fig. VI-47. Gamma-Ray Dose Measurements behind Lid Tank Mockups of Reflector-Moderated Reactor and Shield.

[redacted]

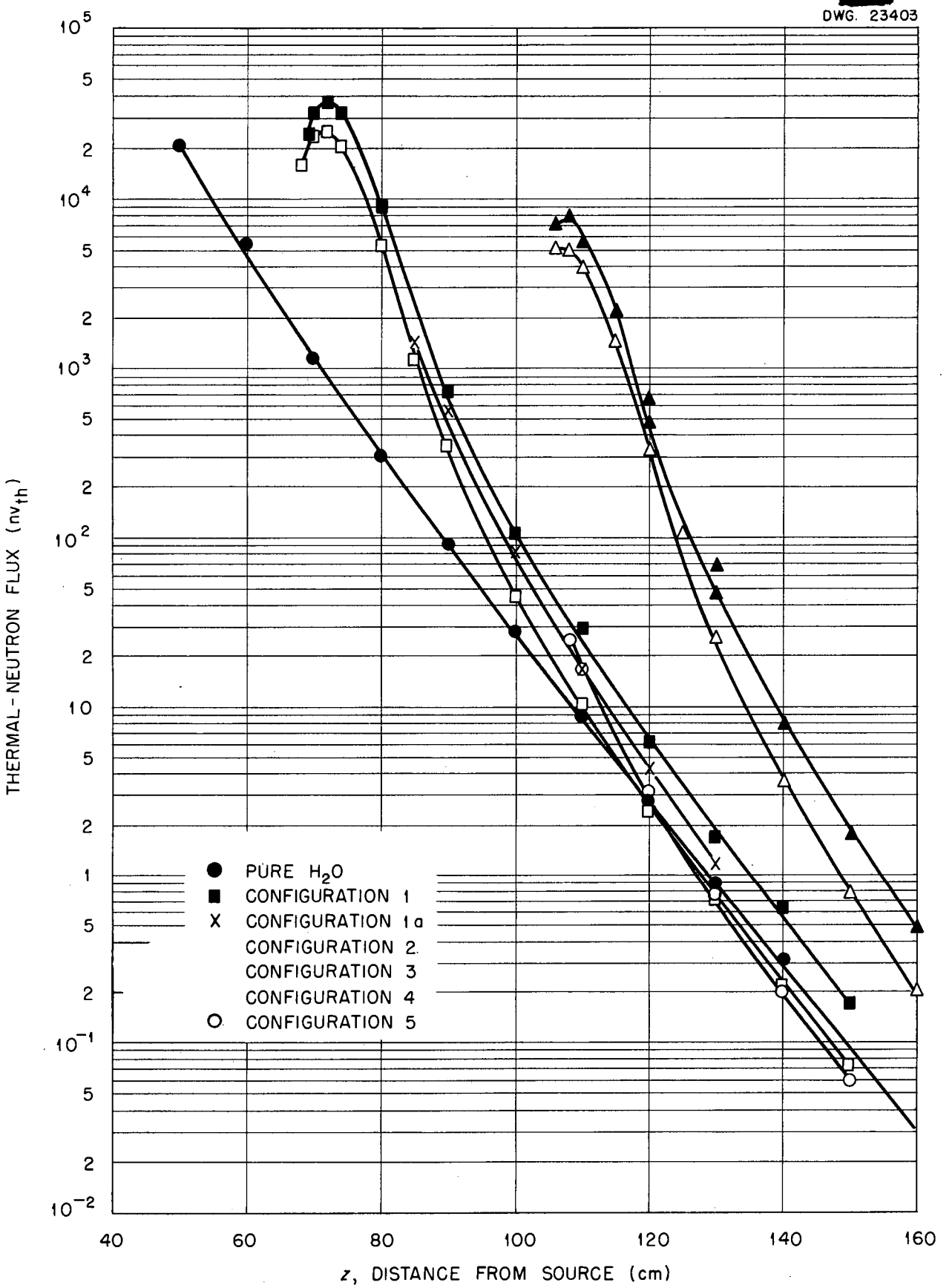

Fig. VI-48. Thermal-Neutron Flux Measurements behind Lid Tank Mockups of Reflector-Moderated Reactor and Shield.

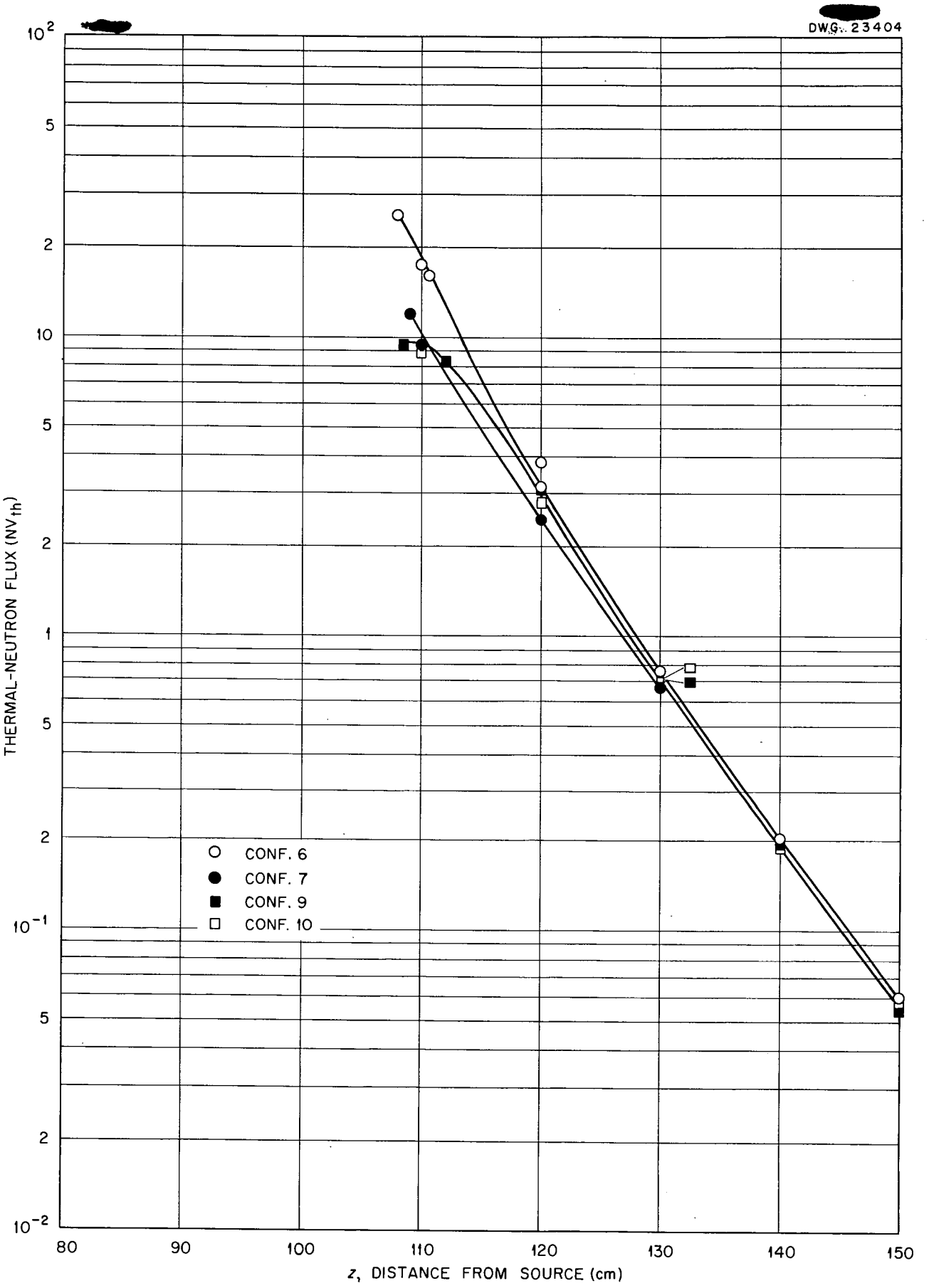

Fig. VI-49. Thermal-Neutron Flux Measurements behind Lid Tank Mockups of Reflector-Moderated Reactor and Shield.

[redacted]

[redacted]

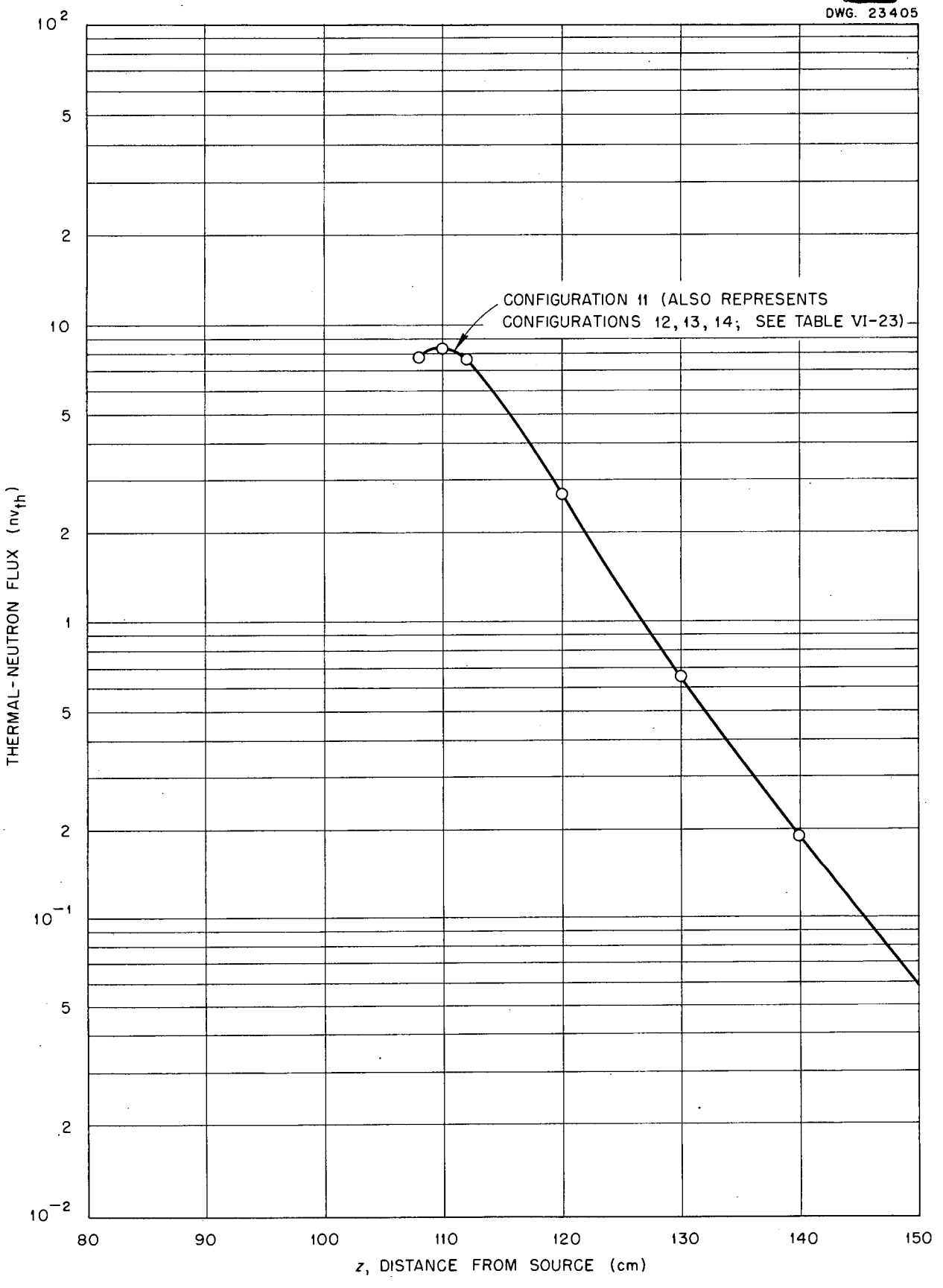

Fig. VI-50. Thermal-Neutron Flux Measurements behind Lid Tank Mockups of Reflector-Moderated Reactor and Shield.

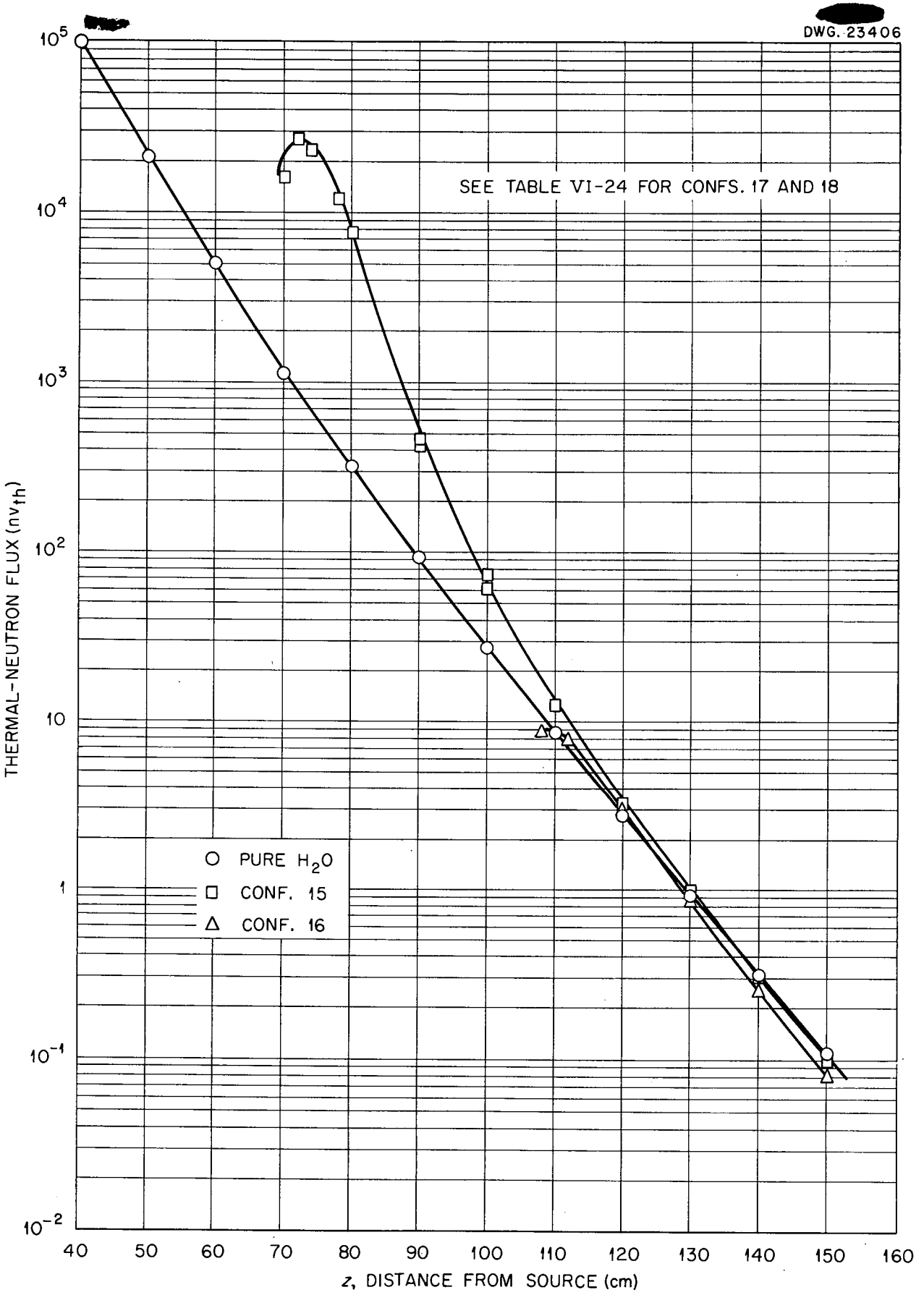

Fig. VI-51. Thermal-Neutron Flux Measurements behind Lid Tank Mockups of Reflector-Moderated Reactor and Shield.

[redacted]

[redacted]

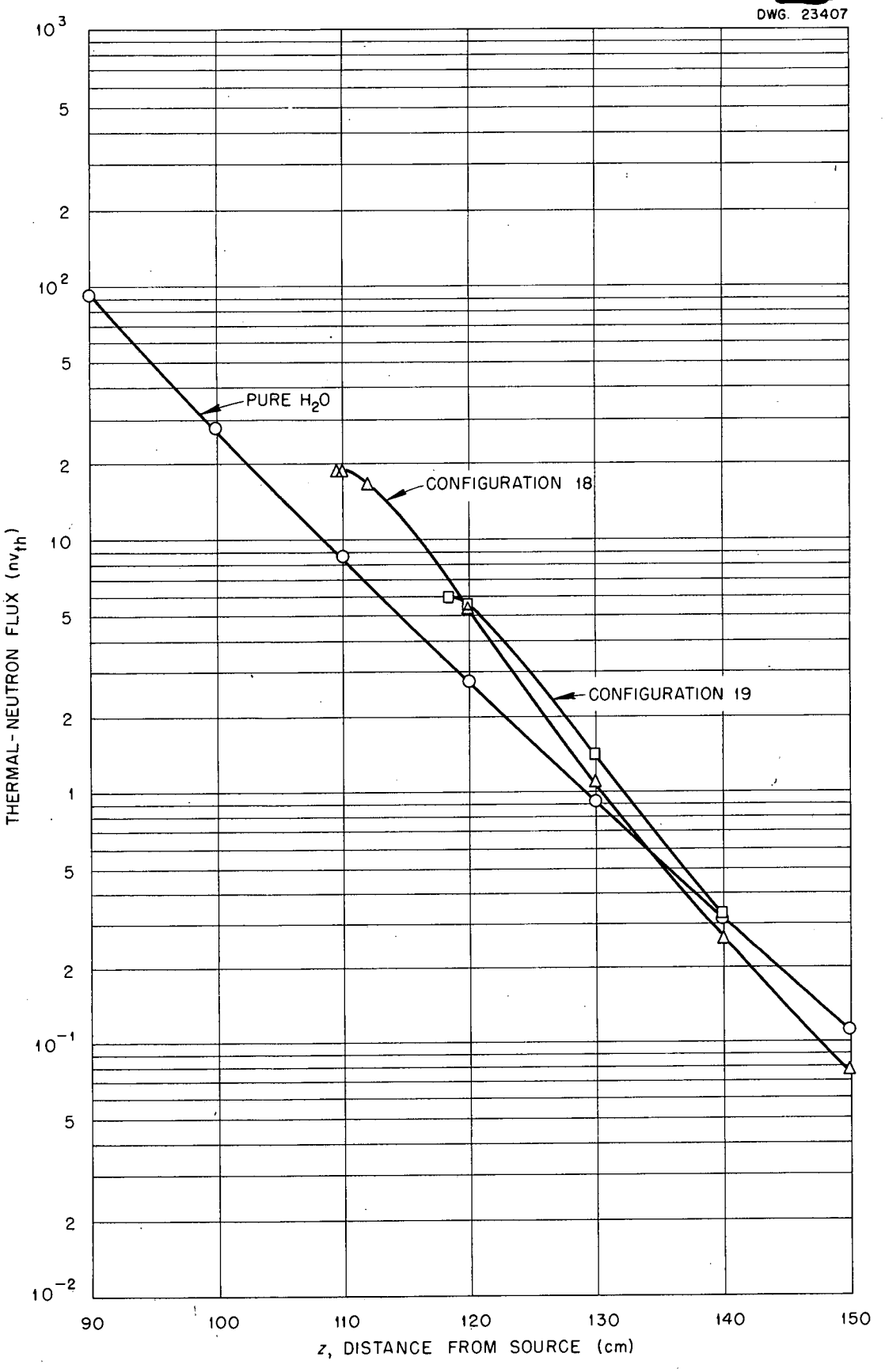

Fig. VI-52. Thermal-Neutron Flux Measurements behind Lid Tank Mockups of Reflector-Moderated Reactor and Shield.

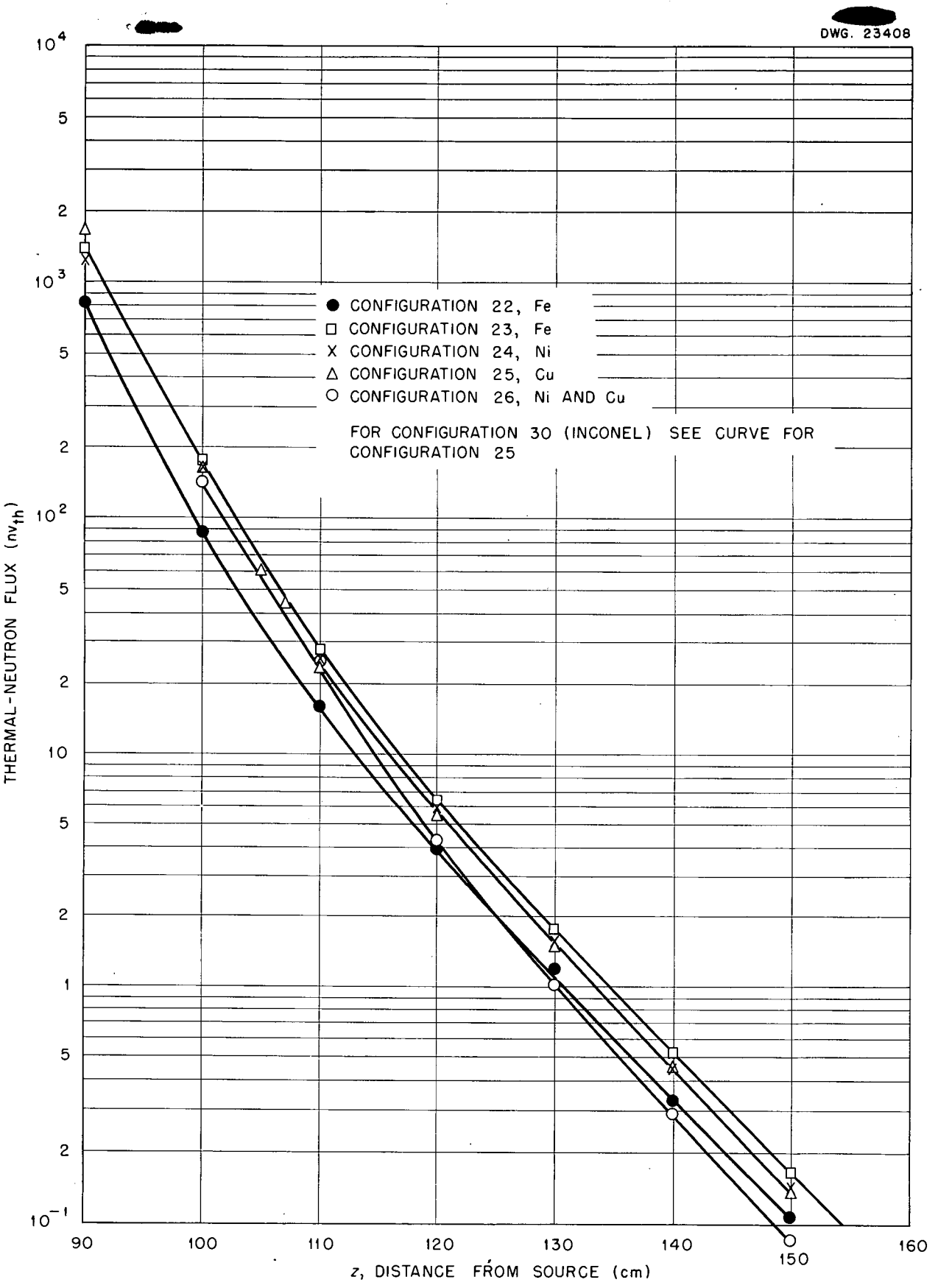

Fig. VI-53. Thermal-Neutron Flux Measurements behind Lid Tank Mockups of Reflector-Moderated Reactor and Shield.

[redacted] [redacted]

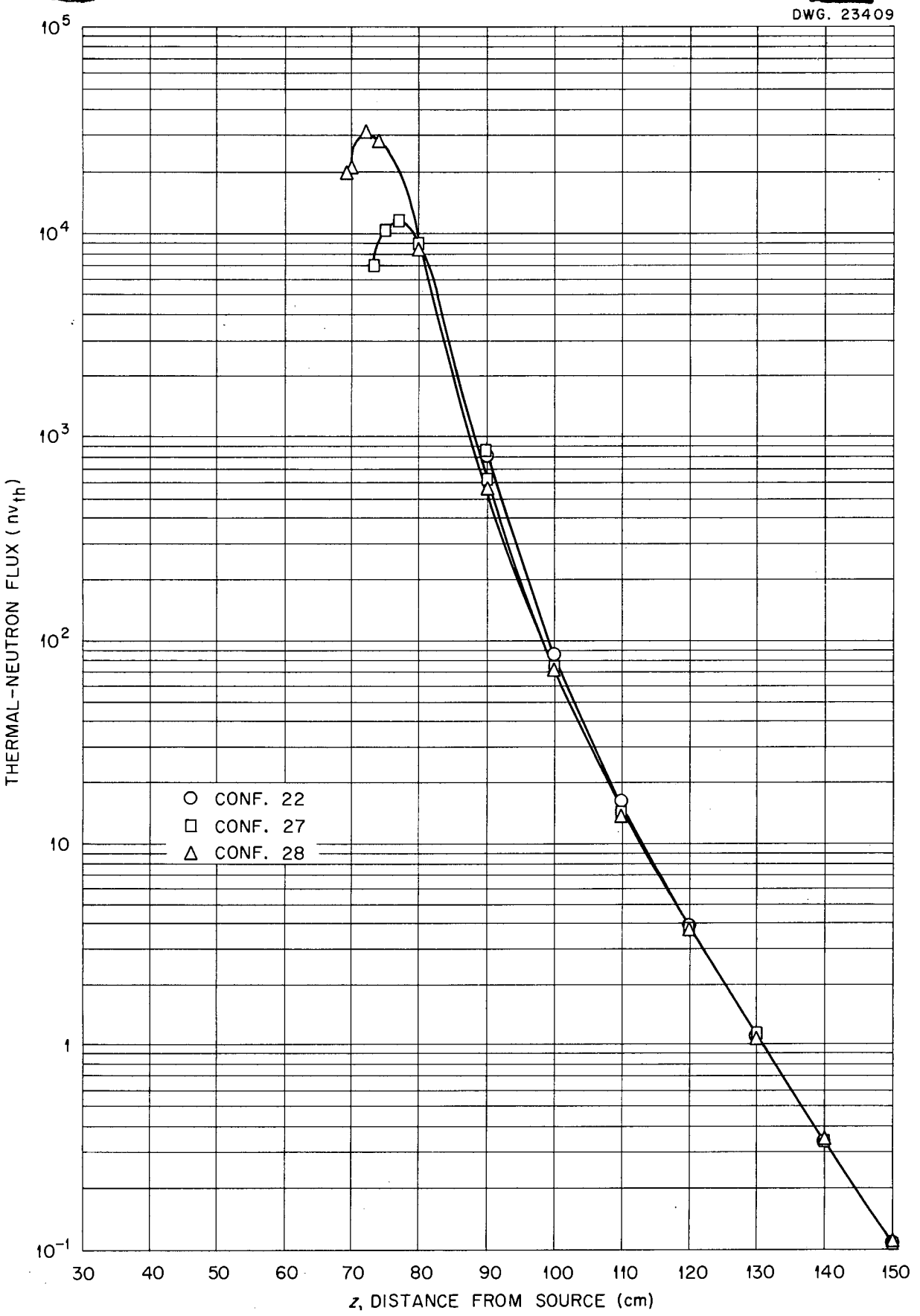

Fig.VI-54. Thermal-Neutron Flux Measurements behind Lid Tank Mockups of Reflector-Moderated Reactor and Shield.

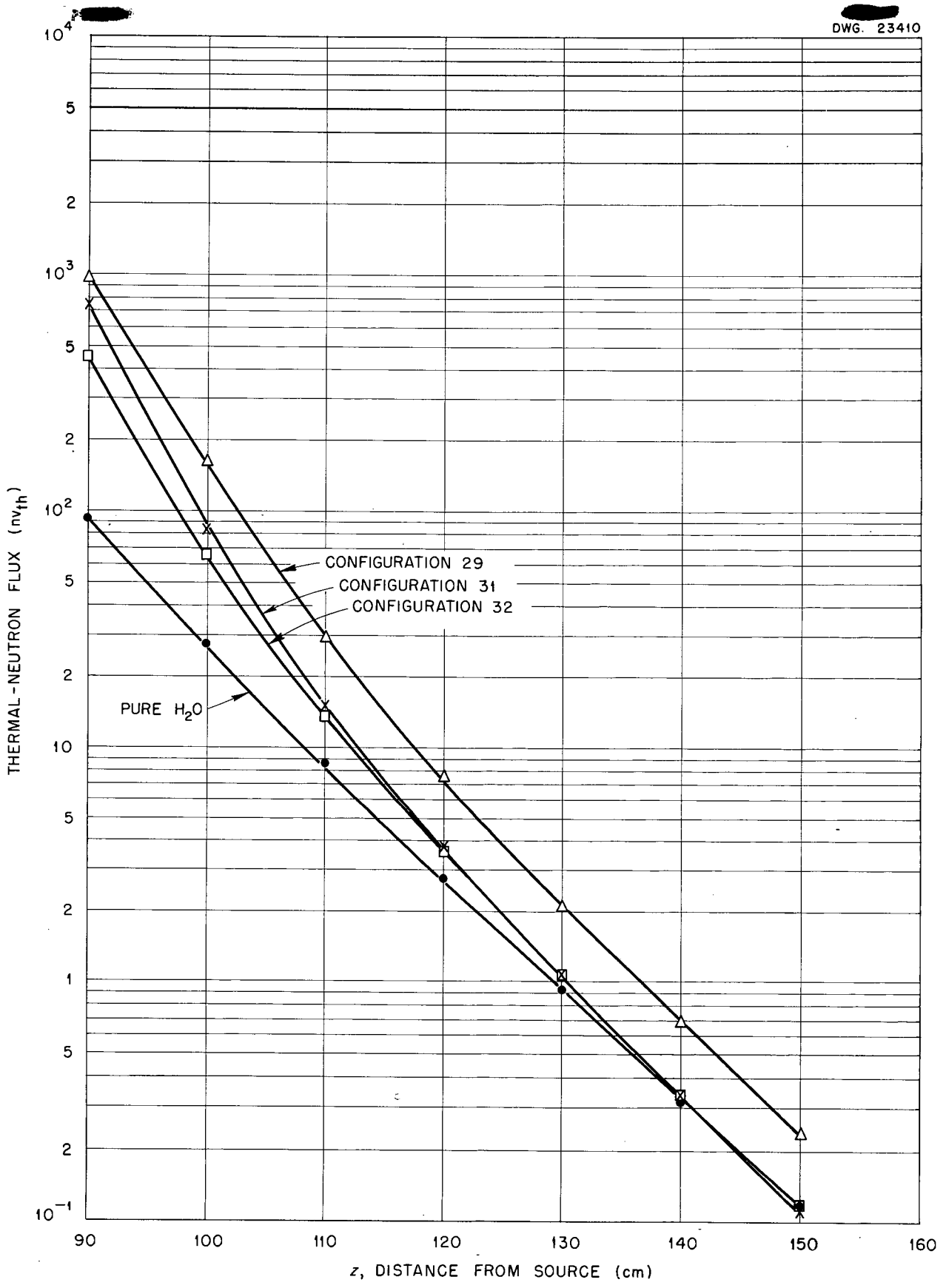

Fig. VI-55. Thermal-Neutron Flux Measurements behind Lid Tank Mockups of Reflector-Moderated Reactor and Shield.

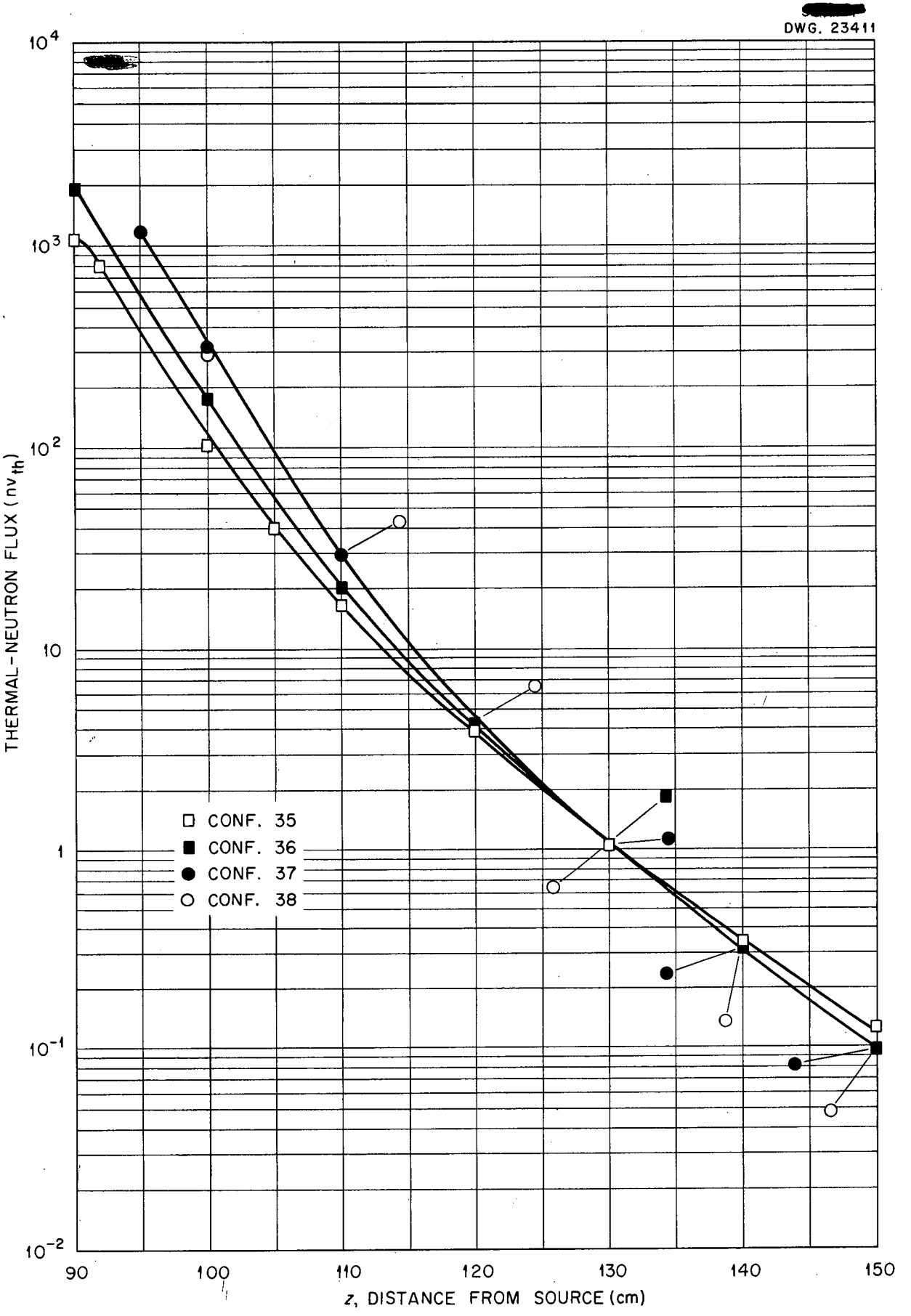

Fig. VI-56. Thermal-Neutron Flux Measurements behind Lid Tank Mockups of Reflector-Moderated Reactor and Shield.

[redacted]

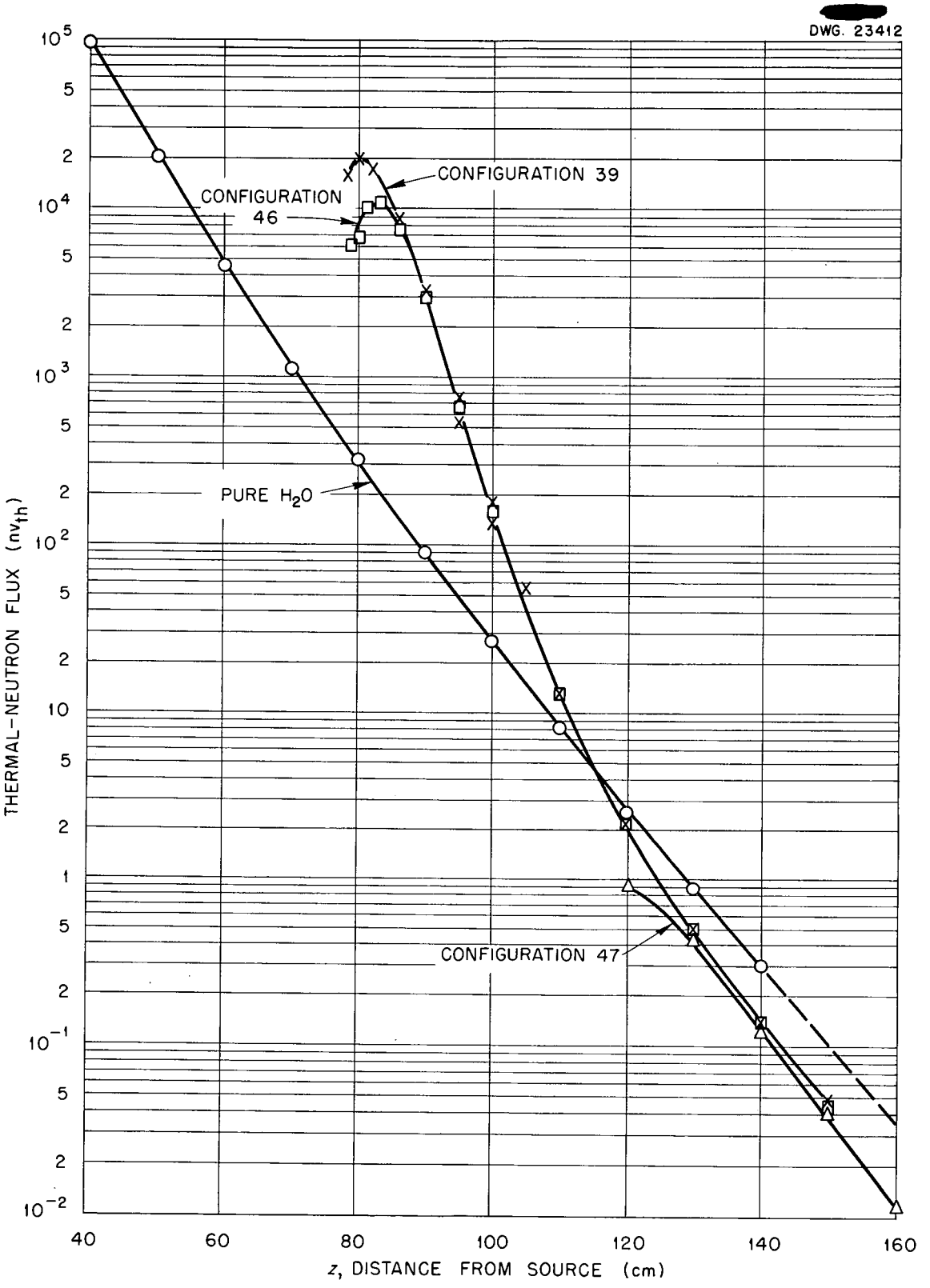

Fig. VI-57. Thermal-Neutron Flux Measurements behind Lid Tank Mockups of Reflector-Moderated Reactor and Shield.

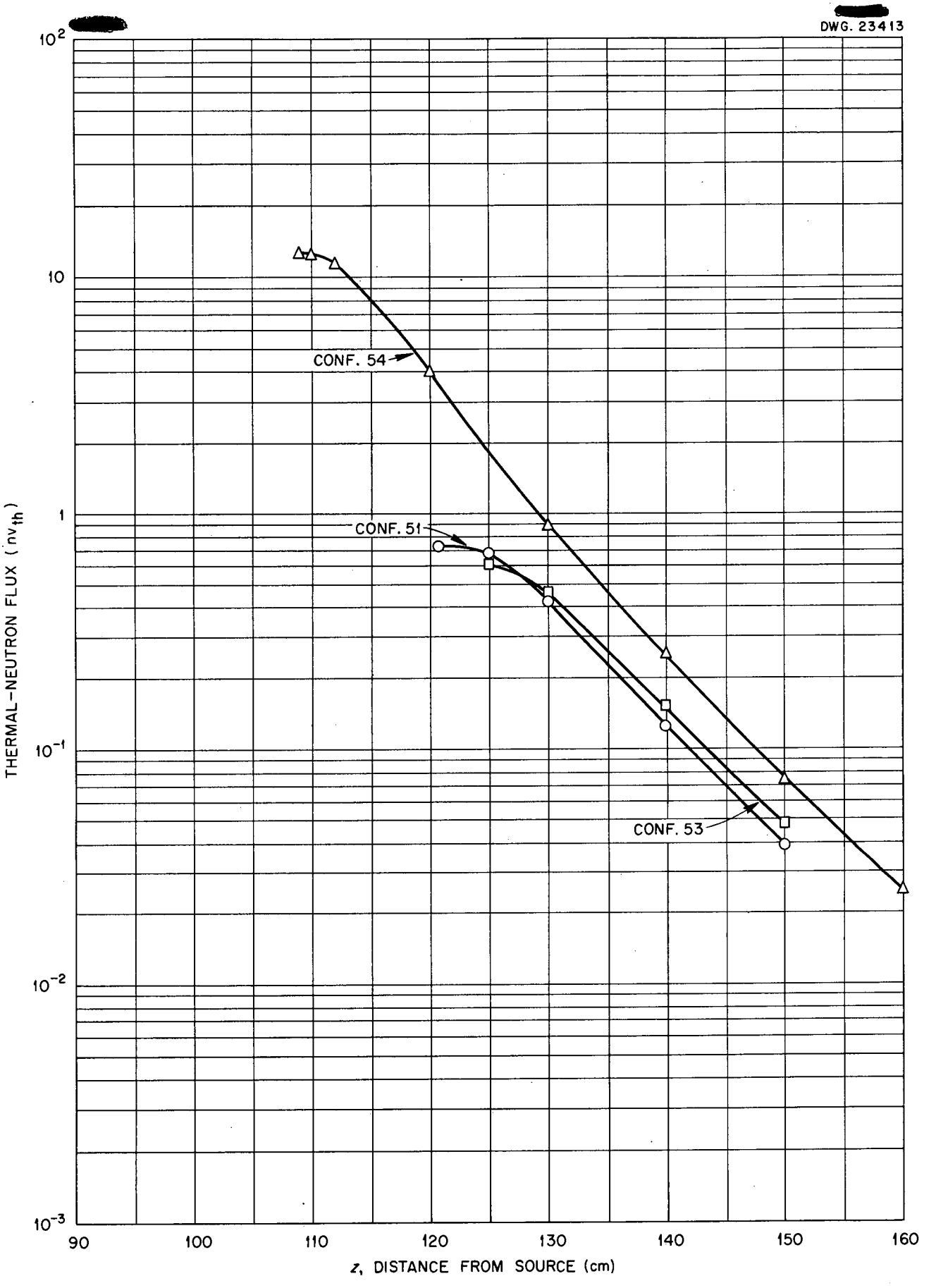

Fig. VI-58. Thermal-Neutron Flux Measurements behind Lid Tank Mockups of Reflector-Moderated Reactor and Shield.

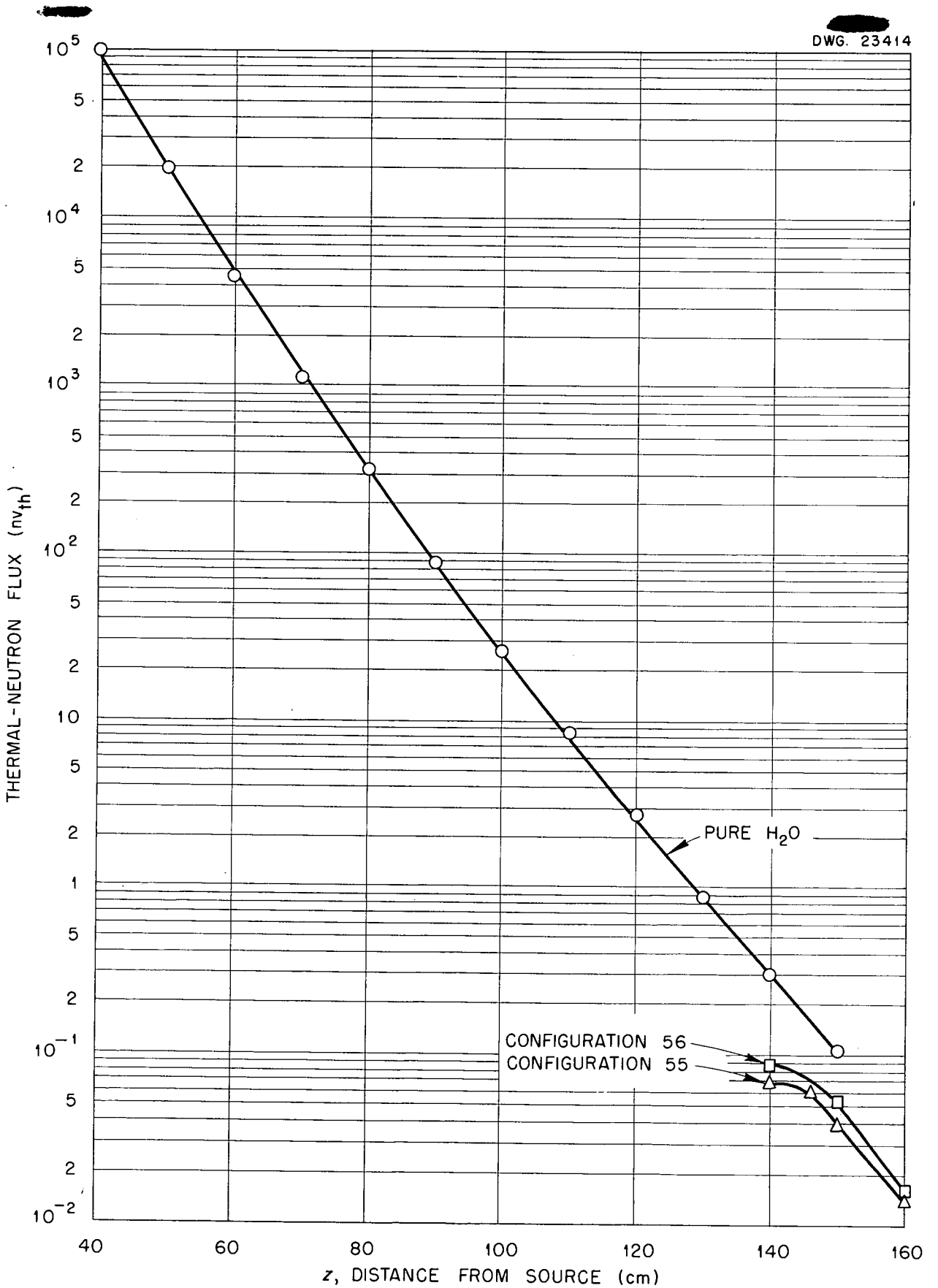

Fig. VI-59. Thermal-Neutron Flux Measurements behind Lid Tank Mockups of Reflector-Moderated Reactor and Shield.

[redacted]

[redacted]

DWG. 23415

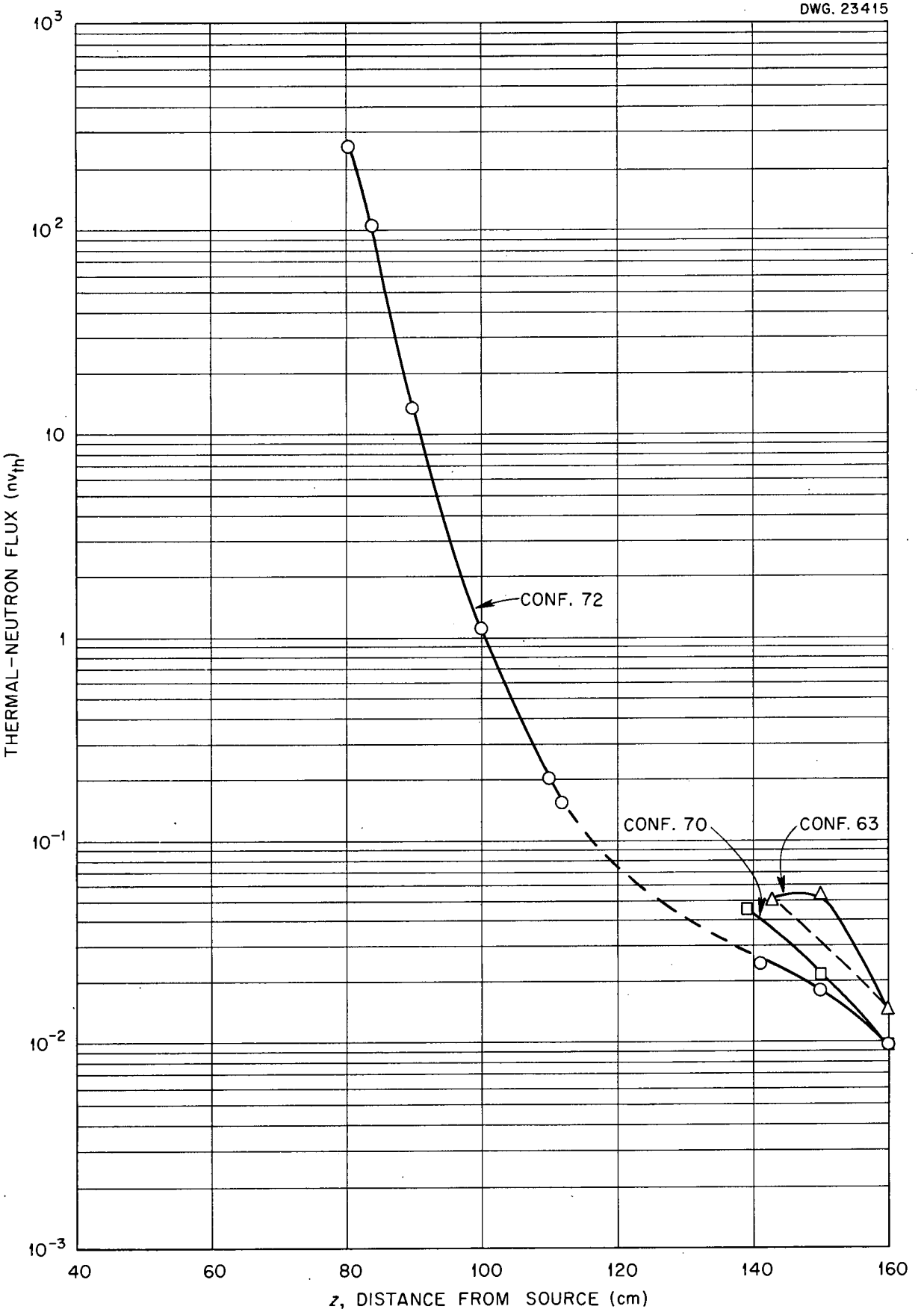

Fig. VI-60. Thermal-Neutron Flux Measurements behind Lid Tank Mockups of Reflector-Moderated Reactor and Shield.

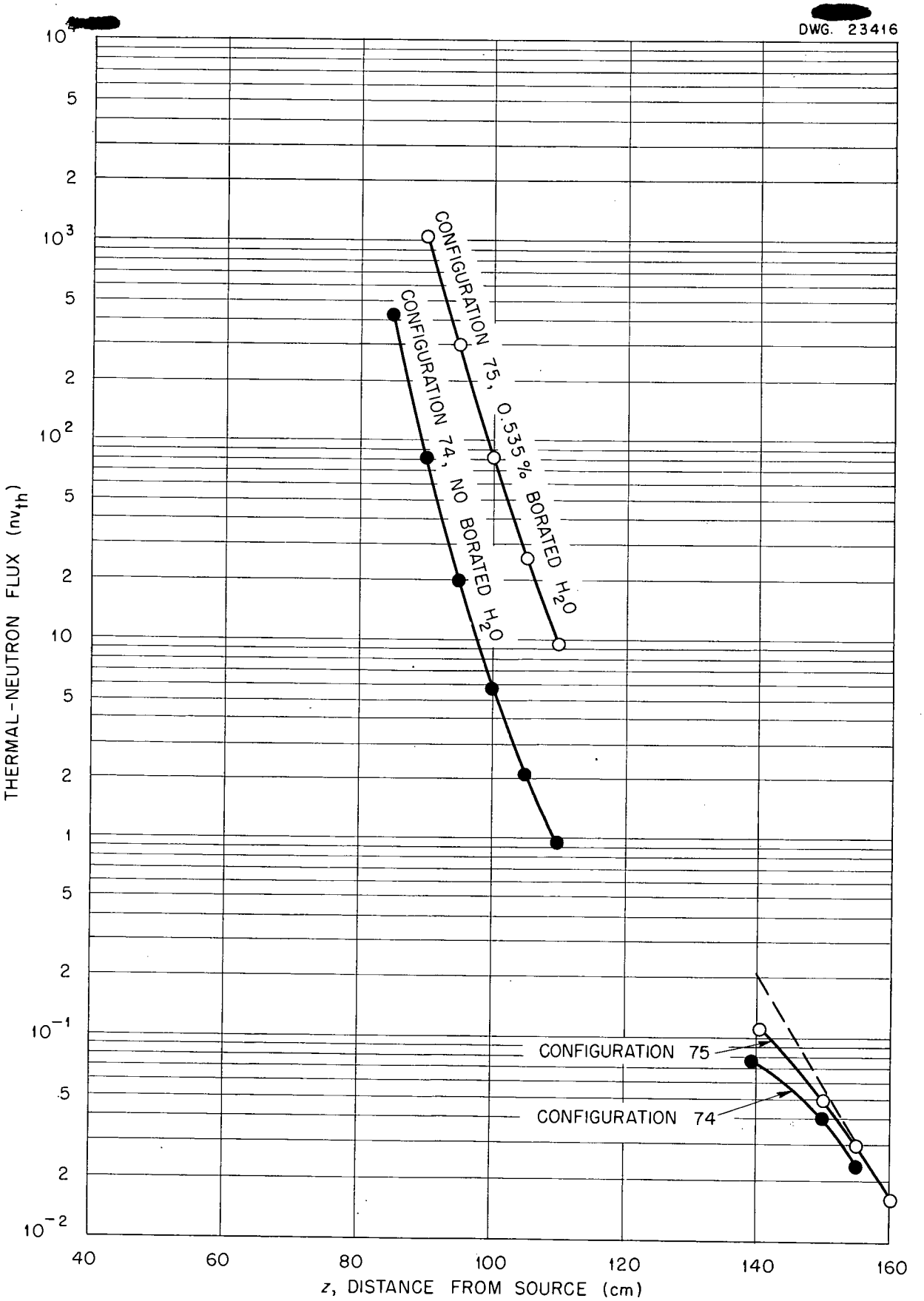

Fig. VI-61. Thermal-Neutron Flux Measurements behind Lid Tank Mockups of Reflector-Moderated Reactor and Shield.

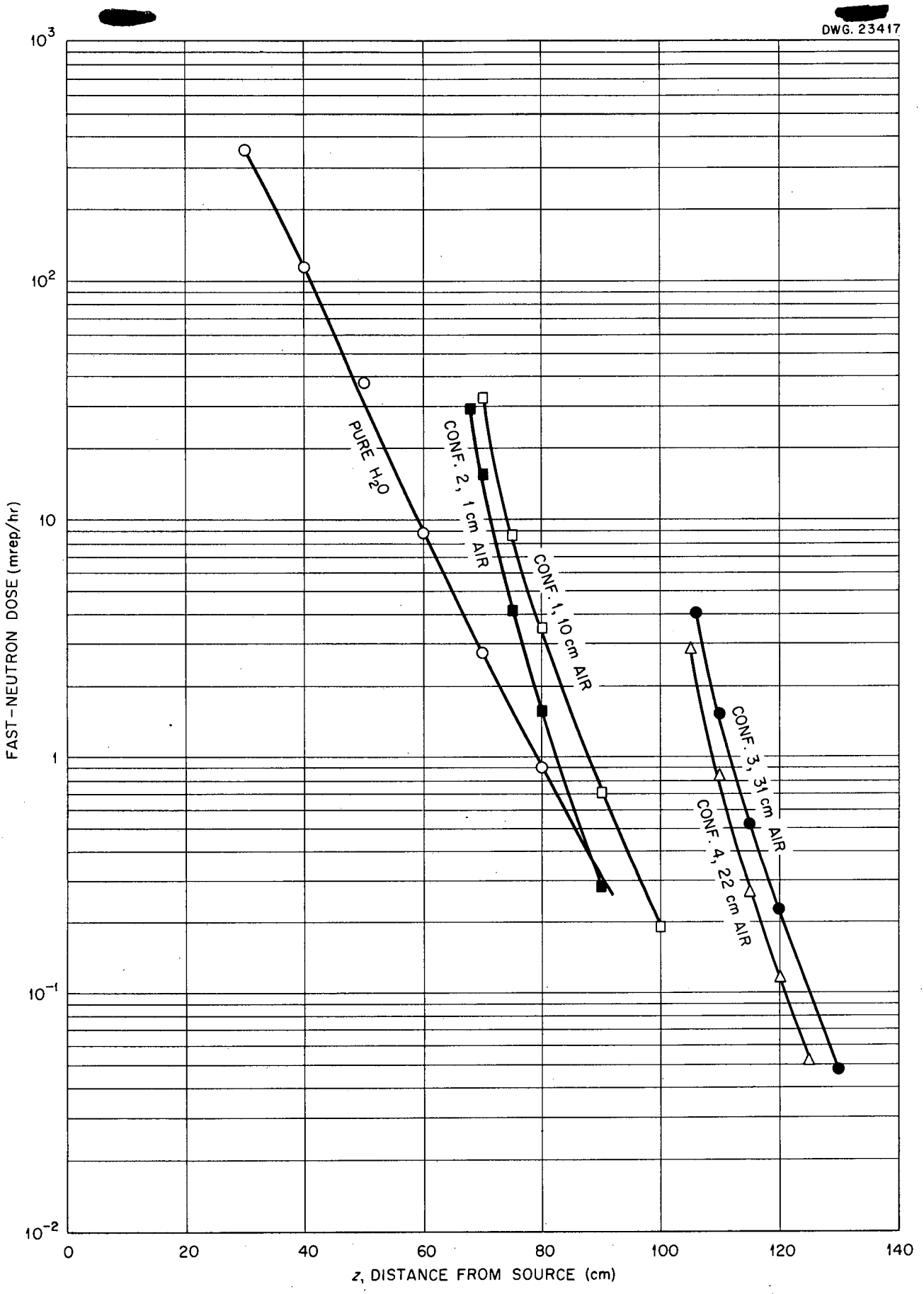

Fig. VI-62. Fast-Neutron Dose Measurements behind Lid Tank Mockups of Reflector-Moderated Reactor and Shield.

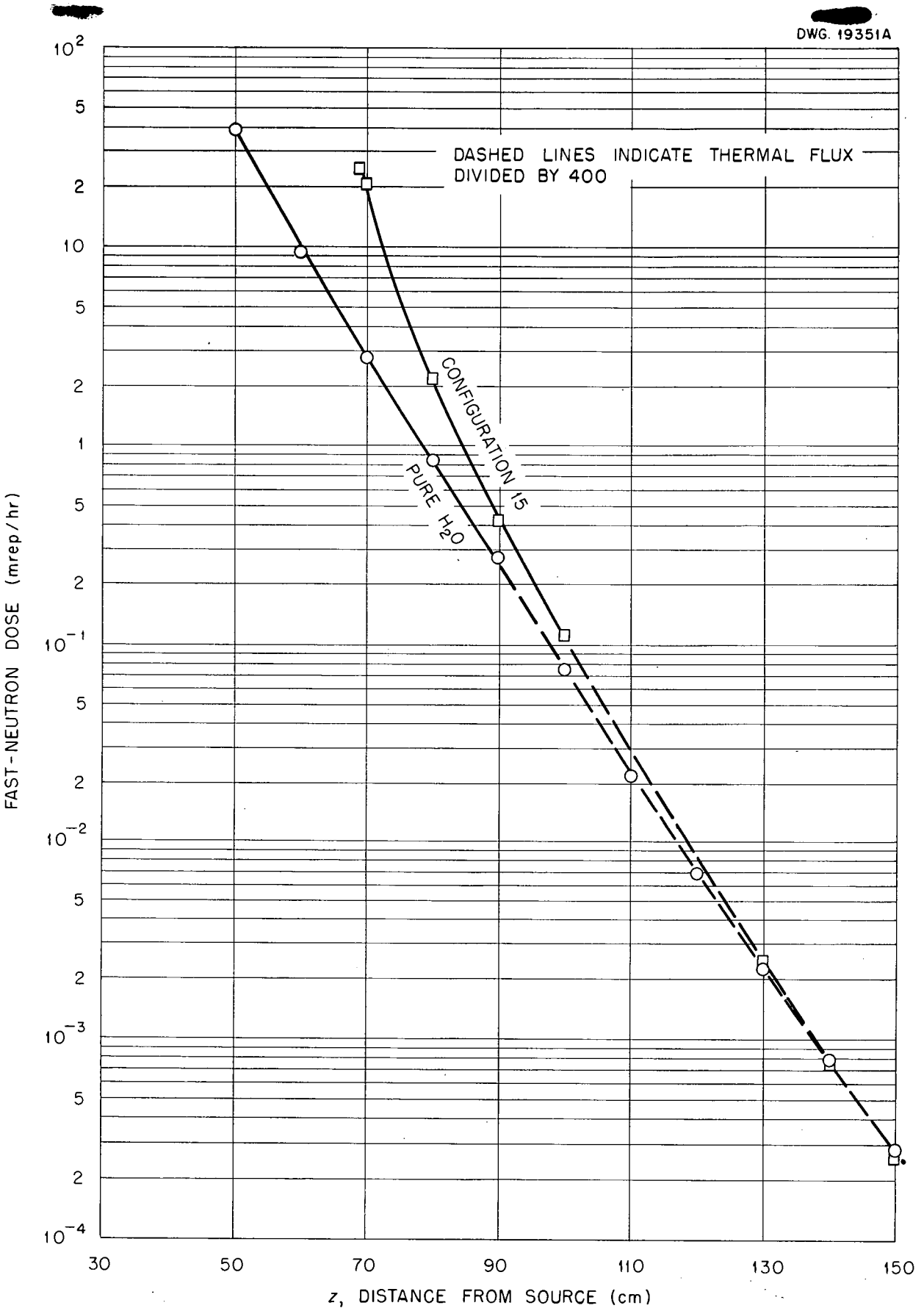

Fig. VI-63. Fast-Neutron Dose Measurements behind Lid Tank Mockups of Reflector-Moderated Reactor and Shield.

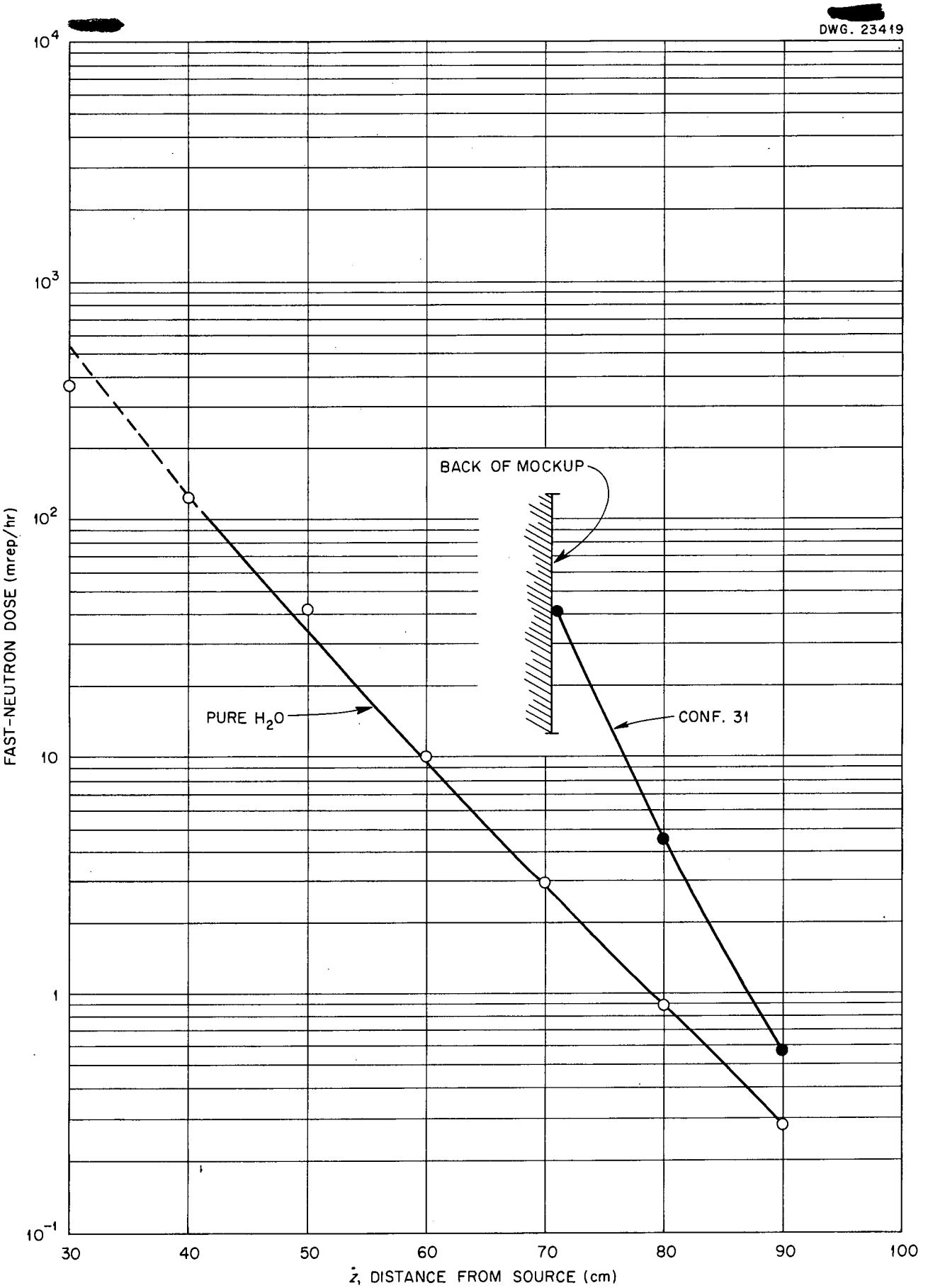

Fig. VI-64. Fast-Neutron Dose Measurements behind Lid Tank Mockups of Reflector-Moderated Reactor and Shield.

[redacted]

[redacted]

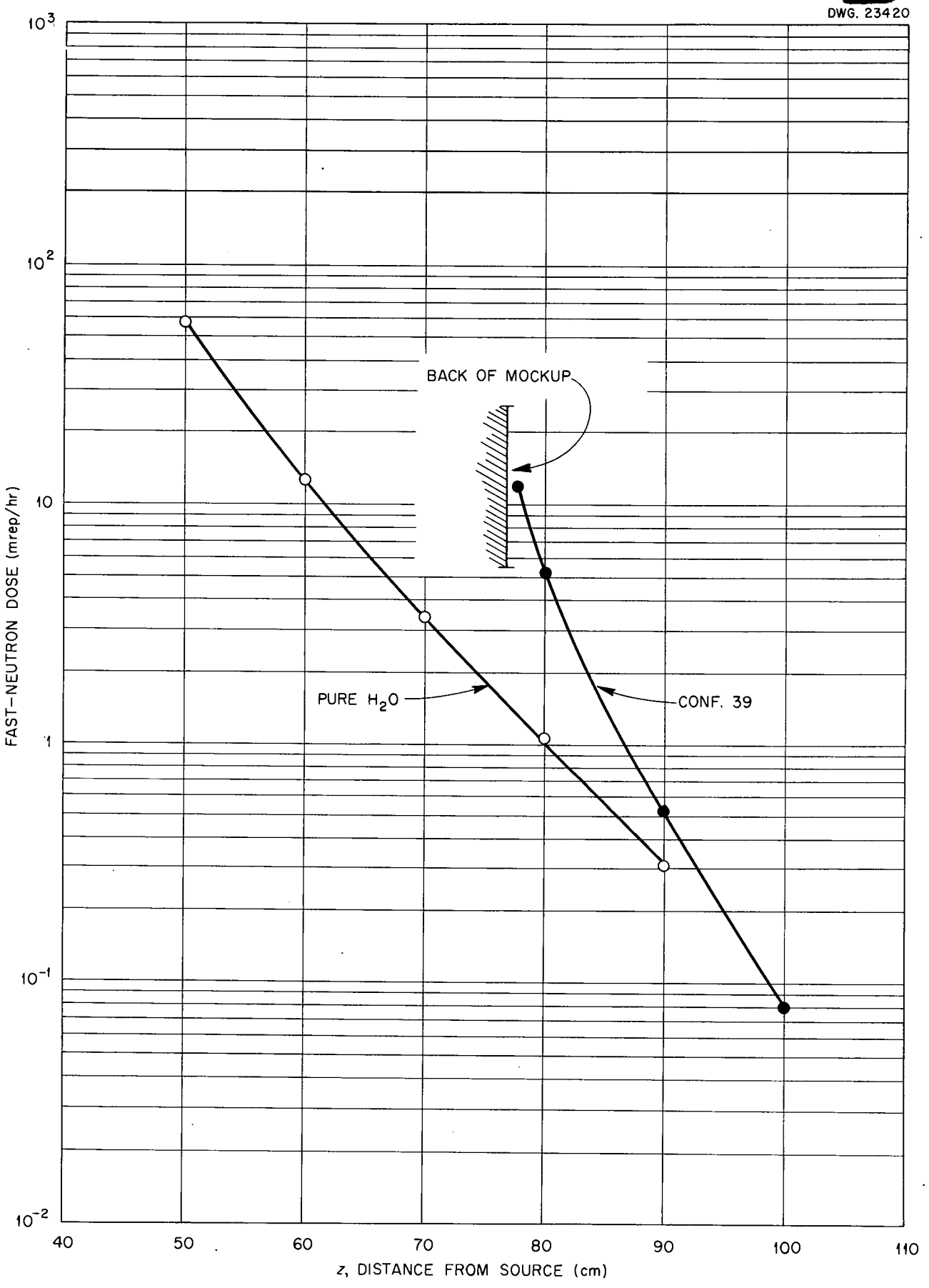

Fig. VI-65. Fast-Neutron Dose Measurements behind Lid Tank Mockups of Reflector-Moderated

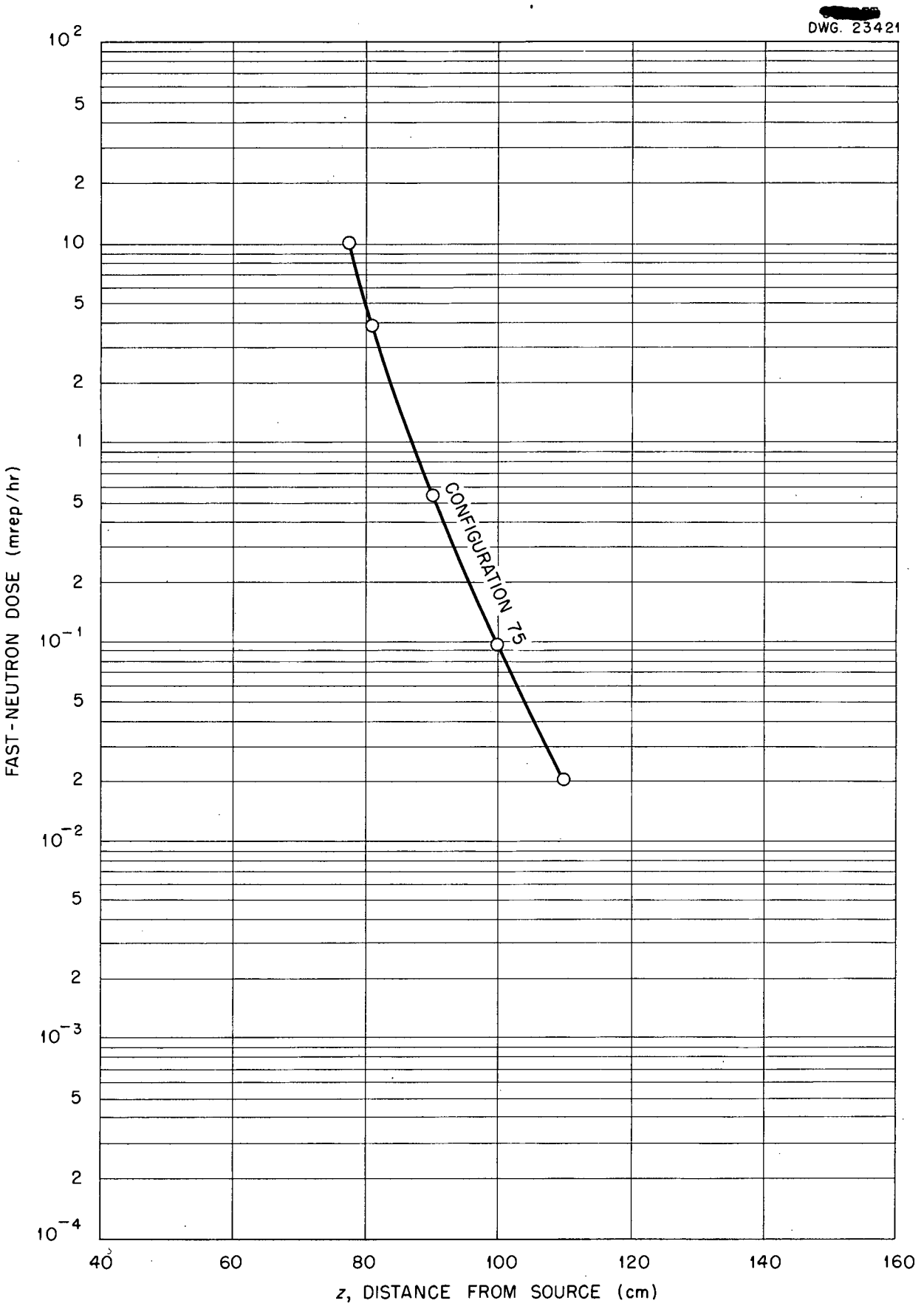

Fig. VI-66. Fast-Neutron Dose Measurements behind Lid Tank Mockups of Reflector-Moderated Reactor and Shield.

Table VI-2

Gamma-Ray Dose Measurements in Water behind Configurations 1 through 5

z, Distance from Source (cm)	Gamma-Ray Dose (mr/hr)						
	Pure H_2O[a]	Conf. 1	Conf. 1a	Conf. 2	Conf. 3	Conf. 4	Conf. 5
60	2.44×10^{3}						
70	1.44×10^{3}						
73.2				4.77×10^{1}			
73.9		5.62×10^{2}					
76				5.03×10^{1}			
80	8.80×10^{2}	4.28×10^{2}	3.97×10^{2}	3.89×10^{1}			
				3.38×10^{1}			
90	5.64×10^{2}	2.71×10^{2}	2.52×10^{2}	2.16×10^{1}			
				1.95×10^{1}			
100	3.46×10^{2}	1.76×10^{2}	1.63×10^{2}	1.27×10^{1}			
				1.18×10^{1}			
110	2.18×10^{2}	1.14×10^{2}	1.08×10^{2}	8.23×10^{0}			
				8.00×10^{0}			
112.6						4.82×10^{0}	
112.8					8.33×10^{0}		
113.2						4.97×10^{0}	
						4.97×10^{0}	
114.5							5.97×10^{-1}
120	1.39×10^{2}	7.70×10^{1}	7.20×10^{1}	5.17×10^{0}	4.97×10^{0}	2.62×10^{0}	3.80×10^{-1}
						2.72×10^{0}	
130	8.97×10^{1}	5.12×10^{1}	4.83×10^{1}	3.31×10^{0}	2.58×10^{0}	1.33×10^{0}	1.95×10^{-1}
						1.38×10^{0}	
135						1.00×10^{0}	
						9.84×10^{-1}	
140	6.03×10^{1}	3.60×10^{1}	3.39×10^{1}	2.15×10^{0}	1.53×10^{0}	7.65×10^{-1}	1.16×10^{-1}
						8.41×10^{-1}	1.17×10^{-1}
150	3.96×10^{1}	2.42×10^{1}		1.47×10^{0}	9.55×10^{-1}	4.61×10^{-1}	7.01×10^{-1}
						4.65×10^{-1}	6.63×10^{-2}
160	2.67×10^{1}	1.72×10^{1}		9.83×10^{-1}	5.94×10^{-1}	2.86×10^{-1}	4.67×10^{-2}
						2.59×10^{-1}	

[a] Measurements in pure water were made at various times throughout the tests and are reported accordingly.

Table VI-3

Gamma-Ray Dose Measurements in Water behind Configurations 6 through 10

z, Distance from source (cm)	Gamma-Ray Dose (mr/hr)				
	Conf. 6	Conf. 7	Conf. 8	Conf. 9	Conf. 10
114.3	3.10×10^{-1}				
114.9				3.50×10^{-2}	6.93×10^{-2}
120	2.04×10^{-1}		See Optimi-	2.78×10^{-2}	4.91×10^{-2}
				2.84×10^{-2}	
130	1.08×10^{-1}		zation	1.52×10^{-2}	3.46×10^{-2}
140	6.48×10^{-2}	4.72×10^{-1}		1.09×10^{-2}	2.16×10^{-2}
150	4.20×10^{-2}	2.74×10^{-1}	Discussion,	7.72×10^{-3}	1.51×10^{-2}
	4.05×10^{-2}		Section III		
151.3				7.10×10^{-3}	
				6.87×10^{-3}	
				7.75×10^{-3}	
				6.95×10^{-3}	
160	2.61×10^{-2}	1.63×10^{-1}		5.31×10^{-3}	1.03×10^{-2}
	2.61×10^{-2}				

Table VI-4

Gamma-Ray Dose Measurements in Water behind Configurations 11 through 14

z, Distance from source (cm)	Gamma-Ray Dose (mr/hr)			
	Conf. 11	Conf. 12	Conf. 13	Conf. 14
113				5.33×10^{-1}
114.4	4.30×10^{-2}			
115	4.30×10^{-2}			
115.4			3.29×10^{-2}	
			3.56×10^{-2}	
115.5		2.46×10^{-2}		
		2.45×10^{-2}		
120	3.31×10^{-2}	2.09×10^{-2}	2.96×10^{-2}	4.40×10^{-1}
	3.22×10^{-2}	2.04×10^{-2}	2.73×10^{-2}	
125		1.57×10^{-2}		
130	2.29×10^{-2}	1.24×10^{-2}	2.33×10^{-2}	2.72×10^{-1}
	2.18×10^{-2}	1.15×10^{-2}	1.97×10^{-2}	
140	1.53×10^{-2}	8.94×10^{-3}	1.48×10^{-2}	2.01×10^{-1}
	1.67×10^{-2}	8.19×10^{-3}	1.33×10^{-2}	1.66×10^{-1}
150	1.04×10^{-2}	6.60×10^{-3}	1.20×10^{-2}	1.30×10^{-1}
	1.06×10^{-2}	5.43×10^{-3}	9.45×10^{-2}	
160	7.60×10^{-3}	4.74×10^{-3}	8.04×10^{-3}	1.09×10^{-1}
	8.74×10^{-3}	3.82×10^{-3}	7.30×10^{-3}	9.38×10^{-2}

Table VI-5

Gamma-Ray Dose Measurements in Water behind Configurations 15 through 18

z, Distance from source (cm)	Gamma-Ray Dose (mr/hr)				
	Pure H_2O	Conf. 15	Conf. 16	Conf. 17	Conf. 18
60	2.96×10^{3}				
70	1.66×10^{3}				
77.1		2.80×10^{2}			
80	9.84×10^{2}	2.45×10^{2}			
90	5.55×10^{2}	1.53×10^{2}			
100	3.63×10^{2}	9.83×10^{1}			
110	2.26×10^{2}	6.26×10^{1}			
114			1.86×10^{0}		
115.9				1.37×10^{-1}	6.49×10^{-2}
120	1.42×10^{2}	4.29×10^{1}	1.45×10^{0}	1.10×10^{-1}	5.14×10^{-2}
130	8.97×10^{1}	2.91×10^{1}	9.66×10^{-1}	7.36×10^{-2}	3.25×10^{-2}
140	6.03×10^{1}	1.95×10^{1}	6.35×10^{-1}	4.67×10^{-2}	1.93×10^{-2}
150	3.96×10^{1}	1.32×10^{1}	4.35×10^{-1}	3.12×10^{-2}	1.31×10^{-2}
160	2.73×10^{1}	9.51×10^{0}	2.81×10^{-1}	2.11×10^{-2}	8.43×10^{-3}

Table VI-6

Gamma-Ray Dose Measurements in Water
behind Configurations 19 through 20e

z, Distance from Source (cm)	Gamma-Ray Dose (mr/hr)					
	Conf. 19	Conf. 20a	Conf. 20b	Conf. 20c	Conf. 20d	Conf. 20e
122.9		8.84×10^{-1}				
		8.49×10^{-1}				
124.5						2.22×10^{-2}
124.8	1.80×10^{-2}				2.08×10^{-2}	
					2.19×10^{-2}	
					2.23×10^{-2}	
130	1.25×10^{-2}	6.11×10^{-1}	2.10×10^{-1}	3.51×10^{-2}	1.60×10^{-2}	1.66×10^{-2}
	1.31×10^{-2}	6.09×10^{-1}	2.05×10^{-1}	3.43×10^{-2}	1.84×10^{-2}	
			1.89×10^{-1}		1.79×10^{-2}	
140	9.29×10^{-3}	4.27×10^{-1}	1.28×10^{-1}	2.43×10^{-2}	9.21×10^{-3}	9.95×10^{-3}
	1.01×10^{-2}	3.98×10^{-1}	1.33×10^{-1}	2.40×10^{-2}	1.04×10^{-2}	
			1.30×10^{-1}	2.74×10^{-2}	9.75×10^{-3}	
150	5.46×10^{-3}	2.85×10^{-1}	8.10×10^{-2}	1.66×10^{-2}	6.11×10^{-3}	6.17×10^{-3}
		2.98×10^{-1}	7.65×10^{-2}	1.55×10^{-2}	7.72×10^{-3}	
			9.43×10^{-2}	2.08×10^{-2}	7.56×10^{-3}	
				1.74×10^{-2}	7.49×10^{-3}	
					6.89×10^{-3}	
					7.24×10^{-3}	
160	3.56×10^{-3}	2.13×10^{-1}	5.22×10^{-2}	1.37×10^{-2}	5.52×10^{-3}	5.54×10^{-3}
			5.10×10^{-2}	1.24×10^{-2}	5.20×10^{-3}	5.07×10^{-3}
			5.39×10^{-2}	1.46×10^{-2}	5.94×10^{-3}	
					5.42×10^{-3}	
					5.58×10^{-3}	

Table VI-7

Gamma-Ray Dose Measurements in Water behind Configuration 21 -- with and without Transformer Oil Placed behind Borated Water Tank

z, Distance from source (cm)	Gamma-Ray Dose (mr/hr)	
	Without Oil	With Oil
124.1	5.44×10^{-2}	
	5.18×10^{-2}	
130	4.08×10^{-2}	
	3.55×10^{-2}	
	3.80×10^{-2}	
140	2.77×10^{-2}	
	2.93×10^{-2}	
150	1.54×10^{-2}	
	1.73×10^{-2}	
160	1.15×10^{-2}	
163.1		1.24×10^{-2}
165		1.02×10^{-2}
170		9.16×10^{-3}

Table VI-8

Gamma-Ray Dose Measurements in Water behind Configurations 22 through 26

z, Distance from source (cm)	Gamma-Ray Dose (mr/hr)				
	Conf. 22	Conf. 23	Conf. 24	Conf. 25	Conf. 26
84.4	1.33×10^{2}				
90	1.05×10^{2}				
90.1		1.17×10^{2}			
90.6				7.61×10^{1}	
91.6			7.75×10^{1}		
96.4					1.99×10^{1}
100	6.72×10^{1}	7.65×10^{1}	5.34×10^{1}	5.02×10^{1}	1.70×10^{1}
110	4.34×10^{1}	5.11×10^{1}	3.54×10^{1}	3.29×10^{1}	1.10×10^{1}
120	2.98×10^{1}	3.46×10^{1}	2.34×10^{1}	2.16×10^{1}	7.36×10^{0}
130	2.04×10^{1}	2.32×10^{1}	1.58×10^{1}	1.48×10^{1}	4.91×10^{0}
140	1.42×10^{1}	1.61×10^{1}	1.11×10^{1}	1.03×10^{1}	3.53×10^{0}
150	9.82×10^{0}	1.10×10^{1}	7.63×10^{0}	6.91×10^{0}	2.24×10^{0}
160	6.58×10^{0}	7.70×10^{0}	5.00×10^{0}	4.28×10^{0}	1.62×10^{0}
				4.82×10^{0}	

Table VI-9

Gamma-Ray Dose Measurements in Water behind Configurations 27 and 28

z, Distance from Source (cm)	Gamma-Ray Dose (mr/hr)	
	Conf. 27	Conf. 28
77.7		1.92×10^{2}
80		1.69×10^{2}
82.3	2.03×10^{2}	
90	1.44×10^{2}	1.04×10^{2}
100	9.27×10^{1}	6.87×10^{1}
110	5.97×10^{1}	4.50×10^{1}
120	4.02×10^{1}	3.02×10^{1}
130	2.69×10^{1}	2.02×10^{1}
140	1.81×10^{1}	1.39×10^{1}
150	1.26×10^{1}	9.64×10^{0}
160	8.57×10^{0}	6.53×10^{0}

Table VI-10

Gamma-Ray Dose Measurements in Water behind Configurations 29 through 32

z, Distance from source (cm)	Gamma-Ray Dose (mr/hr)			
	Conf. 29	Conf. 30	Conf. 31	Conf. 32
78.2			2.61×10^{2}	
80			2.45×10^{2}	2.78×10^{2}
83.7	4.20×10^{2}			
90	3.26×10^{2}		1.52×10^{2}	1.73×10^{2}
91		9.67×10^{1}		
100	2.11×10^{2}	6.58×10^{1}	9.58×10^{1}	1.10×10^{2}
110	1.41×10^{2}	4.34×10^{1}	5.99×10^{1}	7.26×10^{1}
120	9.21×10^{1}	2.89×10^{1}	4.13×10^{1}	4.70×10^{1}
130	6.24×10^{1}	1.93×10^{1}	2.78×10^{1}	3.21×10^{1}
140	4.37×10^{1}	1.37×10^{1}	1.89×10^{1}	2.21×10^{1}
150	2.95×10^{1}	8.84×10^{0}	1.31×10^{1}	1.54×10^{1}
160	2.11×10^{1}	6.56×10^{0}	8.98×10^{0}	1.06×10^{1}

Table VI-11

Gamma-Ray Dose Measurements in Water behind Configurations 33 through 38

z, Distance from Source (cm)	Gamma-Ray Dose (mr/hr)					
	Conf. 33	Conf. 34	Conf. 35	Conf. 36	Conf. 37	Conf. 38
81.2			7.59×10^{1}			
82.9	6.49×10^{1}					
83		6.21×10^{1}				
85.7				2.06×10^{1}		
90	4.49×10^{1}	4.43×10^{1}	4.89×10^{1}	1.54×10^{1}	1.17×10^{1}	
					1.18×10^{1}	
100	2.82×10^{1}	2.77×10^{1}	2.99×10^{1}	8.19×10^{0}	5.01×10^{0}	7.88×10^{0}
				8.07×10^{0}	5.00×10^{0}	
110	1.76×10^{1}	1.79×10^{1}	1.91×10^{1}	5.00×10^{0}	2.37×10^{0}	4.04×10^{0}
				4.74×10^{0}	2.40×10^{0}	
120	1.16×10^{1}	1.14×10^{1}	1.22×10^{1}	3.03×10^{0}	1.32×10^{0}	2.26×10^{0}
				2.98×10^{0}	1.26×10^{0}	
130	7.68×10^{0}	7.74×10^{0}	8.28×10^{0}	1.95×10^{0}	8.43×10^{-1}	1.39×10^{0}
				1.85×10^{0}	8.06×10^{-1}	1.42×10^{0}
140	5.23×10^{0}	5.32×10^{0}	5.47×10^{0}	1.20×10^{0}	5.83×10^{-1}	9.08×10^{-1}
				1.26×10^{0}	6.09×10^{-1}	
150	3.77×10^{0}	3.64×10^{0}	3.77×10^{0}	7.33×10^{-1}	3.88×10^{-1}	6.21×10^{-1}
				7.86×10^{-1}	3.92×10^{-1}	6.77×10^{-1}
160	2.54×10^{0}	2.58×10^{0}	2.52×10^{0}	5.24×10^{-1}	2.30×10^{-1}	4.21×10^{-1}
				5.33×10^{-1}	2.32×10^{-1}	

Table VI-12

Gamma-Ray Dose Measurements in Water behind Configurations 39 through 44

z, Distance from Source (cm)	Gamma-Ray Dose (mr/hr)						
	Pure H_2O	Conf. 39	Conf. 40	Conf. 41	Conf. 42	Conf. 43	Conf. 44
60	2.80×10^{3}						
70	1.65×10^{3}						
80	9.46×10^{2}						
84.7					1.89×10^{1}		
84.9		2.50×10^{1}					
		2.35×10^{1}					
85.6						2.27×10^{1}	
88.1			1.114×10^{1}	9.94×10^{0}			
90	5.74×10^{2}	1.67×10^{1}	9.87×10^{0}	8.45×10^{0}	1.24×10^{1}	1.57×10^{1}	
		1.63×10^{1}					
95							8.28×10^{0}
100	3.46×10^{2}	7.51×10^{0}	4.45×10^{0}	3.58×10^{0}	5.49×10^{0}	7.10×10^{0}	5.78×10^{0}
		7.37×10^{0}					
110	2.08×10^{2}	4.05×10^{0}	2.27×10^{0}	1.79×10^{0}	2.93×10^{0}	3.73×10^{0}	3.16×10^{0}
			2.26×10^{0}				
120	1.33×10^{2}	2.31×10^{0}	1.32×10^{0}	1.01×10^{0}	1.85×10^{0}	2.14×10^{0}	1.90×10^{0}
					1.62×10^{0}		
130	8.62×10^{1}	1.34×10^{0}	7.87×10^{-1}	5.66×10^{-1}	9.40×10^{-1}	1.26×10^{0}	1.24×10^{0}
140	5.79×10^{1}	8.73×10^{-1}	4.81×10^{-1}	3.55×10^{-1}	5.87×10^{-1}	7.72×10^{-1}	8.32×10^{-1}
							8.44×10^{-1}
150	3.86×10^{1}	5.18×10^{-1}	3.18×10^{-1}	2.11×10^{-1}	3.69×10^{-1}	4.96×10^{-1}	5.35×10^{-1}
160	2.56×10^{1}	3.43×10^{-1}	1.95×10^{-1}		2.22×10^{-1}	3.16×10^{-1}	3.47×10^{-1}

Table VI-13

Gamma-Ray Dose Measurements in Water behind Configurations 45 through 50

z, Distance from Source (cm)	Gamma-Ray Dose (mr/hr)					
	Conf. 45	Conf. 46	Conf. 47	Conf. 48	Conf. 49	Conf. 50
85.7	1.33×10^{1}					
86.3		1.28×10^{1}				
90	9.68×10^{0}	9.66×10^{0}				
100	4.07×10^{0}	3.95×10^{0}				
110	2.05×10^{0}	1.93×10^{0}				
120	1.11×10^{0}	1.05×10^{0}				
126.3					7.37×10^{-2}	
126.6						6.17×10^{-1}
126.9				1.84×10^{-1}		
127.1			1.99×10^{-1}			
130	6.60×10^{-1}	5.74×10^{-1}	1.67×10^{-1}	1.64×10^{-1}	6.12×10^{-2}	5.63×10^{-1}
						5.63×10^{-1}
140	3.66×10^{-1}	3.52×10^{-1}	9.76×10^{-2}	1.01×10^{-1}	4.10×10^{-2}	3.58×10^{-1}
		3.34×10^{-1}				3.62×10^{-1}
150	2.57×10^{-1}	2.13×10^{-1}	6.63×10^{-2}	6.63×10^{-2}	3.02×10^{-2}	2.25×10^{-1}
		2.07×10^{-1}			3.04×10^{-2}	2.33×10^{-1}
160	1.51×10^{-1}		4.48×10^{-2}	4.68×10^{-2}	2.15×10^{-2}	1.42×10^{-1}
					2.06×10^{-2}	1.36×10^{-1}

Table VI-14

Gamma-Ray Dose Measurements in Water behind Configurations 51 through 54; Also Configuration 17

z, Distance from Source (cm)	Gamm-Ray Dose (mr/hr)					Ratio: Conf. 54 / Conf. 17
	Conf. 51	Conf. 52	Conf. 53	Conf. 54[a]	Conf. 17[a]	
115.5				1.46×10^{-1}		
115.9					1.37×10^{-1}	
120				1.15×10^{-1}	1.10×10^{-1}	1.009
				1.07×10^{-1}		
126.4		4.40×10^{-1}				
127.8	3.56×10^{-1}					
130	3.28×10^{-1}	3.67×10^{-1}		6.38×10^{-2}	7.36×10^{-2}	0.893
				6.77×10^{-2}		
131.3			4.33×10^{-1}			
140	1.99×10^{-1}	2.23×10^{-1}	2.76×10^{-1}	4.46×10^{-2}	4.67×10^{-2}	0.935
				4.27×10^{-2}		
150	1.26×10^{-1}	1.40×10^{-1}	1.77×10^{-1}	2.99×10^{-2}	3.12×10^{-2}	0.958
160	8.12×10^{-2}	9.38×10^{-2}	1.12×10^{-1}	1.99×10^{-2}	2.11×10^{-2}	0.983
		9.40×10^{-2}		2.16×10^{-2}		
						0.956 avg.

[a] Configuration 54 is a repeat of Configuration 17, differing only in boron content in water section of shield:

54 -- 1.0% B
17 -- 2.8% B

Table VI-15

Gamma-Ray Dose Measurements in Water behind Configurations 55 through 59

z, Distance from Source (cm)	Gamma-Ray Dose (mr/hr)					
	Pure H_2O	Conf. 55[a]	Conf. 56	Conf. 57	Conf. 58	Conf. 59
100	3.65×10^{2}					
110	2.28×10^{2}					
120	1.41×10^{2}					
130	9.51×10^{1}					
140	6.33×10^{1}					
146.2		3.03×10^{-2}				
		3.37×10^{-2}				
146.6						4.92×10^{-2}
147.7				4.56×10^{-2}	4.06×10^{-2}	
148		3.14×10^{-2}	3.81×10^{-2}			
150	4.31×10^{1}	2.87×10^{-2}	3.15×10^{-2}	4.26×10^{-2}	3.50×10^{-2}	4.34×10^{-2}
			3.40×10^{-2}	4.40×10^{-2}	3.72×10^{-2}	
160	2.90×10^{1}	1.98×10^{-2}	2.71×10^{-2}	3.02×10^{-2}	2.84×10^{-2}	3.22×10^{-2}
				3.23×10^{-2}	2.77×10^{-2}	
170		1.27×10^{-2}	2.12×10^{-2}	2.45×10^{-2}	2.00×10^{-2}	2.18×10^{-2}
			2.03×10^{-2}			2.46×10^{-2}

[a] See also Configuration 55R.

Table VI-16

Gamma-Ray Dose Measurements in Water behind Configurations 60 and 61

z, Distance from Source (cm)	Gamma-Ray Dose (mr/hr)	
	Conf. 60	Conf. 61
146.6	2.24×10^{-2}	2.10×10^{-2}
150	2.15×10^{-2}	1.95×10^{-2}
160	1.65×10^{-2}	1.52×10^{-2}
170	1.30×10^{-2}	1.17×10^{-2}

Table VI-17

Gamma-Ray Dose Measurements in Water behind Configurations 62 through 65

z, Distance from Source (cm)	Gamma-Ray Dose (mr/hr)			
	Conf. 62	Conf. 63	Conf. 64[a]	Conf. 65
146.5	4.67×10^{-2}			
	4.78×10^{-2}			
147.7				1.27×10^{-1}
147.9			3.80×10^{-2}	
150	4.00×10^{-2}	3.19×10^{-2}	3.53×10^{-2}	1.17×10^{-1}
155		2.72×10^{-2}		
160	3.07×10^{-2}	2.44×10^{-2}	2.89×10^{-2}	8.17×10^{-2}
			2.70×10^{-2}	
165		2.02×10^{-2}		
170	2.20×10^{-2}	1.91×10^{-2}	1.90×10^{-2}	5.41×10^{-2}
		2.13×10^{-2}		
		1.83×10^{-2}		

a See also configuration 64R.

Table VI-18

Table 17. Gamma-Ray Dose Measurements in Water behind Configurations 66 through 72

z, Distance from Source (cm)	Gamma-Ray Dose (mr/hr)						
	Conf. 66	Conf. 67	Conf. 68	Conf. 69	Conf. 70	Conf. 71	Conf. 72
90							1.08×10^{0}
							1.12×10^{0}
95							7.63×10^{-1}
100							5.89×10^{-1}
							6.11×10^{-1}
105							4.27×10^{-1}
110							3.45×10^{-1}
							3.54×10^{-1}
115							2.63×10^{-1}
116.3							2.85×10^{-1}
145.1			1.39×10^{-1}				
145.9					1.48×10^{-1}		
146.5						3.70×10^{-2}	
146.7				2.47×10^{-2}			
147.8	2.85×10^{-2}						
147.9		1.15×10^{-2}					9.32×10^{-2}
		1.16×10^{-2}					
150	2.70×10^{-2}	1.25×10^{-2}	1.11×10^{-1}	2.25×10^{-2}	1.33×10^{-1}	3.54×10^{-2}	9.06×10^{-2}
		1.33×10^{-2}		2.31×10^{-2}			9.36×10^{-2}
		1.16×10^{-2}					
155				2.14×10^{-2}			
				1.87×10^{-2}			
160	1.96×10^{-2}	8.56×10^{-3}	7.69×10^{-2}	1.92×10^{-2}	1.20×10^{-1}	3.16×10^{-2}	6.42×10^{-2}
		9.90×10^{-3}			1.21×10^{-1}		
165	1.81×10^{-2}			1.66×10^{-2}			
170	1.55×10^{-2}	7.55×10^{-3}	5.33×10^{-2}	1.42×10^{-2}	1.06×10^{-1}	2.72×10^{-2}	5.17×10^{-2}
		9.04×10^{-3}		1.32×10^{-2}	1.03×10^{-1}		4.77×10^{-2}

Table VI-19

Gamma-Ray Dose Measurements in Water behind Configurations 73 through 75; Also Configuration 55R

z, Distance from Source (cm)	Gamma-Ray Dose (mr/hr)			
	Conf. 55R	Conf. 73	Conf. 74	Conf. 74
84.8			4.27×10^{0}	
85.3				1.01×10^{1}
				1.03×10^{1}
90			2.61×10^{0}	6.91×10^{0}
				6.68×10^{0}
95			1.69×10^{0}	
100			1.17×10^{0}	2.86×10^{0}
			1.25×10^{0}	2.93×10^{0}
105			8.76×10^{-1}	
110			6.75×10^{-1}	1.51×10^{0}
			6.90×10^{-1}	1.57×10^{0}
115			5.12×10^{-1}	
115.3				1.22×10^{0}
146.3		1.13×10^{-1}		
146.6			1.34×10^{-1}	
146.7				3.32×10^{-1}
147.2	3.44×10^{-2}			
150	2.96×10^{-2}	9.30×10^{-2}	1.13×10^{-1}	2.78×10^{-1}
		1.08×10^{-1}		
160	2.57×10^{-2}	7.36×10^{-2}	8.88×10^{-2}	1.73×10^{-1}
	2.19×10^{-2}		7.67×10^{-2}	
	2.15×10^{-2}			
170	1.75×10^{-2}	5.08×10^{-2}	5.45×10^{-2}	1.17×10^{-1}

Table VI-20

Gamma-Ray Dose Measurements in Water behind Configurations 76 and 77; Also Configuration 64R

z, Distance from Source (cm)	Gamma-Ray Dose (mr/hr)		
	Conf. 76.	Conf. 64R	Conf. 77
83.7		2.57×10^{0}	
90		1.33×10^{0}	
		1.36×10^{0}	
100		6.07×10^{-1}	
110		3.25×10^{-1}	
117.4		2.00×10^{-1}	
147.9	5.89×10^{-2}		
148		4.24×10^{-2}	
150	5.41×10^{-2}	3.79×10^{-2}	4.09×10^{-2}
		4.18×10^{-2}	
155		3.44×10^{-2}	3.28×10^{-2}
160	3.97×10^{-2}	2.86×10^{-2}	3.09×10^{-2}
		2.79×10^{-2}	
165			2.54×10^{-2}
170	2.82×10^{-2}	2.18×10^{-2}	2.18×10^{-2}

Table VI-21

Thermal-Neutron Flux Measurements in Water behind Configurations 1 through 5

z, Distance from Source (cm)	Thermal-Neutron Flux (nvth)						
	Pure H_2O[a]	Conf. 1	Conf. 1a	Conf. 2	Conf. 3	Conf. 4	Conf. 5
50	2.06×10^{4}						
60	5.66×10^{3}						
68.3				1.75×10^{4}			
68.8		2.41×10^{4}					
70	1.22×10^{3}	3.30×10^{4}		2.39×10^{4}			
72		3.68×10^{4}		2.47×10^{4}			
74		3.27×10^{4}		2.00×10^{4}			
80	3.17×10^{2}	9.17×10^{3}		5.53×10^{3}			
85			1.65×10^{3}	1.60×10^{3}			
				1.12×10^{3}			
90	9.25×10^{1}	7.21×10^{2}	5.87×10^{2}	3.59×10^{2}			
		7.53×10^{2}					
100	2.82×10^{1}	1.11×10^{2}	8.10×10^{1}	4.62×10^{1}			
106						5.13×10^{3}	
106.1					6.98×10^{3}		
108					7.02×10^{3}	4.89×10^{3}	2.50×10^{1}
110	8.71×10^{0}	2.90×10^{1}	1.67×10^{1}	1.00×10^{1}	5.61×10^{3}	3.94×10^{3}	1.71×10^{1}
				9.19×10^{0}			
115					2.27×10^{3}	1.50×10^{3}	
120	2.81×10^{0}	5.97×10^{0}	4.39×10^{0}	2.45×10^{0}	4.74×10^{2}	3.53×10^{2}	3.10×10^{0}
				2.51×10^{0}	6.82×10^{2}	4.30×10^{2}	
125						9.34×10^{1}	
						1.14×10^{2}	
130	9.16×10^{-1}	1.74×10^{0}	1.22×10^{0}	7.01×10^{-1}	4.68×10^{1}	2.73×10^{1}	7.38×10^{-1}
140	3.14×10^{-1}	5.55×10^{-1}		2.19×10^{-1}	7.68×10^{0}	3.63×10^{0}	2.02×10^{-1}
150		1.83×10^{-1}		7.36×10^{-2}	1.76×10^{0}	7.69×10^{-1}	6.03×10^{-2}
160					4.79×10^{0}	2.01×10^{-1}	

[a] Measurements in pure water were taken at various times throughout the tests and are reported accordingly.

Table VI-22

Thermal-Neutron Flux Measurements in Water behind Configurations 6, 7, 9, and 10

z, Distance from Source (cm)	Thermal-Neutron Flux (nv_{th})			
	Conf. 6	Conf. 7	Conf. 9	Conf. 10
108	2.52×10^{1}	1.19×10^{1}		
108.4			9.31×10^{0}	
110	1.73×10^{1}	9.40×10^{0}	9.63×10^{0}	8.85×10^{0}
			9.45×10^{0}	
110.6	1.59×10^{1}			
112			8.23×10^{0}	
120	3.80×10^{0}	2.44×10^{0}	3.02×10^{0}	2.78×10^{0}
	3.11×10^{0}			
130	7.88×10^{-1}	6.76×10^{-1}	6.96×10^{-1}	6.88×10^{-1}
	7.27×10^{-1}			
140	2.06×10^{-1}		1.94×10^{-1}	1.89×10^{-1}
150	6.01×10^{-2}		5.44×10^{-2}	5.60×10^{-2}

Table VI-23

Thermal-Neutron Flux Measurements in Water behind Configurations 11 through 14

z, Distance from Source (cm)	Thermal-Neutron Flux (nvth)			
	Conf. 11	Conf. 12	Conf. 13	Conf. 14
107.2				6.55×10^{0}
108.1	7.83×10^{0}			
109		7.33×10^{0}		
109.1			6.44×10^{0}	
110	8.32×10^{0}	7.67×10^{0}	6.95×10^{0}	6.53×10^{0}
	8.21×10^{0}			4.40×10^{0}
112	7.57×10^{0}		6.61×10^{0}	
113				4.41×10^{0}
114		6.07×10^{0}	5.58×10^{0}	4.61×10^{0}
120	2.67×10^{0}	2.77×10^{0}	2.67×10^{0}	2.26×10^{0}
				2.23×10^{0}
130	6.54×10^{-1}	7.17×10^{-1}	6.81×10^{-1}	6.32×10^{-1}
				6.17×10^{-1}
140	1.91×10^{-3}	1.89×10^{-1}	1.98×10^{-1}	1.97×10^{-1}
150		5.93×10^{-2}	5.79×10^{-2}	6.02×10^{-2}

Table VI-24

Thermal-Neutron Flux Measurements in Water behind Configurations 15 through 18

z, Distance from Source (cm)	Thermal-Neutron Flux (nv_{th})				
	Pure H_2O	Conf. 15	Conf. 16	Conf. 17	Conf. 18
30	5.56×10^{5}				
40	1.01×10^{5}				
50	2.13×10^{4}				
60	4.99×10^{3}				
70	1.21×10^{3}	1.70×10^{4}			
72		2.57×10^{4}			
74		2.37×10^{4}			
78		1.22×10^{4}			
80	3.15×10^{2}	7.71×10^{3}			
90		4.64×10^{2}			
	9.26×10^{1}	4.10×10^{2}			
100		6.26×10^{1}			
	2.76×10^{1}	7.33×10^{1}			
107.8			8.79×10^{0}		
109.6				1.16×10^{1}	1.79×10^{1}
110	8.62×10^{0}	1.31×10^{1}	8.92×10^{0}	1.15×10^{1}	1.80×10^{1}
112			7.83×10^{0}	1.08×10^{1}	1.68×10^{1}
120	2.75×10^{0}	3.33×10^{0}	3.09×10^{0}	4.07×10^{0}	5.40×10^{0}
130	9.16×10^{-1}	9.61×10^{-1}	8.48×10^{-1}	9.38×10^{-1}	1.09×10^{0}
140	3.14×10^{-1}	3.00×10^{-1}	2.58×10^{-1}	2.65×10^{-1}	2.64×10^{-1}
150	1.15×10^{-1}	1.02×10^{-1}	8.06×10^{-2}	8.53×10^{-2}	7.71×10^{-2}

Table VI-25

Thermal-Neutron Flux Measurements in Water behind Configuration 19

z, Distance from Source (cm)	Thermal-Neutron Flux (nv_{th})	
	Pure H_2O	Conf. 19
90	9.26×10^{1}	
100	2.76×10^{1}	
110	8.62×10^{0}	
118.5		5.99×10^{0}
120	2.75×10^{0}	5.51×10^{0}
130	9.16×10^{-1}	1.41×10^{0}
140	3.14×10^{-1}	3.32×10^{-1}
150	1.15×10^{-1}	

Table VI-26

Thermal-Neutron Flux Measurements in Water behind Configurations 22 through 26; Also Configuration 30

z, Distance from Source (cm)	Thermal-Neutron Flux (nv_{th})					
	Conf. 22	Conf. 23	Conf. 24	Conf. 25	Conf. 26	Conf. 30
90	8.20×10^{2}	1.40×10^{3}	1.23×10^{3}	1.66×10^{2}		1.30×10^{3}
100	8.72×10^{1}	1.76×10^{2}	1.70×10^{2}	1.64×10^{2}	2.36×10^{2}	1.65×10^{2}
			1.65×10^{2}	1.69×10^{2}		
105				5.94×10^{1}		
107				4.34×10^{1}		
				4.16×10^{1}		
110	1.59×10^{1}	2.76×10^{1}	2.55×10^{1}	2.40×10^{1}	2.50×10^{1}	2.49×10^{1}
				2.48×10^{1}		
120	3.90×10^{0}	6.31×10^{0}	5.82×10^{0}	5.40×10^{0}	4.27×10^{0}	5.62×10^{0}
130	1.19×10^{0}	1.77×10^{0}	1.57×10^{0}	1.50×10^{0}	1.02×10^{0}	1.51×10^{0}
140	3.37×10^{-1}	5.29×10^{-1}	4.62×10^{-1}	4.62×10^{-1}	2.95×10^{-1}	4.63×10^{-1}
150	1.10×10^{-1}	1.68×10^{-1}	1.46×10^{-1}	1.40×10^{-1}	8.56×10^{-2}	1.46×10^{-1}

Table VI-27

Thermal-Neutron Flux Measurements in Water behind Configurations 27 and 28; Also Configuration 22

z, Distance from Source (cm)	Thermal Neutron Flux (nv_{th})		
	Conf. 22	Conf. 27	Conf. 28
69.4			1.93×10^{4}
70			2.15×10^{4}
72			3.12×10^{4}
73.3		6.98×10^{3}	
74			2.85×10^{4}
75		1.06×10^{4}	
77		1.20×10^{4}	
80		9.00×10^{3}	8.60×10^{3}
			8.71×10^{3}
90	8.20×10^{2}	6.31×10^{2}	5.40×10^{2}
		8.64×10^{2}	6.51×10^{2}
100	8.72×10^{1}	7.50×10^{1}	7.11×10^{1}
		8.78×10^{1}	7.09×10^{1}
110	1.59×10^{1}	1.45×10^{1}	1.44×10^{1}
120	3.90×10^{0}	3.76×10^{0}	3.73×10^{0}
130	1.19×10^{0}	1.06×10^{0}	1.12×10^{0}
140	3.37×10^{-1}	3.39×10^{-1}	3.63×10^{-1}
150	1.10×10^{-1}	1.10×10^{-1}	1.12×10^{-1}

Table VI-28

Thermal-Neutron Flux Measurements in Water behind Configurations 29, 31, and 32

z, Distance from Source (cm)	Thermal-Neutron Flux (nv_{th})			
	Pure H_2O	Conf. 29	Conf. 31	Conf. 32
90	9.26×10^{1}	9.83×10^{2}	7.38×10^{2}	4.49×10^{2}
100	2.76×10^{1}	1.46×10^{2}	8.27×10^{1}	6.46×10^{1}
110	8.62×10^{0}	2.97×10^{1}	1.49×10^{1}	1.36×10^{1}
120	2.75×10^{0}	7.61×10^{0}	3.72×10^{0}	3.55×10^{0}
130	9.16×10^{-1}	2.10×10^{0}	1.05×10^{0}	1.05×10^{0}
140	3.14×10^{-1}	6.67×10^{-1}	3.24×10^{-1}	3.36×10^{-1}
150	1.15×10^{-1}	2.30×10^{-1}	1.08×10^{-1}	1.11×10^{-1}

Table VI-29

Thermal-Neutron Flux Measurements in Water behind Configurations 35 through 38

z, Distance from Source (cm)	Thermal-Neutron Flux (nv_{th})			
	Conf. 35	Conf. 36	Conf. 37	Conf. 38
90	1.13×10^{3}	1.94×10^{3}		
92	8.05×10^{2}			
95			1.28×10^{3}	
100	1.06×10^{2}	1.67×10^{2}	3.41×10^{2}	3.25×10^{2}
	1.05×10^{2}			
105	3.98×10^{1}			
110	1.66×10^{1}	1.96×10^{1}	2.94×10^{1}	2.85×10^{1}
120	3.85×10^{0}	4.08×10^{0}	4.64×10^{0}	4.68×10^{0}
130	1.06×10^{0}	1.09×10^{0}	1.16×10^{0}	1.14×10^{0}
140	3.38×10^{-1}	3.11×10^{-1}	3.13×10^{-1}	3.23×10^{-1}
150	1.24×10^{-1}	9.66×10^{-2}	9.93×10^{-2}	9.66×10^{-2}

Table VI-30

Thermal-Neutron Flux Measurements in Water behind Configurations 39, 46, and 47

z, Distance from Source (cm)	Thermal-Neutron Flux (nv_{th})			
	Pure H_2O	Conf. 39	Conf. 46	Conf. 47
40	9.74×10^{4}			
50	1.97×10^{4}			
60	4.49×10^{3}			
70	1.11×10^{3}			
78.4		1.58×10^{4}		
79			6.09×10^{3}	
80	3.12×10^{2}	1.96×10^{4}	6.62×10^{3}	
	3.06×10^{2}			
81			1.01×10^{4}	
82		1.77×10^{4}		
83			1.08×10^{4}	
86		8.68×10^{3}	7.42×10^{3}	
90	8.84×10^{1}	3.10×10^{3}	2.98×10^{3}	
	9.18×10^{1}			
95		7.65×10^{2}	7.65×10^{2}	
		5.31×10^{2}	5.45×10^{2}	
100	2.70×10^{1}	1.37×10^{2}	1.41×10^{2}	
		1.75×10^{2}	1.74×10^{2}	
105		5.51×10^{1}		
110	8.15×10^{0}	1.28×10^{1}	1.25×10^{1}	
120	2.61×10^{0}	2.08×10^{0}	2.04×10^{0}	
120.4				9.07×10^{-1}
130	8.80×10^{-1}	4.96×10^{-1}	4.99×10^{-1}	4.28×10^{-1}
140	2.98×10^{-1}	1.46×10^{-1}	1.40×10^{-1}	1.24×10^{-1}
150		4.75×10^{-2}	4.64×10^{-2}	4.03×10^{-2}
160				1.13×10^{-2}

Table VI-31

Thermal-Neutron Flux Measurements in Water behind Configurations 51, 53, and 54

z, Distance from Source (cm)	Thermal-Neutron Flux (nv_{th})		
	Conf. 51	Conf. 53	Conf. 54
109.1			1.25×10^{1}
110			1.27×10^{1}
112			1.13×10^{1}
120			4.01×10^{0}
120.8	7.19×10^{-1}		
124.9		6.02×10^{-1}	
125	6.75×10^{-1}		
130	4.22×10^{-1}	4.60×10^{-1}	8.94×10^{-1}
140	1.25×10^{-1}	1.49×10^{-1}	2.52×10^{-1}
150	3.95×10^{-2}	4.77×10^{-2}	7.43×10^{-2}
160			2.44×10^{-2}

Table VI-32

Thermal-Neutron Flux Measurements in Water behind Configurations 55 and 56

z, Distance from Source (cm)	Thermal-Neutron Flux (nv_{th})		
	Pure H_2O	Conf. 55	Conf. 56
30	5.58×10^{5}		
40	9.81×10^{4}		
50	2.01×10^{4}		
60	4.60×10^{3}		
70	1.15×10^{3}		
	1.17×10^{3}		
80	3.08×10^{2}		
	3.06×10^{2}		
90	8.44×10^{1}		
	9.03×10^{1}		
100	2.72×10^{1}		
110	8.50×10^{0}		
120	2.77×10^{0}		
130	8.71×10^{1}		
139.7		6.93×10^{-2}	
140	2.97×10^{-1}		
140.2			8.79×10^{-2}
146		6.04×10^{-2}	
150	1.07×10^{-1}	3.93×10^{-2}	5.28×10^{-2}
		3.95×10^{-2}	
160		1.46×10^{-2}	1.50×10^{-2}
		1.40×10^{-2}	

Table VI-33

Thermal-Neutron Flux Measurements in Water behind Configurations 63, 70, and 72

z, Distance from Source (cm)	Thermal-Neutron Flux (nv_{th})		
	Conf. 63	Conf. 70	Conf. 72
80.5			2.52×10^{2}
84			1.11×10^{2}
90			1.40×10^{1}
100			1.12×10^{0}
110			2.03×10^{-1}
112.1			1.57×10^{-1}
139.1		4.44×10^{-2}	
141.2			2.43×10^{-2}
142.8	4.94×10^{-2}		
150	5.27×10^{-2}	2.16×10^{-2}	1.80×10^{-2}
			1.73×10^{-2}
160	1.39×10^{-2}	9.63×10^{-3}	9.40×10^{-3}

Table VI-34

Thermal-Neutron Flux Measurements in Water behind Configurations 74 and 75

z, Distance from Source (cm)	Thermal-Neutron Flux (nv_{th})	
	Conf. 74	Conf. 75
85	4.28×10^{2}	
90	8.07×10^{1}	1.03×10^{3}
95	1.91×10^{1}	3.00×10^{2}
100	5.69×10^{0}	8.10×10^{1}
105	2.17×10^{0}	2.56×10^{1}
110	9.40×10^{-1}	9.46×10^{0}
139.4	7.58×10^{-2}	
140.3		1.16×10^{-1}
150	4.02×10^{-2}	4.86×10^{-2}
155	2.30×10^{-2}	2.96×10^{-2}
160		1.63×10^{-2}

Table VI-35

Fast-Neutron Dose Measurements in Water behind Configurations 1 through 4

z, Distance from Source (cm)	Fast-Neutron Dose (mrep/hr)				
	Pure H_2O	Conf. 1	Conf. 2	Conf. 3	Conf. 4
30	3.48×10^{2}				
40	1.15×10^{2}				
50	3.73×10^{1}				
60	8.70×10^{0}				
68.1			2.90×10^{1}		
70	2.73×10^{0}	3.26×10^{1}	1.54×10^{1}		
75		8.60×10^{0}	4.05×10^{0}		
80	9.03×10^{-1}	3.46×10^{0}	1.54×10^{0}		
90		6.97×10^{-1}	2.83×10^{-1}		
100		1.93×10^{-1}			
105.4					2.77×10^{0}
105.7				4.01×10^{0}	
110				1.51×10^{0}	8.26×10^{-1}
115				5.18×10^{-1}	2.61×10^{-1}
					2.64×10^{-1}
120				2.25×10^{-1}	1.13×10^{-1}
125					5.09×10^{-2}
130				2.71×10^{-2}	

Table VI-36

Fast-Neutron Dose Measurements in Water behind Configuration 15

z, Distance from Source (cm)	Fast-Neutron Dose (mrep/hr)	
	Pure H_2O	Conf. 15
30	3.54×10^{2}	
40	1.08×10^{2}	
50	3.80×10^{1}	
60	9.31×10^{0}	
68.7		2.46×10^{1}
70	2.75×10^{0}	2.13×10^{1}
80	8.45×10^{-1}	2.24×10^{0}
90	2.73×10^{-1}	4.19×10^{-1}
100	7.41×10^{-2} [a]	1.16×10^{-1}
110	2.16×10^{-2} [a]	
120	6.88×10^{-3} [a]	
130	2.29×10^{-3} [a]	2.40×10^{-3} [a]
140	7.85×10^{-4} [a]	7.51×10^{-4} [a]
150	2.88×10^{-4} [a]	2.56×10^{-4} [a]

[a] Thermal-neutron flux divided by 400.

[redacted]

Table VI-37

Fast-Neutron Dose Measurements in Water behind Configurations 31, 39, and 75

z, Distance from Source (cm)	Fast-Neutron Dose (mrep/hr)			
	Pure H_2O	Conf. 31	Conf. 39	Conf. 75
30	3.72×10^{2}			
40	1.23×10^{2}			
50	4.22×10^{1}			
60	1.00×10^{1}			
70	2.93×10^{0}			
70.9		4.13×10^{1}		
77.7				1.00×10^{1}
77.8			1.20×10^{1}	
80	8.82×10^{-1}	3.53×10^{0}	5.17×10^{0}	
81.2				3.88×10^{0}
90	2.78×10^{-1}	5.67×10^{-1}	5.20×10^{-1}	5.44×10^{-1}
100			7.86×10^{-2}	9.73×10^{-2}
110				2.10×10^{-2}

[redacted]